The Role of 16α-Hydroxyestradiol in Pulmonary Arterial Hypertension

Rosemary Anne Gaw MPharm MSc

Submitted in fulfilment of the requirements of the degree of Doctor of Philosophy

Strathclyde Institute of Pharmacy & Biomedical Sciences
University of Strathclyde

16th April 2024

Declaration of Authenticity and Author's Rights

This thesis is the result of the author's original research. It has been composed by the author and has not been previously submitted for examination which has led to the award of a degree.

Signed:

Date: 16/04/24

Acknowledgements

First and foremost, I would like to thank my supervisor Professor Mandy MacLean for the wonderful opportunity to work in her lab and for all the guidance she has given me during my PhD. Despite many challenges, Mandy has always supported me, and I am extremely grateful.

I would also like to thank my postdoctoral mentor Dr Smriti Sharma for her support and advice, especially for saving the day when it comes to western blots! I am also very grateful to my previous postdoctoral mentor Dr Nina Denver for her advice and training at the start of this project. In addition, thanks to our technicians Gregor Aitchison and Ayman Gebril who keep the lab running and rest of us (mostly) sane. I would also like to thank the rest of the MacLean lab (past and present) for their support – Dr Hicham Labazi, Dr Josh Dignam, Dr Sofia Laforest, Margaret Nilsen, Dr Ben Cathcart, Dr Kirsty Mair, Dr Stuart McEwen, and Dr Rebecca Openshaw. It has been a privilege to work with such a fantastic group of people.

I am extremely grateful to my parents for all their encouragement and help over my years of studying, and for their financial support without which I could not have completed my studies. Also, thanks to my wonderful wee brother Jonathan who always makes me laugh.

I would also like to thank my friend Kati for being so amazing through this PhD journey and being there for me no matter how tough things were. I would also like to thank her parents Willie and Annukka for their kindness and support. Finally, thanks to all my other friends (particularly Sarah, Youssef, Leah, Alison, Brenda, Souvde, Gillian, and Claire) for your support over the past few years.

Table of Contents

List of Tables

List of Figures

List of Abbreviations

16-OH-DHEA	16α-hydroxydehydroepiandrosterone
16-OH-DHEA-S	16α-hydroxydehydroepiandrosterone sulfate
16OHE1	16α-hydroxyestrone
16OHE2	16α-hydroxyestradiol
17β-HSD1	17β-hydroxysteroid dehydrogenase 1
17β-HSD2	17β-hydroxysteroid dehydrogenase 2
17β-HSD3	17β-hydroxysteroid dehydrogenase 3
2EE	2-ethoxyestradiol
2ME1	2-methoxyestrone
2ME2	2-methoxyestradiol
2OHE1	2-hydroxyestrone
2OHE2	2-hydroxyestradiol
3β-HSD	3β-hydroxysteroid dehydrogenase
4ME1	4-methoxyestrone
4ME2	4-methoxyestradiol
4OHE1	4-hydroxyestrone
4OHE2	4-hydroxyestradiol
5-HT	5-hydroxytryptamine (serotonin)
5-HTP	5-hydroxy-L-tryptophan
α-SMA	alpha-smooth muscle actin
AhR	aryl hydrocarbon receptor
ALK1	activin receptor-like kinase-1
AoSMCs	aorta smooth muscle cells

ARNT	aryl hydrocarbon receptor nuclear translocator
ATP	adenosine triphosphate
BAT	brown adipose tissue
BCA	bicinchoninic acid
BMI	body mass index
BMP	bone morphogenetic protein
BMP2	bone morphogenetic protein 2
BMP9	bone morphogenetic protein 9
BMPR1A	bone morphogenetic protein receptor 1A
BMPR1B	bone morphogenetic protein receptor 1B
BMPR2	bone morphogenetic protein receptor 2
BOEC	blood outgrowth endothelial cell
BSA	bovine serum albumin
cAMP	cyclic adenosine monophosphate
CAV1	caveolin-1
cDNA	complementary deoxyribonucleic acid
cGMP	cyclic guanosine monophosphate
CKD	chronic kidney disease
c-Myc	cellular Myc
COL1A1	collagen, type I, alpha 1
COL3A1	collagen, type III, alpha 1
COMT	catechol-O-methyltransferase
COX	cyclooxygenase
CRP	C-reactive protein
CT	threshold cycle

CYP11A1	cytochrome P450 11A1
CYP17A1	cytochrome P450 17A1
CYP19A1	cytochrome P450 19A1 (aromatase)
CYP1A1	cytochrome P450 1A1
CYP1A2	cytochrome P450 1A2
CYP1B1	cytochrome P450 1B1
CYP3A4	cytochrome P450 3A4
DAG	diacylglycerol
DHEA	dehydroepiandrosterone
DHEA-S	dehydroepiandrosterone sulfate
DHT	dihydrotestosterone
DMEM	Dulbecco's modified eagle medium
DMSO	dimethyl sulfoxide
DNA	deoxyribonucleic acid
dNTPs	deoxyribonucleotide triphosphates
E1	estrone
E2	estradiol
E3	estriol
EC	endothelial cell
EDTA	ethylenediaminetetraacetic acid
ENG	endoglin
eNOS	endothelial nitric oxide synthase
ER	estrogen receptor
ERα	estrogen receptor-alpha
ERβ	estrogen receptor-beta

ERK1	extracellular signal-related kinase 1
ERK2	extracellular signal-related kinase 2
ET	endothelin
FBS	fetal bovine serum
FC	fold change
G1	(±)-1-[(3a*R**,4*S**,9b*S**)-4-(6-Bromo-1,3-benzodioxol-5-yl)-3a,4,5,9b-tetrahydro-3*H*-cyclopenta[*c*]quinolin-8-yl]- ethanone
G15	(3a*S**,4*R**,9b*R**)-4-(6-Bromo-1,3-benzodioxol-5-yl)-3a,4,5,9b-3*H*-cyclopenta[*c*]quinoline
Glut4	glucose transporter type 4
GPER	G protein-coupled estrogen receptor
GTP	guanosine triphosphate
HFL-1	human fetal lung fibroblast-1
HIF1α	hypoxia-inducible factor 1α
HIF1β	hypoxia-inducible factor 1β
Hk2	hexokinase 2
HLF	human lung fibroblast
hPASMCs	human pulmonary artery smooth muscle cells
HRP	horseradish peroxidase
HRT	hormone replacement therapy
Hx	hypoxia
ID	inhibitor of DNA-binding
Id1	inhibitor of DNA-binding 1
Id2	inhibitor of DNA-binding 2
Id3	inhibitor of DNA-binding 3
IL-1β	interleukin-1β

IP	I-prostanoid
IP_3	Inositol triphosphate
KNCK3	potassium channel, subfamily K, member 3
LDS	lithium dodecyl sulfate
LV	left ventricle
LV+S	left ventricle plus septum
MAPK	mitogen-activated protein kinase
MCT	monocrotaline
miR	micro-ribonucleic acid
MPP	1,3-*Bis*(4-hydroxyphenyl)-4-methyl-5-[4-(2-piperidinylethoxy)phenol]-1*H*-pyrazole dihydrochloride
mRNA	messenger ribonucleic acid
NF-κβ	nuclear factor- κβ
NO	nitric oxide
Nox1	nicotinamide adenine dinucleotide phosphate oxidase 1
NRF2	nuclear factor erythroid 2-related factor 2
p38 MAPK	p38 mitogen-activated protein kinase
PAECs	pulmonary artery endothelial cells
PAH	pulmonary arterial hypertension
PASMCs	pulmonary artery smooth muscle cells
PBS	phosphate buffered saline
PBS-T	Tween 20 in PBS
PBS-TT	phosphate buffered saline-Tween 20-Triton X-100
PCR	polymerase chain reaction
PDE-5	phosphodiesterase-5

PDGF	platelet derived growth factor
PH	pulmonary hypertension
PHD	prolyl hydroxylase
PHTPP	4-[2-Phenyl-5,7-*bis*(trifluoromethyl)pyrazolo[1,5-*a*]pyrimidin-3-yl]phenol
PI3K	phosphoinositide 3-kinase
PPARγ	peroxisome proliferator-activated receptor gamma
PV	pressure-volume
PVAT	perivascular adipose tissue
PVDF	polyvinylidene difluoride
PVR	pulmonary vascular resistance
qRT-PCR	quantitative real-time polymerase chain reaction
RNA	ribonucleic acid
ROCK	Rho-associated protein kinase
ROS	reactive oxygen species
rPASMCs	rat pulmonary artery smooth muscle cells
RV	right ventricle
RVEF	right ventricular ejection fraction
RVSP	right ventricular systolic pressure
s/c	subcutaneous
SEM	standard error of the mean
SERT	serotonin transporter
sGC	soluble guanylate cyclase
SNP	single nucleotide polymorphism
SOD	superoxide dismutase

SOX17	SRY-related HMG-box 17
SSRI	selective serotonin reuptake inhibitor
SuHx	sugen-hypoxic
TASK-1	TWIK-related acid-sensitive potassium channel-1
TBS	tris-buffered saline
TBST	tris-buffered saline-Tween-20
TGF-β	transforming growth factor-beta
TMS	(E)-2,3',4,5'-tetramethoxystilbene
TNF-α	tumour necrosis factor-α
TPH1	tryptophan hydroxylase 1
TPH2	tryptophan hydroxylase 2
TXA_2	thromboxane A_2
UCP-1	uncoupling protein-1
VAT	visceral adipose tissue
VEGF	vascular endothelial growth factor
VEGFR2	vascular endothelial growth factor receptor 2
WAT	white adipose tissue
WHO	World Health Organization

Abstract

Pulmonary arterial hypertension (PAH) is a life-limiting disease characterised by progressive remodelling of distal pulmonary arteries. PAH is predominant in females, affecting up to four-fold more women than men. This has led to extensive research into the role of estrogens in PAH. 16α-hydroxyestradiol (16OHE2) is produced during pregnancy. Plasma levels of 16OHE2 are increased in female idiopathic PAH patients, and males and females with portopulmonary PAH. However, its function is undetermined.

Many paradoxes have been observed in PAH, and here we provide evidence that the effects of 16OHE2 are also paradoxical. The *in vitro* effects of 16OHE2 are mainly pathogenic. 16OHE2 increased migration of male and female rat pulmonary artery smooth muscle cells (rPASMCs) but had no effect on proliferation. Mutations in bone morphogenetic protein receptor 2 (BMPR2) account for ~80% of hereditary PAH cases. However, BMPR2 levels are generally reduced in PAH patients regardless of mutation status. 16OHE2 decreased *Bmpr2*, *Smad1*, *Smad4* and *Smad5* mRNA expression in male rPASMCs. Decreased *Smad4* expression was attenuated by the estrogen receptor-α antagonist MPP. 16OHE2 also decreased *BMPR2* and *SMAD4* in human male control (non-PAH) PASMCs. However, 16OHE2 decreased expression of the fibrosis marker *Col1a1* in male rPASMCs. 16OHE2 may also mediate pathogenic effects in the aorta.

16OHE2 mediates both pathogenic and protective effects *in vivo*. 16OHE2 did not induce PAH in male or female C57BL/6 mice but increased right ventricular (RV) hypertrophy in female mice, suggesting that it acts directly on the heart. In lung tissue, 16OHE2 decreased BMPR2 protein levels in female mice but increased p-Smad1,5,9 in both sexes. In the RV, 16OHE2 increased protective *Id1*, *Id3 and Sox17* mRNA expression and decreased pathogenic *Col1a1* in female mice, and decreased Col*3a1* in both sexes. Paradoxical effects may result from peripheral 16OHE2 synthesis (e.g., in lung or adipose) versus exogenous administration.

Chapter 1

Introduction

1.1 Pulmonary Arterial Hypertension

In the circulation, the right ventricle pumps deoxygenated blood into the pulmonary artery[1]. This branches off into small distal pulmonary arteries and capillaries (which envelop the alveoli)[1]. Carbon dioxide is released and exhaled, and oxygen enters the bloodstream[1]. Oxygenated blood is then returned to the heart via the pulmonary vein and left atrium before being pumped to the rest of the body by the left ventricle[1]. Following circulation, deoxygenated blood returns to the right ventricle via the vena cava and right atrium (Figure 1.1)[1].

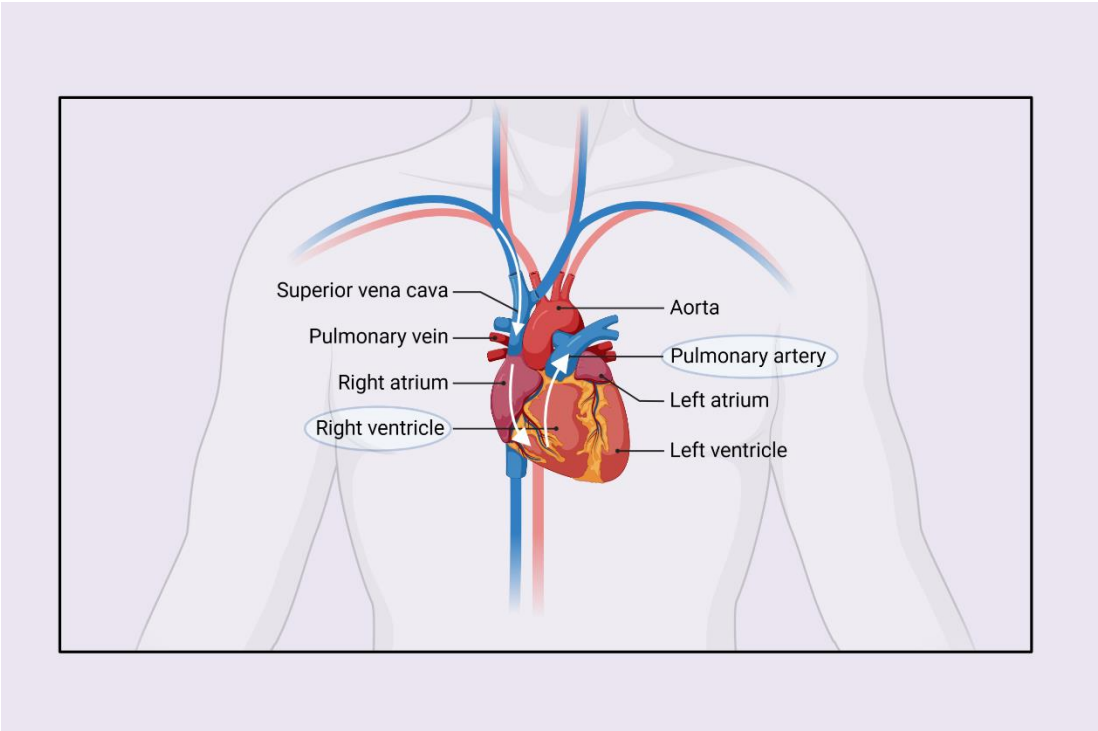

Figure 1.1: The pulmonary circulation.
Deoxygenated blood is returned to the heart via the superior vena cava. It flows through the right atrium to the right ventricle, where it is pumped into the pulmonary artery and reoxygenated in the lungs before returning to the heart via the pulmonary vein and left atrium. Adapted from "Cross-Section Heart with Human Background (Layout)", by BioRender.com (2024)[2].

Pulmonary hypertension (PH) is defined as a mean pulmonary arterial pressure >20mmHg at rest (as recommended by the 6th World Symposium on Pulmonary Hypertension 2018; previously defined as >25mmHg)[3]. There are five distinct classes of PH set out by the World Health Organization (Table 1.1)[4].

Table 1.1: World Health Organization Classification of Pulmonary Hypertension

Group	Causes
Class I – Pulmonary Arterial Hypertension (PAH)	• Idiopathic PAH (unknown) • Heritable PAH (e.g., *BMPR2*, *ALK1*, *ENG*, *SMAD9*, *KCNK3, CAV1*, *EIF2AK4*, other mutations) • Drug or toxin-induced PAH • PAH associated with HIV, connective tissue disease, schistosomiasis, portal hypertension or congenital heart disease • Pulmonary veno-occlusive disease or pulmonary capillary haemangiogenesis
Class II – PH due to left heart disease	
Class III – PH due to lung disease and/or hypoxia	
Class IV – Chronic thromboembolic PH	
Class V – PH with unclear and/or multi-factorial mechanisms	• Haematological disorders (chronic haemolytic anaemia, myeloproliferative disorders) • Splenectomy • Systemic disorders (e.g. sarcoidosis, neurofibromatosis) • Metabolic disorders (e.g. thyroid disease, Gaucher disease) • Other disease (e.g. chronic renal failure)

Pulmonary arterial hypertension (PAH) is a rare life-limiting condition affecting around 15-50 people in one million[4]. It is characterised by progressive obstruction of distal pulmonary arteries resulting in increased pulmonary arterial pressure and right ventricular (RV) hypertrophy, leading to RV failure and ultimately death[4]. Survival rates are poor, with the US REVEAL registry reporting 1-year, 3-year, 5-year and 7-year survival rates of 85%, 68%, 57% and 49% respectively[5]. As the early symptoms of PAH are non-specific (e.g., fatigue, dizziness), it is often not diagnosed until late stages where patient prognoses and outcomes are poor[4]. Furthermore, a definitive diagnosis of PAH requires invasive right heart catheterisation (although an estimate of pulmonary arterial pressure may be obtained by echocardiogram)[4]. This also contributes to delays in diagnosing PAH[4].

According to Humbert et al, "Vasoconstriction, remodeling of the pulmonary vessel wall, and thrombosis contribute to the increased pulmonary vascular resistance in PAH. However, it is now recognized that pulmonary arterial obstruction by vascular proliferation and remodeling is the hallmark of PAH pathogenesis"[6(p.13S)]. The process of pulmonary vascular remodelling is complex, with several known mechanisms affecting all layers of the arterial wall[6]. These include genetic mutations, altered microRNA function, inflammation, mitochondrial dysfunction and oxidative stress[6,7]. Increased pulmonary vascular resistance increases strain on the RV, leading to maladaptive remodelling and failure (Figure 1.2)[7].

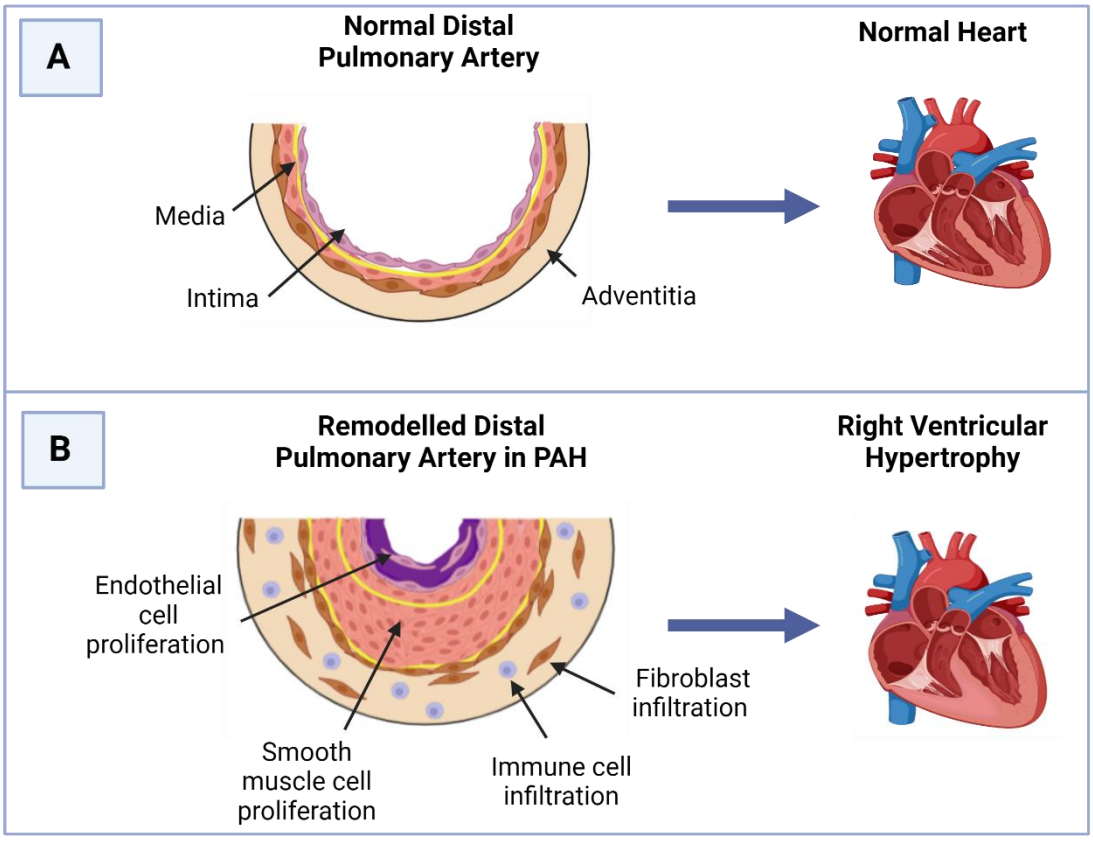

Figure 1.2: Pulmonary vascular remodelling in PAH.
(A) The normal distal pulmonary artery is comprised of three layers – the outer adventitial layer, the medial (middle) layer of smooth muscle cells, and the intimal (inner) layer of endothelial cells. These facilitate blood flow through the artery. (B) In pulmonary arterial hypertension, immune cells and fibroblasts infiltrate into the adventitial layer leading to inflammation and fibrosis. Increased proliferation of smooth muscle cells leads to narrowing of the vessel. Proliferation and migration of endothelial cells leads to further occlusion of the vessel. Increased pulmonary arterial pressure places strain on the right ventricle (RV). This leads to RV remodelling, hypertrophy, failure, and ultimately death. Created with BioRender.com.

Current medicines for PAH target three key pathways: endothelin, prostacyclin, and nitric oxide (Figure 1.3)[8].

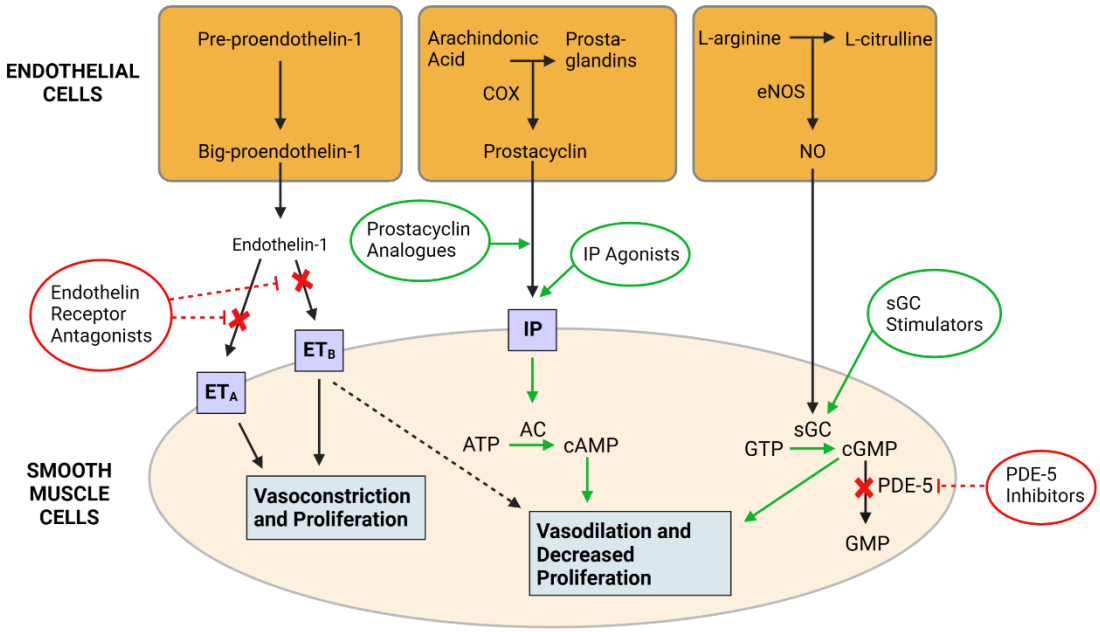

DRUGS AVAILABLE ON THE MARKET	ENDOTHELIN RECEPTOR ANTAGONISTS	PROSTACYCLIN ANALOGUES	IP RECEPTOR AGONISTS	SGC STIMULATORS	PDE-5 INHIBITORS
	Bosentan (Non-selective) Macitentan (Non-selective) Ambrisentan (ET_A selective)	Iloprost Epoprestenol Treprostinil	Selexipag	Riociguat	Sildenafil Tadalafil

Figure 1.3: Therapeutic targets for PAH and drugs currently available on the market. Current medicines for PAH target three key pathways: endothelin, prostacyclin, and nitric oxide[8]. ET = endothelin, COX = cyclooxygenase, IP = I-prostanoid, ATP = adenosine triphosphate, AC = adenylate cyclase, cAMP = cyclic adenosine monophosphate, eNOS = endothelial nitric oxide synthase, NO = nitric oxide, GTP = guanosine triphosphate, sGC = soluble guanylate cyclase, cGMP = cyclic guanosine monophosphate, PDE-5 = phosphodiesterase-5, GMP = guanosine monophosphate. Created with BioRender.com.

Endothelin-1 (ET-1) is a potent vasoconstrictor which acts via the G protein-coupled receptors ET_A and ET_B[9]. ET_A receptors are present in pulmonary artery smooth muscle cells (PASMCs) whereas ET_B receptors are present in both smooth muscle and endothelial cells[9]. In PASMCs, ET_A and ET_B mediate the pathogenic effects of ET-1 through G_q-coupled activation of phospholipase C, which hydrolyses phosphatidylinositol 4,5-bisphosphate to inositol triphosphate (IP_3) and

diacylglycerol (DAG)[10]. IP_3 acts as a second messenger to release stored intracellular Ca^{2+} from the endoplasmic reticulum into the cytosol, leading to increased smooth muscle cell contractility and migration[10]. DAG activates protein kinase C, leading to increased cell proliferation (via activation of mitogen-activated protein kinases (MAPKs))[10]. On the other hand, activation of ET_B in endothelial cells increases protective prostacyclin and nitric oxide (NO) production, leading to vasodilation and decreased proliferation[9]. Endothelial ET_B receptors also contribute to clearance of ET-1 through internalisation of the receptor complex upon ET-1 binding[11,12]. Approximately 50% of circulating ET-1 is removed in the lung due to the high surface area of the pulmonary vasculature, which may explain its very low physiological levels (e.g., average of 1.36 pg/mL in a cohort of 3223 African American individuals enrolled in The Jackson Heart Study)[12,13]. In PAH patients, ET_A and ET_B expression are increased in pulmonary vascular smooth muscle, whereas endothelial ET_B expression is decreased[9]. Furthermore, plasma levels of ET-1 are elevated in PAH patients compared to control subjects, suggesting that clearance is decreased[8]. ET_A is considered a key therapeutic target in PAH[14]. There are two distinct groups of endothelin receptor antagonists: ET_A-selective and non-selective[14]. ET_A-selective antagonists are designed to maintain the beneficial ET-1 clearance and vasodilation mediated by ET_B in endothelial cells, while blocking the adverse effects mediated by ET_A receptors[14]. The ET_A-selective antagonist ambrisentan was approved in 2007 and is still in clinical use[14]. Sixatentan has a higher ET_A selectivity than ambrisentan but was withdrawn from the market in 2010 due to concerns over severe hepatotoxicity[14]. Non-selective ET-antagonists (e.g. bosentan, macitentan) are also commercially available but indiscriminately block both the ET_A and ET_B receptors[14].

Prostacyclins are produced in endothelial cells from arachidonic acid via cyclooxygenase (COX)[8]. They bind to specific I-prostanoid (IP) receptors in smooth muscle cells leading to G_s protein-coupling to adenylate cyclase, increased production of cyclic adenosine monophosphate (cAMP) and subsequent activation of protein kinase A[15,16]. Protein kinase A inactivates myosin light chain kinase in PASMCs leading to smooth muscle relaxation and vasodilation[16]. Prostacyclins also reduce smooth muscle cell proliferation and have anti-thrombotic and anti-inflammatory effects[8]. In PAH, the pathway shifts and arachidonic acid is converted to the alternative pro-inflammatory product thromboxane A_2 (TXA_2)[8]. TXA_2 mediates vasoconstriction, cell proliferation, and platelet aggregation via activation of TXA_2

receptors and subsequent activation of several G protein isotypes (e.g., G_q, G_{12})[8,17]. Prostacyclin production and IP receptor expression are decreased in the lung tissue of PAH patients[8]. There are currently two types of drugs which act on the prostacyclin pathway: prostacyclin analogues and the IP receptor agonist selexipag[8]. These drugs activate IP receptors, stimulating adenylate cyclase conversion of adenosine triphosphate (ATP) to cAMP[15,16]. This results in vasorelaxation, decreased cell proliferation and reduced inflammation[15,16].

NO is an endogenous vasodilator which plays a key role in maintaining a healthy vasculature[8]. It is produced in endothelial cells by endothelial nitric oxide synthase (eNOS) during oxidation of L-arginine to L-citrulline[8]. NO diffuses into the underlying PASMCs and binds to soluble guanylate cyclase (sGC), which converts guanosine triphosphate (GTP) to cyclic guanosine monophosphate (cGMP)[8,16]. This activates protein kinase G which phosphorylates several target proteins leading to a decrease in intracellular Ca^{2+} concentration resulting in vasorelaxation, decreased cell proliferation, decreased platelet aggregation and reduced thrombosis[16,18]. NO bioavailability and signalling are decreased in PAH patients[19]. While some studies have attributed pulmonary vasoconstriction to decreased eNOS expression, other studies in experimental animal models and human PAH have observed no change or even increased eNOS expression[18,20,21]. For example, Mason et al. demonstrated that increased expression of eNOS may be specifically localised to plexiform lesions[21]. Variable eNOS expression may explain why only a small subset of PAH patients (~13%) respond to vasodilator therapy[22]. However, the anti-proliferative effects of NO may still be of benefit in 'non-responders' to prevent further vascular remodelling[8]. There are currently two drug classes acting on the NO pathway: soluble guanylate cyclase (sGC) stimulators and phosphodiesterase-5 (PDE-5) inhibitors[8]. Riociguat enhances sGC activity, increasing availability of cGMP and activation of protein kinase G, leading to vasodilation and decreased cell proliferation[8,16]. PDE-5 inhibitors (e.g. sildenafil, tadalafil) prevent conversion of cGMP to GMP, increasing cGMP/protein kinase G signalling[8,16]. However, concomitant administration of PDE-5 inhibitors with nitrates or NO-producing drugs is contraindicated, as increased cGMP in the vascular network may lead to widespread vasorelaxation, severe drop in blood pressure, and potentially death[16]. Calcium channel blockers (e.g. amlodipine, diltiazem) may also be effective in the small subset of PAH patients who respond to vasodilator therapy (response being defined as a >10mmHg reduction in mean pulmonary arterial pressure)[22,23].

While treatment of PAH has progressed over recent decades, current therapeutic strategies are suboptimal[8]. The current aims of treatment are to achieve a low-risk status (<5% risk of mortality within the next year), preserve quality of life and minimise future mortality risk[8]. Current therapies generally alleviate the symptoms of PAH but fail to address the underlying pulmonary vascular remodelling[8]. In addition, some treatments are invasive (e.g. continuous intravenous infusion of treprostinil) and have undesirable side effects[24]. As a result, most patients will inevitably require a lung transplant or succumb to the disease[25]. Therefore, novel medicines are required to attenuate the underlying pulmonary vascular remodelling in PAH and to regenerate obliterated distal pulmonary arteries[25].

1.2 Sex and PAH

1.2.1 The Estrogen Paradox in PAH

First noted by Dresdale et al. in 1951, the incidence of PAH is significantly higher in females with up to four-fold more women developing PAH than men[26,27]. This has led to the hypothesis that female sex hormones (or 'estrogens') may mediate development of PAH. On the other hand, once PAH has developed women have better survival than men[28]. For example, according to the Swedish Pulmonary Arterial Hypertension Registry, 5-year survival was 68% in women but 55% for men between 2008 and 2016[28]. Furthermore, estrogens are protective in certain animal models of PAH[29]. These issues are collectively known as the 'estrogen paradox'[29].

The are three main estrogens: estrone (E1), estradiol (E2) and 16α-hydroxyestradiol (16OHE2)[29]. E2 synthesised in the ovarian follicles and corpus luteum is predominant in premenopausal women, whereas E1 synthesised in peripheral tissues (particularly adipose) is predominant in postmenopausal women and men[29]. 16OHE2 (also known as estriol (E3)) is predominant during pregnancy[29]. Circulating E2 levels are higher in men and postmenopausal women with PAH compared to control subjects, and are associated with worse disease outcomes[30,31]. It is

challenging to study E2 levels in premenopausal women with PAH due to the natural variations associated with the menstrual cycle[32]. However, Baird et al. recently conducted a study in premenopausal women with PAH where E2 levels and 6-minute walk distance (a measure of exercise capacity) were assessed weekly across a 4-week menstrual cycle[32]. E2 levels were higher and less variable in premenopausal female PAH patients compared to control subjects and were inversely associated with 6-minute walk distance[32]. While it is widely accepted that E2 and its metabolites play a key role in PAH, many controversies remain including the question of whether endogenous and exogenous E2 attenuates or induces PAH[29]. There are many hypotheses for the estrogen paradox in PAH including extragonadal E2 synthesis in peripheral tissues (e.g., lung, adipose), altered E2 metabolism, context-specific effects of E2, and poor translation of animal models to human PAH[29,33-35]. E2 may also contribute to improved survival in women with PAH by protecting RV function[29].

Several studies have observed that endogenous E2 mediates protective effects against pulmonary vascular remodelling, haemodynamic alterations, and RV hypertrophy in certain animal models of PAH[36,37,38]. On the other hand, exogenous E2 from oral contraceptives and hormone replacement therapy (HRT) may unmask or worsen pre-existing PAH in women with additional predisposing factors (e.g., genetic susceptibility, connective tissue disease)[32,29]. Many of the autoimmune diseases associated with PAH are also female predominant, e.g., systemic lupus erythematosus, systemic sclerosis, and autoimmune hepatitis[40]. The effects of E2 in the circulation may be different to the effects of extragonadal E2 synthesised in the peripheral tissues (e.g., lung, adipose)[33,34]. Mair et al. observed that E2 is synthesised endogenously in the smooth muscle layer of human pulmonary arteries via aromatase[33]. Aromatase has been demonstrated to be pathogenic in PAH, and its expression is higher in the smooth muscle layer of pulmonary arteries from female control subjects compared to males[33]. Adipose tissue is also a major source of E2 production, particularly in postmenopausal women[41]. Obesity may be more prevalent in PAH patients. For example, the Scottish Government in 2019 reported that 29% of adults were affected by obesity, whereas McLean et al. (also in 2019) reported from Scottish Pulmonary Vascular Unit data that 35.7% of PAH patients were obese[42,43]. Similarly, 17% of adults in France are obese whereas, according to the French Pulmonary Hypertension Network Registry, 30% of PAH patients are obese[44,45]. On the other hand, ~42% of adults in the US are currently obese,

whereas according to Pulmonary Hypertension Association Registry data (2015-2019), around 40% of American PAH patients are obese[46,47]. However, according to the World Health Organisation, the global obesity rate is approximately 16%[48]. Therefore, the average obesity rate of 30-40% in PAH patients from different registries across the globe may be higher than in the general population[41]. Increased fat mass in obesity is positively correlated with increased E2 synthesis via aromatase[49,50]. According to the REVEAL registry, the average patient age at PAH diagnosis is 53 years old, suggesting that extragonadal E2 synthesis in adipose tissue may contribute to the high prevalence of PAH in postmenopausal women[51].

RV hypertrophy and failure is the major cause of mortality in PAH[52]. The right ventricular ejection fraction (RVEF) is a key prognostic marker of survival in PAH, which expresses the amount of deoxygenated blood pumped out of the RV (stroke volume) divided by the total amount of blood in the RV (end-diastolic volume) as a percentage[53,54]. According to Kawut et al., a 5% lower RVEF at PAH diagnosis was associated with a 60% increased risk of death between January 1994 and June 2002[55]. Both the Framingham Heart Study and Multi-Ethnic Study of Atherosclerosis (MESA) reported that baseline RVEF is higher in women than men in the absence of cardiovascular disease[56,57]. Higher circulating E2 levels in postmenopausal women receiving HRT were also associated with increased RV function compared to non-HRT users[58]. Increased RVEF is also observed in female PAH patients compared to male patients, and improved RV adaptability to high pulmonary pressures may contribute to better survival in females[59].

Sex also affects response to current PAH treatments. Jacobs et al. observed a similar reduction in pulmonary vascular resistance in male and female PAH patients following one year of mono- or combination therapy with prostacyclin analogues, endothelin receptor antagonists, and PDE-5 inhibitors[60]. However, RV function improved in response to treatment in female PAH patients but deteriorated further in male patients[60]. In general, prostacyclin analogues and endothelin receptor antagonists appear to be more effective in female PAH patients than male patients[61,62]. However, the PDE-5 inhibitor tadalafil may be more effective in males[63]. Therefore, sex differences in response to treatment of PAH may be associated with improved survival in female PAH patients[60]. Overall, despite recent progress in understanding the estrogen paradox, this remains a challenge and further investigation is required to fully elucidate the underlying mechanisms of PAH.

1.2.2 Pregnancy and PAH

Pregnancy is associated with physiological changes that increase pulmonary vascular flow including increased circulatory volume and cardiac output[64]. However, the role of 16OHE2 in these changes is undetermined. The healthy pulmonary vasculature responds to the demands of pregnancy by dilating and recruiting previously non-perfused vessels, thus maintaining normal pulmonary vascular resistance (PVR)[65]. This compensatory response is absent or decreased in PAH patients and those who develop PAH during pregnancy, leading to increased pulmonary arterial pressure and PVR[65]. This results in significant strain on the RV and is associated with high rates of mortality[65]. As a result, pregnancy should be avoided in women with PAH wherever possible due to high maternal and fetal mortality rates[65]. The risk of decompensation with subsequent RV failure is especially high between 20-24 weeks gestation, and during the third trimester and postpartum period[65].

1.2.3 Animal Models of PAH

Several animal models of PAH are available, and these are generally classified as ‘classical’ or ‘alternative’[29]. Classical models include chronic hypoxia in rodents and a single injection of the toxic pyrrolizidine alkaloid monocrotaline in rats[29]. In contrast to human PAH, these models demonstrate a male bias where the disease phenotype is more severe in male animals and the effects of E2 appear to be protective[66,67]. Furthermore, depletion of endogenous estrogens by ovariectomy induces a more severe PAH phenotype in female animals[66,68]. While these classical models have undoubtedly contributed to a better understanding of PAH, it is generally conceded that these poorly translate to human PAH and that research into the female-prevalence of the disease has been hampered by a lack of appropriate *in vivo* models[58]. Several alternative models (e.g. sugen-hypoxia) have been developed with the aim to more closely mimic human PAH[29,69].

1.2.3.1 Classical Models of PAH

Chronic hypoxia (under both normal atmospheric pressure and hypobaric conditions) can induce PAH in a variety of animal species but is most studied in rodents[70]. While pulmonary arterial pressure and vascular resistance are increased, these animals lack the plexiform lesions and irreversible intimal fibrosis characteristic of human PAH[69]. Although RV remodelling and hypertrophy occur, RV failure and subsequent death are rare[70]. Therefore, this model poorly translates to human PAH. Furthermore, there is significant variability in response to chronic hypoxia according to animal species[70]. For example, male C57BL/6 mice develop less pulmonary vascular remodelling than male Sprague-Dawley rats[70]. There is also variability within species according to strain[70]. For example, BALB/c and FVB/N mice display pulmonary vascular remodelling in response to chronic hypoxia, whereas the C57BL/6 strain shows minimal changes in medial wall thickness[71,72,73]. Therefore, these factors need to be considered during experimental design.

Monocrotaline (MCT) is a toxic pyrrolizidine alkaloid first observed to induce PAH in rats by Kay et al. in 1967[74]. It is hypothesised to mediate endothelial cell injury and accumulation of mononuclear inflammatory cells (particularly macrophages) but its precise mechanism is undetermined[75-79]. MCT is ineffective in mice as they lack the CYP3A enzyme required to metabolise MCT in the liver to its active form dehydromonocrotaline[80]. Attempts to directly introduce dehydromonocrotaline to mice via intraperitoneal injection have resulted in a less severe PAH phenotype than observed in rats[80]. Therefore, the MCT model of PAH is almost exclusively studied in rats[80]. Treatment with MCT results in a more severe PAH phenotype than chronic hypoxia[70]. Severe RV failure develops following a single MCT injection, with a 5-week survival rate of ~35% in male Long-Evans rats[70,81]. However, plexiform lesions are not observed, and MCT-induced PAH appears to be readily reversed by most therapeutic agents including prostanoids and endothelin receptor antagonists (in contrast to human PAH)[70,82,83]. Controversially, Mitani et al. observed that the anorexigen dexfenfluramine (which is well-established to induce PAH in female rodents and in humans) attenuated MCT-induced PAH in female Sprague-Dawley rats[84]. The toxic effects of MCT in the liver, kidney, and heart also have the potential to confound study results[81] Therefore, the MCT model is a poor reflection of human

PAH but may be useful in investigating toxin-induced damage of the pulmonary vasculature and other organs.

The MCT/Pneumonectomy model of PAH was developed with the aim to potentiate the effects of MCT in the pulmonary vasculature by altering haemodynamic conditions[85,86]. As pneumonectomy is well tolerated in both animals and humans (e.g., for removal of lung cancer), altered haemodynamics appear to be insufficient to induce pulmonary vascular remodelling in the absence of endothelial cell injury[87,88]. However when combined with the 'second hit' of MCT, intimal remodelling occurs in the distal pulmonary arteries but plexiform lesions are generally not observed in this model[85,86]. Therefore, this model is also a limited reflection of human PAH.

Aminorex, fenfluramine, and dexfenfluramine are serotonin transporter substrates which were originally marketed as appetite suppressants for weight loss[89,90]. However, aminorex was withdrawn in 1968, and fenfluramine and dexfenfluramine were withdrawn in 1997 due to their association with PAH[89,90]. Fenfluramine is still currently prescribed under specialist supervision as an adjunctive therapy for seizures associated with Dravet syndrome[91]. However, it has stringent monitoring requirements including regular echocardiograms[91]. Dempsie et al. observed that dexfenfluramine only induced PAH in female C57BL/6 mice[92]. This was attenuated by ovariectomy, suggesting that dexfenfluramine-induced PAH is E2-dependent[92]. Female CYP1B1$^{-/-}$ mice also do not develop dexfenfluramine-induced PAH, suggesting that altered estrogen metabolism plays a key role in this model[92]. An increased incidence of PAH has also been observed in users of methamphetamine, which is structurally similar and shares pharmacological properties with dexfenfluramine[93,94]. Labazi et al. recently observed that male and female C57BL/6 mice did not develop PAH in response to methamphetamine, but RV hypertrophy significantly increased in female mice[95].

Pulmonary arterial banding is a classic model of RV hypertrophy independent of changes to the pulmonary vasculature[96]. Labazi et al. recently observed that RV hypertrophy in response to moderate pulmonary trunk banding was more severe in male Wistar rats compared to females[97]. This fits with the decreased RV adaptability and survival observed in male PAH patients compared to females[59].

1.2.3.2 Alternative Models of PAH

Several alternative models of PAH have recently been developed with the aim to translate to human PAH more closely[69]. The sugen-hypoxic (SuHx) model was designed to mimic the formation of obliterative plexiform lesions based on the concept that vascular endothelial growth factor (VEGF) inhibition disrupts maintenance and differentiation of vascular endothelial cells, resulting in hyperproliferation[69]. The vascular endothelial growth factor receptor 2 (VEGFR2) inhibitor Sugen 5416 is known to cause mild pulmonary vascular remodelling[69]. However, when combined with hypoxia it induces severe pulmonary vascular remodelling associated with occlusion, RV remodelling and failure, and death[69]. Plexiform lesions may also form if re-exposure to normoxia is prolonged following SuHx, e.g., for 10-11 weeks in male Sprague-Dawley rats[98]. However, prolonged re-exposure to normoxia is associated with poor survival[98]. Rats are known to exhibit a more severe PAH phenotype in response to SuHx than mice[99,100]. Overall, SuHx is a useful *in vivo* model given its similar phenotype to human PAH.

Transgenic mouse models have been developed to study specific pathways involved in PAH. Only females develop PAH in serotonin-dependent models including $SERT^{+}$ mice overexpressing the human serotonin transporter gene and $S100A4/MTS^{+}$ mice overexpressing the calcium-binding protein S100A4/MTS[101,102,103]. Similarly, only female $Smad1^{+/-}$ heterozygous knockout mice spontaneously develop PAH[104]. Bmpr2-mutant transgenic mouse models include $Bmpr2^{R899X}$ mice (with a knock-in of the human R899X mutation) and $Bmpr2^{delx4+}$ mice (with a T-insertion at base 504 resulting in a premature stop codon)[105,106]. Many of these transgenic mice spontaneously develop mild PAH. For example, female $SERT^{+}$ mice develop PAH at around 5 months old[101]. However, a ‘second hit’ (e.g., hypoxia) is often required to induce a robust PAH phenotype due to their unpredictable pulmonary vascular remodelling and relatively mild haemodynamic alterations[80].

1.2.3.3 Sex Differences in Animal Models of PAH

There are considerable sex differences in animal models of PAH (Table 1.2). In chronic hypoxia- and MCT-induced PAH, male rodents display a more severe disease phenotype than females and the effects of E2 appear to be protective[66,67]. For example, pulmonary vascular remodelling in response to chronic hypoxia was decreased by continuous subcutaneous (s/c) administration of E2 in male Sprague-Dawley rats[107]. Daily s/c injection with E2 also attenuated MCT-induced PAH in male Sprague-Dawley rats[67]. Furthermore, depletion of endogenous E2 by ovariectomy induces a more severe PAH phenotype in both chronic hypoxic and MCT-induced PAH[66,68]. On the other hand, Frump et al. observed that Sprague-Dawley rats develop SuHx-induced PAH without any sex bias[108]. However, continuous s/c administration of E2 attenuated RV hypertrophy in both male and ovariectomised female SuHx rats[108]. A key difference between these studies is the dose of E2 used. A circulating concentration of <1 nmol/L E2 is considered physiologically relevant[101]. Frump et al. used a dose of 75 µg/kg/day E2 by s/c pellet in male chronic hypoxic Sprague-Dawley rats, and in both male and ovariectomised female SuHx Sprague-Dawley rats[107,108]. Although Frump et al. did not measure the plasma concentrations of E2, Resta et al. had previously observed that this dose resulted in physiologically relevant plasma concentrations (45.6 ± 9.0 pg/mL (equivalent to ~0.17 nmol/L)) in chronic hypoxic ovariectomised female Sprague-Dawley rats[66]. On the other hand, Liu et al. administered higher doses of 50 mg/kg/day and 100 mg/kg/day E2 to male Sprague-Dawley rats with MCT-induced PAH[67]. As the plasma levels of E2 were not measured, it is uncertain whether this dose of E2 is physiologically relevant[67]. Only female rodents develop PAH in serotonin-dependent models including oral dexfenfluramine, transgenic mice overexpressing the human serotonin transporter gene ($SERT^+$) and transgenic mice overexpressing the calcium-binding protein S100A4 ($S100A4/MTS^+$)[92,101-103]. E2 is critical to the development of PAH in serotonin-dependent models[101]. For example, ovariectomy attenuated the development of PAH in normoxic and chronic hypoxic female $SERT^+$ mice, and this was re-established by continuous s/c administration of E2 (0.1 mg/21-day pellet)[101]. Karas et al. previously observed that this dose of E2 was physiologically relevant (0.43 ± 0.03 nmol/L in female wild-type $ER\alpha^{+/+}\beta^{+/+}$ mice)[109]. Pulmonary arterial pressure is also elevated in female $BMPR2^{R899X}$ transgenic mice compared to male $BMPR2^{R899X}$ mice, however there is no sex difference in RV hypertrophy[105].

Overall, when designing an *in vivo* study, it is important to consider whether the PAH phenotype observed in the species, strain and sex of the animal model translates to the characteristic of interest in human PAH. For example, the SuHx model is associated with severe pulmonary vascular and RV remodelling, and more closely translates to the human PAH phenotype than other *in vivo* models[69]. On the other hand, BMPR2-mutant transgenic mouse models are valuable for studying hereditary PAH, especially when combined with a 'second hit' (e.g., hypoxia) to induce a more robust disease phenotype[105,106]. The chronic hypoxic model may be more appropriate for studying pulmonary hypertension due to lung disease/hypoxia (WHO Class III, Table 1.1) than PAH (WHO Class I)[69]. Similarly, the MCT model may best translate to toxin-induced PAH rather than idiopathic or hereditary PAH[81].

Table 1.2: Sex Differences in Animal Models of PAH

Animal Model	Species	Male/Female Bias	Effects of E2	References
Chronic hypoxic	Rat/Mouse	Male	Protective	66, 107
Monocrotaline	Rat	Male	Protective	67, 68
Sugen-hypoxic	Rat/Mouse	None	No effect on RVSP but attenuates RV hypertrophy	108
Dexfenfluramine	Rat/Mouse	Only females develop PAH.	Pathogenic	92
$SERT^{+}$	Transgenic Mouse	Only females develop PAH.	Pathogenic	101, 102
$S100A4/MTS^{+}$	Transgenic Mouse	Only females develop PAH.	Pathogenic	103
$Bmpr2^{R899X}$ $Bmpr2^{delx4+}$	Transgenic Mouse	Female	Pathogenic	105, 106
$Smad1^{+/-}$	Transgenic Mouse	Only females develop PAH.	Pathogenic	104

Table 1.2: Sex differences in animal models of PAH.
Male rats/mice develop a more severe pulmonary arterial hypertension (PAH) phenotype in response to chronic hypoxia than females (male bias), and the effects of estradiol (E2) appear to be protective in this model. Only rats develop PAH in response to monocrotaline, with males displaying a more severe disease phenotype. Rats/mice develop PAH in response to Sugen 5416 and chronic hypoxia without any sex bias. Continuous s/c E2 had no effect on right ventricular systolic pressure (RVSP; a measure of pulmonary arterial pressure) but attenuated right ventricular (RV) hypertrophy in Sprague-Dawley rats. Only females develop PAH in serotonin-dependent models including dexfenfluramine, transgenic mice overexpressing the human serotonin transporter ($SERT^{+}$), and transgenic mice overexpressing the calcium-binding protein S100A4 ($S100A4/MTS^{+}$). E2 is critical to development of PAH in serotonin-dependent models. Transgenic mice with bone morphogenetic protein receptor 2 (BMPR2) haploinsufficiency (e.g., $BMPR2^{R899X}$, $BMPR2^{delx4+}$) may spontaneously develop PAH, and disease penetrance is higher in females. Only female $Smad1^{+/-}$ heterozygous transgenic mice develop PAH.

1.3 Sex Hormones and PAH

1.3.1 Estrogen Biosynthesis and Metabolism

The first step in estrogen biosynthesis (Figure 1.4) is derivation of cholesterol to its mitochondrion form pregnenolone by cytochrome P450 11A1 (CYP11A1)[7]. Pregnenolone is then converted to progesterone by 3β-hydroxysteroid dehydrogenase (3β-HSD)[7]. Both pregnenolone and progesterone are converted by cytochrome P450 17A1 (CYP17A1) to form androgens – dehydroepiandrosterone (DHEA) and androstenediol respectively[7]. These are further converted to androstenedione and testosterone by 3β-HSD, before aromatisation to E1 and E2[7]. E1 and E2 are metabolised by various cytochrome P450 enzymes to 2-hydroxy-, 4-hydroxy- and 16α-hydroxyestrogens[7]. The 2- and 4-hydroxyestrogens (collectively known as catechol estrogens) are further metabolised to 2- and 4-methoxyestrogens by catechol-O-methyltransferase (COMT)[7]. Androgens, estrogens, and their respective metabolites are maintained in constant equilibrium by 17β-hydroxysteroid dehydrogenase enzymes (17β-HSD1 and 17β-HSD2)[7]. The CYP450 enzymes mediating estrogen metabolism may vary according to type of tissue. For example, Badawi et al. observed that 16α-hydroxylation was mainly catalysed by cytochrome P450 1A2 (CYP1A2) in human liver microsomes[110]. However, 16α-hydroxylation via cytochrome P450 1B1 (CYP1B1) in lung and adipose tissue may mediate development of PAH[34,35].

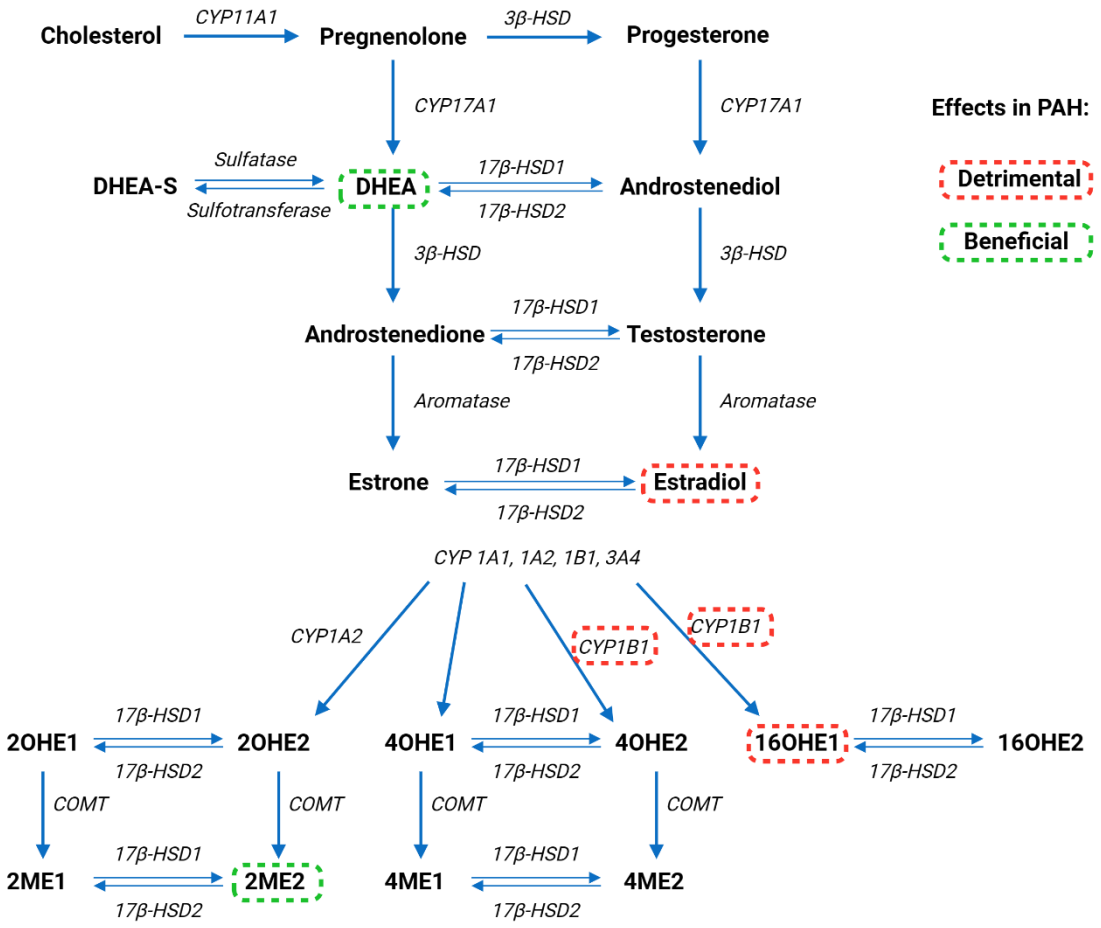

Figure 1.4: Estrogen biosynthesis and metabolism.

Cholesterol is derivatised to its mitochondrion form pregnenolone by cytochrome P450 11A1 (CYP11A1). Pregnenolone is then converted to progesterone by 3β-hydroxysteroid dehydrogenase (3β-HSD). Pregnenolone and progesterone are converted by cytochrome P450 17A1 (CYP17A1) to the androgens dehydroepiandrosterone (DHEA) and androstenediol. DHEA and dehydroepiandrosterone sulfate (DHEA-S) are interconverted by sulfotransferase and sulfatase. DHEA and androstenediol are further converted to androstenedione and testosterone by 3β-HSD, before aromatisation to estrone (E1) and estradiol (E2). E1 and E2 are metabolised by various cytochrome P450 enzymes to 2-hydroxy-,4-hydroxy- and 16α-hydroxyestrogens. The 2- and 4-hydroxyestrogens (catechol estrogens) are further metabolised to 2- and 4-methoxyestrogens by catechol-O-methyltransferase (COMT). Androgens, estrogens, and their respective metabolites are maintained in constant equilibrium by 17β-hydroxysteroid dehydrogenase enzymes (17β-HSD1 and 17β-HSD2). The effects of key metabolites in pulmonary arterial hypertension (PAH) are indicated – detrimental in red and protective in green. Created with BioRender.com.

1.3.2 Estrogen Receptors

Estrogen receptors (ERs) mediate the effects of estrogens and their metabolites on many physiological processes including reproduction, cardiovascular health, and bone integrity[111]. Estrogens primarily act via three receptors: estrogen receptor-alpha (ERα) and estrogen receptor-beta (ERβ) mediate both genomic and non-genomic signalling, whereas G protein-coupled estrogen receptor (GPER) mediates the rapid non-genomic effects of estrogen[102]. In genomic signalling, the nuclear estrogen receptors ERα and ERβ act as ligand-activated transcription factors[112]. Upon E2 binding in the cytoplasm, the receptors undergo a conformational change to form a heterodimer (either ERα/ERα, ERβ/ ERβ, or ERα/ ERβ) then translocate to the nucleus[112]. In direct genomic signalling, the heterodimer directly binds to DNA sequences known as estrogen response elements, leading to activation or suppression of target genes[112]. ERα and ERβ can also mediate indirect genomic signalling through complex interactions with other transcription factors and response elements[112]. Non-genomic signalling can also occur through ERα and ERβ receptors at the cell membrane, for example by interaction with scaffold proteins (e.g., caveolin-1), G proteins, membrane receptors (e.g., tyrosine kinase, insulin growth factor 1) and signalling molecules (e.g., PI3 kinase, Ras)[112]. This leads to activation of intracellular signalling cascades (e.g., MAPK and Akt signalling)[112]. GPER expression is localised to the endoplasmic reticulum and cell membrane[113]. E2 exerts rapid non-genomic effects through GPER by triggering intracellular signalling cascades including the phospholipase C/protein kinase C, Ras/Raf/MAPK, PI3/Akt, and cAMP/protein kinase A pathways[112,113]. Subsequent phosphorylation of transcription factors by these protein kinases leads to changes in gene expression[113].

ER dysfunction has been implicated in several disease pathologies including cancers, osteoporosis, cardiovascular disease, insulin resistance and obesity[29,111]. In the lung, ERα and ERβ are expressed in epithelial cells, pulmonary artery endothelial cells (PAECs), PASMCs, and alveolar macrophages[114,115]. It is unclear whether the estrogen receptors mediate beneficial or harmful effects of E2 in PAH. For example, Frump et al. observed a significant decrease in pulmonary vascular remodelling in response to chronic hypoxia in male wild type and ERα knockout mice treated with continuous s/c E2, but not in ERβ knockout mice[107]. While there

was no difference between the wild type and ERα knockout mice, pulmonary vascular remodelling was significantly increased in ERβ knockout mice compared to wild type mice, suggesting that ERβ may be protective against PAH[107]. On the other hand, ERα expression is markedly increased in human pulmonary artery smooth muscle cells (hPASMCs) from female PAH patients[102]. Furthermore, the ERα antagonist MPP attenuates PAH in normoxic and chronic hypoxic female $SERT^{+}$ mice[102]. MPP also inhibited E2-induced proliferation of female control subject hPASMCs, but the ERβ antagonist PHTPP and GPER antagonist G15 had no effect[102]. Expression of the ERα gene *ESR1* is also upregulated in the lung tissue of PAH patients compared to control subjects[116].

Fulvestrant is an ERα antagonist currently approved for the treatment of metastatic estrogen receptor-positive breast cancer[117]. It blocks dimerization of ERα, decreases ERα expression, and limits nuclear translocation of transcriptional activating factors[117]. During a small proof-of-concept trial, Kawut et al. observed that fulvestrant may improve PAH in postmenopausal women, as measured by an increase in 6-minute walk distance and RV function[117,118]. Therefore, fulvestrant may be worth investigating in further clinical trials. However, fulvestrant is not recommended in premenopausal women as it is non-selective, resulting in the adverse effects of early menopause (e.g., increased risk of osteoporosis)[119]. Tamoxifen is a selective ERα antagonist in breast tissue and partial agonist in other tissues (e.g., endometrium)[120]. Therefore, it is considered a suitable alternative to fulvestrant for premenopausal women with ER-positive breast cancer[120]. Tamoxifen has also been investigated for PAH in preclinical studies and a small Phase 2 clinical trial (results not yet available)[120,121]. However, Chen et al. observed that tamoxifen was less effective than fulvestrant at attenuating PAH in female $Bmpr2^{delx4+}$ mice[120].

GPER is well-established to mediate the protective effects of E2 in the systemic circulation. These include vasorelaxation and reduced oxidative stress, leading to a decrease in blood pressure[122,123,124]. At present, only two studies have focused on the effects of GPER in PAH[125,126]. Alencar et al. observed that activation of GPER with the selective agonist G1 attenuated MCT-induced PAH in male Wistar rats[125]. G1 also attenuated MCT-induced PAH in ovariectomised female Wistar rats[126]. However, these studies are limited to the MCT model which, as previously discussed, poorly translates to human PAH. Therefore, future studies could

investigate the role of G15 in SuHx-induced PAH since this translates more closely to human PAH[69].

Overall, sex differences in ER-mediated signalling may potentially contribute to increased susceptibility but improved survival in female PAH patients compared to males. However, this is also likely to be influenced by many additional factors including age, menopausal status, genetic susceptibilities, body weight, and enivironment[127]. Therefore, it is important to consider that ER-mediated signalling may be stimulus-specific, and development of PAH may require a 'second hit' (e.g., hypoxia, obesity)[127].

1.3.3 Androgens and PAH

Androgens may also be involved in the development of PAH. DHEA is a precursor for both estrogen and testosterone synthesis[7]. It is synthesised by the adrenal cortex in postmenopausal women and men, and in the ovaries and placenta of premenopausal or pregnant women[128,129]. DHEA is converted to dehydroepiandrosterone sulfate (DHEA-S) by sulfotransferase, and DHEA-S can be reversed back to DHEA by steroid sulfatase (Figure 1.4)[128].

At the cellular level, DHEA reduces accumulation of hypoxia-inducible factor 1α (HIF1α) in human PAECs in response to hypoxia[130]. DHEA may also decrease oxidative stress, as it stimulates nitric oxide release in bovine aortic endothelial cells and eNOS activation in human umbilical vein endothelial cells[131]. DHEA is protective in animal models of PAH. For example, SuHx-induced PAH and RV hypertrophy were attenuated in male Sprague-Dawley rats receiving food containing 1% DHEA (for 3 weeks)[132]. Dietary supplementation with 1% DHEA also inhibited MCT-induced PAH in pneumonectomized male Sprague-Dawley rats[133]. Higher circulating levels of E2 and decreased levels of DHEA-S were recently observed in men and postmenopausal women with PAH[30,31]. Lower DHEA-S levels were associated with poor outcomes including worse haemodynamics, increased RV dilatation and dysfunction, and shorter 6-minute walking distance[30,31]. Similarly, Baird et al. observed that DHEA-S levels were lower in premenopausal women with PAH than

in control subjects across the menstrual cycle[32]. DHEA is commonly used as a food supplement to build muscle and resist the effects of aging[134]. It is readily available and short-term use has minimal known side effects[134]. However, the effects of long-term use are not established[134]. In a pilot study, Dumas de La Roque et al. observed that DHEA supplementation improved 6-minute walk distance, pulmonary haemodynamics, and lung function of patients with PH associated with COPD (WHO Class III; Table 1.1)[135]. However, the long-term safety of DHEA requires further investigation before clinical trials in PAH patients, particularly given that it could increase E2 synthesis which may potentially exacerbate pulmonary vascular remodelling[7].

The effects of testosterone in PAH are unclear. For example, testosterone induces dose-dependent dilation of isolated pulmonary arteries from male and female Wistar rats[136]. This was also observed in human pulmonary arteries from lung carcinoma patients[137]. On the other hand, Wen et al. observed that endogenous testosterone depletion by castration attenuated MCT-induced PAH in male Sprague-Dawley rats, and this was re-established by daily s/c injection with dihydrotestosterone (DHT)[138]. Testosterone and DHT act via the androgen receptor, with DHT exerting a higher receptor affinity and stronger androgenic activity[138]. In men without cardiovascular disease, Ventetuolo et al. recently identified two tightly linked single nucleotide polymorphisms (SNPs) in the androgen receptor gene (rs1337080 and rs5918764) associated with an increased RV mass[139]. Therefore, testosterone may modulate RV hypertrophy in male PAH patients, but its effects are unclear.

1.4 Key Pathways in PAH

1.4.1 Bone Morphogenetic Protein Receptor 2 Signalling

Around 80% of hereditary PAH cases are associated with mutations in bone morphogenetic protein receptor 2 (BMPR2)[140]. Unusually, the mutation can occur at any locus along the gene, with over 400 different *BMPR2* mutations reported[140]. While *BMPR2* mutations are inherited as an autosomal dominant trait, penetrance of the PAH disease phenotype is low and predominantly affected by sex (penetrance is around 14% in males and 42% in females)[141]. However, disease penetrance may also be influenced by additional 'hits', for example altered estrogen metabolism and serotonergic drugs (e.g., fenfluramine)[106,142]. As BMPR2 levels are generally reduced in PAH patients regardless of mutation status, this is of interest across all PAH patients[140]. However, hereditary PAH typically presents in younger patients and is generally fatal around 10 years earlier than idiopathic PAH[143]. For example, based on data from the French Network of Pulmonary Hypertension, Sztrymf et al. observed that PAH patients carrying a *BMPR2* mutation were on average diagnosed at 36.5 ± 14.5 years old, whereas non-carriers presented at 46.0 ± 16.1 years old[143].

BMPR2 forms a heterodimer with a BMP Type 1 Receptor (BMPR1A or BMPR1B) upon ligand binding, which then phosphorylates Smads 1,5, and 9 to form a complex with Smad4 and translocate to the nucleus (Figure 1.5)[144]. This upregulates expression of the inhibitor of DNA-binding proteins (Id1, Id2, Id3) which play a key role in cell cycle regulation[145]. The BMPR2 heterodimer also phosphorylates p38 mitogen-activated protein kinases (p38 MAPKs) which translocate to the nucleus[145]. On the other hand, decreased BMPR2 signalling is associated with hyperactivation of the transforming growth factor-beta (TGF-β) pathway[105]. Increased p-Smad2,3 signalling decreases expression of Ids1-3, leading to increased cell proliferation, increased differentiation, and decreased apoptosis[105,146]. The BMPR2 pathway is regulated by the inhibitory Smads - Smad6 competes with Smad4 for complex formation with p-Smad1 and Smad7 blocks TGF-β from accessing the receptor[145].

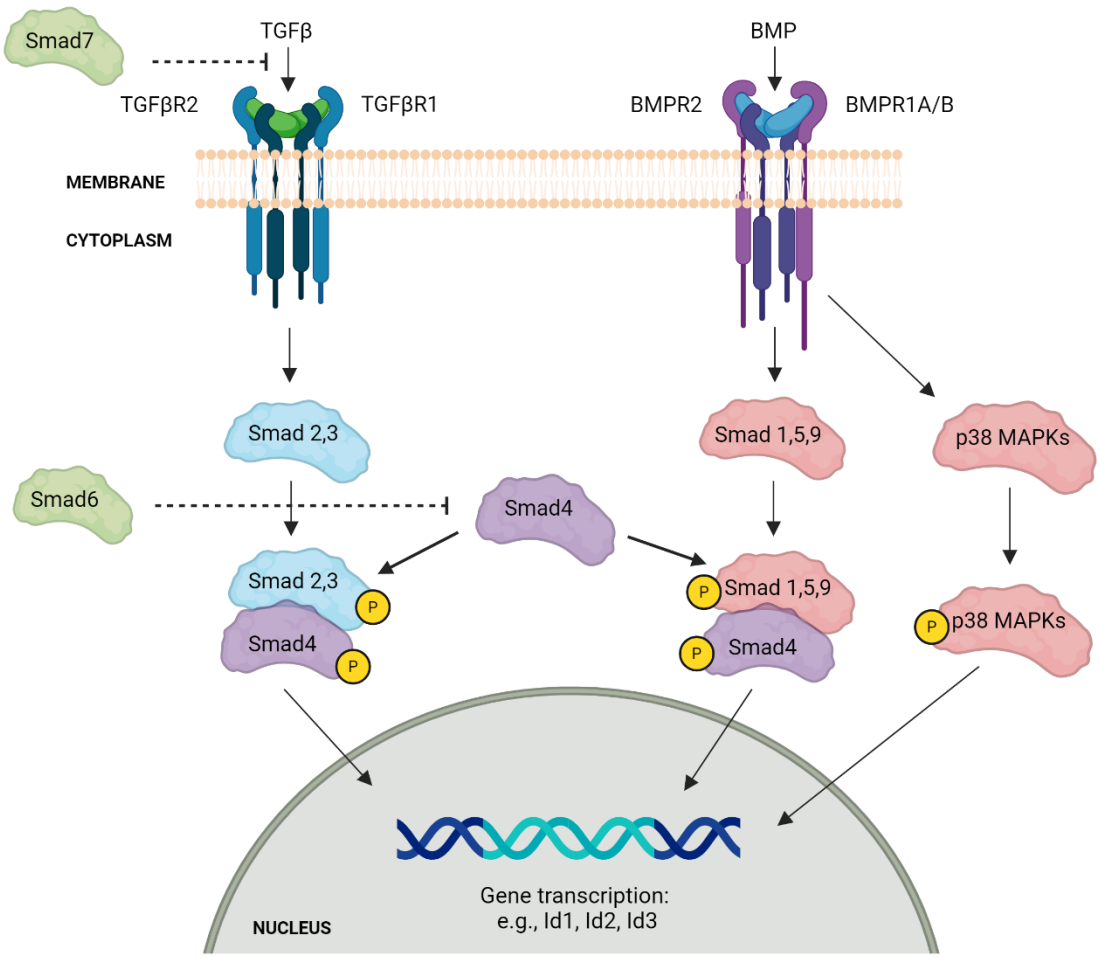

Figure 1.5: The bone morphogenetic protein receptor 2 signalling pathway.
BMPR2 signalling through p-Smad1,5,9 upregulates transcription of the inhibitor of DNA binding genes Id1, Id2 and Id3, which play a key role in cell cycle regulation. TGF-β signalling through p-Smad2,3 suppresses Id1-3 expression, leading to increased cell proliferation and decreased apoptosis. These pathways are regulated by the inhibitory Smads - Smad6 completes with Smad4 for complex formation with p-Smad1 and Smad7 blocks TGF-β from accessing the receptor. BMPR2 = bone morphogenetic protein receptor 2, BMP= bone morphogenetic protein, BMPR1A/B = bone morphogenetic protein receptor 1A or 1B, TGF-β = transforming growth factor-β, TGFβR1 = transforming growth factor-β receptor 1, TGFβR2 = transforming growth factor-β receptor 2, p38 MAPKs = p38 mitogen-activated protein kinases, Id1 = inhibitor of DNA-binding 1, Id2 = inhibitor of DNA-binding 2, Id3 = inhibitor of DNA-binding 3. Created with BioRender.com.

The female predominance of hereditary PAH has led to the hypothesis that E2 may mediate disease penetrance[141]. In the absence of PAH, basal messenger ribonucleic acid (mRNA) and protein expression of BMPR2, Smad1, Id1 and Id3 is lower in female hPASMCs than male hPASMCs[104]. Furthermore, Mair et al. observed that stimulation of male control subject hPASMCs with E2 suppressed Id1 and Id3 expression to a similar level observed in female hPASMCs[104]. This suggests that E2 may suppress BMPR2 signalling[104]. ERα is highly expressed in hPASMCs from female PAH patients[102]. Austin et al. observed that transfection of increasing quantities of ERα in COS-7 cells (which lack endogenous estrogen receptors) strongly correlates with decreasing BMPR2 expression[147]. Basal *Bmpr2* mRNA expression is also significantly lower in female $SERT^+$ mouse lung tissue compared to their wild type littermates, and this was attenuated by continuous s/c dosing with the ERα antagonist MPP[102]. On the other hand, Chen et al. observed that ERβ primarily mediates the increased PAH penetrance observed in female $Bmpr2^{R899X}$ mice compared to male $Bmpr2^{R899x}$ mice, with ERα only partially involved[120]. Ichimori et al. observed that BMPR2 signalling in human PAECs increased in response to E2 under normoxic conditions but decreased under acute hypoxia (1% O_2), and these effects were attenuated by the ERα inhibitor fulvestrant (ICI 182,780)[148]. Therefore, the effects of E2 on BMPR2 signalling may differ according to species, tissue, and stimulus.

Rarely, hereditary PAH can arise from mutations in other genes involved in the BMPR2 pathway including activin receptor-like kinase-1 (*ALK1*), endoglin *(ENG*) and *SMAD9*[140]. Approximately 20% of hereditary PAH families lack a detectable mutation but clearly demonstrate autosomal dominant transmission of the disease[140]. In keeping with *BMPR2*-associated hereditary PAH, penetrance of the disease phenotype in other gene mutations may be influenced by sex and additional 'hits'[140]. As *BMPR2* mutations are germline and presumably present in every cell in the body, this raises the question of whether other organs are affected in addition to the pulmonary vasculature[140]. This is pertinent given that mutations elsewhere in the BMPR2 signalling pathway are associated with systemic effects. For example, PAH occurs in conjunction with haemorrhagic telangiectasis (vascular dysplasia resulting in excessive bleeding and arteriovenous malformations) in patients with *ALK1* and *ENG* mutations[149,150]. PAH is also associated with an abnormally high bone mass in patients with *SMAD9* mutations[151]. *De novo* somatic mutations in the lung may also be involved in the development of PAH[152]. For example, Aldred et al. identified a

somatic mutation in *SMAD9* in the lung of a hereditary PAH patient - an additional insult to *BMPR2* mutation[153].

MicroRNAs (miRs) are small non-coding RNA molecules that negatively regulate gene expression[154]. BMPR2 signalling directly controls processing of a subset of miRs through a noncanonical role of the receptor regulated Smads (particularly Smad9)[155]. miR29 expression is upregulated in the lung tissue of female hereditary PAH patients[156]. It was also two-fold higher in the lung tissue of male BMPR2^{delx4+} mice compared to their wild type littermates[156]. Antagonism of miR29 significantly decreased right ventricular systolic pressure (RVSP), pulmonary vascular resistance, and pulmonary vascular remodelling in male and female BMPR2^{R899X} mice following a high fat diet[156]. However, there are barriers to investigating miR29 antagonists in clinical trials[157]. For example, strategies to deliver miR mimics or inhibitors to the lungs are in early development[157]. In addition, miR29 expression is strongly suppressed in pulmonary fibrosis patients[158]. Therefore, pulmonary fibrosis could potentially be a serious side effect of miR29 antagonists in PAH patients.

1.4.2 Novel Genes Associated with PAH

Genetic variants associated with deficiency of SRY-related HMG-box 17 (*SOX17*) were recently observed in PAH patients[159]. SOX17 is specifically expressed in endothelial cells, and its expression is reduced in the lung endothelium of PAH patients compared to control subjects[159]. Sangam et al. observed that basal SOX17 expression was lower in the lung tissue of female Sprague-Dawley rats compared to males, suggesting that E2 may suppress SOX17[159]. SOX17 may be protective against PAH as it is known to interact with SMAD3, preventing formation of the p-Smad2,3 complex and the downstream effects of TGF-β signalling such as suppression of the Id genes[146,160]. A direct link between bone morphogenetic protein 2 (BMP2) and SOX17 has been identified during cardiogenesis, where BMP2 and SOX17 form a positive feedback loop and trigger induced pluripotent stem cells to become cardiac progenitor cells[161]. However, it is undetermined whether there is any direct link between *SOX17* deficiency and increased disease penetrance in hereditary PAH.

Other novel genes associated with PAH include *KNCK3* (potassium channel, subfamily K, member 3) and *CAV1* (Caveolin-1). Missense mutations in *KCNK3* have been reported in hereditary and idiopathic PAH patients[162]. *KCNK3* encodes TWIK-related acid-sensitive potassium channel-1 (TASK-1))[162]. TASK-1 may decrease pulmonary vascular resistance through complex interplay between ion channels to regulate membrane depolarization (via Ca^{2+})[163]. However, its precise mechanism is undetermined[163]. TASK-1 function may be partially restored by the phospholipase inhibitor ONO-RS-082[162]. However, drug design to specifically target the TASK-1 or other ion channels is challenging[164]. Frameshift mutations associated with loss of *CAV1* function were identified in hereditary PAH patients without a *BMPR2* mutation[165]. However, CAV1 is known to directly interact with BMPR2 and increase bone morphogenetic protein 9 (BMP9)-dependent Smad1,5 phosphorylation and induction of Id1[166]. Daily s/c injection of the elastin inhibitor elafin attenuated SuHx-induced PAH in male Sprague-Dawley rats by promoting interaction of CAV1 and BMPR2 to enhance BMP signalling[167]. Elafin is under investigation for treatment of PAH and recently completed an initial clinical trial to assess its safety in healthy volunteers[168].

1.4.3 Serotonin and PAH

Serotonin plays a complex role in many biological systems including the gastrointestinal, cardiovascular, pulmonary, genitourinary, central and peripheral nervous systems, where it can act as a hormone, neurotransmitter, and mitogen[169,170]. Around 90% of the serotonin in the body is produced by intestinal enterochromaffin cells[170]. It is secreted luminally and basolaterally, leading to serotonin uptake and storage by circulating platelets[170]. In the gastrointestinal tract, serotonin release increases the speed of the digestive process and contributes to satiety while eating[170]. When a blood clot forms, serotonin is re-released from the platelets into the circulation[170]. At lower levels, serotonin facilitates endothelial nitric oxide release, leading to vasodilation[170]. On the other hand, elevated levels of serotonin resulting from excessive release from enterochromaffin cells leads to contraction of vascular smooth muscle cells and vasconstriction[170]. Only 10% of

serotonin is produced by neurons in the central nervous system, where it regulates mood, sleep, appetite, and memory[170]. As serotonin does not cross the blood-brain barrier, the central nervous serotonin system is separate from the rest of the body[171,172]. L-tryptophan is the precursor for serotonin[173]. L-tryptophan is converted to 5-hydroxy-L-tryptophan (5-HTP) by two isoforms of tryptophan hydroxylase (TPH1 and TPH2)[171,172]. 5-HTP decarboxylase then converts 5-HTP to serotonin (also known as 5-hydroxytryptamine (5-HT))[173]. TPH1 is expressed in several tissues including endothelial cells, intestinal mucosa, spleen, pineal gland, and thymus. However, TPH2 is only expressed in neurons[171,172].

The serotonin hypothesis of PAH was first proposed by Hervé et al. in 1995 based on the observation that PAH patients had increased plasma levels and decreased platelet storage of serotonin compared to control subjects[174]. Serotonin mediates several effects in the pathogenesis of PAH (Figure 1.6)[175-178]. For example, endothelial cell-derived serotonin can act on the underlying PAMSCs in a paracrine manner, and this is facilitated by connexin intercellular channels[175,176]. In PASMCs, it can activate serotonin receptors leading to increased oxidative stress and activation of downstream signalling pathways including mitogen-activated protein kinase (MAPK) and Rho-associated protein kinase (ROCK)-induced nuclear translocation of extracellular signal-related kinases 1 and 2 (ERK1, ERK2) leading to increased proliferation[177]. Serotonin also increased the susceptibility of male *Bmpr2*$^{+/-}$ heterozygous mice to chronic hypoxia-induced PAH, and inhibited BMPR2 signalling in the lung tissue of their wild type littermates[178].

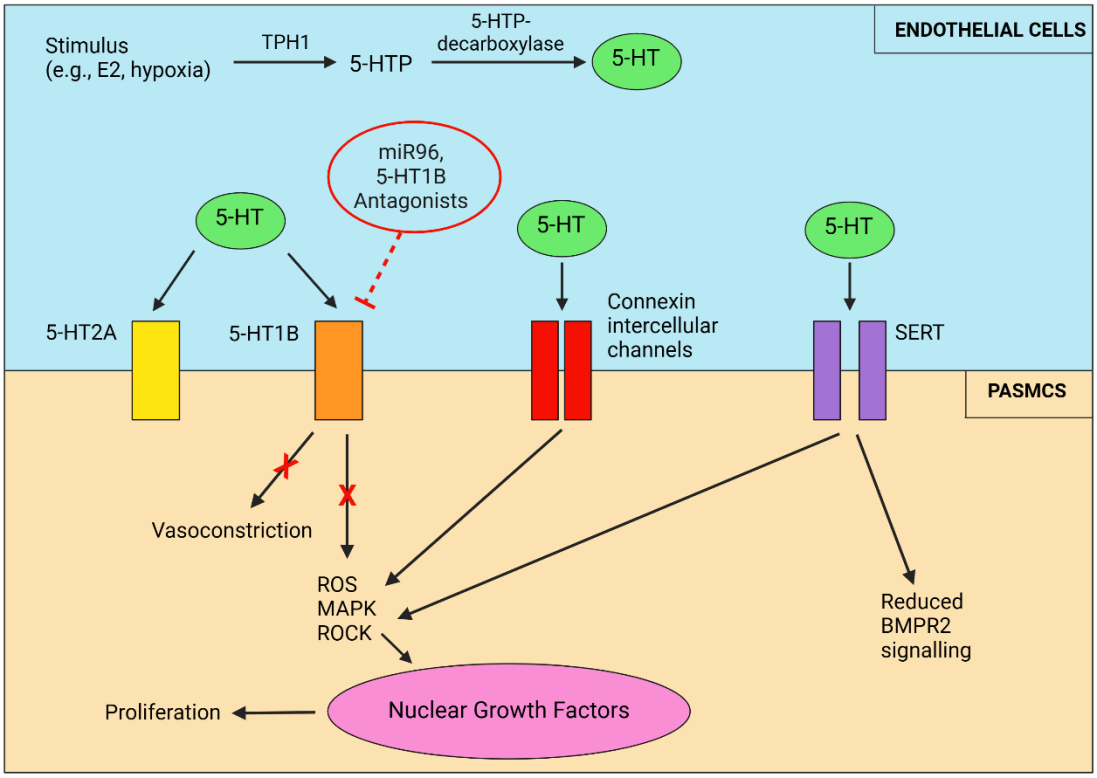

Figure 1.6: The role of the serotonin pathway in PAH.
In response to a stimulus (e.g., hypoxia, estradiol (E2)), L-tryptophan is converted to 5-hydroxy-L-tryptophan (5-HTP) by tryptophan hydroxylase 1 (TPH1) in endothelial cells. 5-HTP is converted to 5-hydroxytryptamine (5-HT), also known as serotonin, by 5-hydroxy-L-tryphophan decarboxylase. 5-HT then binds to one of the serotonin receptors. 5-HT1B mediates pathogenic effects in PAH including vasoconstriction and activation of downstream signalling pathways including reactive oxygen species (ROS), mitogen-activated protein kinase (MAPK) and Rho-associated protein kinase (ROCK). This leads to increased pulmonary artery smooth muscle cell (PASMC) proliferation. These effects are inhibited by miR96 and 5-HT1B antagonists. 5-HT signalling through connexin intercellular channels and the serotonin transporter (SERT) also mediates ROS, MAPK and ROCK signalling. 5-HT signalling through SERT also decreases bone morphogenetic protein receptor 2 (BMPR2) signalling. Created with BioRender.com.

There are many potential therapeutic targets for PAH within the serotonin pathway. Increased TPH1 expression has been observed in PAH patient PAECs compared to those from control subjects[179]. In chronic hypoxic PAH, *Tph1*$^{-/-}$ mice are protected against pulmonary vascular remodelling and increased RVSP but not RV hypertrophy[180]. *Tph1*$^{-/-}$ mice are also protected against dexfenfluramine-induced PAH, suggesting this is dependent on serotonin synthesis[181]. Aiello et al. observed that pharmacological inhibition of TPH1 significantly decreased pulmonary arterial pressure, pulmonary vessel wall thickness and occlusion in male rats with MCT- and SuHx-induced PAH[171]. Imatinib is a tyrosine kinase inhibitor used in several types of cancers (e.g., chronic myeloid leukaemia)[91]. Imatinib also downregulates TPH1 activity in human PAECs and attenuates SuHx-induced PAH in Tph1 wild type mice[182]. While Imatinib was investigated in clinical trials for PAH, these have been terminated due to serious adverse effects (particularly subdural haematomas in patients receiving concomitant anticoagulant therapy)[183,184]. Until recently, design of selective drugs to specifically target the TPH1 isoform has not been possible[185]. However, Petrassi et al. recently identified a novel allosteric inhibitory site on TPH1, enabling development of TPH1-selective drugs[186]. The selective TPH1 inhibitor rodatristat ethyl has been investigated for treatment of PAH in a Phase 2 clinical trial[187]. Selective TPH1 inhibition may also offer therapeutic benefits in obesity and insulin resistance[188].

Involvement of the 5-HT1B receptor in PAH was proposed in 1993 based on the observation that sumatriptan (a selective 5-HT1B/D agonist used for acute migraine) induced pulmonary vasoconstriction[189]. In human pulmonary arteries, 5-HT1B receptors mediate the mitogenic and vasoconstrictive effects of serotonin through multiple mechanisms including inhibition of forskolin-stimulated cAMP accumulation and increased accumulation of [3H]-inositol phosphates through increased G_q-coupled receptor activation[190,191]. In PAH, inhibition of nitric oxide synthesis, removal of the vascular endothelium and small increases in vascular tone synergise such that the effects of 5-HT1B activation are significantly amplified in the pulmonary arteries[191,192]. Serotonin-induced PASMC proliferation via 5-HT1B may occur due to oxidative stress caused by nicotinamide adenine dinucleotide phosphate oxidase 1 (Nox1) activation and subsequent reactive oxygen species (ROS) production[193]. For example, Hood et al. observed that serotonin-induced proliferation in female control subject hPASMCs was further increased in female PAH patient hPASMCs, and these effects were attenuated by pharmacological inhibition of Nox1 and 5-HT1B[193].

Consistent with this, serotonin-induced proliferation was decreased in female Nox1$^{-/-}$ mouse PASMCs compared to PASMCs isolated from their wild type littermates[193]. Serotonin also decreased activity of the transcription factor nuclear factor erythroid 2-related factor 2 (NRF2) in human PASMCs, which mediates activation of antioxidant genes including superoxide dismutase (*SOD1*), catalase (*CAT*), and thioredoxin (*TXN*)[193].

In non-human mammals (e.g., mouse, rabbit, dog), the vasoconstrictive effects of serotonin are predominantly mediated by 5-HT2A[194,195]. Delaney et al. observed that pharmacological inhibition of the 5-HT2A receptor protected neonatal C57BL/6 mice against pulmonary hypertension associated with bronchopulmonary dysplasia (a chronic lung disease associated with premature birth)[195]. However, it is undetermined whether this translates to human PAH. The 5-HT2B receptor is associated with fenfluramine-associated PAH, for example nordexfenfluramine (the main metabolite of dexfenfluramine) is a selective 5-HT2B agonist[196]. However, it is unclear whether 5-HT2B agonism mediates protective or pathogenic effects in PAH[197]. For example, the 5-HT2B agonist BW 723C86 induces vasorelaxation in pig pulmonary arteries[198]. Blanpain et al. also observed a loss of function mutation in the 5-HT2B gene (*HTR2B*) in a 50-year-old human female with fenfluramine-associated PAH[197]. On the other hand, West et al. observed that continuous s/c administration of the 5-HT2B antagonist SB204741 prevented spontaneous development of PAH in male Bmpr2^{R899X} mice[199]. Furthermore, 5-HT2B$^{-/-}$ mice are protected against chronic hypoxia-induced PAH[196]. Therefore, the effects of 5-HT2B in PAH are unclear and may be specific to different species.

The serotonin transporter (SERT) is a monoamine protein which transports serotonin into cells[177]. In PAH patients, serotonin promotes pulmonary vascular remodelling and PASMC proliferation via 5-HT1B and SERT[200-203]. SERT is encoded by a single gene (*SLC6A4*) on chromosome 17 (17q11-17q12)[201]. A polymorphism in the upstream promoter region of *SLC6A4* affects SERT expression and function, with the long allele inducing a higher rate of gene transcription than the short allele[201]. Around 65% of PAH patients are homozygous for the long-allelic variant, but this was only present in 27% of control subjects[201]. Female transgenic mice overexpressing the human serotonin transporter gene (SERT^{+}) spontaneously develop PAH at around 5 months of age[101]. However, this is E2-dependent, as PAH in normoxic and chronic hypoxic female SERT^{+} mice was attenuated by ovariectomy

and reestablished by continuous s/c administration of E2[101]. SERT and 5-HT1B may also act synergistically in serotonin-induced pulmonary vasconstriction[202]. The combined 5-HT1B receptor/SERT antagonist LY393558 was a more potent inhibitor of serotonin-induced pulmonary artery vasoconstriction in normoxic and hypoxic Fawn hooded rats than the 5-HT1B receptor antagonist SB224289 alone[202]. The combined action of SERT and 5-HT1B may also mediate PASMC proliferation via ROCK activation and nuclear translocation of ERK1/ERK2[203.204].

Selective serotonin reuptake inhibitors (SSRIs) are a class of antidepressants which target SERT (e.g., citalopram, escitalopram, fluoxetine)[91,202]. The effects of SSRIs in PAH have been extensively studied. For example, Hood et al. observed that citalopram inhibited serotonin-induced proliferation and ROS production in female PAH patient hPASMCs but not in female control subject hPASMCs[193]. While clinical trials of fluoxetine and escitalopram have been conducted in PAH patients, it is uncertain whether these drugs will be effective as extracellular accumulation of serotonin may potentially worsen pulmonary vascular remodelling by subsequent activation of 5-HT1B receptors[202,205-207]. Sadoughi et al. observed that SSRI use in PAH patients was associated with increased mortality and worse clinical outcomes (e.g, reduced 6-minute walk distance, increased risk of transplantation) compared to PAH patients not taking antidepressants[208]. Fox et al. also reported that use of any type of antidepressant was associated with a 67% increased risk of idiopathic PAH[209]. However, as the rate of idiopathic PAH was similar across all antidepressant classes and there was no dose-response relationship, this is likely to be a non-causal association[209]. Therefore, simultaneous antagonism of 5-HT1B and SERT may be a preferable therapeutic strategy in PAH. However, this has not yet been investigated in clinical trials.

It is well-established that only female rodents develop PAH in serotonin-dependent models including oral dexenfluramine, $SERT^+$ transgenic mice, and $S100A4/MTS^+$ mice, and that this is dependent on E2[92,101-103]. E2 also increases expression of TPH1, 5-HT1B, and SERT in female hPASMCs[101]. Based on the observation that E2 can regulate expression of miRs in cancer, Wallace et al. hypothesised that miRs may contribute to E2-induced PASMC proliferation in PAH[210,211]. miR96 levels are decreased in female PAH patient hPASMCs compared to female control subject hPASMCs, and this is accompanied by an increase in 5-HT1B expression[211]. Transfection of a miR96 precursor into female PAH patient hPASMCs decreased 5-

HT1B expression and inhibited serotonin-induced proliferation[211]. Docherty et al. recently observed that direct delivery of a miR96 mimic to the lungs by weekly intratracheal administration (for 3 weeks) decreased RVSP, pulmonary vascular remodelling, and RV hypertrophy in female Sprague-Dawley rats with SuHx-induced PAH[212]. Therefore, the 5-HT1B/miR96 axis may present a potential therapeutic target for PAH[212]. However, further work is required to optimise miR96 formulation and administration[212].

1.4.4 Obesity and Insulin Resistance in PAH

Obesity is a global public health issue characterised by excess body fat and an increased body mass index (BMI) of 30 kg/m^2 or higher[41]. According to Scottish Pulmonary Vascular Unit and French Pulmonary Hypertension Network data, obesity may be more prevalent in PAH (35.7% patients vs. 29% general population in Scotland; 30% patients vs. 17% general population in France)[42-45]. However, this was not the case in the US (40% PAH patients vs. 42% general population are obese)[46,47]. In the absence of cardiovascular disease, increased BMI is associated with increased pulmonary arterial pressure[213,214]. On the other hand, once cardiovascular disease (e.g., heart failure, coronary heart disease) has developed, morbidity and mortality are generally decreased in obese patients compared to their lean counterparts[215]. However, it is unclear whether this is the case in PAH. An ‘obesity paradox’ has been observed in some PAH cohorts, where obesity is associated with subclinical RV dysfunction but paradoxically may confer a protective effect on RV function once PAH develops[216,217,218]. However, the Scottish Pulmonary Vascular Unit and French Pulmonary Hypertension Network Registry recently reported that no such paradox exists, and that obesity was associated with significantly worse 6-minute walk distance, functional class, and haemodynamic parameters in PAH patients[43,45].

Chronic availability of excess nutrients leads to expansion of adipose tissue by two mechanisms: hypertrophy and hyperplasia[219]. Hypertrophy (increased size of individual adipocytes) is associated with inflammation, dyslipidaemia, and impaired glucose homeostasis[219]. In hyperplasia, new adipocytes are recruited from a

reservoir of progenitor cells[219]. In obesity, decreased hyperplasia and increased adipocyte hypertrophy results in limited capacity of adipose tissue to store fat, leading to pathogenic deposition of excess free fatty acids in non-adipose tissue (e.g., liver, heart)[219]. Adipose tissue is now recognised as an important endocrine organ which releases adipokines (e.g., leptin, adiponectin, apolipoprotein E) to facilitate communication between adipocytes and other tissues[220]. These influence many physiological processes including reproduction, cardiovascular function, immunity, and metabolism[220]. There are many shared pathophysiological mechanisms between obesity and PAH including oxidative stress, inflammation, and an adverse adipokine profile (e.g., elevated pro-inflammatory leptin and low anti-inflammatory adiponectin)[220-226].

Adipose tissue develops in multiple discrete locations (or deposits), generally classified as white or brown adipose tissue (Figure 1.7)[220]. White subcutaneous adipose is predominant in lean, healthy human subjects (~80% of total adipose)[221]. However, many obese individuals accumulate intra-abdominal visceral white adipose tissue (known as 'central obesity')[221]. This is highly metabolically active and continuously releases free fatty acids into the portal circulation, leading to inflammation and a combination of cardiovascular disease risk factors (e.g., insulin resistance) known as the metabolic syndrome[221]. On the other hand, brown adipose tissue (BAT) located in the neck and supraclavicular regions is composed of highly specialised adipocytes that dissipate stored energy in the form of heat through uncoupling protein-1 (UCP-1)[227]. Active BAT is always present in early childhood and plays a critical role in neonatal thermoregulation as newborn babies cannot shiver[227]. However, metabolically active BAT is only present in around 50% of adolescents and is associated with lower BMI, increased insulin sensitivity, and improved metabolic health in adulthood[227,228].

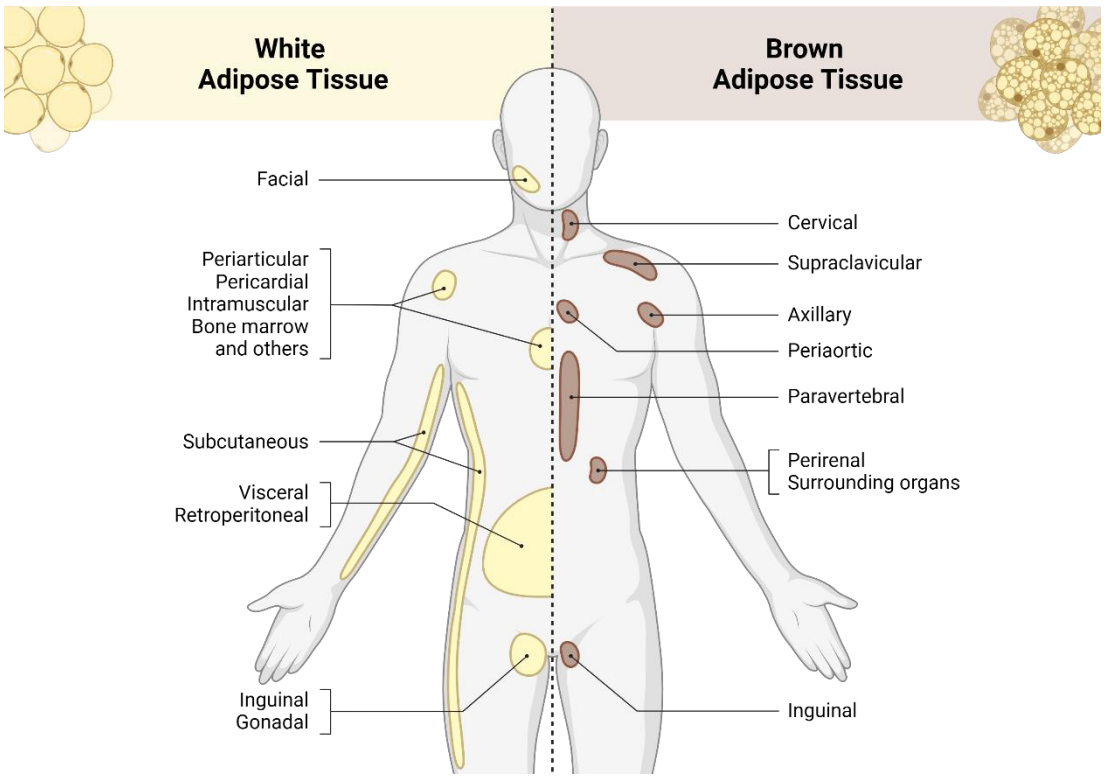

Figure 1.7: White and brown adipose tissue deposits in humans.
There are many different adipose tissue deposits in the human body, which are generally classified as white or brown adipose tissue. Reprinted from "Adipose Tissue Depots", by BioRender.com (2024)[229].

Perivascular adipose tissue (PVAT) plays an important role in vascular physiology[41]. It directly adheres to blood vessels and has a distinct phenotype from other adipose deposits, which varies depending on location[41]. In healthy individuals, PVAT normally has anti-proliferative, anti-inflammatory, and anti-contractile effects on blood vessels[230]. However, adipocyte dysfunction in obesity causes inflammation, oxidative stress and hypoxia resulting in loss of the protective effects of PVAT[231]. Due to its proximity to the pulmonary artery, PVAT is hypothesised to contribute to development of PAH in obesity[231]. For example, increased tumour necrosis factor-α (TNF-α) and endothelin-1 expression have been observed in the PVAT of small arteries isolated from visceral adipose tissue biopsies in obese individuals, resulting in impaired nitric oxide release[231]. In obesity, PVAT expansion within the human lung has not yet been characterised[231]. However, Shields et al. observed areas of localised asymmetric intense lipid staining near the lung vasculature of male Sprague-Dawley rats with SuHx-induced PAH, which suggests the existence of lipid-

laden cells within the lung[232]. Therefore, further studies are required to elucidate the potential role of PVAT in the pathogenesis of PAH.

In the thorax, two main adipose deposits surround the heart: epicardial and pericardial adipose tissue[41]. Thoracic adipose tissue is of particular interest in PAH, as its lymphatics drain directly into the pulmonary circulation where it can exert local and systemic effects[233]. Epicardial adipose is located between the myocardium and visceral layer of the pericardium and covers around 80% of the heart's surface area[234]. In healthy individuals, epicardial adipocytes express high levels of UCP-1 and can therefore actively generate heat, providing the heart with thermal protection in addition to mechanical cushioning[234]. Epicardial adipose tissue also secretes adipokines which mediate cardiac function (e.g., adiponectin)[235]. However, in obesity, increased epicardial adipose tissue deposition and expansion increases the workload on the heart and contributes to cardiac hypertrophy[236].

Extragonadal E2 synthesis in peripheral tissues is a key hypothesis for the estrogen paradox in PAH[33,34]. Although adipose tissue does not synthesise sex steroids *de novo*, it highly expresses the E2-synthesising enzyme aromatase and interconverts stored or circulating sex steroids (Figure 1.8)[41,237]. Increased fat mass in obesity is positively correlated with increased E2 synthesis via aromatase[49,50]. This effect is more pronounced in postmenopausal women as adipose tissue is the primary source of E2 production after menopause[238]. According to the REVEAL registry, the average patient age at PAH diagnosis is 53 years old, suggesting that E2 synthesis in adipose may play an important role in the predisposition of postmenopausal women to PAH[51]. Adipose tissue is also known to mediate estrogen metabolism[239]. CY1P1B1 is one of several CYP450 enzymes which converts E1 and E2 to 16α-hydroxyestrogens[34]. CYP1B1 is highly expressed in visceral adipose tissue (VAT) and is also overexpressed in the pulmonary artery lesions of PAH patients[34,35,239,240]. Genetically obese *ob/ob* mice spontaneously develop PAH, and the disease severity increases following a second hit with chronic hypoxia[34]. Mair et al. recently observed that expression of aromatase and CYP1B1 were upregulated in the peri-renal VAT of male *ob/ob* mice compared to their wild type littermates[34]. Daily intraperitoneal injection of the aromatase inhibitor anastrozole attenuated PAH in both male and female *ob/ob* mice. In keeping with overexpression of CYP1B1 in VAT, urinary levels of 16OHE1 were also elevated in male *ob/ob* mice[34]. Daily intraperitoneal injection of the CYP1B1 inhibitor TMS ((E)-2,3',4,5'-tetramethoxystilbene) attenuated PAH in

male *ob/ob* mice[34]. Mair et al. also incubated cell culture media with VAT isolated from male *ob/ob* mice for 24 hours[34]. 16OHE1 levels were significantly higher in VAT-conditioned media compared to control media, suggesting that 16OHE1 is released into the circulation by VAT[34]. In keeping with this, Denver et al. observed that plasma levels of 16OHE1 are elevated in male idiopathic PAH patients but not in females[241]. It is undetermined whether 16OHE2 is synthesised and released by adipose tissue.

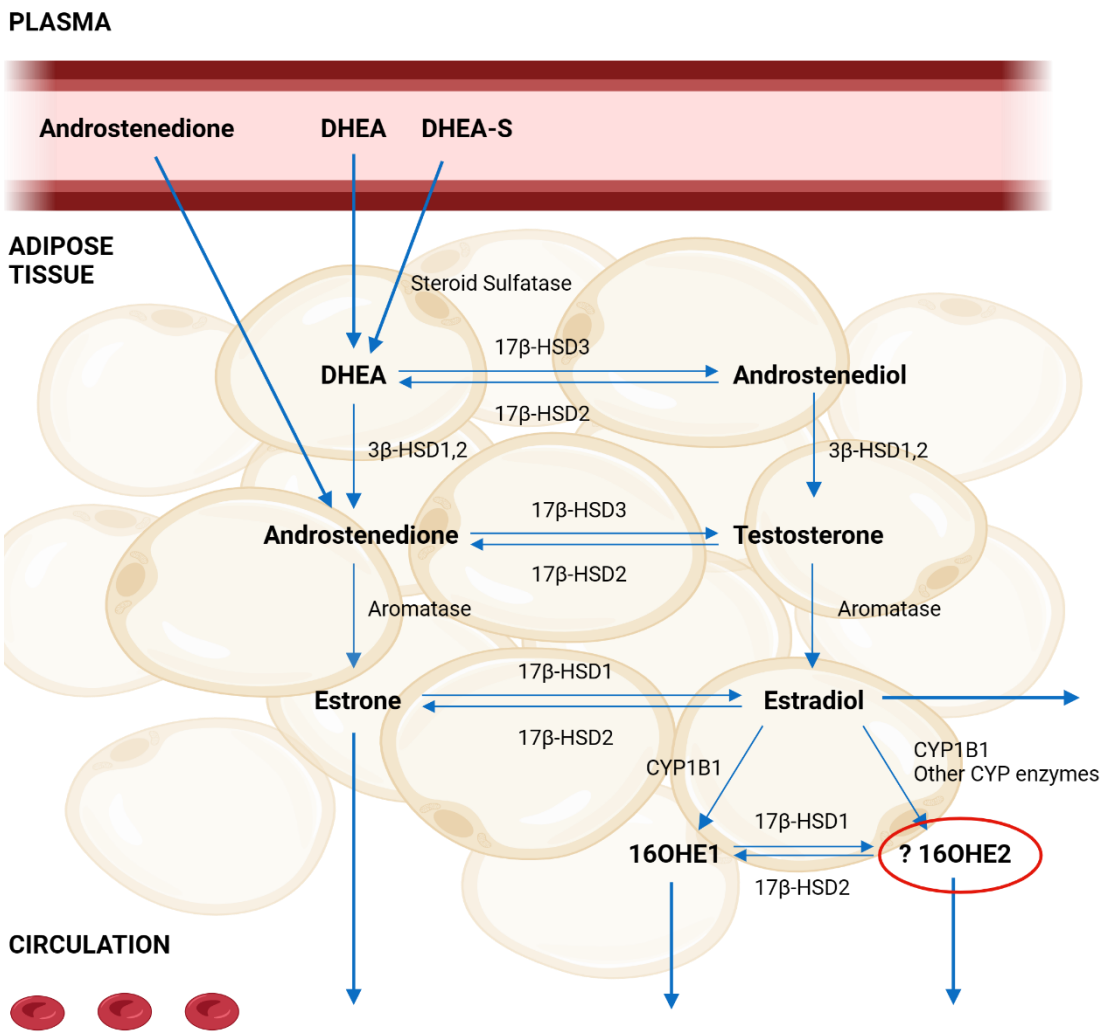

Figure 1.8: Estrogen synthesis and metabolism in adipose tissue from circulating precursors. Localised synthesis, metabolism, and release of estrogens in human adipose tissue from the circulating precursors androstenedione, dehydroepiandrosterone (DHEA), and dehydroepiandrosterone-sulfate (DHEA-S). 17β-HSD1 = 17β-hydroxysteroid dehydrogenase 1, 17β-HSD2 = 17β-hydroxysteroid dehydrogenase 2, 17β-HSD3 = 17β-hydroxysteroid dehydrogenase 3, CYP1B1 = cytochrome P450 1B1, 16OHE1 = 16α-hydroxyestrone, 16OHE2 = 16α-hydroxyestradiol. Created with BioRender.com.

Insulin is a peptide hormone which reduces blood glucose levels by inducing its uptake into insulin-sensitive tissues (e.g., adipose, skeletal muscle, heart) and by inhibiting glucose production in the liver, kidney and small intestine[242]. Binding of insulin to the insulin receptor (a tyrosine kinase receptor) triggers autophosphorylation of tyrosine residues, leading to activation of the insulin receptor substrate (IRS-1)[243]. This activates the PI3K signalling pathway, leading to activation of Akt, which induces translocation of the glucose transporter 4 (GLUT4) to the cell surface and diffusion of circulating glucose down its concentration gradient into cells[243]. In addition, insulin induces cell proliferation (via MAPK pathway induction and subsequent activation of ERK1/2), stimulates synthesis of fatty acids and glycogen, and promotes mitochondrial function[242,243]. Inhibition of the insulin signalling pathway leads to insulin resistance, where sensitive tissues fail to respond to insulin[242]. It is closely linked to obesity and may lead to development of Type 2 diabetes mellitus, often associated with both hyperglycaemia and hyperinsulinaemia[242]. For example, Narayan et al. observed that for a BMI >35 kg/m^2, the lifetime diabetes risk was 70% in men and 74% in women, whereas in those with a healthy BMI (18.5-24.9 kg/m^2) the lifetime risk was 7% in men and 12% in women[244]. A relationship between insulin resistance and PAH was first reported by Zamanian et al. in 2009, with female PAH patients nearly twice as likely to be insulin resistant than control subjects[245]. Pugh et al. subsequently observed that unrecognised glucose intolerance is common in PAH - 56% of patients were insulin resistant and 15% had Type 2 diabetes[246]. However, it is uncertain whether the relationship between obesity, insulin resistance, and PAH represents an association or a direct cause-and-effect relationship[247].

Many of the underlying mechanisms associated with insulin resistance in obesity are also involved in PAH. For example, the transcription factor peroxisome proliferator-activated receptor gamma (PPARγ) increases insulin sensitivity by protecting non-adipose tissues (e.g., liver, skeletal muscle) against lipid overload through stimulating uptake of free fatty acids and lipid storage in adipocytes[248]. Decreased activity of PPARγ in obesity is a key mediator of insulin resistance[249]. Although predominantly expressed in adipose tissue, PPARγ is also expressed in vascular endothelial cells and macrophages[250]. Many of the target genes of PPARγ are implicated in the pathogenesis of PAH, for example endothelin-1 and interleukin-6 are downregulated by PPARγ[251,252]. PPARγ expression is decreased in the lungs of PAH patients compared to control subjects, resulting in dysregulation of the

endothelial cell cycle leading to increased proliferation and resistance to apoptosis[253]. Furthermore, BMPR2 dysfunction in PAH leads to decreased PPARγ activity, resulting in increased PASMC proliferation via the PDGF-β pathway[254]. West et al. observed increased weight gain in male BMPR2^{R899X} mice compared to their wild type controls[249]. 39% of these BMPR2^{R899X} mice were insulin resistant whereas none of the wild type controls were[249]. Adiponectin is an anti-inflammatory adipokine which directly inhibits PDGFR-β ligand binding and decreases MAPK activation leading to reduced PASMC proliferation[254]. Plasma levels of adiponectin are decreased in obesity, insulin resistance and PAH, but increase in response to weight loss and PPARγ activation[255,256]. Decreased adiponectin secretion leads to increased activation of the pro-inflammatory AMPK/mTOR and NF-κβ pathways[257]. Increased circulating levels of pro-inflammatory cytokines (e.g., IL-1β, IL-6) have also been observed in both PAH and obesity[242,258]. Obese individuals also exhibit higher levels of oxidative stress in white adipose tissue, including elevated ROS levels and decreased antioxidant activity[259]. Similarly, Mair et al. observed increased oxidative stress in the lungs of male *ob/ob* mice with obesity-induced PAH[34].

Thiazolidinedione PPARγ agonists (e.g., pioglitazone, rosiglitazone) are widely used for Type 2 diabetes and may potentially have therapeutic benefits in PAH[250]. For example, Legchenko et al. observed that daily oral administration of pioglitazone attenuated SuHx-induced PAH, pulmonary vascular remodelling, and RV failure in male Sprague-Dawley rats[260]. A preliminary clinical trial of pioglitazone has been conducted in PAH patients[261]. However, further studies have been hampered by safety concerns due to their possible association with serious cardiovascular side effects (e.g., myocardial infarction)[262,263].

1.4.5 Fibrosis and PAH

A key characteristic of PAH is remodelling of the extracellular matrix in pulmonary arteries[264]. In PAH patients, collagen deposition and cross-linkage (converting soluble collagen to insoluble collagen) is increased in the perivascular and intravascular compartments of pulmonary arteries, leading to stiffening and reduced compliance[264]. Collagen deposition is highest in the intima, followed by the media and adventitia[265]. Fibril-forming collagens (e.g., COL1A1, COL3A1) assemble to build a microfibril and, when stabilised by cross-linking, provide structure and strength for the vessel wall[265]. Collagen deposition also plays a key role in RV dysfunction in PAH[266]. RV hypertrophy may be classed as 'adaptive' or 'maladaptive'[266]. In adaptive RV hypertrophy, cardiac fibroblasts remain concentric with retained function[266]. However, maladaptive RV hypertrophy is characterised by transition of cardiac fibroblasts into myofibroblasts leading to excess collagen formation, disruption of cross-linking and collagen turnover, loss of extracellular matrix integrity, RV diastolic stiffness, and disruption of co-ordination and contraction[266]. Increased breakdown of elastin in the pulmonary arteries of PAH patients (fragmenting the internal elastic lamina) leads to excess smooth muscle cell prolfieration[264,267]. The extracellular matrix glycoproteins fibronectin and tenascin also accumulate in the pulmonary arteries of PAH patients leading to increased development of fibrous tissue (fibrosis), smooth muscle cell proliferation, and pulmonary vascular remodelling[264,268]. Increased vascular calcification (differentiation of vascular smooth muscle cells into osteoblast-like cells) is also observed in the pulmonary arteries of PAH patients[269].

Female sex is associated with adaptive RV hypertrophy in PAH, suggesting that E2 may be protective against maladaptive RV remodelling[59]. In keeping with this, Liu et al. observed that daily s/c injection with E2 decreased collagen deposition and fibrosis in the RV of male Sprague-Dawley rats with MCT-induced PAH[67]. Petrov et al. observed that E2 significantly increased *Col1a1* and *Col3a1* mRNA expression in cardiac fibroblasts isolated from male Wistar rats[270]. However, in cardiac fibroblasts isolated from female Wistar rats, E2 significantly decreased *Col1a1* and *Col3a1* expression[270]. Erewele et al. also observed that collagen deposition was increased in the lungs of male and female BMPR2^{R899X} transgenic mice compared to their wild type littermates[105].

1.5 Estrogen Metabolism and PAH

There is increasing evidence that metabolic dysfunction is a key driver of PAH[271]. A shift from oxidative phosphorylation to glycolysis (known as the 'Warburg effect') is frequently observed in tumours but has also recently been observed in the pulmonary arteries and RV of PAH patients[271]. This is associated with hyperproliferation of PASMCs and endothelial dysfunction leading to pulmonary vascular remodelling[271]. Furthermore, BMPR2 may be protective against the Warburg effect. For example, following re-exposure to normoxic conditions, mitochondrial function was preserved in wild type mice with chronic hypoxia-induced PAH but not in EC-BMPR2$^{-/-}$ mice (with endothelial-cell specific BMPR2 knockout)[272]. Therefore, the Warburg effect may present a potential therapeutic target for both cancer and PAH[272,273]. Several other metabolic processes are also altered in PAH patients including the tricyclic acid cycle and fatty acid oxidation[271]. Therefore, the emerging field of metabolomics has significant potential to identify novel mechanisms of PAH.

Altered estrogen metabolism is a key hypothesis for the estrogen paradox in PAH[274]. Estrogen metabolites are known to be active in several diseases including breast cancer, endometriosis, and systemic lupus erythematosus[275,276,277]. The CYP450 system is highly active in the lung, with CYP1A1, CYP1A2, CYP1B1 and other CYP450s oxidising E1 and E2 at the C2, C4 or C16 positions to produce 2-,4- or 16α-hydroxyestrogens[7]. The catechol 2-hydroxy- and 4-hydroxyestrogens are further metabolised to 2- and 4-methyoxyestrogens by COMT (Figure 1.4)[7].

1.5.1 Aromatase

Aromatase (*CYP19A1*) is the rate-limiting enzyme which catalyses estrogen synthesis through aromatisation of androstenedione and testosterone[274]. It is locally expressed in the smooth muscle (medial) layer of human and rodent pulmonary arteries[33]. Aromatase expression in postmenopausal female control subject hPASMCs is significantly higher than in male control subject hPASMCs[33]. However,

no difference was observed between female PAH patient hPASMCs and female control subject hPASMCs[33]. On the other hand, aromatase expression is significantly increased in the pulmonary arteries of male and female chronic hypoxic C57BL/6 mice and SuHx Wistar Kyoto rats compared to their normoxic controls[33]. Overexpression of *CYP19A1* associated with the rs7175922 polymorphism may be associated with an increased risk of portopulmonary hypertension[278].

Aromatase inhibitors (e.g., anastrozole, letrozole) are widely used for ER-positive breast cancer[91]. Mair et al. observed that daily s/c injection or oral dosing with anastrozole attenuated PAH in female chronic hypoxic C57BL/6 mice and female SuHx Wistar Kyoto rats[33]. However, no response was observed in males[33]. Anastrozole also increased *Bmpr2* mRNA expression in the lung tissue of female normoxic C57BL/6 mice, female chronic hypoxic C57BL/6 mice and female SuHx rats[33]. However, no change in *Bmpr2* was observed in males[33]. On the other hand, circulating E2 levels are higher in both men and postmenopausal women with PAH compared to control subjects[30,31]. Therefore, aromatase inhibitors may potentially benefit PAH patients of both sexes. Anastrozole has been studied in small cohorts of PAH patients in Phase 2 clinical trials[279,280,281]. Kawut et al. observed that anastrozole significantly reduced plasma E2 levels, improved 6-minute walk distance, and was well tolerated in men and postmenopausal women with PAH[279]. Therefore, further clinical trials of anastrozole in PAH patients may be warranted[279].

Metformin is a well-established treatment for Type 2 Diabetes Mellitus[282]. Dean et al. recently observed that daily oral metformin attenuated SuHx-induced PAH in female Wistar Kyoto rats via inhibition of aromatase[283]. Given that insulin resistance is a common comorbidity with PAH, metformin is currently in clinical trials to investigate whether it can be repurposed as a novel therapy for PAH[245,246,284]. This also leads to the question of whether the recommended lifestyle interventions for obesity and insulin resistance (e.g., diet, weight loss) could improve the symptoms of PAH[285].

1.5.2 Cytochrome P450 Enzymes and PAH

CYP1B1 predominantly metabolises E1 and E2 to 4-hydroxyestrogens, but also plays a role in formation of 16α-hydroxyestrogens[110]. Although CYP1B1 can also mediate formation of the 2-hydroxyestrogens, these are predominantly formed by CYP1A2 and (to a lesser extent) CYP1A1[110]. Altered estrogen metabolism through CYP1B1 may play a key role in hereditary PAH[286]. For example, Austin et. al observed that female *BMPR2* mutation carriers homozygous for the N/N genotype of *CYP1B1 N453S* have a four-fold greater incidence of hereditary PAH[286]. CYP1B1 expression is also decreased in lymphocytes from hereditary PAH patients compared to unaffected BMPR2 mutation carriers and control subjects[287].

CYP1B1 is expressed within all cell types in the pulmonary vascular wall including smooth muscle and endothelial cells[35]. CYP1B1 expression is upregulated in the pulmonary arteries of idiopathic and hereditary PAH patients[35]. It is also overexpressed in the pulmonary arteries of male and female C57BL/6 mice with chronic hypoxia- and SuHx-induced PAH[35]. In both sexes, White et al. observed that chronic hypoxia-induced PAH was attenuated in CYP1B1$^{-/-}$ mice, and that the CYP1B1 antagonist TMS attenuated both chronic hypoxic- and SuHx PAH in C57BL/6 mice[35]. TMS also attenuated E2-induced proliferation in female hPASMCs, and this inhibitory effect was 100-fold more potent in hPASMCs isolated from PAH patients compared to control subjects[35]. On the other hand, Johansen et al. observed that TMS did not reverse PAH in MCT-treated male and female Wistar rats, but prolonged survival[240]. CYP1B1 may also mediate serotonin-dependent PAH. For example, female CYP1B1$^{-/-}$ mice are not susceptible to dexfenfluramine-induced PAH, and daily intraperitoneal injection of TMS attenuates PAH in female SERT^{+} mice[92,240]. Mair et al. recently observed that daily intraperitoneal injection of TMS also attenuates PAH and pulmonary vascular remodelling in male genetically obese *ob/ob* mice[34]. Cell culture media incubated for 24 hours with peri-renal VAT harvested from male *ob/ob* mice contained significantly higher levels of 16OHE1 than control media[34]. Intriguingly, 24 hours stimulation with VAT-conditioned media significantly increased proliferation of PASMCs isolated from male *ob/ob* mice[34]. This was attenuated by both anastrozole and TMS[34]. Therefore, antagonism of CYP1B1 may present a novel therapeutic strategy for PAH.

The aryl hydrocarbon receptor (AhR) is a heterodimeric transcription factor which induces aromatase, CYP1A1, CYP1A2, and CYP1B1[288]. It is highly expressed in the lung, and is also known to influence tumorigenesis, energy metabolism, lipid metabolism and obesity[289,290,291]. The AhR may also play a key role in PAH. AhR expression is significantly higher in hPASMCs from female PAH patients compared to control subjects[292]. Sugen 5416 is a known AhR agonist[292]. Dean et al. recently demonstrated that the AhR plays a key role in SuHx PAH[292]. Activation of the AhR in female SuHx Wistar rats leads to increased expression of CYP1A1 and aromatase in the lungs, resulting in increased E2 synthesis and metabolism[292]. Sugen 5416 increases proliferation of blood outgrowth endothelial cells from female PAH patients, but only causes proliferation of PASMCs when grown in hypoxic conditions[292]. Under hypoxia, HIF1α translocates from the cytoplasm to the nucleus[293]. There is a close link between E2 metabolism and hypoxia as the aryl hydrocarbon receptor nuclear translocator (ARNT), also known as hypoxia-inducible factor 1β (HIF-1β), is shared between the AhR and HIF1α (Figure 1.9)[292,293]. The AhR antagonist CH223191 attenuated SuHx-induced PAH and CYP1A1 overexpression in female Wistar Kyoto rats[292]. Therefore, AhR antagonism may be another potential therapeutic target in PAH.

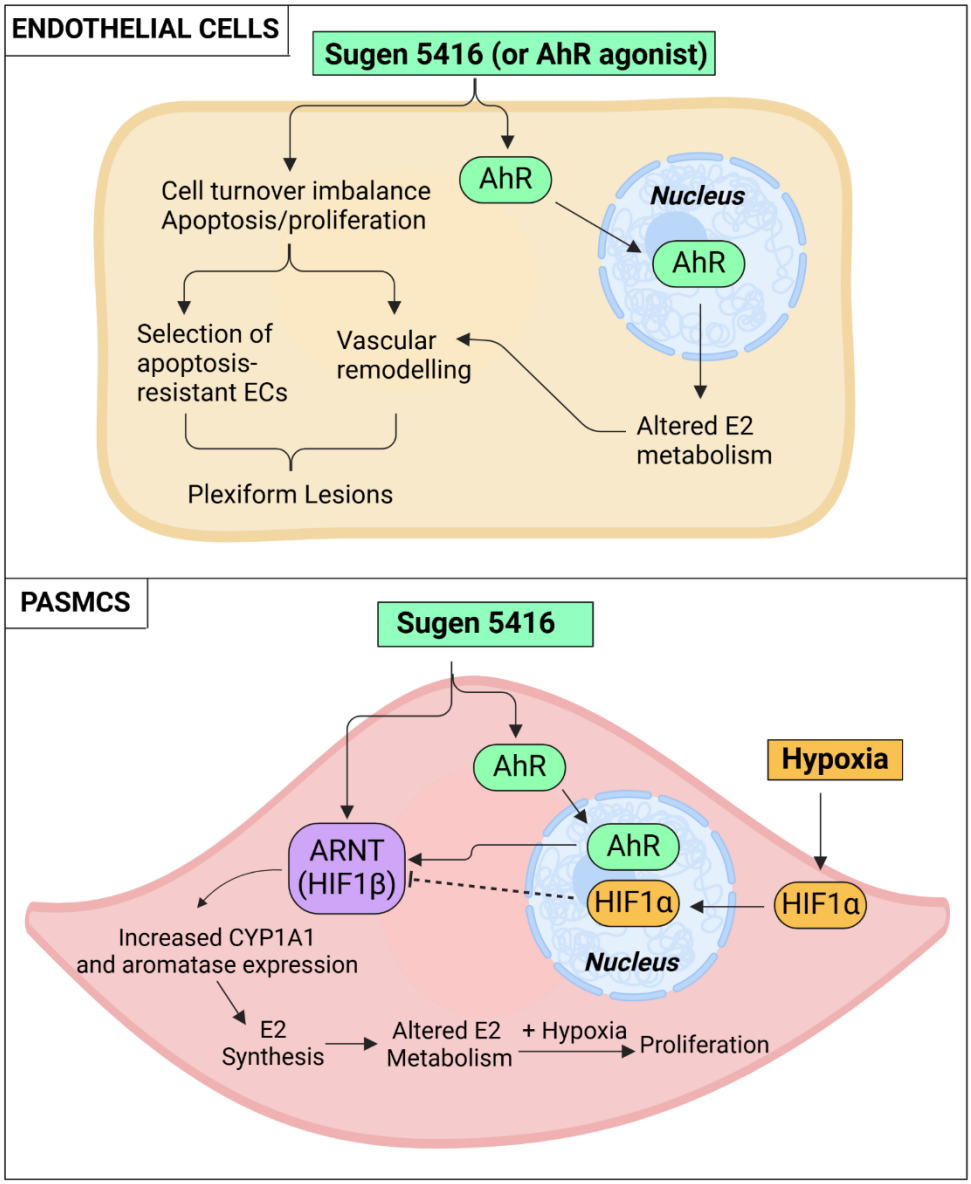

Figure 1.9: The interaction of Sugen 5416, hypoxia, and the aryl hydrocarbon receptor. In endothelial cells, Sugen 5416 activates the aryl hydrocarbon receptor (AhR), leading to nuclear translocation and subsequent alterations in estradiol (E2) metabolism. This results in selection of apoptosis-resistant endothelial cells (ECs) and increased proliferation, leading to pulmonary vascular remodelling and formation of occlusive plexiform lesions. In pulmonary artery smooth muscle cells (PASMCs), Sugen 5416 activates the AhR leading to nuclear translocation. Under hypoxic conditions, hypoxia-inducible factor 1α (HIF1α) translocates from the cytoplasm to the nucleus. The aryl hydrocarbon receptor nuclear translocator (ARNT), also known as hypoxia-inducible factor 1β (HIF1β), is shared by both the AhR and HIF1α. Activation of ARNT by the AhR leads to increased expression of cytochrome P450 1A1 (CYP1A1) and aromatase, resulting in increased E2 synthesis and altered E2 metabolism. When combined with hypoxia, Sugen 5416 induces proliferation of pulmonary artery smooth muscle cells. Created with BioRender.com.

1.5.3 The 2-Hydroxylation Pathway

The 2-hydroxylation pathway accounts for around 50% of E2 metabolism, and its metabolites have no relative estrogenic activity[286]. The 2-hydroxyestrogens are converted to 2-methoxyestrogens by COMT[286]. It is well-established that 2-methyoxyestradiol (2ME2) mediates protective effects in both PAH and cancer[274,294,295]. For example, 2ME2 improves the sensitivity of oesophageal squamous cell carcinomas to radiotherapy[294]. Tofovic et al. observed that continuous s/c administration of 2-hydroxyestradiol (2OHE2) or 2ME2 attenuates development and progression of MCT-induced PAH in male Sprague-Dawley rats[295]. However, the precise mechanism is unclear.

Hypoxia-inducible factors are crucial for adaptation to decreased oxygen availability[296]. Under normoxic conditions, HIF1α is hydroxylated through prolyl hydroxylases (PHDs) then tagged for proteasomal degradation through the E3 ubiquitin-ligase system by Von Hippel-Lindau tumour suppressor protein[293]. In response to hypoxia, the PHDs are inhibited and HIF1α stabilises within the cell, translocates to the nucleus, and interacts with HIF1β (ARNT) and the hypoxic response element to mediate gene transcription[293]. Prolonged HIF1α activation may contribute to pulmonary vascular remodelling in PAH. For example, hypoxia-induced proliferation of human PASMCs is inhibited by knockdown of HIF1α[297]. Chronic hypoxia-induced PAH and pulmonary vascular remodelling is also attenuated in transgenic mice with a smooth muscle cell-specific deletion of HIF1α[298]. Docherty et al. recently observed that basal HIF1α protein expression was higher in female control hPASMCs compared to males, which may potentially contribute to the female predominance of PAH[299] Continuous s/c administration of 2ME2 attenuates chronic hypoxia-induced PAH in male and female Sprague-Dawley rats[299]. HIF1α protein expression significantly increased in the lungs of female rats in response to chronic hypoxia, and this was attenuated by 2ME2[299]. 2ME2 also significantly decreased proliferation in female control human PASMCs, and this was not mediated by ERα, ERβ or GPER[299].

Microtubules are structural components of the cytoskeleton required for cell motility[300]. These regulate a variety of signalling pathways including HIF1α, inducible nitric oxide synthase, and nuclear factor-κβ (NF-κβ)[299,300]. 2ME2 disrupts the cytoskeletal α-tubulin network in both female rPASMCs and female control subject hPASMCs, leading to downregulation of HIF-1α[299]. Intriguingly, serotonin also plays a role in HIF1α expression, as the 5-HT2B receptor activates NF-κβ which regulates HIF1α[301]. Therefore, the therapeutic effects of 2ME2 in PAH may result from inhibition of HIF1α and microtubular disruption in PASMCs.

The specific effects of COMT have not been studied in PAH, however it is reasonable to hypothesise this is protective as it mediates formation of 2ME2[274]. It is well-established that COMT mediates protective effects against both benign and metastatic tumours[302,303]. For example, a leiomyoma is a benign smooth muscle cell tumour often found in the uterus (also known as a uterine fibroid)[302]. COMT overexpression stabilises microtubules, decreases aromatase expression, attenuates E2-induced proliferation, and decreases signalling via ERα in human uterine leiomyoma cells[302]. Intriguingly, women have lower hepatic COMT activity than men[304]. Furthermore, Jiang et al. observed that E2 decreased COMT expression in MCF-7 breast cancer cells, and this was attenuated by the ERα inhibitor fulvestrant (ICI 182780)[303]. Therefore, future studies could investigate whether decreased basal COMT expression in the lung may contribute to the female predominance of PAH.

Overall, 2ME2 has significant therapeutic potential for PAH. It may also be useful as an adjuvant therapy to current treatments as it modifies endothelin synthesis, prostacyclin synthesis, and nitric oxide release[305]. For example, Tofovic et al. investigated the effects of combining 2ME2 with the endothelin receptor antagonist bosentan or the PDE-5 inhibitor sildenafil in male Sprague-Dawley rats with MCT-induced PAH[305]. Combination therapy with 2ME2 improved survival and decreased pulmonary vascular remodelling compared to bosentan or sildenafil alone[305]. While 2ME2 has been investigated in clinical trials for advanced solid tumours, it has not yet been studied in PAH patients[306,307]. 2-ethoxyestradiol (2EE) is a more potent synthetic analogue of 2ME2, therefore may provide more efficient dosing in clinical trials[308]. Tofovic et al. observed that 2EE is anti-mitogenic in human PASMCs, PAECs, and lung fibroblasts[308]. 2EE also attenuated MCT-induced PAH and pulmonary vascular remodelling in male Sprague-Dawley rats[308].

1.5.4 The 4-Hydroxylation Pathway

The 4-hydroxylation pathway accounts for around 5% of E2 metabolism and is predominantly mediated by CYP1B1[274]. The 4-hydroxyestrogens are converted to 4-methoxyestrogens by COMT[274]. In the field of oncology, 4-hydroxyestradiol (4OHE2) is known to produce ROS leading to genotoxic effects and carcinogenesis, for example in ER-positive breast cancer[309]. In PAH, the effects of 4OHE2 appear to have marked sex differences[104]. Mair et al. observed that 4OHE2 significantly decreased proliferation of male control subject hPASMCs and, in keeping with this, increased expression of p-Smad1,5,8, Id1, and Id3[104]. On the other hand, 4OHE2 did not affect proliferation of female control hPASMCs and decreased expression of p-Smad1,5,8, Id1, and Id3[104]. This suggests that 4OHE2 may mediate protective effects against PAH in males but pathogenic effects in females[104]. However, further studies are required to investigate the underlying mechanisms of this sex difference, the effects of 4OHE2 *in vivo*, and whether 4OHE2 may contribute to oxidative stress in PAH.

1.5.5 16α-Hydroxyestrone

16α-hydroxyestrone (16OHE1) is produced by oxidation of E1 at C16 by CYP1A1, CYP1A2, CYP1B1 and CYP3A4[110]. CYP1A1 and CYP1B1 mainly mediate extrahepatic synthesis of 16OHE1, whereas CYP1A2 and CYP3A4 are predominant in the liver[110]. 17β-HSD2 also mediates formation of 16OHE1 by further oxidation of 16OHE2[274]. 16OHE1 forms strong covalent bonds with estrogen receptors, leading to prolonged receptor activation[310]. Therefore, it has a much higher estrogenic activity than the 2- and 4-hydroxyestrogen metabolites and 16OHE2[274,310].

16OHE1 predominantly mediates pathogenic effects in PAH. White et al. observed that daily intraperitoneal injection of 16OHE1 induced PAH in female C57BL/6 mice in the absence of any additional precipitating factors[35]. 16OHE1 induces proliferation of female control subject hPASMCs, and this is further increased in female PAH patient hPASMCs[35,311]. Hood et al. demonstrated that 16OHE1-induced proliferation

is redox-sensitive, primarily acting through Nox1[311]. 16OHE1 induced a rapid, but transient, increase in ROS generation in female control subject hPASMCs, whereas in female PAH patient hPASMCs these effects were sustained[311]. This was mediated via ERα[311]. Female Nox1$^{-/-}$ mice were protected against chronic hypoxic PAH and pulmonary vascular remodelling[311]. 16OHE1 had no significant effect on NRF2 activity in female control hPASMCs, but significantly decreased NRF2 activity in female PAH patient hPASMCs[311]. This effect appears to be dependent on estrogen metabolism to 16OHE1 by CYP1B1, as TMS restored NRF2 activity in female PAH patient hPASMCs[311]. 16OHE1 also decreased expression of the antioxidants SOD1 in female control subject hPASMCs and catalase in female PAH patient hPASMCs[311]. Therefore, 16OHE1 may be a key mediator of oxidative stress in PAH. The NRF2 activator bardoxolone methyl has been investigated in Phase 2 and 3 clinical trials for PAH[312].

16OHE1 may also mediate disease penetrance in hereditary PAH. For example, Austin et al. observed that the urinary 2-hydroxyestrogen/16OHE1 ratio was 2.3-fold lower in hereditary PAH patients compared to unaffected *BMPR2* mutation carriers[286]. Fessel et al. also observed that the urinary 16OHE1/2ME2 ratio was elevated in male hereditary PAH patients compared to healthy control subjects[106]. However, this raises the question of whether this is due to correlation between estrogen metabolite levels, or if PAH is caused by high 16OHE1 or low 2-hydroxyestrogen/2ME2 levels.

Bmpr2-mutant mice spontaneously develop PAH but, in keeping with human hereditary PAH, disease penetrance is low[313]. For example, around 50% of Bmpr2^{R899X} mice spontaneously develop PAH after 6 weeks of transgene activation[313]. Fessel et al. observed that continuous s/c administration of 16OHE1 significantly increased the penetrance of PAH in male Bmpr2^{R899X} and Bmpr2^{delx4+} mice[106]. 16OHE1 also suppressed BMPR2 signalling in the lung tissue of their wild type littermates[106]. However, 2ME2 had no significant protective effect against PAH in male Bmpr2^{R899X} mice[106]. Following this, Chen et al. observed that 16OHE1 exacerbates PAH in *Bmpr2*-mutant mice via upregulation of miR29[156]. Weekly injections of anti-miR29 for 6 weeks attenuated PAH and pulmonary vascular remodelling in male and female BMPR2^{R899X} mice in the presence or absence of 16OHE1[156]. 16OHE1 may also promote insulin resistance in PAH[156]. Chen et al. observed that 16OHE1 significantly decreased PPARγ expression in the lungs of

wild type and *Bmpr2*-mutant mice[156]. This was reversed by miR29 antagonism[156]. In keeping with this, 16OHE1 also decreased mobilisation of GLUT4 in response to insulin in pulmonary microvascular endothelial cells isolated from male Bmpr2^{delx4} mice[156]. Therefore, miR29 antagonism presents a potential therapeutic target against the pathogenic effects of 16OHE1 in PAH.

Finally, Sangam et al. recently observed that 16OHE1 suppresses protective *SOX17* expression in human PAECs[159]. 16OHE1 also suppressed *SOX17* promoter activity in hPASMCs via ERα[159]. Intriguingly, *Tie2-Sox17* transgenic mice overexpressing *Sox17* are protected against 16OHE1-induced PAH and RV hypertrophy[159]. Therefore, *SOX17* may be a key link between altered estrogen metabolism and PAH.

1.5.6 16α-Hydroxyestradiol

16OHE2**,** also known as estriol, is predominant during pregnancy[29]. It is synthesised from 16α-hydroxydehydroepiandrosterone (16-OH-DHEA) in the fetal liver then released into the maternal circulation via the placenta as unconjugated 16OHE2[314]. There, it rapidly undergoes extensive conjugation by enzymes such as β-glucuronidase and is excreted in the urine as 16OHE2-glucuronide (Figure 1.10)[315,316]. During pregnancy, around 80-90 percent of 16OHE2 circulates as 16OHE2-glucuronide and the rest as unconjugated 16OHE2[314]. Elevated plasma levels of 16OHE2 were recently observed in female idiopathic PAH patients, and in male and female patients with portopulmonary PAH (affecting both the lungs and liver)[241,317]. However, the source of 16OHE2 synthesis in PAH patients is undetermined.

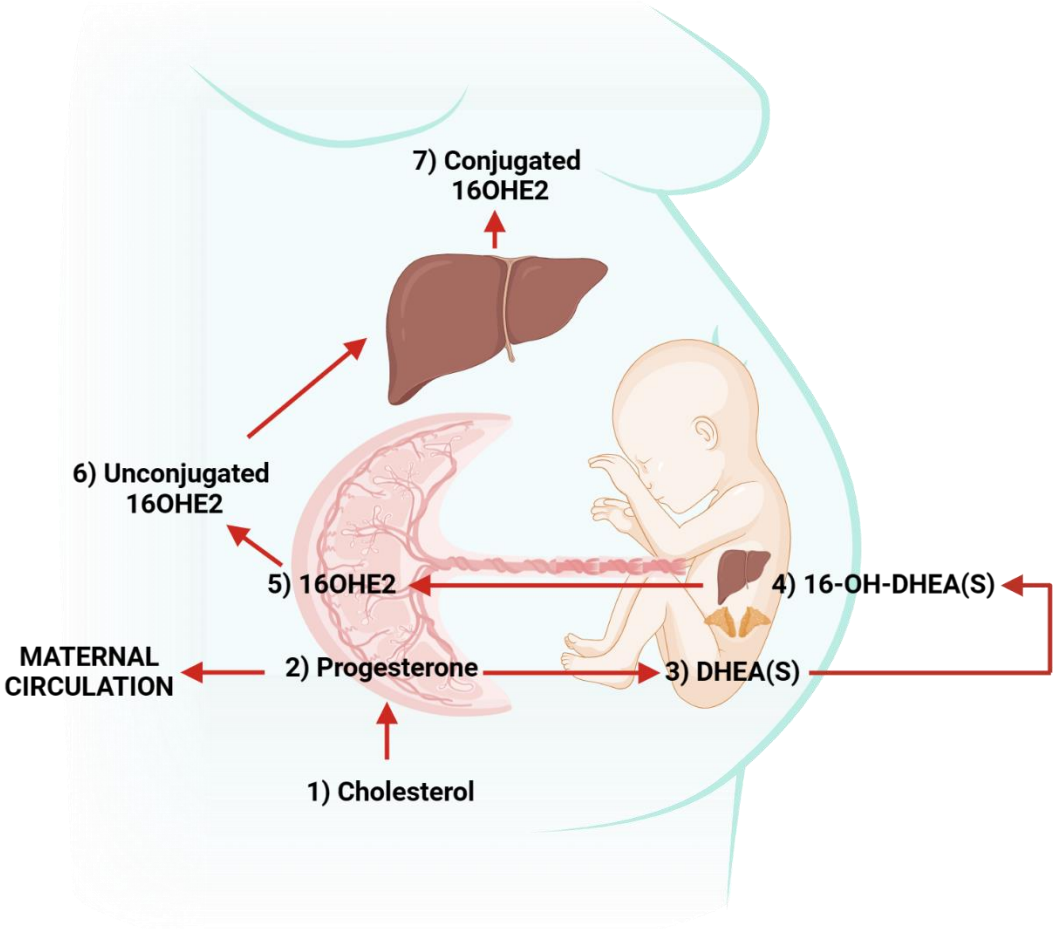

Figure 1.10: Biosynthesis of 16α-hydroxyestradiol during pregnancy.
The mother provides cholesterol to the placenta, which converts it to progesterone for release into the maternal or fetal circulation. Progesterone is converted to dehydroepiandrosterone (DHEA) or dehydroepiandrosterone sulfate (DHEA-S) in the fetal adrenal glands before further metabolism to 16α-hydroxydehydroepiandrosterone or 16α-hydroxydehydroepiandrosterone sulfate (16-OH-DHEA/16-OH-DHEA-S) in the fetal liver. 16-OH-DHEA returns to the placenta and is aromatised to unconjugated 16α-hydroxyestradiol (16OHE2) before secretion into the maternal circulation. 16OHE2 undergoes extensive conjugation in the maternal liver by several enzymes (e.g., β-glucuronidase) before excretion in the urine as 16OHE2-glucuronide. Created with BioRender.com.

At present, little is known about the function of 16OHE2 in PAH. In a preliminary study, Denver et al. observed that 16OHE2 induced proliferation of female PAH patient hPASMCs, and increased migration of blood outgrowth endothelial cells (BOECs) from male and female PAH patients[241]. 16OHE2-induced migration was attenuated by the NRF2-activator bardoxolone, suggesting that this may be dependent on redox signalling[241]. Intriguingly, Kawut et al. observed that the ERα inhibitor fulvestrant decreased plasma 16OHE2 levels in postmenopausal women

with PAH[117]. Watson et al. also observed that 16OHE2 increased proliferation of GH3/B6/F10 rat pituitary tumour cells, but this did not occur in a subline of these cells expressing low levels of ERα[318]. During a study primarily focused on E2, Austin et al. (2012) incidentally observed that 24 hours stimulation with 16OHE2 suppressed *BMPR2* expression in human pulmonary microvascular endothelial cells[147]. However, this observation was made before increased plasma levels of 16OHE2 were detected in PAH patients (Denver et al. 2020)[241]. While preliminary evidence suggests that 16OHE2 may be pathogenic in PAH, substantial work is required to elucidate the mechanisms underlying its functional effects *in vitro*, its molecular effects, and its effects *in vivo*.

1.6 Aims and Objectives

Female sex is a significant risk factor for PAH, with up to four-fold more women developing PAH than men[27]. On the other hand, once PAH has developed, women have better survival than men[28]. Recent evidence suggests that this 'estrogen paradox' may be mediated by a shift in estrogen metabolism from the protective 2-hydroxylation pathway to pathogenic 16α-hydroxylation[274]. Elevated plasma levels of 16OHE2 were recently observed in female idiopathic PAH patients, and in male and female patients with portopulmonary PAH[241,317]. However, little is known about the function of 16OHE2 in PAH. Therefore, the principal aim of this research was to investigate the role of 16OHE2 in the pathogenesis of PAH. This was addressed by the following project aims:

1. To functionally characterise the effects of 16OHE2 *in vitro*.

2. To investigate the molecular effects of 16OHE2 *in vitro*.

3. To investigate the haemodynamic, physiological, and molecular effects of 16OHE2 *in vivo.*

Chapter 2

Material and Methods

2.1 Chemical Reagents and Equipment

All chemical reagents were purchased from Fisher Scientific (UK) or Sigma-Aldrich (UK) unless stated otherwise. Plastic-ware for cell culture was supplied by Corning, ThermoFisher Scientific (UK). Reagents for RNA and protein analyses were purchased from Qiagen (UK) and ThermoFisher Scientific (UK) respectively unless stated otherwise. Certified nuclease-free plastic-ware for experimental protocols involving RNA was supplied by VWR International (UK).

2.2 Cell Culture

2.2.1 Dede Hamster Lung Fibroblasts

Dede hamster lung fibroblasts, an immortalised cell line derived from female Chinese hamsters, were purchased from ATCC (Manassas, US). Dede hamster lung fibroblasts were removed from liquid nitrogen and stored on dry ice before rapid defrosting in a water bath (37°C). Once the contents of the vial had thawed, the exterior was wiped with 70% ethanol (Fisher Chemical, UK) in distilled water to prevent contamination. Dede hamster lung fibroblasts were placed in a T-75 flask with 10 mL Dulbecco's Modified Eagle Medium (DMEM; Gibco, UK) containing 10% fetal bovine serum (FBS; Sera Laboratories International, UK) and 1% antibiotic antimycotic solution (containing 0.25 µg/mL amphotericin B, 10,000 U/mL penicillin, 100 µg/mL streptomycin; Sigma-Aldrich, UK). Penicillin prevents bacterial growth by inhibiting cell wall synthesis, streptomycin inhibits bacterial protein synthesis, and amphotericin B is an antifungal agent. DMEM contains the pH indicator phenol red, which progresses from a red to yellow colour as the pH of the medium decreases. This most commonly occurs in response to waste products released from the cells but can also result from bacterial infection or cell death. Cells were placed in a 37°C, 5% CO_2, 95% air humidified incubator and fresh media was provided every 2-3 days.

2.2.2 Subculture of Dede Hamster Lung Fibroblasts

Dede hamster lung fibroblasts were cultured to 90-100% confluency. The media was aspirated, and the cells washed with 10 mL phosphate buffered saline (PBS; Gibco, UK). 1 mL trypsin 0.1% (w/v) EDTA in PBS (Life Technologies, UK) was added to the flask and the cells incubated for 3-5 minutes until detached (sometimes aided by a gentle tap following removal from the incubator). Trypsin digests adhesive proteins, detaching cells from the flask. EDTA chelates divalent ions in the media. 9 mL media was added to each flask to inactivate the trypsin and the cell suspension centrifuged at 1500 rpm for 5 minutes to pellet the cells. The supernatant was aspirated, and the cells re-suspended in 10 mL media. A Neubauer Improved Haemocytometer Counting Chamber BS.748 (Hawksley, UK) was used to count the cells. Cells were seeded in a 6-well plate at $3x10^5$ cells/well for the Countess proliferation assay (2.5) and grown to 50-60% confluency.

2.2.3 Isolation of Rat Pulmonary Artery Smooth Muscle Cells

All *in vivo* procedures including euthanasia, tissue harvest, and pulmonary artery dissection were performed by Dr Hicham Labazi. Male and female Sprague-Dawley rats (Envigo, UK) aged 11-13 weeks weighing 320-344g (males) and 210-265g (females) were euthanised by CO_2 inhalation (BOC, UK) in accordance with Schedule 1 of the Animals (Scientific Procedures) Act 1986. The heart and lungs were excised, rinsed in sterile PBS, and placed in 2 mL sterile Ham's F-12 nutrient mixture media (Gibco, UK). The intra-lobar artery and aorta were dissected using micro-dissection forceps and placed in new Eppendorf tubes containing 2 mL sterile Ham's F-12 media. The right ventricle (RV) was separated from the left ventricle and septum (LV+S), and both were weighed.

The following digestive enzyme mix was prepared: 10 mg bovine serum albumin (BSA; Sigma-Aldrich, UK), 5mg collagenase type I (Sigma-Aldrich, UK), 0.6 mg elastase type III (Sigma-Aldrich, UK), 1.8 mg soybean trypsin inhibitor (Sigma-Aldrich, UK) in 10 mL F-12 Ham's media. Collagenase and elastase break down

collagen and elastin to compromise the integrity of the blood vessel wall and allow cell migration into the media. BSA inhibits the collagenase and slows down the digestion process to prevent damage to cells. Soybean trypsin inhibitor was used to prevent cell damage during cell dissociation from the vessel. The digestion enzyme mix was filtered through a 0.22 µm syringe filter under sterile conditions into a 35 mm culture dish. The pulmonary arteries were carefully transferred to one culture dish using fine tweezers. The dishes were incubated overnight.

As only one lung from each rat was available during earlier experiments, three pulmonary arteries from different rats were pooled to form one cell line as these are very small and one pulmonary artery alone does not yield sufficient cells. Each cell line was used three times to provide n=3. In later experiments, both lungs from each rat were available and two pulmonary arteries from the same rat were pooled to form one cell line. Each line was used once as n=1.

Vessels were chopped into small pieces using a disposable scalpel, then re-suspended in the media by pipetting up and down 20 times using a Pasteur pipette every 30 minutes for 3 hours. 3 mL F-12 Ham's media was added to the culture plate, and the cells and debris were filtered through a 100 µM nylon cell strainer (FALCON, New York, U.S) into a 50 mL Falcon tube. The plate was washed twice with a further 3 mL F-12 Ham's media and once with 1 mL media to ensure all cells and debris were removed from the plate. This was filtered into the Falcon tube, and a further 5 mL of F-12 Ham's media was run through the cell strainer to clear any remaining cells into the Falcon tube. The cell suspension was centrifuged for 5 minutes at 1500 rpm to pellet the cells.

The pulmonary artery cells were re-suspended in 5 mL DMEM containing 20% FBS and 1% antibiotic antimycotic solution per artery (15 mL for three arteries; 10 mL for two). T-25 flasks were coated with 1 mL gelatin (bovine; Sigma-Aldrich, UK), allowed to dry for 20 minutes, then washed with PBS. The cells were distributed 5 mL per gelatin-coated flask and incubated until adhered. The media was replaced after 1-2 days, and the cells cultured for 5-6 days.

Once 70-80% confluent, the cells were washed with 5 mL PBS, 1 mL trypsin was added, and the cells incubated for 3-5 minutes until detached. 4 mL DMEM was added to each flask to inactivate the trypsin, and the cell suspension taken up into a Falcon tube and centrifuged at 1500 rpm for 5 minutes to pellet the cells. The

supernatant was aspirated, and the cells re-suspended in 10 mL media then placed in T-75 flasks to allow culture expansion.

Once the T-75 flasks were confluent, the cells were washed with 10 mL PBS. 1 mL trypsin was added, and the cells incubated for 3-5 minutes until detached. 9 mL DMEM was added to each flask and the cell suspension centrifuged at 1500 rpm for 5 minutes to pellet the cells. The supernatant was aspirated, and the cell pellet was re-suspended in 2 mL 10% dimethyl sulfoxide (DMSO; ThermoFisher Scientific, UK) in DMEM. DMSO is a cryoprotectant that aids in reducing cell death during the slow-freezing process for storage in liquid nitrogen. 1 mL cell suspension was added to each cryogenic storage vial and the cells were slowly frozen at a rate of approximately -1°C/min in a Mr Frosty™ Freezing Container (ThermoFisher Scientific, UK) insulated with 100% isopropyl alcohol (Fisher Chemical, UK). The cells were moved into long-term storage in liquid nitrogen (-196°C).

2.2.4 Culture of Rat Pulmonary Artery Smooth Muscle Cells

Rat pulmonary artery smooth muscle cells (rPASMCs) were removed from liquid nitrogen and kept on dry ice before rapid defrosting in a water bath. Once the contents of the vial had thawed, the exterior was wiped with 70% ethanol to prevent contamination. rPASMCs were suspended in 10mL DMEM (containing 20% FBS and 1% antibiotic-antimycotic solution) in a T-75 flask or 25 mL DMEM in a T-175 flask depending on the number of cells required and left to adhere for ~24 hours. Fresh media was provided every 2-3 days.

2.2.5 Subculture of Rat Pulmonary Artery Smooth Muscle Cells

rPASMCs (passage 2-6) were grown to 90-100% confluency. 1 mL culture media was taken for *Mycoplasma* testing, initially using a PCR Mycoplasma Test Kit (Supplemental Methods 8.1; PromoCell, UK) and later using a MycoStrip™ Mycoplasma Detection Kit (Supplemental Methods 8.2; InvivoGen, San Diego, USA) as this was less time consuming. One cell line tested positive for *Mycoplasma* and was treated with Plasmocin™ Treatment (InvivoGen, San Diego, USA) 12.5 µg/mL for two passages, then repeat testing confirmed successful *Mycoplasma* eradication. Plasmocin™ Treatment is a broad-spectrum anti-mycoplasma agent containing two bactericidal components: one interfering with ribosome translation and the other acting on DNA replication.

The culture media was aspirated, and the cells washed with 10 mL or 25 mL PBS for T-75 and T-175 flasks respectively. 1 mL or 3 mL trypsin was added, and the cells incubated for 3-5 minutes until detached. PASMCs develop a round morphology upon detachment. 9 mL or 22 mL media was added to inactivate the trypsin and the cell suspension taken up into a Falcon tube. The cell suspension was centrifuged at 1500 rpm for 5 minutes to form a pellet. The supernatant was aspirated, and the pellet re-suspended in 10 mL or 25 mL media for T-75 and T-175 flasks respectively. The cells were counted using the haemocytometer.

For immunocytochemistry, rPASMCs were seeded in 12-well plates onto collagen coated coverslips (prepared as per 2.3) at $1x10^5$ cells/well in DMEM containing 20% FBS. For the Countess proliferation assay, male rPASMCs were seeded at $3x10^5$ cells/well and female rPASMCs at $2x10^5$ cells/well in a 6-well plate and grown to 50-60% confluency in DMEM containing 10% FBS. Different seeding densities were required because female rPASMCs grow more rapidly than male rPASMCs. For wound migration, rPASMCs were seeded in gelatin coated 6-well plates (prepared as per 2.6) at $3x10^5$ cells/well in DMEM containing 20% FBS. rPASMCs were initially seeded at $3x10^5$ cells/well in 6-well plates in DMEM containing 20% FBS for RNA and protein extraction, but this was later changed to $2.2x10^6$ cells in a 100 mm dish to yield more RNA and protein.

2.2.6 Isolation of Pulmonary Artery Smooth Muscle Cells from Sugen-Hypoxic and Chronic Hypoxic Rats

An attempt was made to isolate PASMCs from male and female Sprague-Dawley rats treated with a single 20 mg/kg dose of Sugen 5416 (Bio-techne Ltd, UK) followed by 3 weeks hypoxia (reduced atmospheric pressure of 550 mBar) then re-exposure to normal atmospheric pressure (~1050 mBar) for 3 weeks. All *in vivo* procedures including Sugen dosing, maintenance in chronic hypoxia, euthanasia, tissue harvest, and pulmonary artery dissection were carried out by Dr Hicham Labazi. As this was a preliminary study, rats were used as available. The male rats were aged 13 weeks and weighed 269-300g. The female rats were aged 15 weeks and weighed 205-241g. Euthanasia, tissue harvest, and PASMC isolation were carried out as per 2.2.3. The RV was separated from the LV+S. Both parts were weighed to calculate the Fulton index (RV Weight/ LV+S Weight). In all rats, the Fulton index was >0.34 confirming the presence of RV hypertrophy characteristic of PAH (Supplementary Tables 9.1 and 9.2). As fewer cells were expected to adhere to the flask following isolation, the cells from four rat pulmonary arteries were pooled in each flask and cultured as per 2.2.4. Although the cells adhered unfortunately their growth was very poor, and the cultures had to be abandoned around 5 weeks later.

It was hypothesised that the sugen-hypoxic rPASMCs failed to grow due to the severe PAH phenotype associated with this model. Therefore, an attempt was made to isolate PASMCs from female Sprague-Dawley rats following 2 weeks of hypoxia alone. As previously, all *in vivo* procedures including maintenance in chronic hypoxia, euthanasia, tissue harvest, and pulmonary artery dissection were carried out by Dr Hicham Labazi. The female rats were aged 18 weeks and weighed 241-260g. Euthanasia, tissue harvest and PASMC isolation were carried out as per 2.2.3. The RV was separated from the LV+S and both were weighed. In all rats, the Fulton index was >0.34 confirming the presence of the RV hypertrophy (Supplementary Table 9.2). The cells were cultured as per 2.2.4 and sub-cultured as per 2.2.5. However, these cells were highly sensitive to quiescence in 0.2% DMEM (as per 2.5.2) prior to experiments and stopped growing. Therefore, the decision was made to focus on other studies.

2.2.7 Isolation of Rat Aorta Smooth Muscle Cells

Aorta smooth muscle cells (AoSMCs) were isolated from the same male and female Sprague-Dawley rats at the same time as the PASMCs using the same method as per 2.2.3. As the aorta is much larger than the pulmonary artery and yields more cells, one aorta was transferred to each dish for each individual cell line. Following isolation, rat AoSMC cultures were expanded then stored in liquid nitrogen as per 2.2.3.

2.2.8 Culture of Rat Aorta Smooth Muscle Cells

Culture, subculture, and RNA collection from rat AoSMCs were carried out by Mr Gregor Aitchison. AoSMCs were removed from liquid nitrogen and kept on dry ice before rapid defrosting in a water bath (37°C). Once the contents of the vial had thawed, the exterior was wiped with 70% ethanol to prevent contamination. AoSMCs were suspended in 10 mL DMEM (containing 10% FBS and 1% antibiotic-antimycotic solution) in a T-75 flask and left to adhere for ~24 hours. Fresh media was provided every 2-3 days.

2.2.9 Subculture of Rat Aorta Smooth Muscle Cells

AoSMCs (passage 2-3) were grown to 90-100% confluency. 1 mL culture media was taken for *Mycoplasma* testing. The culture media was aspirated, and the cells washed with 10 mL PBS. 1 mL trypsin was added, and the cells incubated for ~3 minutes until detached. 9 mL DMEM was added to inactivate the trypsin and the cell suspension taken up into a Falcon tube. The cell suspension was centrifuged at 1200 rpm for 3 minutes to pellet the cells. The cells were re-suspended in 10 mL media, counted, and seeded into 6-well plates at $3x10^5$ cells/well for RNA collection. The cells were grown to ~70% confluency.

2.2.10 Human Fetal Lung Fibroblast-1 Cells

Human fetal lung fibroblast-1 cells (HFL-1; ATCC, Manassas, US) were used as a fibroblast control for immunocytochemistry characterisation of the newly isolated rPASMCs and AoSMCs. HFL-1 cells were removed from liquid nitrogen and stored on dry ice before rapid defrosting in a water bath. Once the contents of the vial had thawed, the exterior was wiped with 70% ethanol to prevent contamination. Cells were suspended in 10 mL Ham's F-12K (Kaighn's) Medium (Gibco, UK) with 10% FBS and 1% antibiotic-antimycotic solution in a T-75 flask, then incubated. Cells were left to adhere overnight, and fresh media provided every 2-3 days.

2.2.11 Subculture of Human Fetal Lung Fibroblast-1 Cells

HFL-1 cells were grown to 90-100% confluency in a T-75 flask. The culture media was aspirated, and the cells washed with 10 mL PBS. 1mL trypsin was added to the flask and the cells incubated for ~3 minutes until detached. The HFL-1 cells were seeded in 12-well plates onto collagen-coated coverslips at $1x10^5$ cells/well. The cells were incubated until 50-60% confluent.

2.2.12 Human Pulmonary Artery Smooth Muscle Cells

Experimental procedures using human cells conform to the principles outlined in the Declaration of Helsinki. Human pulmonary artery smooth muscle cells (hPASMCs) were provided by Professor Nick Morrell (University of Cambridge, UK) with ethical permission. Primary cultures were isolated from the small distal pulmonary arteries (<1mm external diameter). Subject characteristics are provided in Tables 3.1, 3.2 and 4.12.

hPASMCs were stored in liquid nitrogen in 10% DMSO in DMEM (with 10% FBS and 1% antibiotic-antimycotic solution). hPASMCs were removed from liquid nitrogen and stored on dry ice before rapid defrosting in a water bath. Once the contents of the vial had thawed, the exterior was wiped with 70% ethanol to prevent

contamination. Cells were suspended in 10 mL DMEM containing 20% FBS and 1% antibiotic-antimycotic solution, then incubated. Cells were left to adhere for ~24 hours, and fresh media was provided every 2-3 days.

2.2.13 Subculture of Human Pulmonary Artery Smooth Muscle Cells

hPASMCs were grown to 90-100% confluency in a T-75 flask. 1 mL culture media was taken for *Mycoplasma* testing. The culture media was aspirated, and the cells washed with 10 mL PBS. 1 mL trypsin was added to the flask and the cells were incubated for ~3 minutes until detached. 9 mL media was added to inactivate the trypsin and the cell suspension was taken up into a Falcon tube. The cells were centrifuged at 1200 rpm for 3 minutes, and the cell pellet re-suspended in 10 mL media. The cells were counted. For immunocytochemistry (2.3), female PAH patient hPASMCs were seeded onto collagen-coated coverslips in 12-well plates at $1x10^5$ cells/well in DMEM containing 20% FBS and incubated until 50-60% confluent. For the Countess proliferation assay (2.5), female PAH patient hPASMCs were seeded in 6-well plates at $2x10^5$ cells/well in DMEM containing 10% FBS and incubated until ~50% confluent. For RNA extraction (2.8.1.3), male control subject hPASMCs were seeded in 100 mm dishes at $2.2x10^6$ cells/well in DMEM containing 20% FBS and incubated until ~70% confluent.

2.3 Immunocytochemistry Characterisation of Rat PASMCs and AoSMCs

19 mm glass coverslips (VWR International, UK) were sterilised in 100% ethanol, placed on 70% ethanol-sprayed tissue paper in the cell culture hood, and allowed to dry for a few minutes. The coverslips were placed into 12-well plates. A solution of 20 mM acetic acid was prepared from glacial acetic acid (Fisher Chemical, UK) diluted in distilled water and sterilised using a Minisart™ 0.2 µm syringe filter (Sartorius, UK). A 50 µg/mL solution of Collagen I Rat Tail (Gibco, UK) was prepared

in 20 mM acetic acid and used to coat each coverslip. Collagen I is an extracellular matrix protein and coating promotes cell adherence to coverslips. The coverslips were left to dry in the hood for 20 minutes, washed with PBS, and the plates were sealed and stored in the fridge until use.

rPASMCs, AoSMCs, HFL-1 cells, and female PAH patient hPASMCs were cultured to 90-100% confluency then seeded onto the collagen-coated coverslips at a density of $1x10^5$ cells/well. The cells were left to adhere for 24 hours then washed twice with PBS to remove interference from the serum in the media. 500 µL 10% neutral buffered formalin (Sigma-Aldrich, UK) was added per well and the plates left on ice for 10 minutes to fix the cells. Formalin is a chemical fixative which acts by formation of covalent bond cross links between molecules. After a quick rinse with PBS, the cells were washed twice with PBS for 5 minutes at room temperature. PBS-Tween-Triton X-100 (PBS-TT) was prepared as follows: 0.05% Tween 20 (Sigma-Aldrich, UK), 0.1% Triton X-100 (Sigma-Aldrich, UK) in PBS. Tween 20 is a surfactant used to prevent non-specific binding of antibodies to the cells. Triton X-100 permeabilises the cells, which is essential to allow antibodies to cross the cell membrane. Fixation is essential prior to permeabilization as the cellular material would otherwise not be preserved. The cells were permeabilized in PBS-TT at room temperature for 20 minutes.

After a quick rinse, the cells were washed twice with PBS for 5 minutes at room temperature. A blocking buffer was made up as follows: 4% BSA, 10% goat serum (Sigma-Aldrich, UK) in PBS-TT. The blocking buffer prevents non-specific antibody binding and reduces subsequent fluorescent background in fixed cells. Goat serum carries antibodies which bind to reactive sites and prevent non-specific binding of secondary antibodies. BSA also binds to and blocks non-specific sites. 500 µL blocking buffer was added to each well, and the cells were incubated for one hour at room temperature.

A primary antibody buffer was made up of 4% BSA in PBS-TT. The following primary antibodies were diluted in the buffer: ab5694 anti-alpha smooth muscle actin produced in rabbit 1:500 dilution (Abcam, UK), ab8978 anti-vimentin antibody [RV202] produced in mouse 1:500 dilution (Abcam, UK). Alpha-smooth muscle actin (α-SMA) is highly expressed in PASMCs and other types of smooth muscle cells, whereas vimentin is highly expressed in fibroblasts and mesenchymal cells. Different host species were selected to minimise secondary antibody cross-reactivity

and improve specificity. PBS was used as a negative control to assess any non-specific binding. 150 µL of each primary antibody was added to the other wells and the cells incubated overnight in a cold room.

The primary antibodies were aspirated, and the cells washed four times for 5 minutes in 0.05% Tween 20 in PBS (PBS-T) after a quick initial rinse. The following secondary antibodies were diluted in PBS-TT: A-11008 Goat anti-Rabbit IgG (H+L) Cross-Adsorbed Secondary Antibody, Alexa Fluor 488 1:500 dilution (Invitrogen, UK), A-11005 Goat anti-Mouse IgG (H+L) Cross-Adsorbed Secondary Antibody, Alexa Fluor 594 1:500 dilution (Invitrogen, UK). The primary antibody binds directly to the target antigen. The secondary antibodies bind to the primary antibodies, with their attached fluorophores providing a green (488 nm) or red (594 nm) fluorescent signal. 150 µL of both secondary antibodies was added to each well, and the plates wrapped in foil to protect the fluorophores from light and incubated at for 1 hour at room temperature.

The secondary antibody was aspirated, and the cells were washed with PBS three times for 5 minutes after a quick initial rinse. The glass coverslips were lifted using forceps and mounted onto microscope slides using a drop of Vectashield Antifade Mounting Medium with DAPI H-1200-10 (Novus Biologicals, UK). DAPI is a marker for membrane viability and is highly fluorescent when bound to double-stranded DNA in the nucleus, with an emission wavelength in the blue region of the spectrum (461 nm). The coverslips were sealed with clear nail varnish and left to set overnight. The slides were wrapped in foil to protect the fluorophores from light and stored in the fridge until imaging. The cells were imaged using a Nikon Eclipse E600 fluorescence microscope (Nikon, Japan) with a x40 objective (Nikon Japan S Fluor 40X/1.30 Oil) and oil immersion (Type DF; Cargille Laboratories, USA). Oil immersion increases the resolving power (ability to distinguish objects located at a small angular distance) of the microscope. The images were recorded using WinFluor Software (V3.8.5.; University of Strathclyde, UK) and analysed using ImageJ (v1.53e; National Institutes of Health, Bethesda, US).

2.4 Validation of the Hypoxic Chamber

Immunocytochemistry and quantitative real-time polymerase chain reaction (qRT-PCR) were used to validate that 72-hours incubation in 1% O_2 /5% CO_2 /nitrogen mix (BOC, UK) using a Modular Incubator Chamber (Billups-Rothenberg, Del-Mar, US) induces a hypoxic response in rPASMCs. HIF1α was selected as a marker of cellular hypoxia as its translocation from the cytoplasm into the nucleus under hypoxic conditions can be visualised[293]. However, HIF1α degrades quickly upon exposure to normoxia (half-life ~5 minutes) therefore expression of its more stable target gene hexokinase 2 (*Hk2*) was also measured using qRT-PCR[293,319-321].

2.4.1 Immunocytochemistry

Collagen-coated coverslips were prepared as per 2.3. Female rPASMCs were seeded onto the coverslips in two 12-well plates and grown to 50-60% confluency in DMEM (containing 10% FBS + 1% antibiotic-antimycotic solution). A 200 μM dilution of cobalt chloride (VWR, UK) in DMEM was prepared from a 25 mM stock solution and sterilised using a Minisart™ 0.2 μm syringe filter. The media was refreshed on both 12-well plates, and 200 μM cobalt chloride added to two wells of the normoxic plate as a positive control. Cobalt chloride stabilises HIF1α in the cell, where it can translocate to the nucleus and interact with HIF1β and the hypoxic response element to mediate gene transcription[322].

The other 12-well plate was placed in hypoxic conditions using a Modular incubator chamber as follows. The hypoxic chamber was cleaned with 70% ethanol and a 100 mm dish of sterile water was placed in the bottom of the chamber. The first mesh rack was placed over the top, the cell culture plate added to the space between the racks, and the chamber was sealed. 100 L of gas (1% O_2/ 5% CO_2/nitrogen) was passed through the chamber at a rate of 10 L/min. The chamber was placed in the incubator for one hour, then flushed with a further 100 L of gas to remove any gases that may have been trapped in the media. The two 12-well plates were incubated in normoxic and hypoxic conditions respectively for 72 hours.

The cells were fixed, and immunocytochemistry carried out as per 2.3. The following primary and secondary antibodies were used: NB100-134 anti-HIF-1α produced in rabbit 1:200 dilution (Novus Biologicals, UK) and A-11008 Goat anti-Rabbit IgG (H+L) Cross-Adsorbed Secondary Antibody, Alexa Fluor 488 1:500 dilution (Invitrogen, UK).

2.4.2 Quantitative Real-Time Polymerase Chain Reaction

Female rPASMCs were seeded into two 6-well plates at $2x10^5$ cells/well in DMEM, left to adhere overnight and grown to 60-70% confluency. One 6-well plate was incubated in normoxic conditions and the other placed in hypoxia (as per 2.4.1) for 72 hours. RNA was collected from both plates and qRT-PCR carried out (as per 2.8) to quantify *Hk2* expression.

2.5 Countess Proliferation Assay

The Countess proliferation assay was carried out in Dede hamster lung fibroblasts, male and female rPASMCs under normoxic and acute hypoxic conditions (72 hours in 1% O_2 /5% CO_2 /nitrogen mix) and female PAH patient hPASMCs. Dede hamster lung fibroblasts were cultured as per 2.2.1 and subcultured in 6-well plates until 50-60% confluent as per 2.2.2. rPASMCs were cultured as per 2.2.4 and subcultured in 6-well plates until 50-60% confluent as per 2.2.5. Female PAH patient hPASMCs were cultured as per 2.2.12 and subcultured in 6-well plates until 50-60% confluent as per 2.2.13.

2.5.1 Charcoal Stripping Fetal Bovine Serum

The estrogens endogenous to FBS (and other sera) may potentially have a confounding effect when studying the effects of steroid hormones *in vitro*. Therefore, FBS was charcoal-stripped to deplete estrogen levels to $<10^{-11}M$[323]. Charcoal-

stripped FBS was used for all experiments involving quiescence and stimulation of cells. 0.1g/10 mL dextran-coated charcoal (Sigma-Aldrich, UK) was added to FBS. This was placed on a shaker in the cold room overnight. The following day, it was centrifuged at 1811G and 4°C for 30 minutes, the stripped serum decanted, and vacuum filtered under sterile conditions. A further 0.1 g/10 mL dextran-coated charcoal was added, and the serum placed on a shake table in the cold room overnight. The centrifugation and filtration steps were repeated, and the stripped serum was aliquoted and stored at -20°C.

2.5.2 Quiescence of Cells

Dede hamster lung fibroblasts were quiesced with 0.5% charcoal stripped FBS in phenol red-free DMEM (Gibco, UK) for 24 hours prior to stimulation. This was reduced to 0.2% charcoal stripped FBS for all subsequent experiments with rPASMCs, hPASMCs and AoSMCs. Quiescence synchronises cells into the G0 phase of the cell cycle. Phenol red-free media was used because the weak estrogenic properties of phenol red may potentially have a confounding effect[324]. Following quiescence, stimulations were carried out in phenol red-free DMEM with either 2% charcoal-stripped FBS (countess proliferation assay in Dede hamster lung fibroblasts) or 1% charcoal-stripped FBS (all other experiments).

2.5.3 Cell Stimulation for the Countess Proliferation Assay

10 mM stock solutions of estradiol (E2), 16α-hydroxyestrone (16OHE1) and 16α-hydroxyestradiol (16OHE2; Steraloids, Newport, US) were prepared in ethanol (absolute 99.8%; Fisher Scientific, UK) and stored at -20°C. Serial dilutions to the desired concentrations (1 nM E2, 1 nM 16OHE1 and 10 nM 16OHE2) were performed immediately before use in phenol red-free DMEM containing either 2% (Dede hamster lung fibroblasts) or 1% charcoal stripped FBS (all other experiments) and 1% antibiotic-antimycotic solution. For the Countess proliferation assay in Dede hamster lung fibroblasts, drugs were added to phenol red-free DMEM in the presence of 2% FBS. For all other experiments, drugs were added in the presence

of 1% FBS. 2% phenol red-free DMEM was used as a negative control for the Countess proliferation assay in Dede hamster lung fibroblasts, whereas 1% was used for all other experiments. 10 nM ethanol was used as a vehicle control. In the initial experiment, Dede hamster lung fibroblasts were stimulated with 1 nM 16OHE1 and 10 nM 16OHE2 for 2, 6, 24 and 48 hours. Subsequent experiments were carried out at 48 hours. rPASMCs were stimulated with 1 nM E2, 1 nM 16OHE1 and 10 nM 16OHE2 under normoxic and acute hypoxic conditions. Female PAH patient hPASMCs were stimulated with 10 nM 16OHE2 for 48 hours.

2.5.4 Countess Proliferation Assay

Cell proliferation experiments were performed on a Countess II Automated Cell Counter (Life Technologies, UK). The 6-well plates were removed from the incubator, the stimulation media aspirated, and the cells washed with 2 mL PBS. 600 µL trypsin was added to each well and the cells incubated for ~3-5 minutes until detached. The cells in trypsin were transferred to a 1.5 mL Eppendorf tube, kept on ice, and then centrifuged at 4900g for 3 minutes at 4°C. The supernatant was removed, and the cell pellets washed with 100 µL PBS. A further 15 µL PBS was added to each pellet and the Eppendorf tube was placed on ice until ready for analysis. 15 µL trypan blue (Sigma-Aldrich, UK) was added immediately before counting as the solution is toxic to cells within 3 minutes, and the cells were re-suspended by mixing with the pipette. Trypan blue is an indicator of cell viability - live cells have an intact membrane and do not absorb the dye whereas dead cells are permeable and appear a dark blue colour. 15 µL cell suspension was added to each chamber of the Countess cell counting slide (Life Technologies, UK) and the slide inserted into the machine. The average total cell count from both chambers of the slide was calculated for each sample using Microsoft Excel (2019, Microsoft Office, Washington, US), then plotted using GraphPad Prism (Version 10, Prism Training & Consultancy, UK).

Normality was confirmed using the Shapiro-Wilk test. For rPASMCs and hPASMCs, analysis was carried out in GraphPad Prism using one-way ANOVA with Tukey post-hoc test and unpaired t-test respectively. A two-way ANOVA was required for Dede hamster lung fibroblast analysis. However, in GraphPad Prism, one of the

independent variables when carrying out a two-way ANOVA is limited to a maximum of two levels (e.g., could include all time points but only 1% and 10% FBS). Therefore, a 2-way ANOVA with post-hoc Tukey test was carried out in IBM SPSS Statistics (Version 29.0.1.0 (171); Armonk, New York, US). The assumption of homogeneity of variances for each combination of the groups of the two independent variables was not met (Levene's test). All other assumptions were met and the groups were of equal sample size.

2.6 Wound Migration Assay

The wound migration assay was carried out in male and female rPASMCs. In the sterile hood, the base of a 6-well plate was marked in red pen as per Figure 2.1 to divide the plate into four locations for imaging designated A, B, C and D. All images were taken directly below the upper horizontal line for each quadrant.

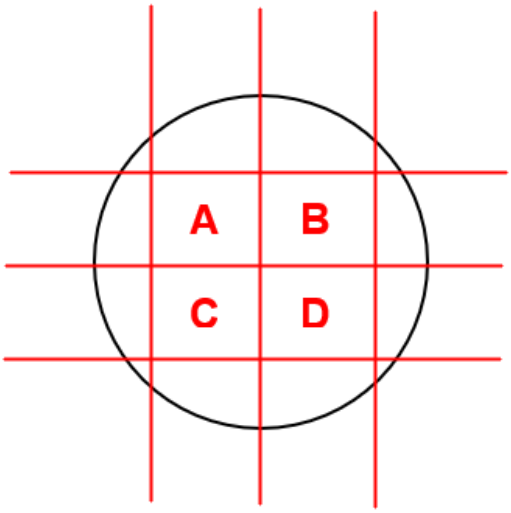

Figure 2.1: Division of 6-well plate into four imaging locations designated A, B, C and D for wound migration assay.
Created with BioRender.com.

6-well plates were coated with 1 mL gelatin, left to dry for 20 minutes, then washed with 1 mL PBS. rPASMCs were cultured as per 2.2.4 and seeded at $3x10^5$ cells/well and subcultured as per 2.2.5 until 90-100% confluent. The cells were quiesced in 0.2% phenol red-free DMEM for 24 hours. Serial dilutions of 16OHE2 were prepared from a 10 mM stock solution to 100 pM, 1 nM and 10 nM in phenol red-free DMEM containing 1% charcoal stripped FBS. Serial dilutions of E2 and 16OHE1 were prepared from a 10 mM stock to 1 nM. The vehicle control ethanol was serially diluted to 1 nM or 10 nM depending on the study. 1% and 10% phenol red-free DMEM were used as negative and positive controls.

After 24 hours quiescence, the 6-well plates were removed from the incubator and two vertical wounds were created using 200 µL pipette tips – one running through the centre of quadrants A and C, and the other running through the centre of quadrants B and D. The cells were washed three times with 2 mL PBS to remove any dead cells and debris, then stimulated with 100 pM, 1 nM or 10 nM 16OHE2 in the presence of phenol red-free DMEM containing 1% charcoal-stripped FBS or a control. Four images were taken per well (at locations A, B, C, and D) at 0, 2, 4, 6, 8, and 24 hours after stimulation using an EVOS™ XL Core Imaging System (ThermoFisher, UK) with EVOS® LPlan PH2 4x/0.13 objective (Life Technologies, UK). Wound area in each image was measured using the freehand selections tool in ImageJ (Figure 2.2) and plotted in Microsoft Excel. The entire background area for all images was measured using ImageJ and plotted in Microsoft Excel. The average wound area for each well at every time point was calculated and made relative to the background image area to normalise for differences in wound thickness. The average wound area relative to the background area at 0 hours was set as 100%, and the percentage wound area remaining at 2, 4, 6, 8, and 24 hours calculated relative to this. As the percentage wound area remaining is inversely proportional to cell migration, the percentage wound area closed was calculated by subtracting the area remaining from 100%.

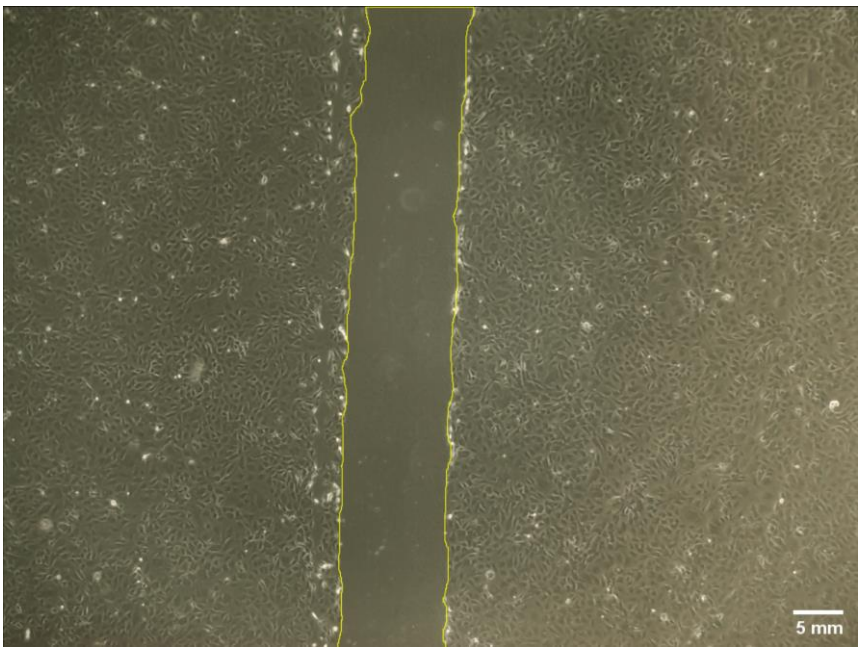

Figure 2.2.: Measuring the wound area at 0 hours in female rat pulmonary artery smooth muscle cells immediately after stimulation with 1% FBS control using the freehand selections tool in ImageJ.

The wound area is highlighted in yellow. FBS = fetal bovine serum. Scale bar = 5 mm.

The percentage wound area closed was plotted in GraphPad Prism. No outliers were detected using Grubb's test and the data were normally distributed (Shapiro-Wilk test). Analysis was carried out by 2-way ANOVA with Tukey post-hoc test in IBM SPSS Statistics. The assumption of homogeneity of variances for each combination of the groups of the two independent variables was not met (Levene's test). However, all other assumptions were met, and the groups were of equal sample size.

2.7 Investigation of the *In Vivo* Effects of 16α-Hydroxyestradiol in C57BL/6 Mice

All experimental procedures were carried out in accordance with the United Kingdom Animal Procedures Act (1986) and the US National Institutes of Health Guide for the Care and Use of Laboratory Animals (1996). All *in vivo* procedures were performed by Dr Smriti Sharma including dosing, assessment of right ventricular systolic pressure (RVSP), and tissue harvest. All animals were housed in the Strathclyde Institute of Pharmacy & Biomedical Sciences Biological Procedures Unit and maintained in the same environmental conditions, with a continuous 12-hour light/dark cycle and *ad libitum* access to fresh food and water.

2.7.1 General Experimental Design

C57BL/6 mice aged 23-25 weeks were provided by the Biological Procedures Unit, University of Strathclyde, UK. According to the US REVEAL registry, the average patient age at PAH diagnosis is 53 years old[51]. C57BL/6 mice are considered mature adults at 23-25 weeks old (~6 months)[325]. Furthermore, increased age is associated with disease penetrance in transgenic mouse models of PAH[101,326]. For example, BMPR2^{R899X} mice are known to spontaneously develop mild PAH at around 6 months old[326]. Female SERT^{+} mice also spontaneously develop PAH at around 5 months[101]. Therefore, the C57BL/6 mice were used at 23-25 weeks as age may increase susceptibility to PAH. C57BL/6 mice were randomised into groups and studied blindly. Group identity was revealed after pressure-volume (PV) loop and qRT-PCR results had been analysed.

Power calculations for *in vivo* studies were based on changes in RVSP as this is an indirect measure of pulmonary arterial pressure. In previous studies by the MacLean lab, the RVSP in control male and female C57BL/6 mice was ~22 mmHg[33,35]. Based on this, a 5 mmHg increase in RVSP was deemed to be physiologically relevant. Mair et al. observed that the standard deviation in RVSP was 2.65 in female control C57BL/6 mice[33]. Thus, to detect a 5 mmHg change in RVSP with a power of 0.80

and Type I error probability of 0.05, 6 animals per group are needed[327]. Our group sizes of 10-12 mice exceeded this requirement.

2.7.2 16α-Hydroxyestradiol Study

Male and female C57BL/6 mice were randomly allocated to receive either 1.5 mg/kg/day 16OHE2 or vehicle control (4% ethanol) intraperitoneally for 14 days. Groups were unblinded on completion of analysis. 16OHE2 was prepared fresh prior to use in 4% ethanol at 0.15 mg/mL. Injection volume was adjusted according to mouse weight to give 1.5 mg/kg/day.

2.7.3 Assessment of Right Ventricular Systolic Pressure

All *in vivo* procedures were performed by Dr Smriti Sharma. Following 14 days treatment with 16OHE2 or vehicle, C57BL/6 mice were anaesthetised with inhaled isoflurane (3% in O_2 for induction, 1-1.5% in O_2 for maintenance; Zoetis, UK). The required level of anaesthesia was confirmed by absence of pedal reflex to toe pinch and was carefully monitored throughout the procedure. PV loop relation measurements were performed to investigate for any changes in haemodynamics following treatment with 16OHE2. A pressure catheter (Millar Instruments, Houston, US) was inserted into the RV via the right jugular vein. After a period of stabilisation, steady state measurements were recorded and RVSP, heart rate and ventricular contractility were evaluated. RVSP was taken as an indirect method of assessing pulmonary arterial pressure as it is technically challenging to accurately obtain pulmonary arterial pressure by diaphragmatic catheterisation in mice. All haemodynamic readings were recorded and analysed using LabChart Pro (v8.1.25; ADINSTRUMENTS, UK). At the end of the procedure, mice were sacrificed by exsanguination under terminal anaesthesia (5% isoflurane).

2.7.4 Tissue Harvest

All procedures were carried out by Dr Smriti Sharma. The heart and lungs were gently flushed with cold PBS. The heart was separated into the RV and LV+S, and both were weighed to allow assessment of the Fulton index (RV weight/LV+S weight). The spleen was also weighed, and tibia length measured. The right lung and RV were flash frozen in liquid nitrogen then stored at -80°C for future molecular studies.

2.8 RNA Analysis

RNA was extracted from cells and C57BL/6 mouse lung tissue using the RNeasy® Mini Kit (Qiagen, UK). RNA was extracted from C57BL/6 mouse RV tissue using the ReliaPrep™ RNA Tissue Miniprep System (Promega, Madison, US) protocol for fibrous tissue.

2.8.1 Harvest of RNA from Cells

2.8.1.1 Rat Pulmonary Artery Smooth Muscle Cells

The experimental protocol for RNA analysis in male and female rPASMCs is summarised in Figure 2.3. In the initial study, rPASMCs were cultured as per 2.2.4, seeded in 6-well plates at $3x10^5$ cells/well, and subcultured as per 2.2.5 until ~70% confluent. In further studies, rPASMCs were subcultured in 100 mm dishes to increase the RNA yield. On the day after seeding (Day 2), the media was refreshed and rPASMCs were either maintained in normoxia or placed into acute hypoxia as per 2.4.1. Hypoxia (1% O_2/ 5% CO_2/ nitrogen mix) was continued for 72 hours. On Day 3, rPASMCs were quiesced in phenol red-free DMEM with 0.2% charcoal-stripped FBS for 24 hours.

All stimulations were carried out in the presence of phenol red-free DMEM containing 1% charcoal-stripped FBS. During the initial study to investigate the estrogen pathway, rPASMCs were stimulated as per 2.5.3 with 1 nM E2, 1 nM 16OHE1, 10 nM 16OHE2, and a vehicle control (10 nM ethanol) for 24 hours. In a further study to investigate the BMPR2 signalling pathway, rPASMCs were stimulated with 10 nM 16OHE2 and the vehicle (10 nM ethanol) for 24 hours. Male rPASMCs were also stimulated with 10 nM 16OHE2 and the vehicle for 2 hours. Finally, the effects of 24 hours stimulation with 10 nM 16OHE2 on the expression of genes within the BMPR2 signalling pathway were investigated in the presence of a 1 μM concentration of the following estrogen receptor antagonists: the ERα antagonist MPP [chemical name- 1,3-*Bis*(4-hydroxyphenyl)-4-methyl-5-[4-(2-piperidinylethoxy)phenol]-1*H*-pyrazole dihydrochloride] (Tocris, UK), the ERβ antagonist PHTPP [chemical name- 4-[2-Phenyl-5,7-*bis*(trifluoromethyl)pyrazolo[1,5-*a*]pyrimidin-3-yl]phenol] (Tocris, UK) and the GPER antagonist G-15 [chemical name- (3a*S**,4*R**,9b*R**)-4-(6-Bromo-1,3-benzodioxol-5-yl)-3a,4,5,9b-3*H*-cyclopenta[*c*]quinoline] (Tocris, UK).

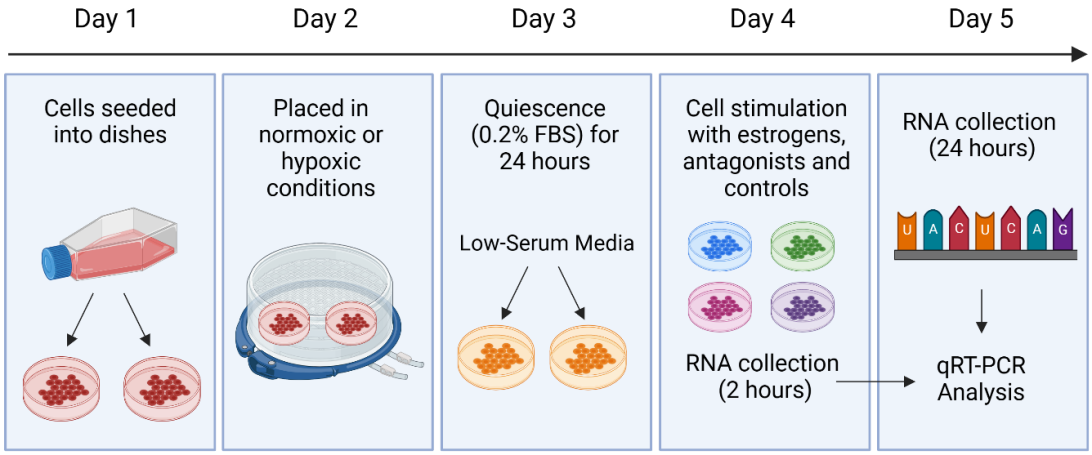

Figure 2.3.: Timeline of culture, quiescence, and stimulation of male and female rat pulmonary artery smooth muscle cells for RNA analysis by quantitative real-time polymerase chain reaction.

FBS = fetal bovine serium, RNA = ribonucleic acid, qRT-PCR = quantitative real-time polymerase chain reaction. Created with BioRender.com.

RNA was also collected from untreated male and female rPASMCs matched at passage 3 to investigate basal expression of the BMPR2 signalling pathway. These were subcultured in 100 mm dishes as per 2.2.5 for 72 hours until 90-100% confluent.

Following stimulation, the media was aspirated, and the cells washed with PBS. For RNA extraction, cells were suspended in 700 µL QIAzol Lysis Reagent (Qiagen, UK), transferred to an RNase-free 1.5 mL Eppendorf tube, and stored at -80°C. QIAzol is an acidic guanidinium-phenol based reagent. The phenol extracts nucleic acids and protein from the cells, the guanidinium salt serves as a chaotropic agent to denature the protein, and the low pH facilitates separation of RNA from DNA and protein.

2.8.1.2 Rat Aorta Smooth Muscle Cells

Rat AoSMCs were cultured as per 2.2.8, seeded in four wells of a 6-well plate at $3x10^5$ cells/well, and subcultured as per 2.2.9 until ~70% confluent. AoSMCs were quiesced for 24 hours in phenol red-free DMEM with 0.2% charcoal stripped FBS, then two wells were stimulated with 10 nM 16OHE2 and the other two with the vehicle control (10 nM ethanol) for 24 hours in the presence of phenol red-free DMEM with 1% charcoal-stripped FBS as per 2.5.3. Following stimulation, the media was aspirated, and the cells washed with 2 mL PBS. The cells were suspended in 350 µL QIAzol Lysis Reagent and transferred to an RNase-free 1.5 mL Eppendorf tube. The cells from two wells treated with 16OHE2 or vehicle were pooled to increase the RNA yield. The samples were stored at -80°C.

2.8.1.3 Human Pulmonary Artery Smooth Muscle Cells

Male control subject hPASMCs were cultured as per 2.2.12, seeded into 100 mm dishes at $2.2x10^6$ cells/dish, and subcultured as per 2.2.13 until ~70% confluent. hPASMCs were quiesced for 24 hours in phenol red-free DMEM with 0.2% charcoal stripped FBS, then stimulated with 10 nM 16OHE2 or vehicle control (10 nM ethanol) for 24 hours in the presence of phenol red-free DMEM containing 1% FBS

as per 2.5.3. The cells were lysed in 700 µL QIAzol and stored at -80°C as per 2.8.1.1.

2.8.2 Harvest of RNA from Tissue

Harvest of RNA from the lung and RV tissue of C57BL/6 mice was carried out by Dr Smriti Sharma.

2.8.2.1 Harvest of RNA from Lung Tissue

700 µL QIAzol Lysis Reagent was added to a piece of lung tissue weighing ~20 mg. Two 5 mm stainless steel beads (Qiagen, UK) were added, and the tissue homogenised using a Tissue Lyser II (Qiagen, UK).

2.8.2.2 Harvest of RNA from Right Ventricle Tissue

500 µL 1-Thioglycerol in LBA Buffer (Promega, Madison, US) was added to a piece of RV tissue weighing ~20 mg. Two 5mm stainless steel beads were added, and the tissue homogenised using the Tissue Lyser II followed by pipetting 7-10 times to shear the DNA. The samples were centrifuged at 14,000g for 3 minutes to pellet tissue debris, and the supernatant was transferred to a clean Eppendorf tube. 500 µL RNA Dilution Buffer was added, and the samples were mixed by vortexing for 10 seconds then incubated for 1 minute at room temperature. The samples were centrifuged at 10,000g for 3 minutes at room temperature to pellet insoluble debris. The cleared lysates were transferred to a clean Eppendorf tube and used for RNA extraction.

2.8.3 RNA Extraction

2.8.3.1 RNA Extraction from Cell Lysates

RNA was extracted using the RNeasy® Mini Kit (Qiagen, UK). Samples were defrosted on ice then homogenized by vortex mixer. The samples were incubated at room temperature for 5 minutes, then 140 µL chloroform (Qiagen, UK) was added as a phase separation reagent for differential extraction of RNA. The samples were shaken vigorously for 15 seconds, incubated at room temperature for 2-3 minutes, then centrifuged at 12,000g and 4°C for 15 minutes for phase separation. The upper aqueous phase mainly contains RNA, and the interphase and lower organic phase contains DNA, proteins, and lipids. The upper aqueous phase was transferred to a new RNase-free Eppendorf tube, and 525 µL 100% ethanol was added to precipitate the RNA. 700 µL sample was added to the RNeasy® Mini column in a collection tube, which was centrifuged at 8000g for 15 seconds at room temperature, then the flow-through was discarded. This was repeated with the remainder of the sample to ensure all the RNA was on the column.

DNase digestion was performed to prevent co-amplification of genomic DNA at the polymerase chain reaction (PCR) stage, which can confound measurement of gene expression by qRT-PCR. All centrifugation steps from this point were carried out at room temperature. 350 µL Buffer RW1 (Qiagen, UK) was added to the RNeasy® column, which was centrifuged at 8000g for 15 seconds and the flow-through discarded. For each sample, 80 µL DNase incubation mix (10 µL DNase I stock solution (Qiagen, UK) and 70 µL Buffer RDD (Qiagen, UK)) was added to the column and incubated at room temperature for 15 minutes. A further 350 µL Buffer RW1 was added to the column. This was centrifuged at 8000g for 15 seconds, and the flow-through discarded.

700 µL Buffer RWT (Qiagen, UK) was added to the RNeasy® Mini column, which was centrifuged at 8000g for 15 seconds and the flow-through discarded. 500 µL Buffer RPE (Qiagen, UK) was added to the column, which was centrifuged at 8000g for 15 seconds and the flow-through discarded. A further 500 µL Buffer RPE was added to the column and centrifuged at 8000g for 2 minutes. The column was placed into a new 2 mL collection tube, and briefly centrifuged to further dry the

membrane. The RNeasy® Mini column was transferred to an RNase-free 1.5 mL Eppendorf tube. 30 µL RNase-free water (Qiagen, UK) was pipetted directly onto the membrane, which was centrifuged at 8000g for 1 minute to elute the RNA. The RNA was stored at -80°C.

2.8.3.2 RNA Extraction from Lung Tissue

RNA extractions from lung tissue were carried out by Dr Smriti Sharma. RNA was extracted using the RNeasy® Mini Kit as per 2.8.3.1.

2.8.3.3 RNA Extraction from Right Ventricle Tissue

RNA extractions from RV tissue were carried out by Dr Smriti Sharma. RNA was extracted using the ReliaPrep™ RNA Tissue Miniprep System (Promega, Madison, US) protocol for fibrous tissue. 340 µL 100% isopropanol was added to the RV tissue lysate, and the samples vortex mixed for 5 seconds. 700 µL lysate was transferred to a Reliaprep™ Minicolumn and centrifuged at 14,000g for 1 minute at room temperature. The flow-through was discarded, and this was repeated to place the remainder of the sample on the column. 500 µL RNA Wash Solution was added to the column. The samples were centrifuged at 14,000g for 30 seconds, and the flow-through was discarded.

The DNase I incubation mix was prepared by combining (in this order) the following amount of each reagent per sample: 24 µL Yellow Core Buffer, 3 µL 0.09M $MnCl_2$, and 3 µL DNase I enzyme. This was mixed by gentle pipetting. 30 µL DNase I incubation mix was added directly to the membrane, and the samples left for 15 minutes at room temperature. 200 µL Column Wash Solution was added, and the samples centrifuged at 14,000g for 15 seconds. 500 µL RNA Wash Solution was added, the samples centrifuged at 14,000g for 30 seconds and the flow-through discarded. The column was placed in a new collection tube. 300 µL RNA Wash Solution was added, the samples centrifuged at high speed for 2 minutes and the flow-through discarded. The column was transferred into a 1.5 mL Elution Tube, 30

µL RNase-free water added, and centrifuged at 14,000g for 1 minute to elute the RNA. The RNA samples were stored at -80°C.

2.8.4 Reverse Transcription of cDNA

.

Complementary deoxyribose nucleic acid (cDNA) was reverse transcribed from RNA using an Applied Biosystems™ High-Capacity cDNA Reverse Transcription Kit (Applied Biosystems, UK). The RNA samples and cDNA kit were defrosted on ice. The RNA concentration, A260/A280, and A260/A230 ratios of the samples were measured using a NanoPhotometer® N60 (Implen, Munich, Germany). 500 ng RNA was added to a 40 µL reverse transcription reaction. The reagent master mix per reaction was made up as follows:

Master Mix:	**1x40µL Reaction**
10X RT Buffer:	4µL
25 mM $MgCl_2$:	8.8µL
dNTPs	8µL
Random hexamers:	2µL
RNase inhibitor:	0.8µL
MultiScribe™ RT:	1µL
Total RNA + RNase-free Water:	15.4 µL

10X RT Buffer (Applied Biosystems™, UK) maintains a favourable pH and ionic strength for the reaction. Magnesium chloride ($MgCl_2$; Applied Biosystems™, UK) acts as a catalyst. Deoxyribonucleotide triphosphates (dNTPs; Applied Biosystems™, UK) ensure proficient reverse transcription. Random hexamers (Applied Biosystems™, UK) are short oligodeoxyribonucleotides of random sequence which serve as primers for cDNA synthesis by annealing to random complementary sites on the target RNA. RNase inhibitor (Applied Biosystems™, UK) prevents RNA degradation. MultiScribe™ RT (Applied Biosystems™, UK) is a

recombinant Moloney murine leukaemia virus DNA polymerase that uses single-stranded RNA as a template in the presence of a primer to synthesise cDNA.

The master mix for all samples plus excess was made up in an RNase-free Eppendorf tube and added to a 96-well PCR plate. The RNA and RNase-free water were added to each well, and the plate was sealed and briefly centrifuged to ensure all the samples were at the bottom of the well. A 45-minute PCR reaction was carried out in a Venti 96-Well Fast Thermocycler (Applied Biosystems™, UK) as follows: 25°C for 10 minutes, 48°C for 30 minutes, 95°C for 5 minutes, then 4°C as required until the plate was removed. The cDNA was stored at -20°C.

2.8.5 Quantitative Real-Time Polymerase Chain Reaction

TaqMan probes (Tables 2.1-2.3; ThermoFisher, UK) and cDNA preparations were defrosted on ice. All TaqMan probes were labelled with a FAM™ dye. A master mix for each gene was prepared as follows: 5 µL TaqMan master mix (Applied Biosystems™, UK), 3 µL RNase-free water, 0.5 µL probe per reaction. 8.5 µL master mix per well was added to a 384-well plate. 1.5 µL of each cDNA sample was added to two or three wells (i.e., the reaction was carried out in duplicate or triplicate). RNase-free water was used as a non-thermocycler control. The plate was briefly centrifuged to ensure all samples were at the bottom of the well. Using a ViiA™ 7 Real-Time PCR System (Applied Biosystems™, UK), the following PCR programme was run: 50°C for 2 minutes, 95°C for 10 minutes, then 40 cycles of 95°C for 10 seconds and 60°C for 1 minute. β-actin (*Actb*) was selected as the housekeeping gene for all studies, as initial experiments found it to be stable in rPASMCs, hPASMCs and tissue samples, and other studies have found it to remain stable under hypoxic conditions[328,329].

Gene expression was calculated relative to β-actin using the ΔΔCT method in Microsoft Excel, then plotted using GraphPad Prism. Distribution of data was assessed using Shapiro-Wilk test, and analysis was carried out using unpaired t-test, Mann-Whitney test, one-way ANOVA with Tukey post-hoc test, or one-way ANOVA with Kruskal-Wallis test as appropriate.

Table 2.1: List of TaqMan mRNA Primers Used in Rat Samples

Gene	TaqMan Assay ID
Actb	Rn00667869_m1
Bmpr2	Rn01437214_m1
Col1a1	Rn01463848_m1
Col3a1	Rn01437681_m1
Comt	Rn00561037_m1
Cyp1a1	Rn00487218_m1
Cyp1a2	Rn00561082_m1
Cyp1b1	Rn04219389_g1
Cyp19a1	Rn01422547_m1
Esr1	Rn01640372_m1
Esr2	Rn00562610_m1
Gper1	Rn01643280_m1
Hk2	Rn00562457_m1
Hsd17b1	Rn00563388_g1
Hsd17b2	Rn00577779_m1
Id1	Rn00562985_s1
Id2	Rn01495280_m1
Id3	Rn00564927_m1
Smad1	Rn00565555_m1
Smad2	Rn00569900_m1
Smad3	Rn00565331_m1
Smad4	Rn00570593_m1
Smad5	Rn00572484_m1
Smad6	Rn01766978_m1
Smad7	Rn01523958_m1
Smad9	Rn00594023_m1

Table 2.2: List of TaqMan mRNA Primers Used in Mouse Samples

Gene	TaqMan Assay ID
Actb	Mm00667939_s1
Bmpr2	Mm00432134_m1
Col1a1	Mm00801666_g1
Col3a1	Mm00802300_m1
Id1	Mm00775963_g1
Id2	Mm00711781_m1
Id3	Mm00492575_m1
Smad1	Mm00484723_m1
Smad2	Mm00487530_m1
Smad3	Mm01170760_m1
Smad4	Mm03023996_m1
Smad5	Mm01341607_g1
Smad6	Mm00484738_m1
Smad7	Mm00488363_m1
Smad9	Mm00649885_m1
Sox17	Mm00488363_m1

Table 2.3: List of TaqMan mRNA Primers Used in Human Samples

Gene	TaqMan Assay ID
ACTB	Hs01060665_g1
BMPR2	Hs00176148_m1
ID1	Hs00357821_g1
ID2	Hs00747379_m1
ID3	Hs00954037_g1
SMAD1	Hs00195432_m1
SMAD2	Hs00998187_m1
SMAD3	Hs00969210_m1
SMAD4	Hs00232068_m1
SMAD5	Hs00195437_m1
SMAD6	Hs00178579_m1
SMAD7	Hs00998193_m1
SMAD9	Hs00931723_m1

2.9 Protein Analysis

2.9.1 Solubilisation and Preparation of Protein

For *in vitro* experiments, rPASMCs were cultured and subcultured in 100 mm dishes as per 2.2.4. and 2.2.5. rPASMCs were quiesced for 24 hours as per 2.5.2, then stimulated with 10 nM 16OHE2 in the presence or absence of a 1 μM concentration of the estrogen receptor antagonists MPP, PHTPP, and G15 for 48 hours in phenol red-free DMEM containing 1% FBS. Protein was also collected from untreated male and female rPASMCs. The media was aspirated, the cells washed with 10 mL PBS, and 1.5 mL tryspin added per dish. The cells were incubated for 7 minutes until detached. 3 mL PBS was added, and the cell suspension taken up into a Falcon tube. The culture dish was rinsed twice with a further 3 mL PBS to collect any remaining cells. A further 4 mL PBS was added to the Falcon tube to dilute the trypsin. The cell suspension was centrifuged at 1500 rpm for 5 minutes to pellet the cells, and the supernatant was aspirated. The cell pellets were either lysed immediately by repeatedly pipetting up and down in 100-200 μL of a 1:100 solution of Halt Protease Inhibitor Cocktail (ThermoFisher Scientific, UK) in Pierce® RIPA Buffer (Pierce, ThermoFisher, US), or frozen at -20°C until lysis. Following lysis, the protein solutions were transferred to pre-chilled 1.5 mL Eppendorf tubes, left on ice for 20 minutes, and mixed every 5 minutes by pipetting up and down 20 times. The protein solutions were then centrifuged at 14,000g for 20 minutes at 4°C to remove any cell debris. The supernatant was transferred into a further pre-chilled 1.5 mL Eppendorf tube, and the protein solutions stored at -80°C.

Alternatively, when extracting protein from C57BL/6 mouse lung tissue, a piece of frozen tissue weighing ~20 mg was placed in a pre-chilled 2 mL Eppendorf tube containing 300-400 μL of 1:100 Halt Protease Inhibitor Cocktail in T-PER™ Tissue Protein Extraction Reagent (ThermoFisher Scientific, UK) on ice. Two 5 mm stainless steel beads were added, and the tissue homogenised using the Tissue Lyser II. Tissue samples were then centrifuged at 10,000 rpm for 10 minutes at 4°C to pellet debris. The supernatant (solubilised protein) was placed in a pre-chilled 1.5 mL Eppendorf tube and stored at -80°C.

2.9.2 Bicinchoninic Acid Assay

Protein samples were defrosted on ice. The bicinchoninic acid (BCA) assay (Pierce, ThermoFisher, US) was used to determine the protein concentration of collected samples. Copper in the reagent mix is reduced by protein, which reacts with BCA to induce a colour change from green to purple. The more protein present, the more intense a purple colour appears. A standard curve was constructed within the 0-2 mg/mL range, using the BSA 2 mg/mL ampoules provided in the BCA kit diluted in Pierce® RIPA Buffer (*in vitro* studies) or T-PER™ Tissue Protein Extraction Reagent (*in vivo* studies). Protein samples were diluted 1:4 in Pierce® RIPA Buffer or T-PER™ Tissue Protein Extraction Reagent prior to BCA assay to ensure that protein concentrations were within the standard range. 10 µL of each standard and protein sample was added to two wells of a 96-well plate. The required volume of BCA working solution was prepared by adding 50 parts Reagent A: 1 part Reagent B. 200 µL working solution was added to each well, and the 96-well plate was protected from light by wrapping in foil and incubated at room temperature for 30 minutes. The plate was read at 560 nm using a GloMax Explorer microplate reader (Promega, Madison, US). Protein concentration was then evaluated against the standard curve using Microsoft Excel. A representative standard curve is show in Figure 2.4.

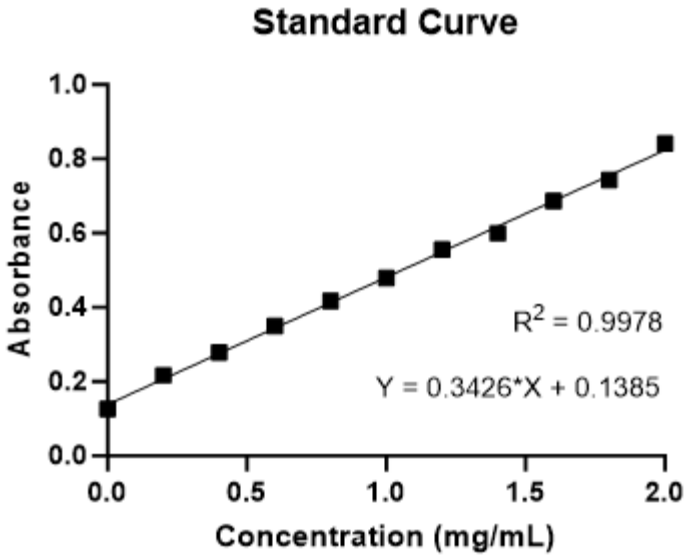

Figure 2.4: Standard curve for bicinchoninic acid protein assay.
A representative standard curve obtained for bovine serum albumin solution (0-2 mg/mL) using the bicinchoninic acid protein assay. Samples were performed in duplicate.

2.9.3 Sodium Dodecyl Sulfate Polyacrylamide Gel Electrophoresis

Protein samples were defrosted on ice. Samples were diluted with RNase-free water to contain equal amounts of protein either to a specific loading amount (10-25 µg) or to the sample of lowest concentration. NuPAGE Sample Reducing Agent (Invitrogen, UK) and NuPAGE Lithium Dodecyl Sulfate (LDS) Sample Buffer (Invitrogen, UK) were added. LDS enhances the activity of the reducing agent, and the sample buffer contains a blue dye for visualisation when loading gels. Samples were heated at 70-85°C for 10 minutes in a heat block to denature and reduce protein disulfide bonds, unfolding the proteins to allow efficient antibody binding. Samples were loaded on to NuPAGE™ Bis-Tris 4-12% Polyacrylamide Gels (Invitrogen, UK) and separated according to protein size using electrophoresis under constant voltage in NuPAGE™ MES running buffer (Invitrogen, UK) containing 0.1% v/v NuPAGE™ Antioxidant – 150V for 1.5 hours for *in vitro* studies and 110V for 2 hours for lung tissue samples. For the small inhibitor of DNA-binding (ID) proteins, gel electrophoresis was run at 150V for 50 minutes in NuPAGE™ MOPS running buffer (Invitrogen UK) with 0.1%

v/v antioxidant. The antioxidant prevents reoxidation of reduced proteins during gel electrophoresis and protein transfer. SeeBlue™ Plus2 Pre-Stained Protein Standard (Invitrogen, UK) was used as the protein ladder to determine approximate protein size.

2.9.4 Protein Transfer

Dry transfer of proteins was attempted using a Trans-Blot Turbo Transfer System (Supplemental Methods 8.3), but wet transfer was found to be more effective for the small amounts of protein available from cells. Once adequate protein separation according to weight was achieved, the proteins were transferred onto a 0.45 µm polyvinylidene difluoride (PVDF) membrane (Pierce®, ThermoFisher Scientific, UK). For the small ID proteins, 0.2 µm PVDF membrane (Amersham™ Hybond™, Cytiva, Marlborough, US) was used. Proteins were transferred in an XCell SureLock™ Mini-Cell and XCell II™ Blot Module wet transfer system (Invitrogen, UK). As PVDF membranes are hydrophobic, the membrane was immersed in 100% methanol for 1 minute prior to use to activate its binding capacity and facilitate effective transfer. A transfer buffer containing 5% v/v Novex® NuPAGE Transfer Buffer 20X (ThermoFisher Scientific, UK) and 20% v/v methanol (100%, VWR International, UK) in distilled water was prepared in advance and placed in the -20°C freezer to cool. For *in vitro* studies, the transfer was run at 40V for 2 hours if transferring two gels or 1.5 hours if transferring one gel. For studies in lung tissue, the transfer was run at 40V for 4 hours with two gels. Transfer efficiency was evaluated by short incubation (<1 minute) in 0.1% w/v Ponceau S stain (Sigma-Aldrich, UK) prepared in 1% v/v acetic acid. The stain was removed by washing the membranes with distilled water then a wash buffer containing 5% v/v 20X Tris-Base Buffered Saline (TBS; ThermoFisher Scientific, UK) with 0.05% v/v Tween-20 (TBST).

2.9.5 Immunoblotting

Membranes were blocked in Superblock™ T20 (TBS) Blocking Buffer (ThermoFisher Scientific, UK) for 1 hour at room temperature to minimise non-specific antibody binding. The primary antibody to detect a specific protein was diluted in 3-10 mL 10% Superblock™ T20 (TBS) Blocking Buffer in TBS or TBST (unless stated otherwise in Table 2.4) in a 50 mL Falcon tube. The membrane was placed inside the tube on a roller overnight in the cold room. After a quick rinse, the membranes were washed 3x10 minutes with TBST on a shaker to remove any unbound primary antibody before incubating in a secondary antibody conjugated with horseradish perioxidase (HRP) prepared in 10% Superblock™ T20 (TBS) Blocking Buffer in TBST for 1 hour at room temperature. After a quick rinse, the membrane was washed 1x10 minutes in TBST and 2x10 minutes in TBS.

In preliminary experiments, antibody binding was detected using an Odyssey® M Imaging System (LI-COR Inc., Lincoln, US; Supplemental Methods 8.4). However, SuperSignal™ West Pico PLUS Chemiluminescent Substrate (ThermoFisher Scientific, UK) was used in subsequent experiments. The secondary antibodies were conjugated with HRP, which catalyses the oxidation of luminol present in the chemiluminescence substrate. The light emitted during the reaction was captured on CL-XPosure™ Film (ThermoFisher Scientific, UK) using a JPI JP 33 X Ray Processor (Raytech Diagnostics, Ottawa, Canada), allowing protein band visualisation.

The membranes were then washed 1x5 minutes with TBST, and the bound antibodies removed by incubating in Restore™ PLUS Western Blot Stripping Buffer (ThermoFisher Scientific, UK) for 15 minutes on a shaker. The membranes were washed 1x5 minutes with TBST to remove the stripping buffer before re-probing for another protein of interest or the loading control. Densitometry was quantified using CLIQS 1D, Version 1.5.170 (TotalLab, UK) and data were analysed in GraphPad Prism. Normal distribution was confirmed using Shapiro-Wilk test and analysis was carried out using unpaired t-test.

Table 2.4: List of Primary Antibodies Used for Immunoblotting

Antibody	Supplier	Antibody Dilution	Detected Band Size
β-Actin (mouse pAb)	Sigma A5441	1: 20,000 10% blocking buffer in TBS	42 kDa
β-Tubulin (rabbit pAb)	Abcam ab6046	1:3000 10% blocking buffer in TSBT	50 kDa
BMPR2 (mouse pAb)	BD Biosciences 612292	1:200 SuperSignal™ Primary Antibody Diluent	130 kDa
BMPR2 (rabbit pAb)	Abcam ab96826	1:3000 10% blocking buffer in TBST	115 kDa
ESR1 (mouse pAb)	Atlas AMAb90867	1:1000 10% blocking buffer in TBS	62 kDa
ESR2 (rabbit pAb)	Invitrogen PA1-311	1:1000 10% blocking buffer in TBS	60 kDa
Id1 (mouse pAb)	Santa Cruz sc-133104	1:300 10% blocking buffer in TBS	15 kDa
p-Smad1,5,9 (rabbit pAb)	Cell Signaling 13820	1:1000 4% BSA in TBST	60 kDa
p-Smad1,5,9 (rabbit pAb)	Abcam ab76296	1:3000 10% blocking buffer in TBST	52 kDa
Smad1 (mouse pAb)	Santa Cruz sc-81378	1:500 4% BSA in TBST	52-56 kDa
Smad1 (rabbit pAb)	Abcam ab633356	1:2000 10% blocking buffer in TBST	60 kDa

Tissue lysates collected from untreated Sprague-Dawley rats for a previous study by the MacLean group were used as positive controls for immunoblotting (Table 2.5).

Table 2.5: List of Positive Controls Used for Immunoblotting

Protein	Positive Control
BMPR2	Rat lung lysate
ESR1	Rat testis lysate
ESR2	Rat testis lysate

2.9.6 Enhancing the Signal of Bone Morphogenetic Protein Receptor 2

Expression of bone morphogenetic protein receptor 2 (BMPR2) is very weak. As immunoblotting for BMPR2 was unsuccessful during *in vitro* studies where <20 µg protein was available for loading, an attempt was made to increase the chemiluminescent signal using a SuperSignal™ Western Blot Enhancer kit (ThermoFisher Scientific, UK). Sodium dodecyl sulfate polyacrylamide gel electrophoresis and protein transfer were carried out as per 2.9.3 and 2.9.4. The blots were rinsed then washed for 2 minutes with distilled water. Ponceau S stain was not used as this can interfere with signal enhancing. The membrane was covered with 10 mL SuperSignal™ Western Blot Enhancer, and the blots incubated for 10 minutes at room temperature on a shaker. The blots were rinsed 5 times with distilled water, then incubated in SuperSignal™ Blocking Buffer for 1 hour. The blots were rinsed with TBST three times, then washed for 5 minutes on a shaker. The blots were incubated in the primary antibody and immunoblotting continued as per 2.9.5.

Chapter 3

The Functional Effects of 16α-Hydroxyestradiol *In Vitro*

3.1 Introduction

Female sex is a significant risk factor for pulmonary arterial hypertension (PAH), with up to four-fold more women developing PAH than men[27]. This suggests that female sex hormones may mediate pathological effects. Circulating estradiol (E2) levels are higher in male and postmenopausal female PAH patients compared to control subjects, and are associated with worse disease outcomes[30,31]. PAH is characterised by remodelling of the pulmonary arterial wall, leading to increased pulmonary vascular resistance, vessel obstruction, and maladaptive right ventricular (RV) hypertrophy and failure[6]. Two key mechanisms of vessel remodelling are proliferation and migration of smooth muscle and endothelial cells[6]. Adventitial fibroblasts are also activated in response to vascular stress (e.g., hypoxia) and undergo phenotypic changes including (but not limited to) proliferation, differentiation, and release of reactive oxygen species (ROS) and pro-inflammatory cytokines[79]. The cytokines (e.g., interleukin-6) stimulate recruitment and retention of circulating progenitor and inflammatory cells (particularly macrophages) to the vessel wall[79]. Many additional precipitating factors (or 'second hits') contribute to the pathogenesis of PAH including genetic susceptibilities (e.g., bone morphogenetic protein receptor 2 (BMPR2) mutation), exposure to certain drugs (e.g., fenfluramines), connective tissue disease, and hypoxia[4,130,140].

Estrogen receptor-alpha (ERα) is overexpressed in the pulmonary artery smooth muscle cells (PASMCs) of female PAH patients[102]. Wright et al. observed that E2 increases proliferation of female PAH patient hPASMCs via ERα[102]. CYP1B1 plays a key role in metabolism of E1 and E2 to the 16α-hydroxyestrogens (Figure 1.4) and is overexpressed in the pulmonary arteries of idiopathic and hereditary PAH patients[35]. The CYP1B1 antagonist TMS attenuated E2-induced proliferation in female hPASMCs, and this inhibitory effect was 100-fold more potent in hPASMCs isolated from PAH patients compared to control subjects[35]. The estrogen metabolite 16α-hydroxyestrone (16OHE1) is known to be mitogenic[35,311]. 16OHE1 increases proliferation of male and female hPASMCs and male mouse PASMCs via ERα and Nox-1 generated ROS[35,311]. On the other hand, 2-methyoxyestradiol (2ME2) is known to be protective and decreases proliferation of female control subject hPASMCs[299]. This has led to the hypothesis that a shift from the protective 2-hydroxylation pathway towards 16α-hydroxylation may mediate PAH[274].

Elevated plasma levels of 16α-hydroxyestradiol (16OHE2) were recently observed in female idiopathic PAH patients, and in males and females with portopulmonary PAH[241,317]. 16OHE2 is predominant during pregnancy and increases proliferation of MCF-7 and T-47D estrogen receptor-positive breast cancer cells, but little is known about its function in PAH[314,330]. In a preliminary study, 16OHE2 increased proliferation of female PAH patient hPASMCs and migration of blood outgrowth endothelial cells (BOECs) from both male and female PAH patients[241]. BOEC migration was attenuated by the nuclear factor erythroid 2-related factor 2 (NRF2)-activator bardoxolone methyl, suggesting that 16OHE2-induced migration may be dependent on redox signalling[241]. This suggests that 16OHE2 may mediate pathogenic effects in PAH[241]. Here, we investigate the functional effects of 16OHE2 *in vitro*.

Aims of this chapter:

1. To characterise the effects of 16OHE2 on proliferation of Dede hamster lung fibroblasts, rat pulmonary artery smooth muscle cells (rPASMCs), and female PAH patient hPASMCs.

2. To investigate the effects of combining 16OHE2 with acute hypoxia as a ‘second hit’ on rPASMC proliferation.

3. To investigate the effects of 16OHE2 on migration of rPASMCs.

3.2 Results

3.2.1 The Effects of 16OHE1 and 16OHE2 on Dede Hamster Lung Fibroblast Proliferation

Proliferation of activated adventitial fibroblasts in response to vascular stress plays a key role in pulmonary vascular remodelling in PAH[79]. As Denver et al. previously observed that 16OHE2 increased proliferation of female PAH patient hPASMCs, we wished to investigate whether this would be the case in fibroblasts[241]. 16OHE1 was also studied. Dede hamster lung fibroblasts, an immortalised cell line derived from female Chinese hamsters, were used for preliminary proliferation studies. Previous studies in hPASMCs have identified the optimal pharmacological concentrations for proliferation as 1 nM 16OHE1 and 10 nM 16OHE2, which are in keeping with physiological concentrations[102,241,311]. In addition, positive and negative controls of phenol red-free DMEM containing 10% and 2% charcoal stripped FBS respectively were used to determine the optimal end time-point for further proliferation studies. 100% ethanol diluted in 2% DMEM to the same concentration of the relevant estrogen metabolite (1 nM or 10 nM) was used as vehicle control. Total cell counts were measured at 2, 6, 24 and 48 hours.

There was no change in proliferation of Dede hamster lung fibroblasts in response to 16OHE1 or 16OHE2 compared to the vehicle control. Dede fibroblast proliferation was significantly increased at 24 hours and further increased at 48 hours by the 10% FBS positive control compared to the 2% FBS control, vehicle control, 16OHE1 and 16OHE2 (Figure 3.1). Therefore, 48 hours was selected as the optimal time point for further proliferation experiments.

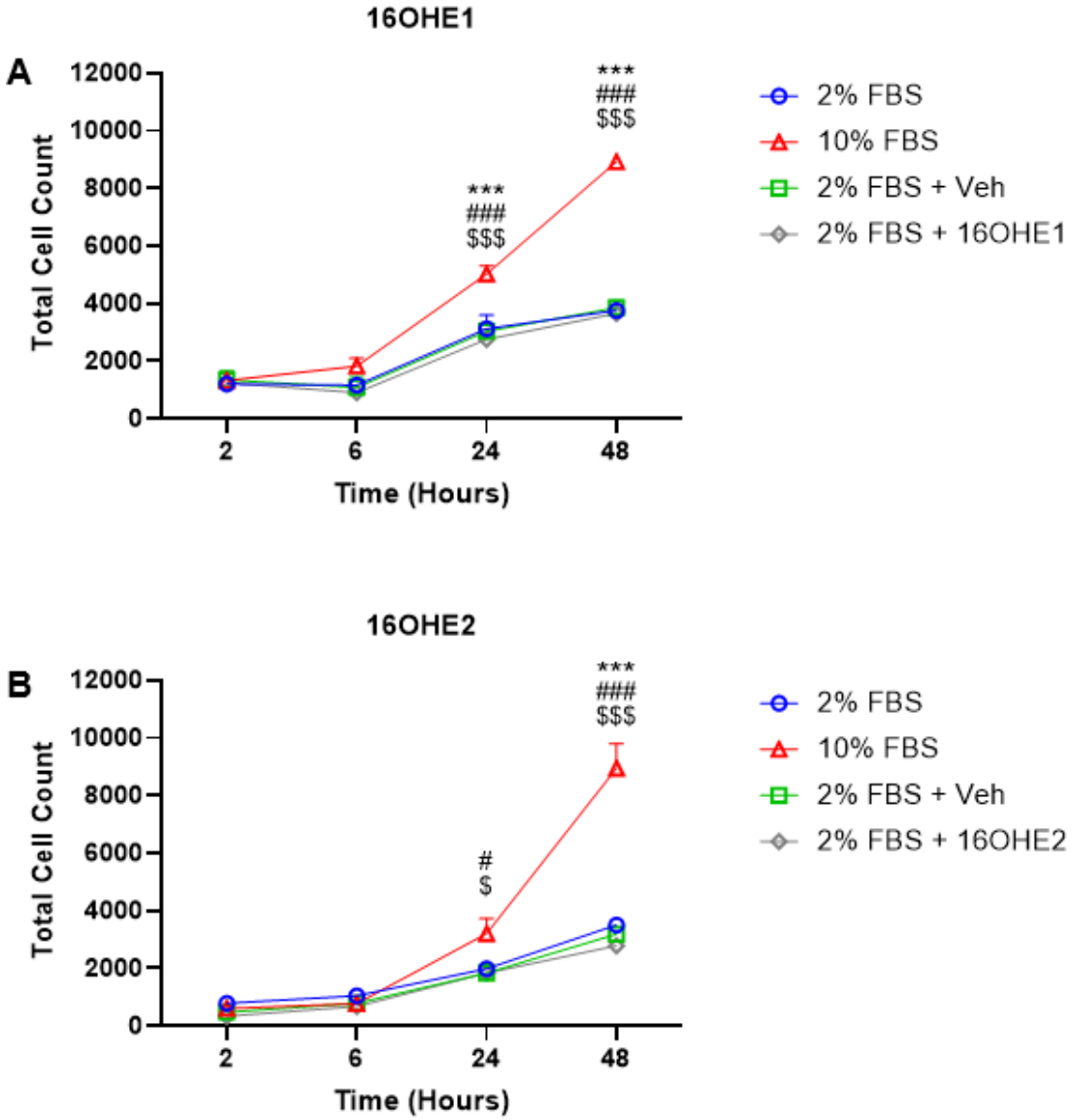

Figure 3.1: Dede hamster lung fibroblast proliferation is not affected by 16OHE1 or 16OHE2. Dede hamster lung fibroblasts were seeded in 6-well plates at $3x10^5$ cells/well, cultured to 50-60% confluency, quiesced for 24 hours (0.5% charcoal stripped fetal bovine serum (FBS)), then stimulated with (A) 1 nM 16α-hydroxyestrone (16OHE1) and controls. (B) 10 nM 16α-hydroxyestradiol (16OHE2) and controls. Experiments were carried out in the presence of 2% charcoal stripped FBS in phenol red-free Dulbecco's Modified Eagle Medium. Veh = vehicle (1 nM or 10 nM ethanol). Total cell counts were assessed at 2, 6, 24, and 48 hours by Countess automated cell counter. Data are expressed as ±SEM and analysed by two-way ANOVA with post-hoc Tukey test. ***$p<0.001$ (2% FBS vs. 10% FBS); #$p<0.05$, ###$p<0.001$ (veh vs. 10% FBS); $$p<0.05$, $$$$p<0.001$ (16OHE1 (A) or 16OHE2 (B) vs. 10% FBS). n=4-8.

3.2.2 Phenotype of Cells Derived from Rat Pulmonary Arteries and Aortae

Previous *in vitro* studies by the MacLean group focused primarily on hPASMCs. However, as the supply of these ceased during the COVID-19 pandemic, most of this work focuses on rPASMCs. The hPASMCs used in this project were isolated from the small distal pulmonary arteries of PAH patients and control subjects and are provided by Professor Nick Morrell (University of Cambridge, UK) with ethical permission.

All *in vivo* work including euthanasia, tissue harvest, and dissection of the pulmonary artery and aorta was carried out by Dr Hicham Labazi. PASMCs were isolated from healthy young adult male and female Sprague-Dawley rats aged 11-13 weeks and weighing 320-344g (males) or 210-265g (females). Aorta smooth muscle cells (AoSMCs) were isolated from the same rats to investigate whether the molecular effects of 16OHE2 in the pulmonary artery are similar in the aorta (Chapter 4).

The isolated cells were examined by immunocytochemistry to confirm these were of smooth muscle phenotype. α-Smooth Muscle Actin (α-SMA) is highly expressed in smooth muscle cells, whereas vimentin is highly expressed in fibroblasts[331,332]. Human fetal lung fibroblast-1 (HFL-1) cells and a female PAH patient hPASMC line were used as positive controls because their morphology was already known. The characteristics of the hPASMC donor (referred to by the anonymous identifier 113MP) are shown in Table 3.1.

Table 3.1: Characteristics of the Human Pulmonary Artery Smooth Muscle Cell Donor Used for α-Smooth Muscle Actin Positive Control

ID	Sex	Age	Conditions	Medications
113MP	Female	45	PAH associated with congenital heart disease	Unknown

PBS was used as a negative control to detect non-specific antibody binding. For each batch of cells, two slides were prepared per cell line and each slide was imaged in three different locations (i.e., six replicates). The images shown in Figure 3.2 are representative of α-SMA and vimentin immunofluorescence. The pulmonary artery and aorta cells had high expression of α-SMA but low vimentin expression, confirming that they were smooth muscle cells. As predicted, the HFL-1 fibroblasts had high vimentin expression and low α-SMA, and the hPASMCs had high α-SMA expression but low vimentin.

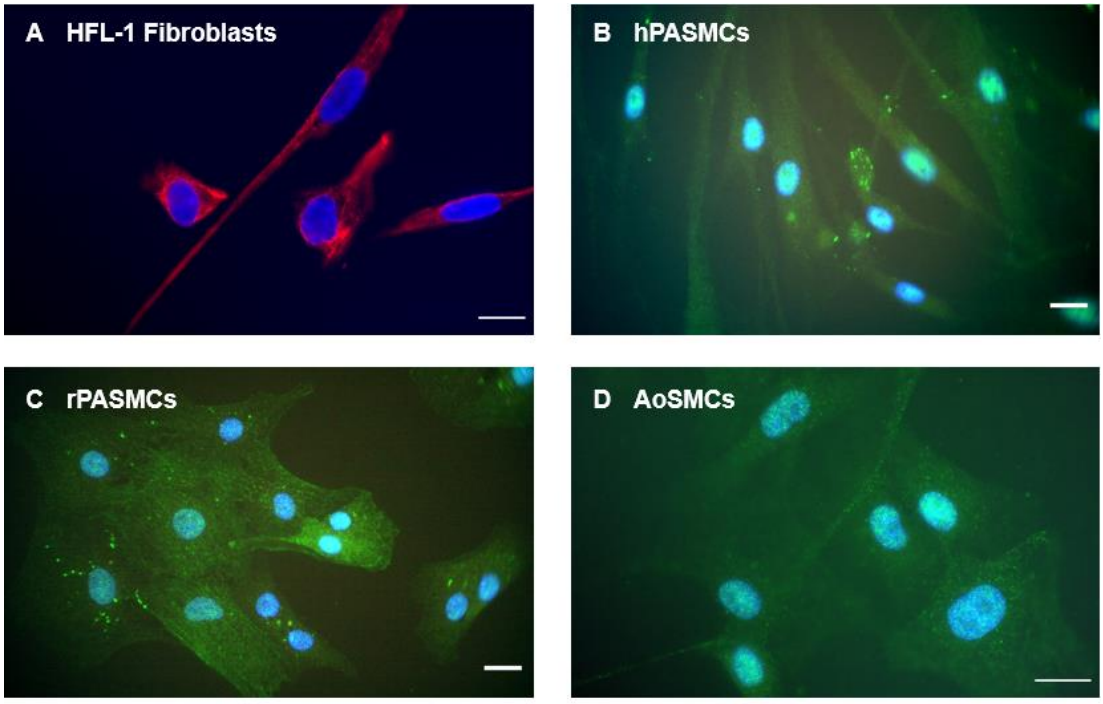

Figure 3.2: Cells derived from rat pulmonary arteries and aortae are smooth muscle cells. Human fetal lung fibroblast-1 (HFL-1) cells, human female pulmonary arterial hypertension (PAH) patient pulmonary artery smooth muscle cells (hPASMCs; passage 8), rat pulmonary artery (passage 3), and rat aorta cells (passage 3) were seeded on to collagen coated coverslips in a 12-well plate at $1x10^5$ cells/well, cultured to 50-60% confluency, and immunocytochemistry carried out as previously described. The nuclear marker DAPI is shown in blue, α-smooth muscle actin (α-SMA) in green, and vimentin in red. Images are representative. (A) Vimentin was strongly expressed in HFL-1 fibroblasts. (B) α-SMA was strongly expressed in female PAH patient hPASMCs. (C) α-SMA was strongly expressed in newly isolated rat pulmonary artery smooth muscle cells (rPASMCs). (D) Newly isolated rat aorta smooth muscle cells (AoSMCs) were positive for α-SMA. Scale bars = 20 μm. n=6.

3.2.3 The Effects of E2, 16OHE1 and 16OHE2 on Rat Pulmonary Artery Smooth Muscle Cell Proliferation in the Presence or Absence of Acute Hypoxia as a 'Second Hit'

Smooth muscle cell proliferation is a key mechanism of pulmonary vascular remodelling in PAH[6]. 1 nM E2 was previously found to increase proliferation of female control subject and PAH patient hPASMCs, as was 1 nM 16OHE1 in male and female hPASMCs and male mouse PASMCs[102,311]. 10 nM 16OHE2 increased proliferation of female PAH patient hPASMCs only[241]. Therefore, we wished to investigate whether these findings would translate to PASMCs isolated from healthy, young adult Sprague-Dawley rats with the intention to further investigate the underlying mechanisms.

No significant difference in proliferation was observed in response to E2, 16OHE1 or 16OHE2 in male or female rPASMCs. However, the cells proliferated in response to the 10% FBS positive control (Figure 3.3 (A, B)). As many additional precipitating factors have been identified in PAH, and increased proliferation in response to 16OHE2 was previously only observed in female PAH patient hPASMCs, it was hypothesised that a 'second hit' with acute hypoxia may enhance the proliferative response of female rPASMCs[241].

72 hours incubation in a hypoxic environment (1% O_2 /5% CO_2 /nitrogen) induced a hypoxic response in female rPASMCs (Figure 3.4). The hypoxic response was determined by examining translocation of hypoxia-inducible factor 1α (HIF1α) from the cytoplasm to the nucleus[293]. Cobalt chloride was used as a positive control as it also stabilises HIF1α, facilitating nuclear translocation under normoxic conditions[333]. HIF1α was present in both the cytoplasm and nucleus under normoxic conditions. Following 72 hours incubation in 1% O_2 or treatment with 200 μM cobalt chloride, HIF1α immunofluorescence was strongly present in the nucleus and weak in the cytoplasm, indicating nuclear translocation (Figure 3.5 (A-C)). The images shown in Figure 3.4 are representative of HIF1α immunofluorescence. As HIF1α degrades quickly upon exposure to normoxia (half-life ~5 minutes), expression of its more stable target gene hexokinase 2 (*Hk2*) was also quantified[321]. *Actb* was selected as a stable housekeeping gene under hypoxic conditions[328,329]. *Hk2* expression significantly increased following 72 hours incubation in 1% O_2 (Figure 3.4 (D)). The basal CT value

of *Hk2* (under normoxic conditions) was 29.6. These results confirm induction of a hypoxic response.

No significant difference in total cell count was observed in response to E2, 16OHE1 or 16OHE2 in male or female rPASMCs under acute hypoxic conditions (Figure 3.3 (C, D)). This contrasted with the hypothesis that a 'second hit' with acute hypoxia may enhance the proliferative response of female rPASMCs[225]. While the male rPASMCs proliferated in response to the 10% FBS positive control under acute hypoxia, there was no significant difference in the female rPASMCs. However, this may be due to high variability in the total cell count.

.

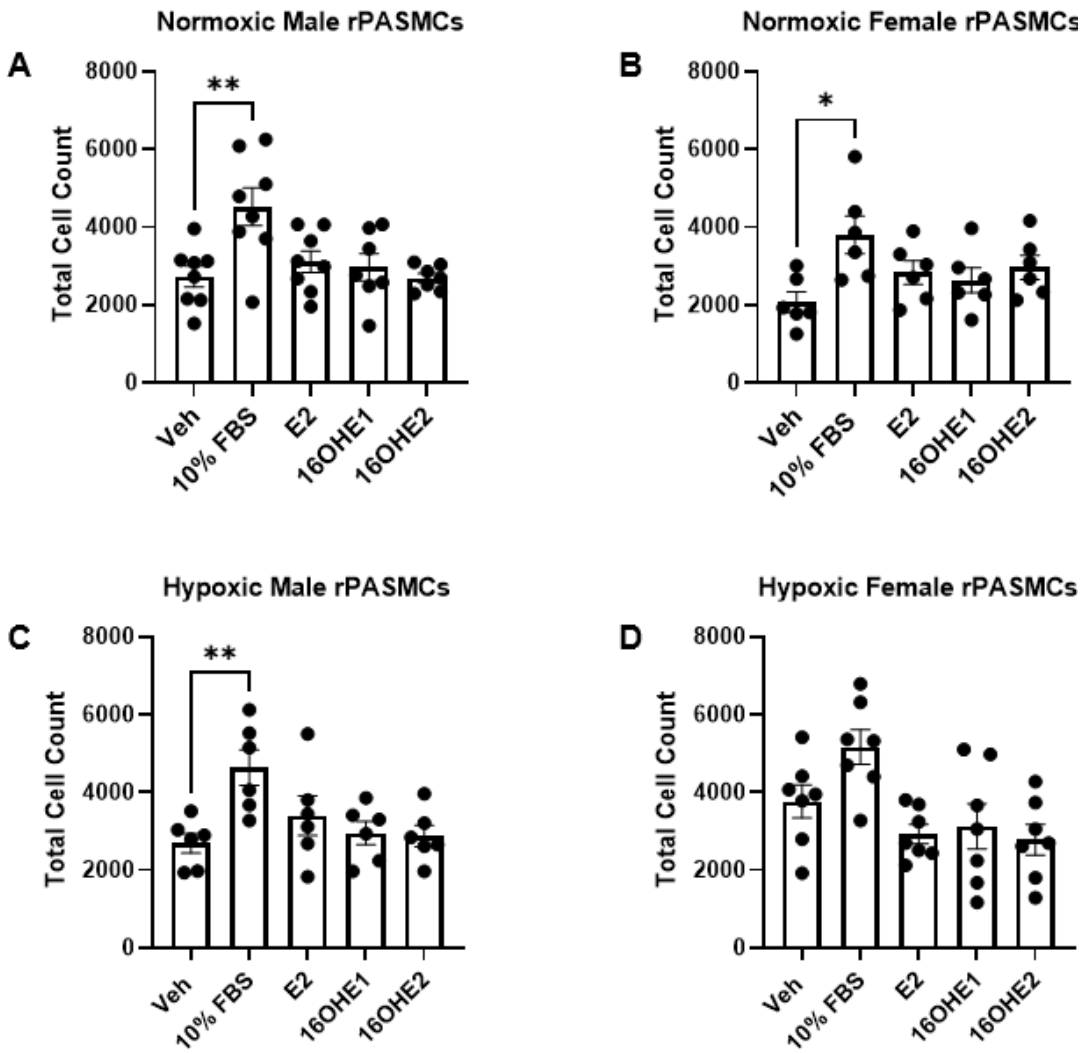

Figure 3.3: The effects of E2, 16OHE1 and 16OHE2 on rPASMC proliferation under normoxic or acute hypoxic conditions (72 hours in 1% O_2).

Rat pulmonary artery smooth muscle cells (rPASMCs) were isolated from male and female Sprague-Dawley rats aged 11-13 weeks and characterised by immunocytochemistry as previously described. rPASMCs were seeded at $3x10^5$ cells/ well (males) or $2x10^5$ cells/well (females) in 6-well plates, cultured to 50-60% confluency, then quiesced (0.2% charcoal stripped fetal bovine serum (FBS)) for 24 hours before stimulation with 1 nM estradiol (E2), 1 nM 16α-hydroxyestrone (16OHE1), 10 nM 16α-hydroxyestradiol (16OHE2), vehicle control (Veh; 10 nM ethanol), or 10% FBS positive control for 48 hours in the presence or absence of 72 hours acute hypoxia (1% O_2/ 5% CO_2/ nitrogen mix). Experiments were carried out in phenol red-free Dulbecco's Modified Eagle Medium (DMEM) in the presence of 1% charcoal stripped FBS. 10 nM ethanol diluted in 1% DMEM was used as the vehicle. Total cell counts were assessed at 48 hours by Countess automated cell counter. (A) Male rPASMCs under normoxic conditions. (B) Female rPASMCs under normoxic conditions. (C) Male rPASMCs under acute hypoxic conditions. (D) Female rPASMCs under acute hypoxic conditions. Data are expressed as ±SEM and analysed by one-way ANOVA with post-hoc Tukey test. *$p<0.05$, **$p<0.01$. n=6-8.

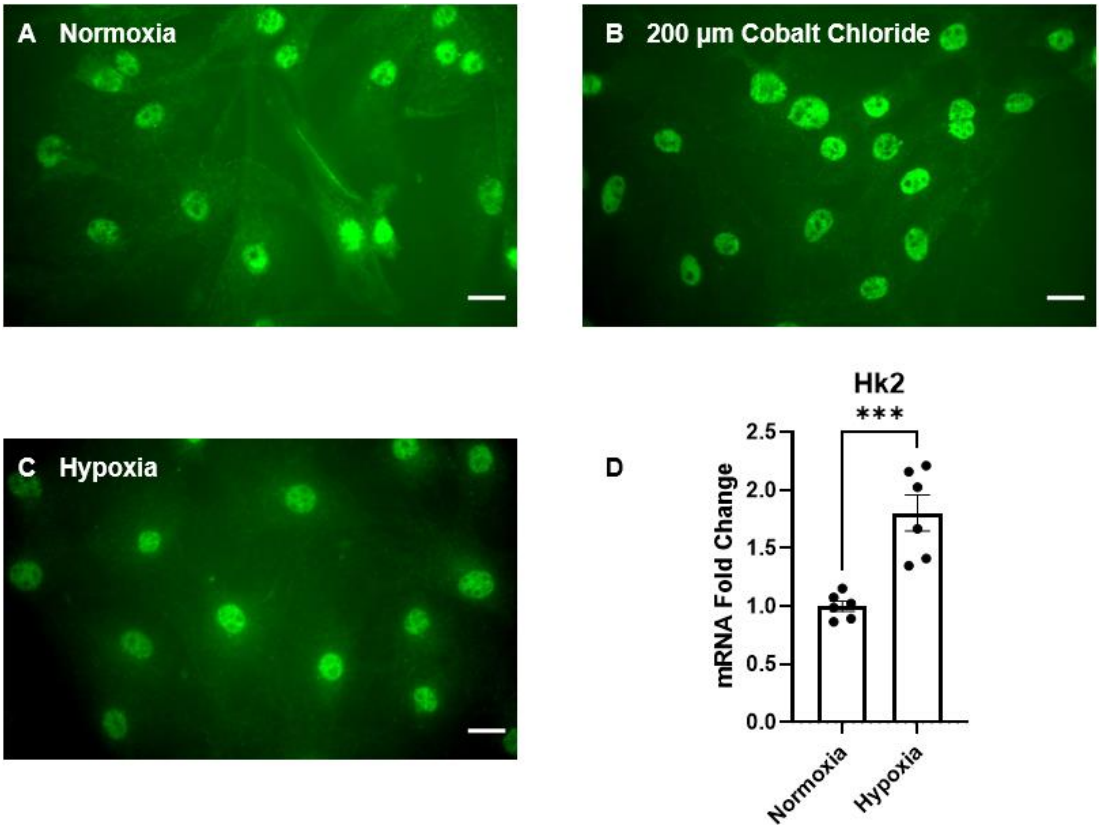

Figure 3.4: 72 hours incubation in 1% O_2 induces a hypoxic response in rPASMCs.
(A-C) Female rat pulmonary artery smooth muscle cells (rPASMCs) at passage 4 were seeded on to collagen coated coverslips in a 12-well plate at $1x10^5$ cells/well, cultured until 50-60% confluent, and immunocytochemistry carried out as previously described. Hypoxia-inducible factor 1α (HIF1α) is shown in green. (A) Under normoxic conditions, HIF1α was expressed in both the cytoplasm and the nucleus. (B) Following 72 hours treatment with 200 µM cobalt chloride, HIF1α expression increased in the nucleus but was weak in the cytoplasm indicating nuclear translocation. (C) Following 72 hours incubation in 1% O_2/ 5% CO_2/nitrogen, HIF1α expression increased in the nucleus and was weak in the cytoplasm indicating nuclear translocation. Images are representative of HIF1α immunofluorescence. Scale bars = 20 µm. (D) Female rPASMCs (passage 4) were seeded into 6-well plates at $3x10^5$ cells/well, cultured until ~70% confluent, and incubated in normoxia or 1% O_2/ 5% CO_2/nitrogen for 72 hours prior to RNA collection. qRT-PCR was carried out as previously described. Fold change was calculated by the ΔΔCT method and is represented as relative to vehicle (where the average vehicle fold change is 1). *Hk2* expression significantly increased following incubation in 1% O_2. Basal *Hk2* CT (normoxia) = 29.6. Data are expressed as ±SEM and analysed by unpaired t-test. *** $p<0.001$. n=6 (technical replicates performed in one female rPASMC cell line).

3.2.4 The Effect of 16OHE2 on Proliferation of Female PAH Patient Pulmonary Artery Smooth Muscle Cells

As a statistically significant increase in proliferation in response to 16OHE2 was not observed in rPASMCs, it was decided to further investigate its effects in female PAH patient hPASMCs when these became available. Denver et al. previously demonstrated that treatment with 10 nM 16OHE2 for 48 hours increased proliferation in these cells[241]. The aim was to replicate these results with the intention to move onto further studies to investigate the underlying mechanism, for example with estrogen receptor antagonists. The characteristics of the human cell donors are shown in Table 3.2. These are referred to by the anonymous internal identifiers 113MP, 117MP, 73MP, and 130MP.

Table 3.2: Characteristics of Female PAH Patient Pulmonary Artery Smooth Muscle Cell Donors

ID	Sex	Age	Conditions	Medications
113MP	Female	45	PAH associated with congenital heart disease	Unknown
117MP	Female	52	PAH associated with septal defect	Unknown
73MP	Female	30	Hereditary PAH (BMPR2^{R899X} mutation)	IV Prostanoids, Warfarin, Zopiclone, Mebeverine, Furosemide
130MP	Female	Unknown	BMPR2 protein-truncating mutation carrier	Unknown

In female PAH patient hPASMCs, total cell count did not significantly change but a wide variation in response to 16OHE2 was noted in line with the heterogeneity of the patients' age and condition. However, the cells proliferated in response to the 10% FBS positive control (Figure 3.5).

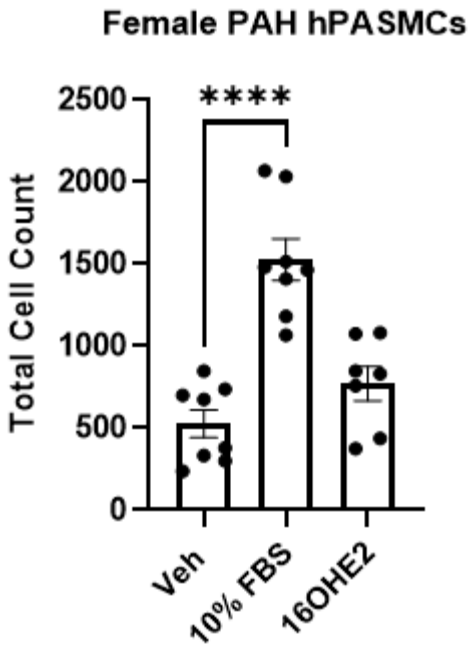

Figure 3.5: The effect of 16OHE2 on proliferation of female PAH patient hPASMCs.
Human pulmonary artery smooth muscle cells (hPASMCs) were seeded in 6-well plates at $2x10^5$ cells/well, cultured to 50-60% confluency, then quiesced for 24 hours (0.2% charcoal stripped fetal bovine serum (FBS) in phenol red-free Dulbecco's Modified Eagle Medium (DMEM)) prior to stimulation with 10 nM 16α-hydroxyestradiol (16OHE2), vehicle control (Veh; 10 nM ethanol) or 10% FBS positive control for 48 hours. Experiments were carried out in phenol red-free DMEM with 1% charcoal stripped FBS. Total cell counts were assessed after 48 hours by Countess automated cell counter. Data are expressed as ±SEM and analysed by one-way ANOVA with post-hoc Tukey test. n=8.

3.2.5 The Effects of 16OHE2 on Migration of Male and Female Rat Pulmonary Artery Smooth Muscle Cells

Cell migration is another key mechanism of pulmonary vascular remodelling in PAH[6]. Denver et al. previously observed that 1 nM 16OHE2 increased migration of BOECs from male and female PAH patients[241]. This was attenuated by the NRF2-activator bardoxolone methyl, suggesting that increased migration may be dependent on redox signalling[241]. However, previous studies have not investigated the effects of 16OHE2 on migration of smooth muscle cells.

A range of concentrations of 16OHE2 from 100 pM to 10 nM were selected. rPASMCs were cultured in 6-well plates until 90-100% confluent. Following 24 hours quiescence, two wounds were created per well of the 6-well plate using a 200 µL pipette tip. Images were taken immediately after stimulation with 16OHE2 or control at 2, 4, 6, 8 and 24 hours. The wound area was measured (Figure 3.6) and the percentage wound area closed analysed as a measure of cell migration (Figure 3.7).

The percentage wound area closed was significantly higher in male and female rPASMCs stimulated with 1 nM 16OHE2 compared to the vehicle control at 8 hours and 24 hours. In male rats, the percentage wound area closed was significantly higher in rPASMCs stimulated with 1 nM 16OHE2 compared to 10 nM 16OHE2 at 24 hours. There were no differences between the vehicle control and 100 pM- or 10 nM 16OHE2 (Figure 3.7). The images shown in Figure 3.6 are representative of cell migration.

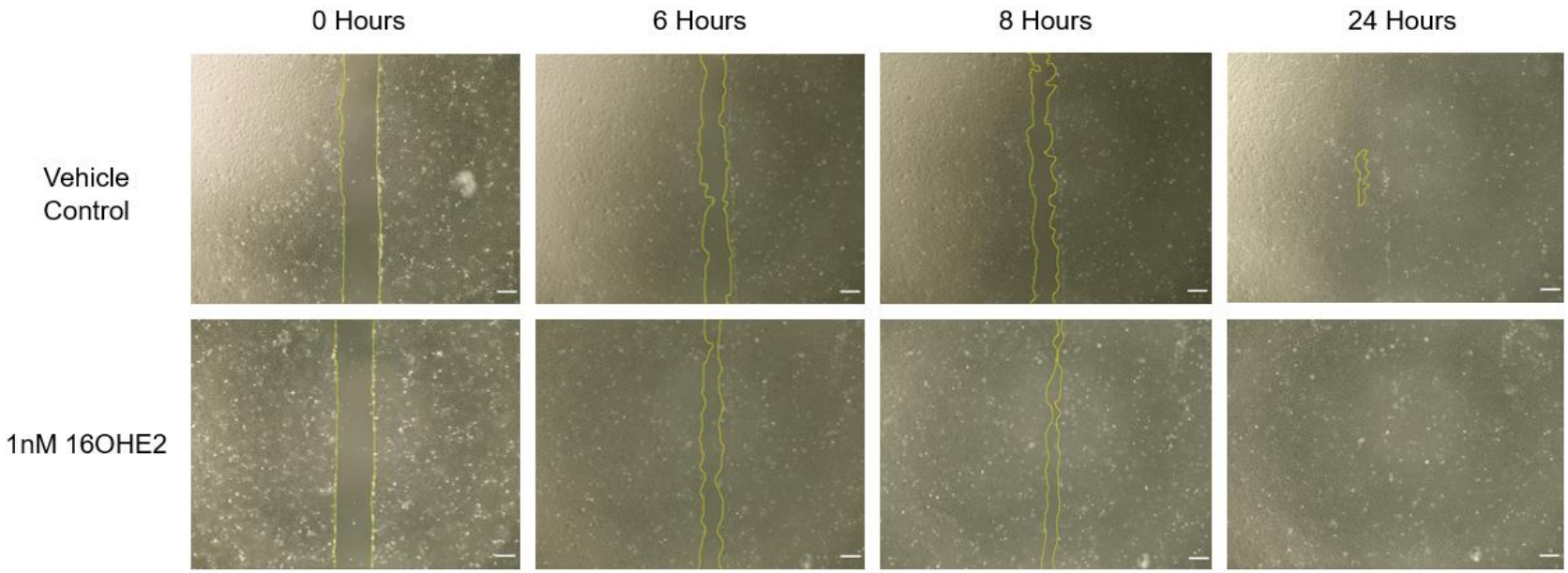

Figure 3.6: Migration is increased in female rPASMCs stimulated with 1 nM 16OHE2 compared to the vehicle.

Female rat pulmonary artery smooth muscle cells (rPASMCs) were seeded in a 6-well plate at $3x10^5$ cells/well, cultured to 90-100% confluency, and quiesced for 24 hours (0.2% charcoal-stripped fetal bovine serum (FBS) in phenol red-free Dulbecco's Modified Eagle Medium (DMEM)). Two wounds were created per well by a 200 µL pipette tip, the cells were washed three times with phosphate buffered saline (PBS), then stimulated with 100 pM, 1 nM, or 10 nM 16α-hydroxyestradiol (16OHE2) or vehicle control (10 nM ethanol). Stimulations were carried out in phenol red-free DMEM with 1% charcoal stripped FBS. Images were taken at 0, 2, 4, 6, 8, and 24 hours at 4X magnification using an EVOS XL Core microscope. Images are representative of cell migration and are female rPASMCs (passage 4). Wound area is highlighted in yellow. Scale bars = 5mm. n=5.

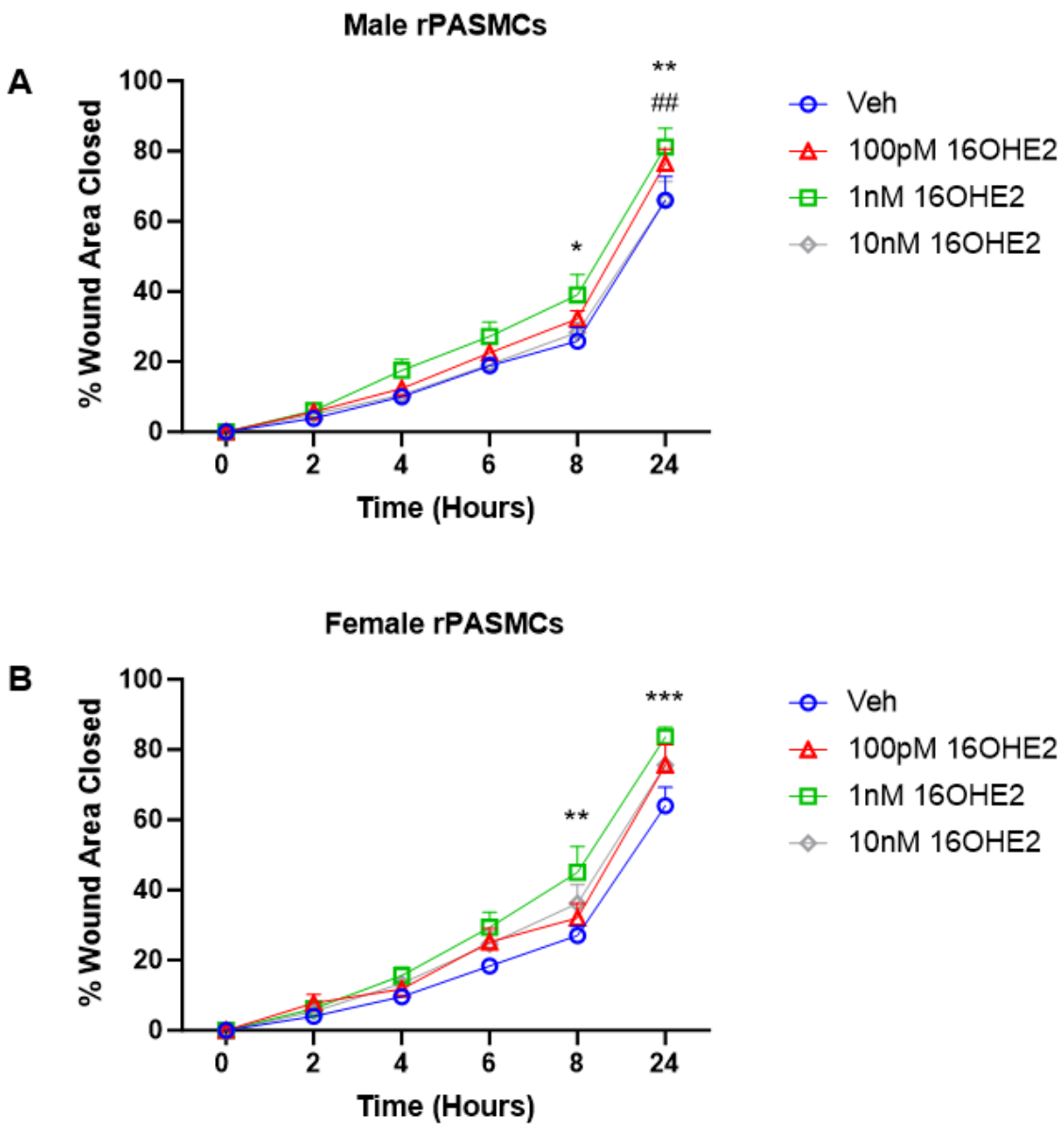

Figure 3.7: Migration of male and female rPASMCs is increased by 1 nM 16OHE2.
Rat pulmonary artery smooth muscle cells (rPASMCs) were seeded in a 6-well plate at $3x10^5$ cells/well, cultured to 90-100% confluency, and quiesced (0.2% charcoal stripped fetal bovine serum (FBS) in phenol red-free Dulbecco's Modified Eagle Medium (DMEM)) for 24 hours. Two wounds were created per well using a 200 µL pipette tip, the cells were washed three times with phosphate buffered saline (PBS), then stimulated with 100 pM, 1 nM, or 10 nM 16α-hydroxyestradiol (16OHE2) or vehicle (Veh; 10 nM ethanol). Stimulations were carried out in phenol red-free DMEM with 1% charcoal stripped FBS. Images were taken at 0, 2, 4, 6, 8, and 24 hours, and the percentage wound area closed calculated as a measure of cell migration. (A) Male rPASMCs. (B) Female rPASMCs. Data are expressed as ±SEM and analysed by two-way ANOVA with post-hoc Tukey test. *p<0.05, **p<0.01, ***p<0.001 (1 nM 16OHE2 vs. Veh); ##p<0.01 (1 nM 16OHE2 vs. 10 nM 16OHE2). n=5-6.

3.2.6 The Effects of E2 and 16OHE1 on Migration of Male Rat Pulmonary Artery Smooth Muscle Cells

As 1 nM 16OHE2 increased migration of male and female rPASMCs, we wished to investigate whether the same concentration of E2 and 16OHE1 would have an effect. Previous data from the MacLean lab showed that 1 nM 16OHE1 did not affect BOEC migration (unpublished). A preliminary study in male rPASMCs (n=3) observed that both 1 nM E2 and 1 nM 16OHE1 significantly increased the percentage wound area closed at 24 hours compared to the vehicle (Figure 3.8). At n=3, 16OHE2 was not significant (Figure 3.8).

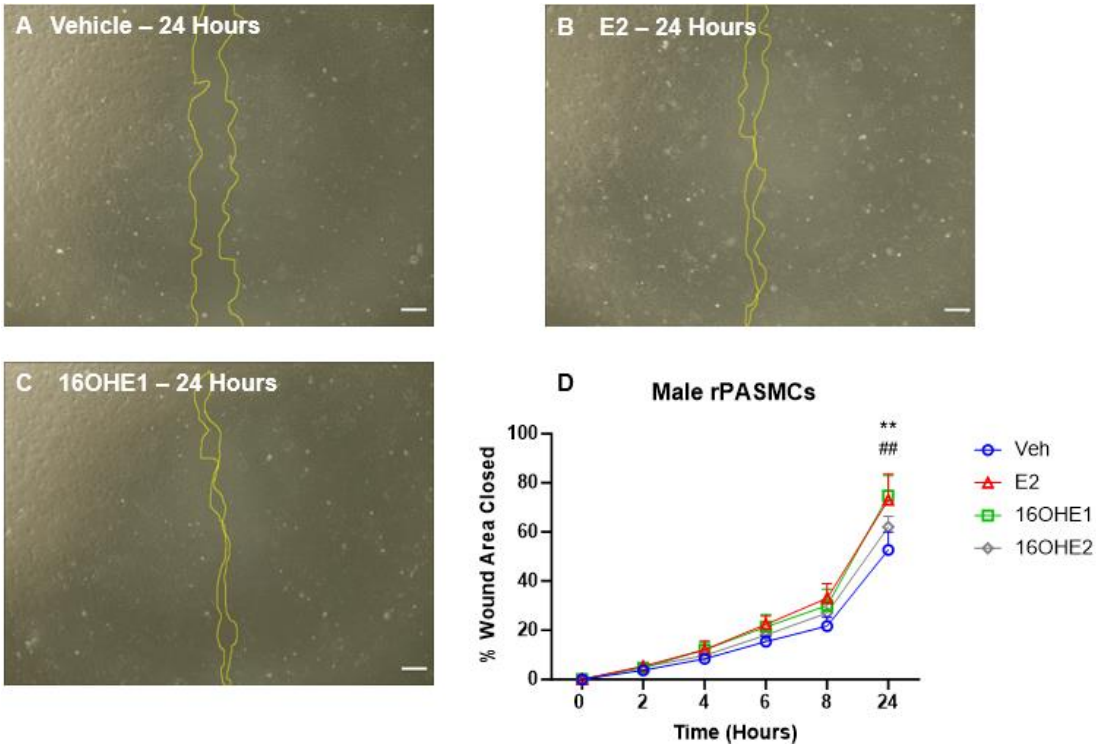

Figure 3.8: Migration of male rPASMCs is increased by E2 and 16OHE1.
Male rat pulmonary artery smooth muscle cells (rPASMCs) were seeded in a 6-well plate at $3x10^5$ cells/well, cultured to 90-100% confluency, and quiesced (0.2% charcoal stripped fetal bovine serum (FBS) in phenol red-free Dulbecco's Modified Eagle Medium (DMEM)) for 24 hours. Two wounds were created per well using a 200 µL pipette tip, the cells washed three times with PBS, then stimulated with 1 nM estradiol (E2), 1 nM 16α-hydroxyestrone (16OHE1), 1 nM 16α-hydroxyestradiol (16OHE2), or vehicle (Veh; 1 nM ethanol). Stimulations were carried out in phenol red-free DMEM with 1% charcoal stripped FBS. Images were taken at 0, 2, 4, 6, 8, and 24 hours, and the images shown are representative of cell migration. (A) 1 nM ethanol vehicle control at 24 hours. (B) 1 nM E2 at 24 hours. (C) 1 nM 16OHE1 at 24 hours. Wound area is highlighted in yellow. Scale bars = 5mm. (D) Percentage wound area closed. Data are expressed as ±SEM and analysed by two-way ANOVA with post-hoc Tukey test. **p<0.01 (E2 vs. Veh); ##p<0.01 (16OHE1 vs. Veh). n=3.

3.3 Discussion

The female predominance of PAH suggests that estrogens and their metabolites may be involved in its pathogenesis[27]. Circulating E2 levels are increased in male and postmenopausal female PAH patients, and are associated with worse disease outcomes[30,31]. Elevated plasma levels of 16OHE2 were recently observed in female idiopathic PAH patients, and in men and women with portopulmonary PAH[241,317]. It is hypothesised that 16OHE2 may contribute to the pathogenesis of PAH, but little is known about its function. Cell proliferation and migration are two key mechanisms of pulmonary vascular remodelling[6]. This work demonstrates that the major effect of 16OHE2 may be increased cell migration in rPASMCs.

Aberrant fibroblast function such as migration, infiltration into the adventitial layer, and proliferation plays a key role in pulmonary vascular remodelling[79]. Initial proliferation experiments were carried out in Dede hamster lung fibroblasts with two aims: to determine whether 16OHE1 or 16OHE2 affected cell proliferation and to determine the optimal end time-point for future proliferation studies. Concentrations of 1 nM 16OHE1 and 10 nM 16OHE2 were selected as previously identified optimal concentrations for smooth muscle cell proliferation, and these are in keeping with physiological levels[35,241,311]. Dede hamster lung fibroblasts are an immortalised cell line derived from female Chinese hamsters. An immortalised cell line was advantageous for experiment optimisation as the growth rate is faster than primary cells, there is lower risk of contamination, and passage numbers are unlimited without differentiation from the primary phenotype. DMEM containing 10% and 2% charcoal stripped FBS were used as positive and negative controls to allow determination of the optimal end time-point.

No difference in proliferation was observed between 16OHE1 or 16OHE2 and the vehicle. Proliferation was significantly increased by 10% FBS at 24 hours, and further increased at 48 hours compared to 2% FBS. Therefore, 48 hours was selected as the optimal end time-point for further proliferation studies.

No published data was found on the effects of estrogens in Dede hamster lung fibroblasts, or on the effects of 16OHE1 or 16OHE2 on fibroblasts in general. However, Martier et al. recently demonstrated that 10 nM E2 increased proliferation of primary human lung fibroblasts (HLFs) from females but not in males[334]. On the other hand, 10 nM dihydrotestosterone increased proliferation in male HLFs but not in females[334]. Increased proliferation in response to E2 has been documented in several types of fibroblasts including primary breast cancer-associated fibroblasts and stromal fibroblasts[335,336]. The effects of testosterone in fibroblasts are unclear[337,338]. However, the MacLean group observed that its metabolite dihydrotestosterone increased proliferation of hPASMCs whereas testosterone had no effect (unpublished data). The effects of 16OHE1 and 16OHE2 could be investigated in the immortalised human HFL-1 cell line to determine whether the proliferative response varies according to species. These could also be used to evaluate a range of metabolite concentrations.

Prior to cell isolation, male and female Sprague-Dawley rats were age-matched to remove this as a confounding factor. This is especially important in the context of PAH, where age has been identified as a risk factor for the disease[51]. For example, according to the REVEAL registry, the average patient age at PAH diagnosis is 53 years old, suggesting that PAH is more prevalent in postmenopausal women[51]. It was vital to study both male and female rats given the sex differences in PAH.

Smooth muscle cell proliferation is a key mechanism of pulmonary vascular remodelling in PAH[6]. It has previously been shown that E2 induces proliferation of female control subject and female PAH patient hPASMCs, and this is attenuated by the ERα antagonist MPP and the CYP1B1 inhibitor TMS[35,102]. It has also been shown that 16OHE1 increases proliferation of male and female hPASMCs and male mouse PASMCs[35,311]. Denver et al. recently observed that 16OHE2 significantly increased proliferation of female PAH patient hPASMCs but had no effect in either male or female control subject hPASMCs[241]. However, little is known about the function of 16OHE2.

In male and female rPASMCs, 48 hours stimulation with E2, 16OHE1 and 16OHE2 had no significant effect on total cell count. The results were highly variable despite using the same seeding density because the primary cell lines grew at different rates. There are several potential reasons for this. For example, the cell lines were used at different passage numbers. One of the female rats had a much higher weight of 265g

compared to the average weight of 226g in female rats (Supplementary Table 9.2). Extragonadal E2 synthesis and metabolism in adipose tissue is known to contribute to the development of PAH[41]. Therefore, increased weight in one female rat may have contributed to the variability in rPASMC total cell count. 16OHE2 is also known to have a short half-life. For example, the half-life of 16OHE2 after intramuscular injection was 3-4 hours in male and female Sprague-Dawley rats and 1.5.-5.3 hours in human female volunteers using the combined contraceptive pill[339,340]. Therefore, the lack of proliferative response may potentially be due to degradation of 16OHE2 *in vitro*. As many additional precipitating factors have been identified in PAH, it was hypothesised that a 'second hit' with acute hypoxia may enhance the proliferative response of female rPASMCs to 16OHE2[4].

Hypoxia is a known risk factor for pulmonary hypertension associated with lung disease (WHO Class III) but is also a consequence of pulmonary vascular remodelling and obstruction in PAH (WHO Class I)[4]. Chronic hypoxia is frequently used to induce pulmonary hypertension *in vivo*, often in combination with the VEGFR2 inhibitor Sugen 5416 to enhance the disease phenotype[69]. HIF1α mediates adaptive response to low O_2 availability[293]. Under normoxic conditions, it is hydroxylated through prolyl hydroxylases then tagged for proteosomal degradation through the E3 ubiquitin-ligase system by Von Hippel-Lindau tumour suppressor protein[293]. When the prolyl hydroxylases are inhibited by decreased oxygen availability, HIF1α translocates to the nucleus and mediates gene transcription through interaction with HIF1β (ARNT)[293]. HIF1β is shared with the aryl hydrocarbon receptor which regulates estrogen synthesis and CYP1A1 expression[292]. Therefore, there is a close link between hypoxia and estrogen metabolism (Figure 1.9).

The level of oxygen depletion required to induce a hypoxic response varies across different cell types[341]. For example, 3% O_2 induces a hypoxic response in neural stem cells isolated from C57BL/6J mice, whereas 1% O_2 induced a hypoxic response in human umbilical vein endothelial cells[342,343]. Tumour cell lines (e.g., MCF-7 breast cancer cells, A2780 ovarian cancer cells) are routinely studied under anoxic conditions with extreme oxygen deprivation (e.g., 0.1% O_2) as the microenvironment of solid tumours is characterised by multiple regions of mild to severe hypoxia due to lack of blood supply to the growing tumour nodules[344]. Dean et al. previously observed that proliferation of female PAH patient hPASMCs did not change in response to Sugen 5416 under normoxic conditions, but significantly increased when

Sugen 5416 was combined with 48 hours acute hypoxia in 1% O_2[292]. Therefore, we also used 1% O_2 for acute hypoxic studies in rPASMCs.

In female rPASMCs, we observed that 24 hours incubation in 1% O_2 was not sufficient to induce a hypoxic response (Supplementary Figure 9.1). 72 hours incubation was confirmed to be sufficient by observation of HIF1α translocation to the nucleus and a significant increase in *Hk2* expression (Figure 3.4). Many online tools are available to assist with selection of an appropriate housekeeping gene, for example NormFinder and geNorm. However, certain housekeepers are unstable under hypoxia, for example TATA box binding protein (*Tbp)*[329]. Tan et al. observed that *Actb* was the most stable housekeeper in cardiac stem cells under hypoxia[329]. We also observed that *Actb* was stable in female rPASMCs following 72 hours acute hypoxia as determined by no statistically significant difference in CT value (Figure 3.9).

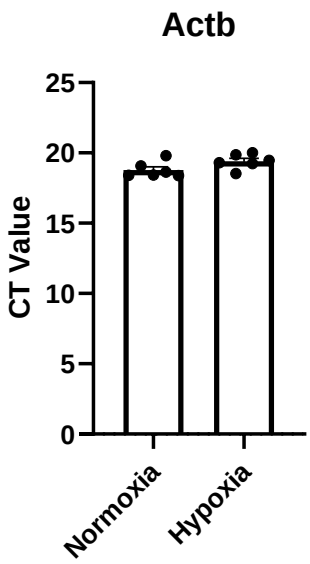

Figure 3.9: *Actb* expression in female rPASMCs is stable following 72 hours acute hypoxia. Female rPASMCs (passage 4) were seeded into 6-well plates at $3x10^5$ cells/well, cultured until ~70% confluent, and incubated in normoxia or 1% O_2/ 5% CO_2/nitrogen for 72 hours prior to RNA collection. qRT-PCR was carried out as previously described. There was no statistically significant difference in CT value for *Actb* in female rPASMCs following 72 hours acute hypoxia. Data are expressed as ±SEM and analysed by unpaired t-test. n=6 (technical replicates performed in one female rPASMC cell line).

Although it was hypothesised that a 'second hit' with acute hypoxia may increase the proliferative response of female rPASMCs, the total cell count was not affected by 16OHE2. Similarly, there was no difference in proliferation in response to 16OHE2 in male rPASMCs under acute hypoxic conditions. There was also no significant difference in total cell count in response to E2 or 16OHE1 in male or female rPASMCs under hypoxia. As chronic hypoxia is an established *in vivo* model and known risk factor for PAH, it was hypothesised that the effects of acute hypoxia may be different. There are several potential reasons for this. For example, in both humans and animal models (e.g., male Wistar rats) acute hypoxia leads to pulmonary vasoconstriction but pulmonary vascular remodelling and PAH only develop following chronic hypoxia[345,346]. Chronic hypoxia is known to induce several molecular changes in PASMCs associated with proliferation including elevation of intracellular calcium concentration ($[Ca^{2+}]_i$) and prolonged activation of HIF1α[297,347]. Therefore, acute hypoxia may be insufficient to induce the molecular changes required to enhance the proliferative response of female rPASMCs to 16OHE2. It is not possible to maintain cells in the hypoxic environment of the modular incubator chamber for long periods time. Therefore, we attempted to isolate cells from male and female Sprague-Dawley rats treated with SuHx, and from chronic hypoxic female Sprague-Dawley rats. However, these were unsuccessful due to poor growth and high sensitivity to quiescence.

Future studies could focus on the effects of combining exogenous hits with 16OHE2 on proliferation of rPASMCs. For example, White et al. investigated the effects of 72 hours stimulation with 2OHE1, 2OHE2, 4OHE1, 4OHE2, 16OHE1 and 16OHE2 in the presence of 10 ng/mL platelet derived growth factor in female control subject hPASMCs[35]. However, out of these estrogen metabolites, proliferation only increased in response to 16OHE1[35]. As serotonin induces proliferation in both female control subject and female PAH patient hPASMCs, this could also be investigated as an exogenous hit[193]. Endothelin-1 is known to induce proliferation in both rat and human PASMCs, therefore could also be explored as an exogenous hit[348,349]. Finally, the effects of 16OHE2 on proliferation could be explored in PASMCs isolated from transgenic mouse models which spontaneously develop PAH (e.g., obese *ob/ob* mice, $Bmpr2^{R899X}$ mice)[34,313].

As we did not observe any significant change in proliferation in response to 16OHE2 in rPASMCs, we investigated this in female PAH patient hPASMCs. The aim was to

replicate the finding by Denver et al. that 16OHE2 increased proliferation of female PAH patient hPASMCs, with the intention to move on to novel studies with estrogen receptor antagonists to investigate the underlying mechanism[241]. However, we did not observe any significant difference in proliferation of female PAH patient hPASMCs in response to 16OHE2. There are several possible reasons for this. We used four PAH patient hPASMC cell lines multiple times due to the shortage of human cells, whereas Denver et al. used each cell line once[241]. Differences in cell passage number and PAH patient hPASMC lines between the studies are also likely to have affected proliferation. For example, the female PAH patient hPASMCs used in this project (Table 3.2) were mostly used at passage 5-7 (except for one vial of cells used at passage 3). On the other hand, the cell lines and passage numbers used by Denver et al. could not be traced and may have come from different female PAH patients. There are many factors which differ between PAH patients including age, weight, condition (e.g., hereditary PAH vs. idiopathic PAH) and medications[4,41,51]. All of these may potentially affect proliferation in response to 16OHE2.

Cell migration is a key mechanism of pulmonary vascular remodelling[6]. 1 nM 16OHE2 significantly increased the percentage wound area closed (a measure of migration) at 8 and 24 hours compared to the vehicle in male and female rPASMCs. Similarly, Denver et al. recently demonstrated that 1 nM 16OHE2 increased migration of BOECs from PAH patients of both sexes[241]. Although concentrations of 100 pM and 10 nM were also tested, only 1 nM increased migration compared to the vehicle. In male rPASMCs, the percentage wound area closed was significantly lower in response to 10 nM 16OHE2 compared to 1 nM. However, there was no significant difference in migration between DMEM containing 1% FBS and the vehicle (Supplementary Figure 9.2), suggesting that the 10 nM ethanol (vehicle) concentration was not responsible for this effect and that migration is dependent on the concentration of 16OHE2. As migration experiments were carried out at the end of the PhD project, time did not allow for further investigation of the underlying mechanism. In the future, this experiment could be repeated in the presence of estrogen receptor antagonists and the NRF2-activator bardoxolone methyl given that this attenuated migration in BOECs[241].

In a preliminary experiment, we also observed that 1 nM E2 and 1 nM 16OHE1 increased migration of male rPASMCs at 24 hours compared to the vehicle (1 nM ethanol). In this case, 16OHE2 did not significantly affect migration which may be due

to lower n-numbers (n=3). Furthermore, this study was carried out in rPASMCs of higher passage number compared to the previous experiment due to the availability of primary cells (P5-6 versus P3-4). Previous studies have observed a loss of cell migration ability with increased passage. For example, Liao et al. demonstrated that the migration capability of human umbilical vein endothelial cells increased with passage until P10, started to decrease at P15, then dramatically reduced after P20[350]. Cao et al. investigated the effects of passage number on the migration of HT29 human colorectal cancer cells at P4, P10 and P16[351]. Migration was highest at P4 and lowest at P16[351]. Therefore, the lack of migration observed in response to 1 nM 16OHE2 and different results from the previous experiment may be due to decreased rPASMC ability to migrate at a higher passage number. While there is little published data on the effects of 16OHE1 and 16OHE2 on migration, the effect of E2 has been studied but is unclear. For example, E2 increased migration of MCF-7 breast cancer cells, and this was reversed by the ERα inhibitor fulvestrant which also decreases plasma levels of 16OHE2 in female PAH patients[117,352]. On the other hand, 10 nM E2 inhibited migration of vascular smooth muscle cells isolated from the thoracic aorta of female Sprague-Dawley rats, and this was reversed by fulvestrant (ICI 182,780)[353]. Therefore, further study is required to determine the underlying mechanism of the increased migration observed in rPASMCs in response to 16OHE2, and whether these effects are specific to the pulmonary vasculature.

3.3.1 Limitations of this Study

Dede hamster lung fibroblasts were used to optimise the end time-point for the Countess proliferation assay because, as an immortalised cell line, they do not have the same limits on passage number as primary cells. However, there may be species-specific differences in hamsters compared to rats and humans. It is also challenging to study the molecular effects of 16OHE2 in Dede hamster lung fibroblasts as many primary antibodies for western blots do not react with this species. Future studies could overcome this limitation by using human HFL-1 fibroblasts.

During hypoxic studies, the modular incubator chamber requires to be opened and the cells re-exposed to normoxia for short periods of time to allow media changes or harvest of RNA/protein. However, this was minimised and does not appear to have affected the hypoxic response. Alternatively, cobalt chloride could have been used as a chemical mimic of hypoxia as it strongly stabilises HIF1α and HIF2α under normoxic conditions[333]. However, unlike low oxygen-induced hypoxia, the response to cobalt chloride lasts several hours and the extent to which this model can be extrapolated to hypoxia is uncertain[333]. Therefore, the use of a modular incubator chamber was preferable.

72 hours incubation in a hypoxic environment (1% O_2 /5% CO_2 /nitrogen) was confirmed to induce a hypoxic response in female rPASMCs by immunocytochemistry observation of HIF1α translocation into the nucleus and increased gene expression of *Hk2*. However, as HK2 protein levels were not analysed, we cannot confirm that increased gene expression of *Hk2* translates to increased protein levels.

There was no significant difference in proliferation in the response to the 10% FBS positive control in female rPASMCs under acute hypoxia. This may be due to high variability in the total cell count associated with different passage number, different primary cell line growth rates, and the higher weight of one female rat compared to the others used in the study. However, the hypoxic environment may also have affected cell growth as a significant increase in total cell count was observed in response to 10% FBS under normoxic conditions. This may potentially have influenced female rPASMC response to E2, 16OHE1 and 16OHE2 under acute hypoxic conditions.

Our supply of hPASMCs ceased during the COVID-19 pandemic. Therefore, it was not possible to add further n-numbers to investigate the effect of 16OHE2 on proliferation of female PAH patient hPASMCs. Those cells we did study were high passage.

Finally, as migration experiments were carried out at the end of the PhD project, time did not allow for investigation of the underlying mechanisms of increased migration in response to 16OHE2 in rPASMCs.

3.3.2 Summary

In summary, Dede hamster lung fibroblast proliferation was not affected by 16OHE1 or 16OHE2, but the optimal end time-point for experiments was determined as 48 hours. 16OHE2 did not increase proliferation of male or female rPASMCs. Acute hypoxia was added as a 'second hit' but this did not increase the proliferative response. 16OHE2 also did not increase proliferation of female PAH patient hPASMCs. 1 nM 16OHE2 increased migration of male and female rPASMCs. In addition, 1 nM E2 and 1 nM 16OHE1 increased migration of male rPASMCs. Overall, these results suggest that increased migration in response to 16OHE2 may contribute to pulmonary vascular remodelling in PAH (Figure 3.10). The molecular effects of 16OHE2 *in vitro* and the effects of 16OHE2 *in vivo* are presented in Chapters 4 and 5.

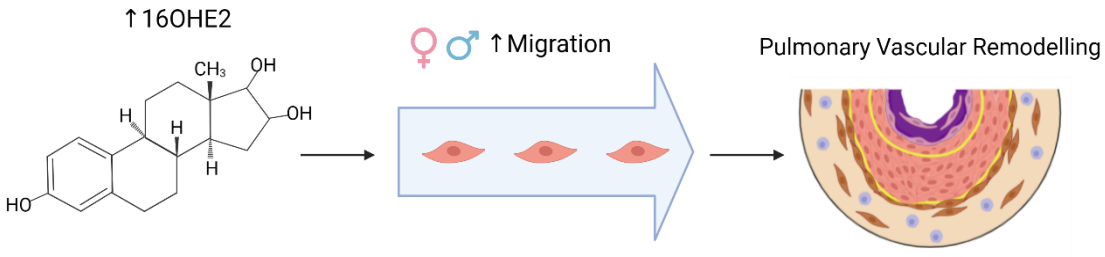

Figure 3.10: Summary of the functional effects of 16OHE2 *in vitro*.
Increased plasma levels of 16α-hydroxyestradiol (16OHE2) were recently observed in female idiopathic pulmonary arterial hypertension (PAH) patients, and in males and females with portopulmonary PAH[225,289]. 1 nM 16OHE2 significantly increased migration of male and female rat pulmonary artery smooth muscle cells. This may contribute to pulmonary vascular remodelling in PAH. Created with BioRender.com.

Chapter 4

The Molecular Effects of 16α-Hydroxyestradiol *In Vitro*

4.1 Introduction

There are several groups of pulmonary arterial hypertension (PAH) including hereditary and idiopathic PAH (Table 1.1)[4]. Around 80% of hereditary PAH cases are associated with mutations in bone morphogenetic protein receptor 2 (BMPR2)[140]. However, as previously discussed in Chapter 1, BMPR2 expression in human pulmonary artery smooth muscle cells (hPASMCs) is generally reduced in PAH patients regardless of mutation status, therefore this is of interest across all PAH patients[140]. In hereditary PAH, disease penetrance is low and is predominantly affected by sex (penetrance is around 14% in males and 42% in females)[141]. This may be driven by many factors including alterations in estrogen metabolism[286]. In the absence of PAH, Mair et al. observed that basal BMPR2 signalling (Figure 1.5) is lower in female control subject hPASMCs than males[104]. Estradiol (E2) suppressed expression of inhibitor of DNA-binding 1 (Id1) and inhibitor of DNA-binding 3 (Id3) in male control subject hPASMCs to a similar level observed in female hPASMCs, suggesting that E2 may suppress BMPR2 signalling[104]. Reduced BMPR2 signalling contributes to hyperactivation of the transforming growth factor-beta (TGF-β) pathway by shifting protective p-Smad1,5,8 signalling to the pathogenic p-Smad2,3 pathway, leading to cell proliferation, migration, and pulmonary vascular remodelling[105].

Estrogens primarily act via three receptors encoded by the genes *Esr1* (ERα), *Esr2* (ERβ) and *Gper1* (GPER)[102]. *ESR1* expression is upregulated in the lung tissue of PAH patients compared to control subjects[116]. Wright et al. observed that ERα protein levels are elevated in female PAH patient hPASMCs compared to female control subjects, whereas ERβ protein levels are elevated in male PAH patient hPASMCs compared to male control subjects[102]. Austin et al. observed that transfection of increasing quantities of ERα in COS-7 cells (which lack endogenous estrogen receptors) strongly correlates with decreasing *BMPR2* expression[147]. *Bmpr2* suppression in the lung tissue of female $SERT^{+}$ mice (overexpressing the human serotonin transporter gene) was also attenuated by continuous subcutaneous (s/c) dosing with the ERα antagonist MPP[102]. On the other hand, Chen et al. observed that ERβ primarily mediates the increased PAH penetrance observed in female $Bmpr2^{R899X}$ mice compared to male $Bmpr2^{R899x}$ mice, with ERα

only partially involved[120]. Furthermore, Ichimori et al. observed that BMPR2 signalling in human pulmonary artery endothelial cells (PAECs) increased in response to E2 under normoxic conditions but decreased under acute hypoxia (1% O_2), and these effects were attenuated by the ERα inhibitor fulvestrant (ICI 182,780)[148]. Therefore, the effects of E2 on BMPR2 signalling may differ according to sex, species, tissue, and stimulus.

Hsd17b1 and *Hsd17b2* encode the 17β-hydroxysteroid dehydrogenase enzymes 17β-HSD1 and 17β-HSD2 which interconvert androgens, estrogens, and their respective metabolites[7]. *Cyp19a1* encodes aromatase which synthesises E1 and E2 from androstenedione and testosterone (Figure 1.4)[7]. Mair et al. observed that aromatase expression is significantly increased in the pulmonary arteries of male and female chronic hypoxic C57BL/6 mice and SuHx Wistar Kyoto rats compared to their normoxic controls[33]. Daily s/c injection or oral dosing with the aromatase inhibitor anastrozole attenuated both PAH and BMPR2 suppression in the lung tissue of female chronic hypoxic C57BL/6 mice and female SuHx Wistar Kyoto rats[33]. However, no response was observed in males[33]. Overexpression of *CYP19A1* due to the rs7175922 polymorphism may be associated with an increased risk of portopulmonary hypertension[278].

Cyp1a1, *Cyp1a2* and *Cyp1b1* encode cytochrome P450 enzymes which metabolise E1 and E2[7]. *Comt* further metabolises 2- and 4-hydroxyestrogens to 2- and 4-methoxyestrogens[7]. Dean et al. observed that CYP1A1 is highly upregulated in the lungs of female SuHx Wistar rats compared in response to activation of the aryl hydrocarbon receptor, leading to increased estrogen metabolism[292]. CYP1B1 is overexpressed in the pulmonary arteries of idiopathic and hereditary PAH patients[35]. The CYP1B1 antagonist TMS attenuates PAH in chronic hypoxic C57BL/6 mice, SuHx C57BL/6 mice, obese male ob/ob mice, and female SERT+ mice[34,35,240]. On the other hand, the COMT metabolite 2-methoxyestradiol (2ME2) mediates several protective effects in PAH, for example decreased proliferation of female rPASMCs and female control subject hPASMCs[299].

16α-hydroxyestrone (16OHE1) is a metabolite of CYP1B1[35]. Increased levels of 16OHE1 may mediate disease penetrance in hereditary PAH[106]. Austin et al observed that female *BMPR2* mutation carriers homozygous for the N/N genotype of *CYP1B1 N453S* have a four-fold greater incidence of hereditary PAH[286]. Fessel et al. observed that continuous s/c administration of 16OHE1 significantly increased

the penetrance of PAH in male Bmpr2^{R899X} and Bmpr2^{delx4+} mice[106]. 16OHE1 also suppressed BMPR2 signalling in the lung tissue of their wild type littermates[106]. This has led to the hypothesis that a shift in estrogen metabolism from the protective 2-hydroxylation pathway to 16α-hydroxylation may mediate the development of PAH[274]. In keeping with this, Austin et al. observed that the urinary 2-hydroxyestrogen/16OHE1 ratio was 2.3-fold lower in hereditary PAH patients compared to unaffected *BMPR2* mutation carriers[286].

16α-hydroxyestradiol (16OHE2) is primarily produced during pregnancy (Figure 1.10)[314]. Increased plasma levels of 16OHE2 were recently observed in female idiopathic PAH patients, and in males and females with portopulmonary PAH[241,317]. During a study primarily focused on E2, Austin et al. (2012) incidentally observed that 24 hours treatment with 16OHE2 (estriol) suppressed *BMPR2* expression in human pulmonary microvascular endothelial cells, with 10 nM being the optimal concentration[147]. However, this observation was made before increased plasma levels of 16OHE2 were detected in PAH patients (Denver et al. 2020)[241]. While preliminary studies have shown it increases proliferation of female PAH patient hPASMCs and migration of blood outgrowth endothelial cells (BOECs) from male and female PAH patients, its molecular function is undetermined[241]. Here, we investigate the molecular effects of 16OHE2 *in vitro*.

Aims of this chapter:

1. To investigate the effects of 16OHE2 on the estrogen pathway, BMPR2 signalling pathway, and fibrosis marker expression in male and female rat pulmonary artery smooth muscle cells (rPASMCs) under normoxic and acute hypoxic conditions.

2. To investigate whether the findings in male rPASMCs translate to male control subject hPASMCs.

3. To investigate the effects of 16OHE2 on the BMPR2 signalling pathway in the systemic circulation using rat aorta smooth muscle cells (AoSMCs).

4.2 Results

4.2.1 Effects of E2, 16OHE1 and 16OHE2 on the Expression of Genes Within the Estrogen Pathway in Rat Pulmonary Artery Smooth Muscle Cells

Estrogen synthesis and metabolism (Figure 1.4) play a key role in PAH and may contribute to its predominance in females[7]. Many of the effects of estrogens result from direct interaction between estrogens and their receptors[130]. For example, E2 increases proliferation of female PAH patient hPASMCs via ERα[102]. Therefore, we wished to investigate the effects of 16OHE2 on expression of genes within the estrogen pathway. As previously described, rPASMCs were isolated from male and female Sprague-Dawley rats (aged 11-13 weeks) and stimulated with 1 nM E2, 1 nM 16OHE1, and 10 nM 16OHE2 for 24 hours prior to RNA collection. These concentrations were selected as they were previously observed to increase proliferation in hPASMCs[35,102,241,311]. However, in Chapter 3, we did not observe any proliferation in response to 48 hours stimulation with 1 nM E2, 1 nM 16OHE1, or 10 nM 16OHE2 in rPASMCs under normoxic or acute hypoxic conditions (72 hours in 1% O_2). Although this may be due to species difference, Denver et al. only observed proliferation in female PAH patient hPASMCs in response to 16OHE2 and not in male or female control subjects[241]. Therefore, the lack of proliferative response may occur because the rPASMCs were isolated from healthy control rats.

We investigated the effects of E2, 16OHE1 and 16OHE2 on the expression of *Esr1*, *Esr2*, *Gper1*, *Hsd17b1*, *Hsd17b2*, *Cyp19a1*, *Cyp1a1*, *Cyp1a2*, *Cyp1b1* and *Comt* in male and female rPASMCs. In male rPASMCs, no significant changes in gene expression were observed (Table 4.1). In female rPASMCs, *Gper1* expression significantly decreased in response to 16OHE1 (Table 4.2). *Hsd17b2* and *Cyp1a2* were not detected. *Cyp19a1* was detected but expression was very low.

Table 4.1: Effects of E2, 16OHE1 and 16OHE2 on the Expression of Genes Within the Estrogen Pathway in Male rPASMCs

PATHWAY	GENES	Basal CT value	E2 vs. Veh		16OHE1 vs. Veh		16OHE2 vs. Veh	
			FC ± SEM	P-value	FC ± SEM	P-value	FC ± SEM	P-value
Estrogen Pathway	***Esr1***	36.1	1.01 ± 0.09	>0.9999	0.82 ± 0.22	>0.9999	0.97 ± 0.31	>0.9999
	Esr2	35.2	1.22 ± 0.18	0.9584	1.93 ± 0.45	0.1894	1.32 ± 0.29	0.8972
	Gper1	33.0	1.05 ± 0.31	>0.9999	1.11 ± 0.40	>0.9999	0.83 ± 0.19	>0.9999
	Hsd17b1	34.3	0.94 ± 0.14	0.9959	0.96 ± 0.21	0.9984	1.04 ± 0.27	0.9992
	Cyp19a1	36.0	1.13 ± 0.17	0.9885	1.17 ± 0.41	0.9744	0.85 ± 0.16	0.9783
	Cyp1a1	35.3	0.53 ± 0.13	0.4421	0.41 ± 0.09	0.3225	0.43 ± 0.12	0.2569
	Cyp1b1	23.0	1.11 ± 0.20	0.9766	1.00 ± 0.21	>0.9999	1.13 ± 0.15	0.9599
	Comt	24.3	1.15 ± 0.12	0.7838	1.01 ± 0.15	0.9998	1.07 ± 0.08	0.9746

Table 4.1: Effects of E2, 16OHE1 and 16OHE2 on the expression of genes within the estrogen pathway in male rPASMCs.
Male rat pulmonary artery smooth muscle cells (rPASMCs) were seeded in a 6-well plate at $3x10^5$ cells/well, cultured to ~70% confluency, and quiesced (0.2% charcoal stripped fetal bovine serum (FBS) in phenol red-free Dulbecco's Modified Eagle Medium (DMEM)) for 24 hours. Cells were stimulated with 1 nM Estradiol (E2), 1 nM 16α-hydroxyestrone (16OHE1), 10 nM 16α-hydroxyestradiol (16OHE2), or vehicle (Veh) control (10 nM ethanol) for 24 hours prior to RNA lysis in QiaZol. Stimulations were carried out in phenol red-free DMEM with 1% charcoal stripped FBS. Basal CT value = average CT value in the vehicle group. FC= Fold change, calculated by ΔΔCT method and represented as relative to the vehicle (where the average vehicle fold change is 1). Normality was assessed by Shapiro-Wilk test. Data are expressed as ±SEM and analysed by one-way ANOVA with post-hoc Tukey test or Kruskal-Wallis test. n=6.

Table 4.2: Effects of E2, 16OHE1 and 16OHE2 on the Expression of Genes Within the Estrogen Pathway in Female rPASMCs

PATHWAY	GENES	Basal CT value	E2 vs. Veh		16OHE1 vs. Veh		16OHE2 vs. Veh	
			FC ± SEM	P-value	FC ± SEM	P-value	FC ± SEM	P-value
Estrogen Pathway	***Esr1***	34.5	1.17 ± 0.13	>0.9999	1.10 ± 0.09	>0.9999	1.19 ± 0.29	>0.9999
	Esr2	34.8	0.91 ± 0.14	0.9946	1.13 ± 0.48	0.9849	0.71 ± 0.16	0.8817
	Gper1	33.6	0.80 ± 0.07	0.4647	0.56 ± 0.10	0.0190*	0.67 ± 0.11	0.1151
	Hsd17b1	32.9	1.09 ± 0.19	0.9816	1.29 ± 0.17	0.6126	0.92 ± 0.18	0.9845
	Cyp19a1	35.8	0.81 ± 0.06	0.9249	0.53 ± 0.21	0.4263	0.85 ± 0.15	0.9504
	Cyp1a1	34.4	1.28 ± 0.30	0.9542	1.22 ± 0.45	0.9762	1.06 ± 0.52	0.9996
	Cyp1b1	24.1	1.02 ± 0.10	>0.9999	0.98 ± 0.09	>0.9999	1.00 ± 0.11	>0.9999
	Comt	25.3	0.97 ± 0.06	0.9995	1.21 ± 0.27	0.8631	1.30 ± 0.21	0.6792

Table 4.2: Effects of E2, 16OHE1 and 16OHE2 on the expression of genes within the estrogen pathway in female rPASMCs.
Female rat pulmonary artery smooth muscle cells (rPASMCs) were seeded in a 6-well plate at $3x10^5$ cells/well, cultured to ~70% confluency, and quiesced (0.2% charcoal stripped fetal bovine serum (FBS) in phenol red-free Dulbecco's Modified Eagle Medium (DMEM)) for 24 hours. Cells were stimulated with 1 nM Estradiol (E2), 1 nM 16α-hydroxyestrone (16OHE1), 10 nM 16α-hydroxyestradiol (16OHE2), or vehicle (Veh) control (10 nM ethanol) for 24 hours prior to RNA lysis in QiaZol. Stimulations were carried out in phenol red-free DMEM with 1% charcoal stripped FBS. Basal CT value = average CT value in the vehicle control group. FC= Fold change, calculated by ΔΔCT method and represented as relative to the vehicle (where the average vehicle fold change is 1). Normality was assessed by Shapiro-Wilk test. Data are expressed as ±SEM and analysed by one-way ANOVA with post-hoc Tukey test or Kruskal-Wallis test. *p<0.05. n=6.

4.2.2 Effects of E2, 16OHE1 and 16OHE2 on the Expression of Genes Within the Estrogen Pathway in Rat Pulmonary Artery Smooth Muscle Cells Under Acute Hypoxia

Pulmonary vascular remodelling in PAH is complex, and many additional precipitating factors (or 'second hits') have been identified including exposure to certain drugs (e.g., fenfluramines), genetic susceptibilities, and hypoxia[92,130,140]. As few changes in expression of genes within the estrogen pathway were observed in response to E2, 16OHE1 or 16OHE2 in rPASMCs, we wished to investigate the effects of adding acute hypoxia as a 'second hit'.

As previously discussed in Chapter 3, 72 hours incubation in a hypoxic environment (1% O_2/5% CO_2/nitrogen) was confirmed to induce a hypoxic response in female rPASMCs by translocation of HIF1α into the nucleus and a significant increase in *Hk2* expression (Figure 3.4). We investigated the effects of 24 hours stimulation with E2, 16OHE1 and 16OHE2 on the expression of *Esr1*, *Esr2*, *Gper1*, *Hsd17b1*, *Hsd17b2*, *Cyp19a1*, *Cyp1a1*, *Cyp1a2*, *Cyp1b1* and *Comt* in male and female rPASMCs under acute hypoxia. No significant changes were observed in male (Table 4.3) or female (Table 4.4) rPASMCs. *Hsd17b2* and *Cyp1a2* were not detected in either sex. *Cyp19a1* was detected at very low levels in female rPASMCs but not detected in males.

Table 4.3: Effects of E2, 16OHE1 and 16OHE2 on the Expression of Genes Within the Estrogen Pathway in Male rPASMCs Under 72 Hours Acute Hypoxia

PATHWAY	GENES	Basal CT value	E2 vs. Veh		16OHE1 vs. Veh		16OHE2 vs. Veh	
			FC ± SEM	P-value	FC ± SEM	P-value	FC ± SEM	P-value
Estrogen Pathway	***Esr1***	36.1	0.70 ± 0.27	>0.9999	0.87 ± 0.22	>0.9999	0.67 ± 0.20	>0.9999
	Esr2	35.3	1.12 ± 0.19	0.9825	0.75 ± 0.13	0.8559	1.08 ± 0.18	0.9955
	Gper1	34.6	0.67 ± 0.20	>0.9999	0.78 ± 0.34	>0.9999	0.48 ± 0.09	>0.9999
	Hsd17b1	34.0	0.85 ± 0.18	0.8640	0.77 ± 0.12	0.6407	0.75 ± 0.15	0.6017
	Cyp1a1	34.8	0.81 ± 0.38	0.9824	0.43 ± 0.12	0.6519	0.72 ± 0.24	0.9398
	Cyp1b1	24.0	0.79 ± 0.22	0.9079	0.80 ± 0.19	0.9073	0.91 ± 0.22	0.9903
	Comt	27.2	0.95 ± 0.19	>0.9999	0.95 ± 0.16	>0.9999	0.94 ± 0.19	>0.9999

Table 4.3: Effects of E2, 16OHE1 and 16OHE2 on the expression of genes within the estrogen pathway in male rPASMCs under 72 hours acute hypoxia. Male rat pulmonary artery smooth muscle cells (rPASMCs) were seeded in a 6-well plate at $3x10^5$ cells/well. The following day, the culture media was refreshed, and the cells placed into acute hypoxia (1% O_2/ 5% CO_2/ nitrogen) for 72 hours as previously described. On day 3, the cells (at ~70% confluency) were quiesced (0.2% charcoal stripped fetal bovine serum (FBS) in phenol red-free Dulbecco's Modified Eagle Medium (DMEM)) for 24 hours. On day 4, cells were stimulated with 1 nM Estradiol (E2), 1 nM 16α-hydroxyestrone (16OHE1), 10 nM 16α-hydroxyestradiol (16OHE2), or vehicle (Veh) control (10 nM ethanol) for 24 hours prior to RNA lysis in QiaZol. Stimulations were carried out in phenol red-free DMEM with 1% charcoal stripped FBS. Basal CT value = average CT value in the vehicle control group. FC= Fold change, calculated by ΔΔCT method and represented as relative to the vehicle (where the average vehicle fold change is 1). Normality was assessed by Shapiro-Wilk test. Data are expressed as ±SEM and analysed by one-way ANOVA with post-hoc Tukey test or Kruskal-Wallis test. n=6.

Table 4.4: Effects of E2, 16OHE1 and 16OHE2 on the Expression of Genes Within the Estrogen Pathway in Female rPASMCs Under 72 Hours Acute Hypoxia

PATHWAY	GENES	Basal CT value	E2 vs. Veh		16OHE1 vs. Veh		16OHE2 vs. Veh	
			FC ± SEM	P-value	FC ± SEM	P-value	FC ± SEM	P-value
Estrogen Pathway	***Esr1***	35.4	0.98 ± 0.14	>0.9999	1.28 ± 0.33	0.7969	0.94 ± 0.16	0.9968
	Esr2	34.7	1.17 ± 0.44	0.9883	1.29 ± 0.48	0.9473	1.09 ± 0.26	0.9983
	Gper1	33.4	0.79 ± 0.14	0.7006	0.84 ± 0.13	0.8338	0.65 ± 0.11	0.3012
	Hsd17b1	33.0	1.30 ± 0.23	0.7485	1.10 ± 0.21	0.9872	1.19 ± 0.25	0.9193
	Cyp19a1	36.4	1.04 ± 0.23	>0.9999	0.94 ± 0.14	0.9955	Only detected in 2 samples	
	Cyp1a1	34.1	0.90 ± 0.16	0.9982	0.94 ± 0.22	0.9996	2.13 ± 0.71	0.2451
	Cyp1b1	24.3	0.95 ± 0.15	0.9991	1.18 ± 0.28	0.9622	1.46 ± 0.34	0.5927
	Comt	25.8	1.12 ± 0.25	0.9715	1.08 ± 0.17	0.9905	1.06 ± 0.21	0.9962

Table 4.4: Effects of E2, 16OHE1 and 16OHE2 on the expression of genes within the estrogen pathway in female rPASMCs under 72 hours acute hypoxia. Female rat pulmonary artery smooth muscle cells (rPASMCs) were seeded in a 6-well plate at $3x10^5$ cells/well. The following day, the culture media was refreshed, and the cells placed into acute hypoxia (1% O_2/ 5% CO_2/ nitrogen) for 72 hours as previously described. On day 3, the cells (at ~70% confluency) were quiesced (0.2% charcoal stripped fetal bovine serum (FBS) in phenol red-free Dulbecco's Modified Eagle Medium (DMEM)) for 24 hours. On day 4, cells were stimulated with 1 nM Estradiol (E2), 1 nM 16α-hydroxyestrone (16OHE1), 10 nM 16α-hydroxyestradiol (16OHE2), or vehicle (Veh) control (10 nM ethanol) for 24 hours prior to RNA lysis in QiaZol. Stimulations were carried out in phenol red-free DMEM with 1% charcoal stripped FBS. Basal CT value = average CT value in the vehicle control group. FC= Fold change, calculated by ΔΔCT method and represented as relative to vehicle (where the average vehicle fold change is 1). Normality was assessed by Shapiro-Wilk test. Data are expressed as ±SEM and analysed by one-way ANOVA with post-hoc Tukey test or Kruskal-Wallis test. n=6.

4.2.3 Effects of 16OHE2 (24 Hours Incubation) on the Expression of Genes Within the BMPR2 Signalling Pathway in Rat Pulmonary Artery Smooth Muscle Cells

BMPR2 signalling (Figure 1.5) is reduced in ~80% of PAH patients regardless of mutation status[140]. BMPR2 expression is also decreased in the lung tissue of male and female chronic hypoxic C57BL/6 mice and SuHx Wistar Kyoto rats in comparison to their normoxic controls[33]. In 2012, Austin et al. incidentally observed that 24 hours treatment with 16OHE2 (estriol) suppressed *BMPR2* expression in human pulmonary microvascular endothelial cells, with 10 nM being the optimal concentration[147]. However, this observation was made before increased plasma levels of 16OHE2 were detected in PAH patients (Denver et al. 2020)[241]. Therefore, we wished to investigate the effects of 16OHE2 on the BMPR2 signalling pathway in PASMCs.

We investigated the effects of 24 hours stimulation with 10 nM 16OHE2 on the expression of the following genes within the BMPR2 signalling pathway: *Bmpr2*, *Smad1*, *Smad2*, *Smad3*, *Smad4*, *Smad5*, *Smad6*, *Smad7*, *Smad9*, *Id1*, *Id2* and *Id3*. In male rPASMCs, *Bmpr2, Smad1* and *Smad4* expression significantly decreased in response to 16OHE2 (Figure 4.1, Table 4.5). No significant changes in gene expression were observed in female rPASMCs (Figure 4.2, Table 4.6).

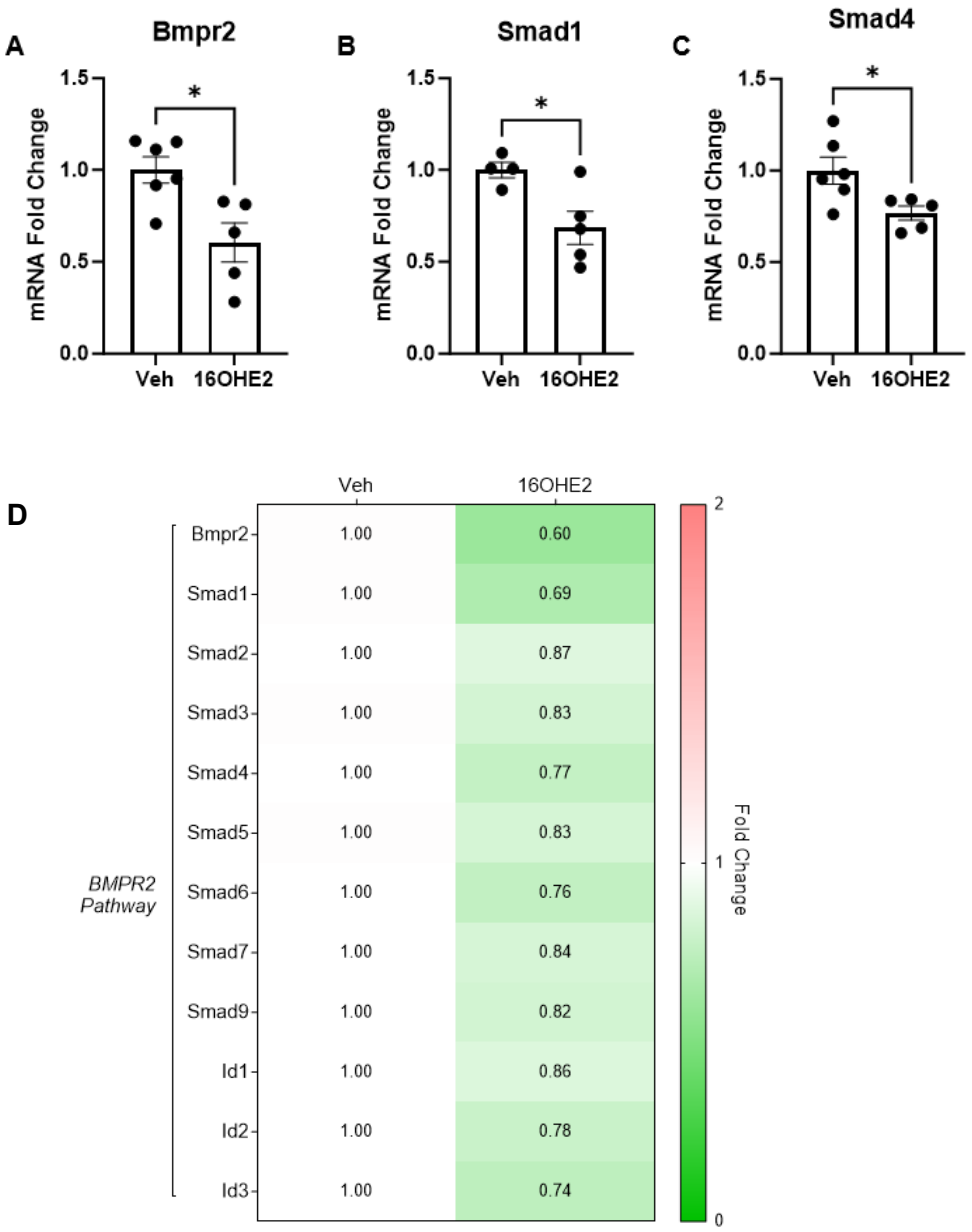

Figure 4.1: Effects of 16OHE2 on expression of genes within the BMPR2 signalling pathway in male rPASMCs.

Male rat pulmonary artery smooth muscle cells (rPASMCs) were seeded in 100 mm dishes at 2.2×10^6 cells/dish, cultured to ~70% confluency, quiesced (0.2% charcoal stripped fetal bovine serum (FBS) in phenol red-free Dulbecco's Modified Eagle Medium (DMEM)) for 24 hours, then stimulated with 10 nM 16α-hydroxyestradiol (16OHE2), or vehicle (Veh) control (10 nM ethanol) for 24 hours prior to RNA lysis. Stimulations were carried out in phenol red-free DMEM with 1% charcoal stripped FBS. Basal CT value = average CT value in the vehicle control group. FC= Fold change, calculated by ΔΔCT method and represented as relative to the vehicle (where the average vehicle fold change is 1). (A) *Bmpr2*. (B) *Smad1*. (C) *Smad4*. (D) Heatmap comparison of the fold change mRNA expression in response to 16OHE2 compared to the vehicle. Green = <1, white = 1, red = >1. Data are expressed as ±SEM and analysed by unpaired t-test. *p<0.05. n=5-6.

Table 4.5: Effects of 16OHE2 on Expression of Genes Within the BMPR2 Signalling Pathway in Male rPASMCs

PATHWAY	GENES	Basal CT value	16OHE2 vs. Veh	
			FC ± SEM	P-value
BMPR2 Pathway	***Bmpr2***	27.9	0.61 ± 0.11	0.0115*
	Smad1	27.6	0.69 ± 0.09	0.0237*
	Smad2	28.9	0.87 ± 0.14	0.4753
	Smad3	27.7	0.83 ± 0.07	0.3117
	Smad4	26.6	0.72 ± 0.04	0.0273*
	Smad5	28.3	0.83 ± 0.05	0.0763
	Smad6	26.8	0.76 ± 0.06	0.0561
	Smad7	28.4	0.84 ± 0.07	0.0960
	Smad9	30.5	0.82 ± 0.10	0.3032
	Id1	29.3	0.86 ± 0.20	0.5540
	Id2	29.0	0.79 ± 0.20	0.3758
	Id3	24.0	0.74 ± 0.11	0.0919

Table 4.5: Effects of 16OHE2 on expression of genes within the BMPR2 signalling pathway in male rPASMCs.

Male rat pulmonary artery smooth muscle cells (rPASMCs) were seeded in 100 mm dishes at 2.2×10^6 cells/dish, cultured to ~70% confluency, quiesced (0.2% charcoal stripped fetal bovine serum (FBS) in phenol red-free Dulbecco's Modified Eagle Medium (DMEM)) for 24 hours, then stimulated with 10 nM 16α-hydroxyestradiol (16OHE2), or vehicle (Veh) control (10 nM ethanol) for 24 hours prior to RNA lysis. Stimulations were carried out in phenol red-free DMEM with 1% charcoal stripped FBS. Basal CT value = average CT value in the vehicle control group. FC= Fold change, calculated by ΔΔCT method and represented as relative to the vehicle (where the average vehicle fold change is 1). Normality was assessed by Shapiro-Wilk test. Data are expressed as ±SEM and analysed by unpaired t-test. *$p<0.05$. n=5-6.

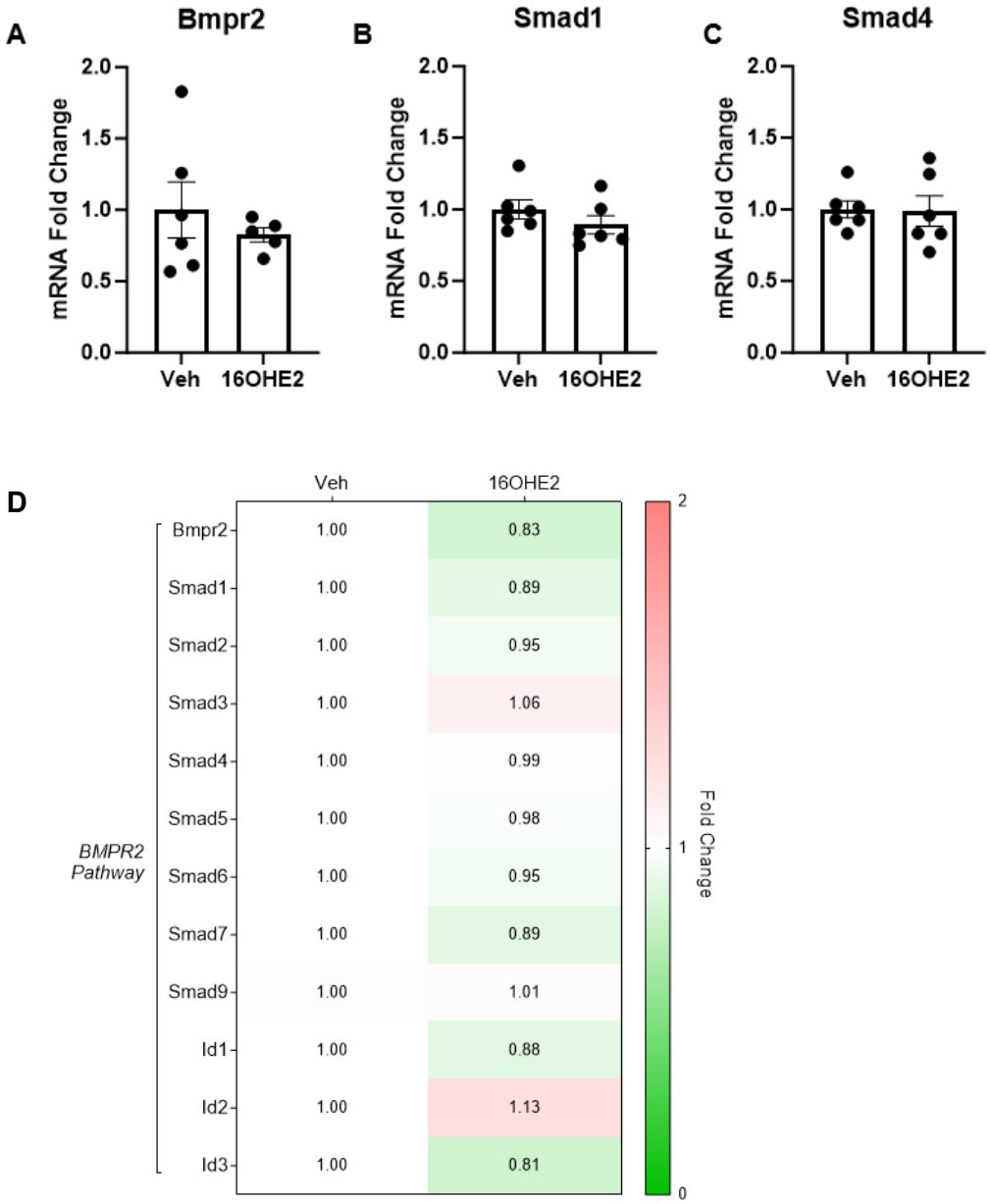

Figure 4.2: Effects of 16OHE2 on expression of genes within the BMPR2 signalling pathway in female rPASMCs.

Female rat pulmonary artery smooth muscle cells (rPASMCs) were seeded in 100 mm dishes at 2.2×10^6 cells/dish, cultured to ~70% confluency, quiesced (0.2% charcoal stripped fetal bovine serum (FBS) in phenol red-free Dulbecco's Modified Eagle Medium (DMEM)) for 24 hours, then stimulated with 10 nM 16α-hydroxyestradiol (16OHE2), or vehicle (Veh; 10 nM ethanol) for 24 hours prior to RNA lysis. Stimulations were carried out in phenol red-free DMEM with 1% charcoal stripped FBS. Basal CT value = average CT value in the vehicle group. FC= Fold change, calculated by ΔΔCT method and represented as relative to the vehicle (where average vehicle fold change is 1). (A) *Bmpr2*. (B) *Smad1*. (C) *Smad4*. (D) Heatmap comparison of the fold change mRNA expression in response to 16OHE2 compared to the vehicle. Green = <1, white = 1, red = >1. Normality was assessed by Shapiro-Wilk test. Data are expressed as ±SEM and analysed by unpaired t-test or Mann-Whitney test. n=6.

Table 4.6: Effects of 16OHE2 on Expression of Genes Within the BMPR2 Signalling Pathway in Female rPASMCs

PATHWAY	GENES	Basal CT value	16OHE2 vs. Veh	
			FC ± SEM	P-value
BMPR2 Pathway	***Bmpr2***	29.9	0.83 ± 0.05	0.4490
	Smad1	29.8	0.89 ± 0.07	0.2767
	Smad2	31.1	0.95 ± 0.04	0.5887
	Smad3	30.5	1.06 ± 0.05	0.7641
	Smad4	27.7	0.99 ± 0.11	0.9258
	Smad5	28.9	0.98 ± 0.11	0.9068
	Smad6	28.4	0.95 ± 0.09	0.6387
	Smad7	29.6	0.89 ± 0.05	0.2522
	Smad9	31.3	1.00 ± 0.16	0.9963
	Id1	31.8	0.88 ± 0.03	0.5887
	Id2	31.6	1.13 ± 0.18	0.5447
	Id3	26.8	0.92 ± 0.02	0.0699

Table 4.6: Effects of 16OHE2 on expression of genes within the BMPR2 signalling pathway in female rPASMCs.

Female rat pulmonary artery smooth muscle cells (rPASMCs) were seeded in 100 mm dishes at $2.2x10^6$ cells/dish, cultured to ~70% confluency, quiesced (0.2% charcoal stripped fetal bovine serum (FBS) in phenol red-free Dulbecco's Modified Eagle Medium (DMEM)) for 24 hours, then stimulated with 10 nM 16α-hydroxyestradiol (16OHE2) or vehicle (Veh) control (10 nM ethanol) for 24 hours prior to RNA lysis. Stimulations were carried out in phenol red-free DMEM with 1% charcoal stripped FBS. Basal CT value = average CT value in the vehicle control group. FC= Fold change, calculated by ΔΔCT method and represented as relative to the vehicle (where the average vehicle fold change is 1). Normality was assessed by Shapiro-Wilk test. Data are expressed as ±SEM and analysed by unpaired t-test or Mann-Whitney test. n=6.

4.2.4 Effects of 16OHE2 (24 Hours Incubation) on the Expression of Genes Within the BMRP2 Signalling Pathway in Rat Pulmonary Artery Smooth Muscle Cells Under Acute Hypoxia

Mair et al. observed that chronic hypoxia suppressed BMPR2 expression in the lung tissue of male and female C57BL/6 mice[33]. Similarly, Maruyama et al. observed that 3- and 6-hours stimulation with the hypoxia mimetic cobalt chloride (100 μM) decreased expression of BMPR2 and Id1 in hPASMCs from control subjects[354]. On the other hand, Ichimori et al. observed that BMPR2 signalling in human PAECs increased in response to E2 under normoxic conditions but decreased under acute hypoxia (1% O_2), and these effects were attenuated by the ERα inhibitor fulvestrant (ICI 182,780)[148]. Therefore, we wished to investigate the effects of 16OHE2 on the BMPR2 signalling pathway under acute hypoxic conditions.

We investigated the effects of 24 hours stimulation with 10 nM 16OHE2 under acute hypoxia (72 hours in 1% O_2, 5% CO_2, nitrogen) on the expression of the following genes within the BMPR2 signalling pathway: *Bmpr2*, *Smad1*, *Smad2*, *Smad3*, *Smad4*, *Smad5*, *Smad6*, *Smad7*, *Smad9*, *Id1*, *Id2* and *Id3*. In male rPASMCs, *Bmpr2, Smad1*, *Smad4* and *Smad5* expression significantly decreased in response to 16OHE2 (Figure 4.3, Table 4.7). On the other hand, *Bmpr2* expression significantly increased in female rPASMCs but there were no other changes in gene expression (Figure 4.4, Table 4.8).

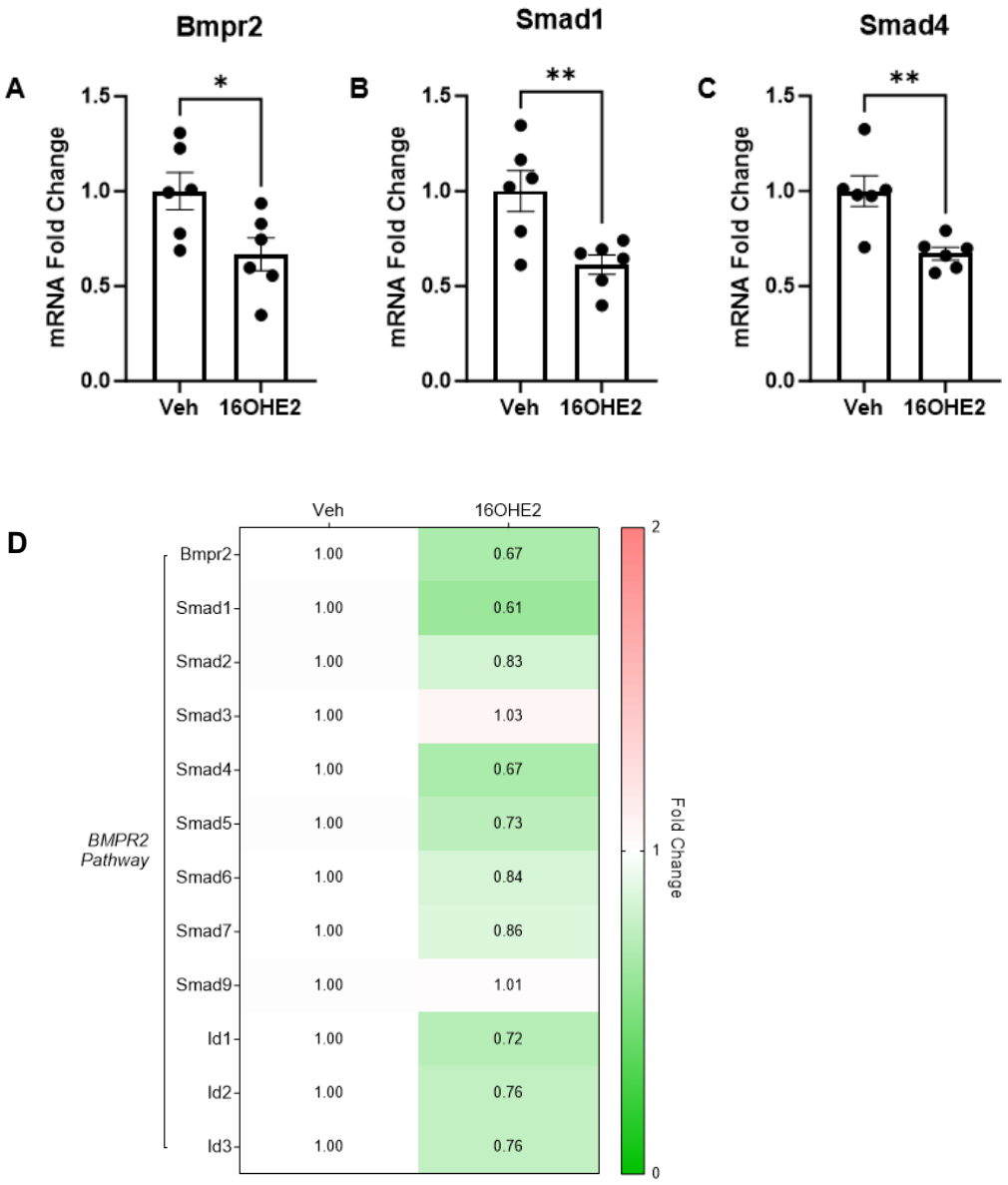

Figure 4.3: Effects 16OHE2 on expression of genes within the BMPR2 signalling pathway in male rPASMCs under 72 hours acute hypoxia.

Male rat pulmonary artery smooth muscle cells (rPASMCs) were seeded in 100 mm dishes at $2.2x10^6$ cells/dish. The following day, the culture media was refreshed, and the cells placed into hypoxia (1% O_2/ 5% CO_2/ nitrogen) for 72 hours as previously described. On day 3, the cells (~70% confluency) were quiesced (0.2% charcoal stripped fetal bovine serum (FBS) in phenol red-free Dulbecco's Modified Eagle Medium (DMEM)) for 24 hours. Cells were stimulated with 10 nM 16α-hydroxyestradiol (16OHE2) or vehicle control (10 nM ethanol) for 24 hours (in phenol red-free DMEM with 1% charcoal stripped FBS). Basal CT value = average CT value in the vehicle control group. FC= Fold change, calculated by ΔΔCT method and represented as relative to the vehicle (where the average vehicle fold change is 1). (A) *Bmpr2.* (B) *Smad1*. (C) *Smad4*. (D) Heatmap comparison of the fold change mRNA expression in response to 16OHE2 compared to the vehicle. Green = <1, white = 1, red = >1. Data are expressed as ±SEM and analysed by unpaired t-test. *p<0.05, **p<0.01. n=6.

Table 4.7: Effects of 16OHE2 on Expression of Genes Within the BMPR2 Signalling Pathway in Male rPASMCs Under 72 Hours Acute Hypoxia

PATHWAY	GENES	Basal CT value	16OHE2 vs. Veh	
			FC ± SEM	P-value
BMPR2 Pathway	***Bmpr2***	29.2	0.67 ± 0.09	0.0300*
	Smad1	27.8	0.61 ± 0.05	0.0089*
	Smad2	29.7	0.83 ± 0.05	0.1845
	Smad3	28.9	1.04 ± 0.04	0.7091
	Smad4	27.5	0.67 ± 0.08	0.0036*
	Smad5	29.7	0.73 ± 0.05	0.0065*
	Smad6	28.1	0.84 ± 0.05	0.2358
	Smad7	29.9	0.86 ± 0.07	0.2398
	Smad9	31.2	1.01 ± 0.09	0.9603
	Id1	30.1	0.72 ± 0.20	0.0924
	Id2	29.9	0.76 ± 0.14	0.3396
	Id3	24.2	0.76 ± 0.10	0.0747

Table 4.7: Effects 16OHE2 on expression of genes within the BMPR2 signalling pathway in male rPASMCs under 72 hours acute hypoxia.

Male rat pulmonary artery smooth muscle cells (rPASMCs) were seeded in 100 mm dishes at 2.2×10^6 cells/dish. The following day, the culture media was refreshed, and the cells placed into hypoxia (1% O_2/ 5% CO_2/ nitrogen) for 72 hours as previously described. On day 3, the cells (~70% confluency) were quiesced (0.2% charcoal stripped fetal bovine serum (FBS) in phenol red-free Dulbecco's Modified Eagle Medium (DMEM)) for 24 hours. Cells were stimulated with 10 nM 16α-hydroxyestradiol (16OHE2) or vehicle (Veh) control (10 nM ethanol) for 24 hours (in phenol red-free DMEM with 1% charcoal stripped FBS). Basal CT value = average CT value in the vehicle control group. FC= Fold change, calculated by ΔΔCT method and represented as relative to the vehicle (where the average vehicle fold change is 1). Normality was assessed by Shapiro-Wilk test. Data are expressed as ±SEM and analysed by unpaired t-test. *$p<0.05$. n=6.

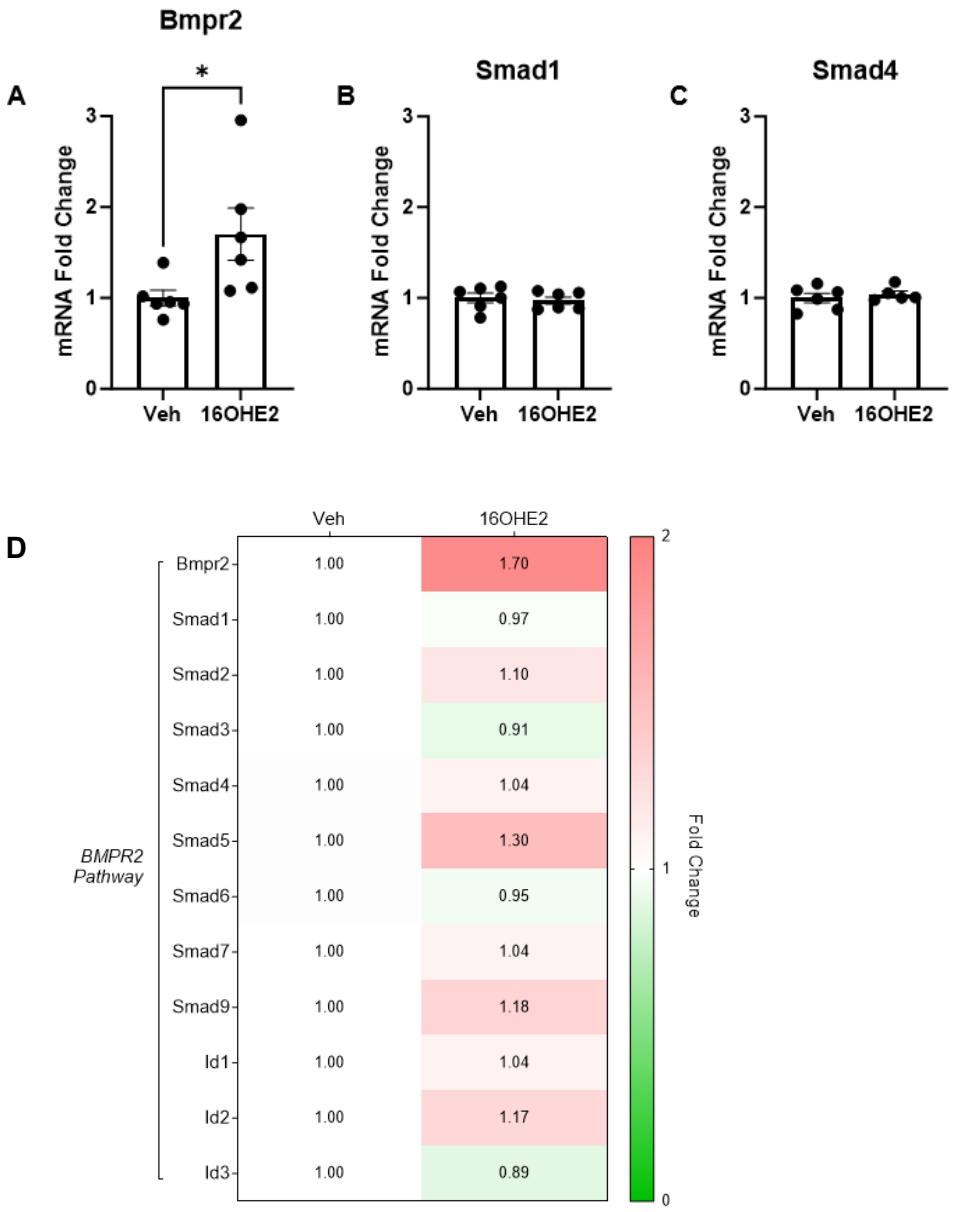

Figure 4.4: Effects 16OHE2 on expression of genes within the BMPR2 signalling pathway in female rPASMCs under 72 hours acute hypoxia.

Female rat pulmonary artery smooth muscle cells (rPASMCs) were seeded in 100 mm dishes at $2.2x10^6$ cells/dish. The following day, the culture media was refreshed, and the cells placed into hypoxia (1% O_2/ 5% CO_2/ nitrogen) for 72 hours as previously described. On day 3, the cells (~70% confluency) were quiesced (0.2% charcoal stripped fetal bovine serum (FBS) in phenol red-free Dulbecco's Modified Eagle Medium (DMEM)) for 24 hours. Cells were stimulated with 10 nM 16α-hydroxyestradiol (16OHE2) or vehicle (Veh) control (10 nM ethanol) for 24 hours in phenol red-free DMEM with 1% charcoal stripped FBS. Basal CT value = average CT value in the vehicle control group. FC= Fold change, calculated by ΔΔCT method and represented as relative to the vehicle (where the average vehicle fold change is 1). (A) *Bmpr2*. (B) *Smad1*. (C) *Smad4*. (D) Heatmap comparison of the fold change mRNA expression in response to 16OHE2 compared to the vehicle. Green = <1, white = 1, red = >1. Data are expressed as ±SEM and analysed by unpaired t-test. *p<0.05. n=6.

Table 4.8: Effects of 16OHE2 on Expression of Genes Within the BMPR2 Signalling Pathway in Female rPASMCs Under 72 Hours Acute Hypoxia

PATHWAY	GENES	Basal CT value	16OHE2 vs. Veh	
			FC ± SEM	P-value
BMPR2 Pathway	***Bmpr2***	27.5	1.70 ± 0.29	0.0407*
	Smad1	27.5	0.97 ± 0.04	0.6910
	Smad2	29.0	1.10 ± 0.10	0.4801
	Smad3	27.8	0.91 ± 0.08	0.4902
	Smad4	26.0	1.04 ± 0.04	0.5246
	Smad5	27.4	1.30 ± 0.18	0.1682
	Smad6	26.4	0.95 ± 0.08	0.7077
	Smad7	27.6	1.04 ± 0.08	0.7713
	Smad9	30.3	1.18 ± 0.09	0.1700
	Id1	30.9	1.04 ± 0.08	0.6398
	Id2	29.6	1.17 ± 0.11	0.2138
	Id3	25.7	0.89 ± 0.08	0.2452

Table 4.8: Effects 16OHE2 on expression of genes within the BMPR2 signalling pathway in female rPASMCs under 72 hours acute hypoxia.
Female rat pulmonary artery smooth muscle cells (rPASMCs) were seeded in 100 mm dishes at $2.2x10^6$ cells/dish. The following day, the culture media was refreshed, and the cells placed into hypoxia (1% O_2/ 5% CO_2/ nitrogen) for 72 hours as previously described. On day 3, the cells (~70% confluency) were quiesced (0.2% charcoal stripped fetal bovine serum (FBS) in phenol red-free Dulbecco's Modified Eagle Medium (DMEM)) for 24 hours. Cells were stimulated with 10 nM 16α-hydroxyestradiol (16OHE2) or vehicle (Veh) control (10 nM ethanol) for 24 hours in phenol red-free DMEM with 1% charcoal stripped FBS. Basal CT value = average CT value in the vehicle control group. FC= Fold change, calculated by ΔΔCT method and represented as relative to the vehicle (where the average vehicle fold change is 1). Normality was assessed by Shapiro-Wilk test. Data are expressed as ±SEM and analysed by unpaired t-test. *$p<0.05$. n=6.

4.2.5 Effects of 16OHE2 on the Expression of Genes Within the BMPR2 Signalling Pathway in the Presence of Estrogen Receptor Antagonists in Male Rat Pulmonary Artery Smooth Muscle Cells

ERα is overexpressed in female PAH patient hPASMCs[102]. Wright et al. observed that the ERα antagonist MPP inhibited E2-induced proliferation of female PAH patient hPASMCs, but the ERβ antagonist PHTPP and GPER antagonist G15 had no effect[102]. Similarly, Austin et al. observed that transfection of increasing quantities of ERα in COS-7 cells (which lack endogenous estrogen receptors) strongly correlates with decreasing *BMPR2* expression[147]. As we observed that 24 hours stimulation with 16OHE2 decreased mRNA expression of *Bmpr2*, *Smad1*, *Smad4* and *Smad5* in male rPASMCs, we wished to investigate whether this effect was mediated by the estrogen receptors.

Male rPASMCs were stimulated with 10 nM 16OHE2 in the presence or absence of 1 μM MPP, 1 μM PHTPP, or 1 μM G15 for 24 hours. Antagonist concentrations of 1 μM were based on a previous study on E2 by Wright et al[102]. The following genes within the BMPR2 signalling pathway were studied: *Bmpr2*, *Smad1*, *Smad4*, *Smad5*, *Smad9*, *Id1*, *Id2* and *Id3*. As previously observed, expression of *Bmpr2*, *Smad1*, *Smad4* and *Smad5* significantly decreased in response to 16OHE2 alone. The decrease in *Smad4* was reversed by MPP, suggesting this effect may occur via ERα. No differences were observed between 16OHE2 alone and the addition of PHTPP or G15 (Figure 4.5, Table 4.9).

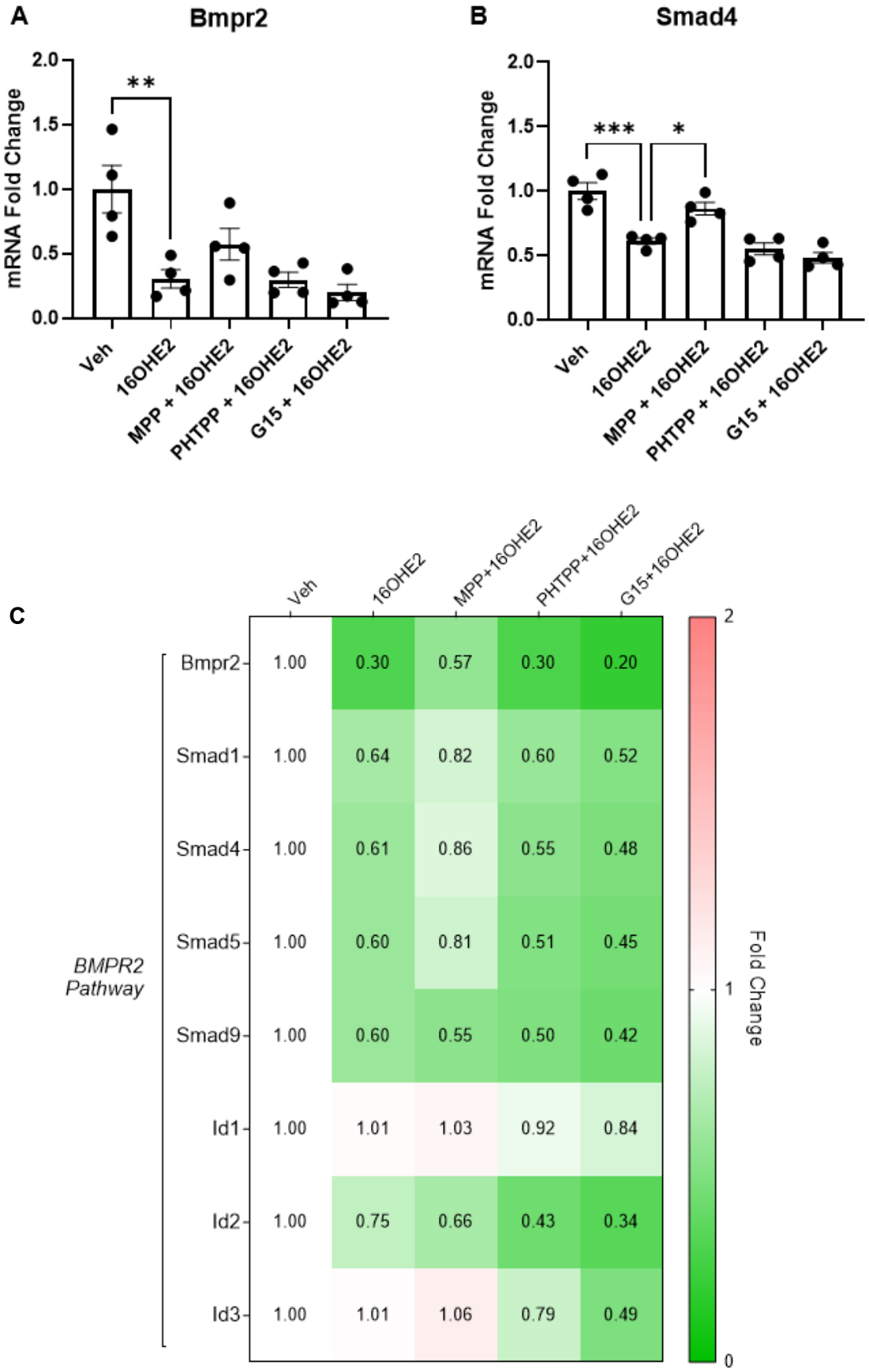
A
Bmpr2
mRNA Fold Change
2.0
1.5
1.0
0.5
0.0
**
Veh
16OHE2
MPP + 16OHE2
PHTPP + 16OHE2
G15 + 16OHE2
B
Smad4
mRNA Fold Change
2.0
1.5
1.0
0.5
0.0
***
*
Veh
16OHE2
MPP + 16OHE2
PHTPP + 16OHE2
G15 + 16OHE2
C
Veh
16OHE2
MPP+16OHE2
PHTPP+16OHE2
G15+16OHE2
BMPR2 Pathway
Bmpr2 1.00 0.30 0.57 0.30 0.20
Smad1 1.00 0.64 0.82 0.60 0.52
Smad4 1.00 0.61 0.86 0.55 0.48
Smad5 1.00 0.60 0.81 0.51 0.45
Smad9 1.00 0.60 0.55 0.50 0.42
Id1 1.00 1.01 1.03 0.92 0.84
Id2 1.00 0.75 0.66 0.43 0.34
Id3 1.00 1.01 1.06 0.79 0.49
Fold Change
2
1
0

Figure 4.5: Effects of 16OHE2 on the expression of genes within the BMPR2 signalling pathway in the presence of estrogen receptor antagonists in male rPASMCs.

Male rat pulmonary artery smooth muscle cells (rPASMCs) were seeded in 100 mm dishes at $2.2x10^6$ cells/dish, cultured to ~70% confluency, quiesced (0.2% charcoal stripped fetal bovine serum (FBS) in phenol red-free Dulbecco's Modified Eagle Medium (DMEM)) for 24 hours, then stimulated with 10 nM 16α-hydroxyestradiol (16OHE2) in the presence or absence of the estrogen receptor antagonists 1 μM MPP (ERα), 1 μM PHTPP (ERβ) or 1 μM G15 (GPER), or with the vehicle (Veh) control (10 nM ethanol) for 24 hours prior to RNA lysis. Stimulations were carried out in phenol red-free DMEM with 1% charcoal stripped FBS. Basal CT value = average CT value in the vehicle control group. FC= Fold change, calculated by ΔΔCT method and represented as relative to the vehicle (where the average vehicle fold change is 1). (A) *Bmpr2.* (B) *Smad4*. (C) Heatmap comparison of the fold change mRNA expression compared to the vehicle. Green = <1, white = 1, red = >1. Normality was assessed using Shapiro-Wilk test. Data are expressed as ±SEM and analysed by one-way ANOVA with post-hoc Tukey test or Kruskal-Wallis test. *p<0.05, **p<0.01, ***p<0.001. n=4.

`

Table 4.9: Effects of 16OHE2 on the Expression of Genes Within the BMPR2 Signalling Pathway in the Presence of Estrogen Receptor Antagonists in Male rPASMCs.

PATHWAY	GENES	Basal CT value	16OHE2 vs. Veh		MPP + 16OHE2 vs. Veh		PHTPP + 16OHE2 vs. Veh		G15 + 16OHE2 vs. Veh	
			FC ± SEM	P-value	FC ± SEM	P-value	FC ± SEM	P-value	FC ± SEM	P-value
BMPR2 Pathway	***Bmpr2***	25.7	0.31 ± 0.07	0.0036*	0.57 ± 0.12	0.0950	0.30 ± 0.06	0.0033*	0.20 ± 0.12	0.0010*
	Smad1	26.6	0.64 ± 0.05	0.0055*	0.82 ± 0.07	0.2559	0.60 ± 0.09	0.0018*	0.52 ± 0.02	0.0003*
	Smad4	25.4	0.61 ± 0.03	0.0002*	0.86 ± 0.05	0.2852	0.55 ± 0.05	<0.0001*	0.48 ± 0.04	<0.0001*
	Smad5	27.2	0.60 ± 0.03	0.0012*	0.81 ± 0.08	0.1566	0.51 ± 0.07	0.0001*	0.45 ± 0.03	<0.0001*
	Smad9	30.1	0.60 ± 0.08	0.0905	0.55 ± 0.04	0.0733	0.50 ± 0.12	0.0250*	0.43 ± 0.06	0.0091*
	Id1	30.3	1.01 ± 0.14	>0.9999	1.03 ± 0.18	>0.9999	0.92 ± 0.21	0.9979	0.84 ± 0.15	0.9657
	Id2	27.5	0.75 ± 0.10	0.3694	0.66 ± 0.05	0.1647	0.43 ± 0.07	0.0050*	0.35 ± 0.08	0.0015*
	Id3	24.7	1.01 ± 0.22	>0.9999	1.06 ± 0.22	>0.9999	0.79 ± 0.24	>0.9999	0.49 ± 0.04	0.2708

Table 4.9: Effects 16OHE2 on the expression of genes within the BMPR2 signalling pathway in the presence of estrogen receptor antagonists in male rPASMCs.

Male rat pulmonary artery smooth muscle cells (rPASMCs) were seeded in 100 mm dishes at 2.2×10^6 cells/dish, cultured to ~70% confluency, quiesced (0.2% charcoal stripped fetal bovine serum (FBS) in phenol red-free Dulbecco's Modified Eagle Medium (DMEM)) for 24 hours, then stimulated with 10 nM 16α-hydroxyestradiol (16OHE2) in the presence or absence of the estrogen receptor antagonists 1 μM MPP (ERα), 1 μM PHTPP (ERβ) or 1 μM G15 (GPER), or with the vehicle (Veh) control (10 nM ethanol) for 24 hours prior to RNA lysis. Stimulations were carried out in phenol red-free DMEM with 1% charcoal stripped FBS. Basal CT value = average CT value in the vehicle control group. FC= Fold change, calculated by ΔΔCT method and represented as relative to the vehicle (where the average vehicle fold change is 1). Normality was assessed using Shapiro-Wilk test. Data are expressed as ±SEM and analysed by one-way ANOVA with post-hoc Tukey test or Kruskal-Wallis test. *p<0.05. n=4.

4.2.6 Effects of 16OHE2 (2 Hours Incubation) on the Expression of Genes Within the BMPR2 Signalling Pathway in Male Rat Pulmonary Artery Smooth Muscle Cells

Most research in PAH has focused on ERα and ERβ, but estrogens can also act through GPER which mediates rapid non-genomic effects, triggering intracellular signalling cascades which alter downstream gene expression[113]. Wright et al. observed that GPER was localised to vascular smooth muscle in the human lung[102]. Activation of GPER with the agonist G1 mediates cardioprotective effects in male and ovariectomised female rats with MCT-induced PAH[125,126]. Furthermore, the half-life of 16OHE2 is short (e.g., 3-4 hours in male and female Sprague-Dawley rats, 1.5-5.3 hours in human female volunteers)[339,340]. Therefore, we wished to investigate the effects of a shorter 2-hour stimulation on expression of genes within the BMPR2 signalling pathway in male rPASMCs.

The following genes within the BMPR2 signalling pathway were studied: *Bmpr2*, *Smad1*, *Smad4*, *Smad5*, *Smad9*, *Id1*, *Id2* and *Id3*. *Id2* expression significantly decreased in male rPASMCs following 2 hours stimulation within 10 nM 16OHE2. No other changes in gene expression were observed (Figure 4.6, Table 4.10).

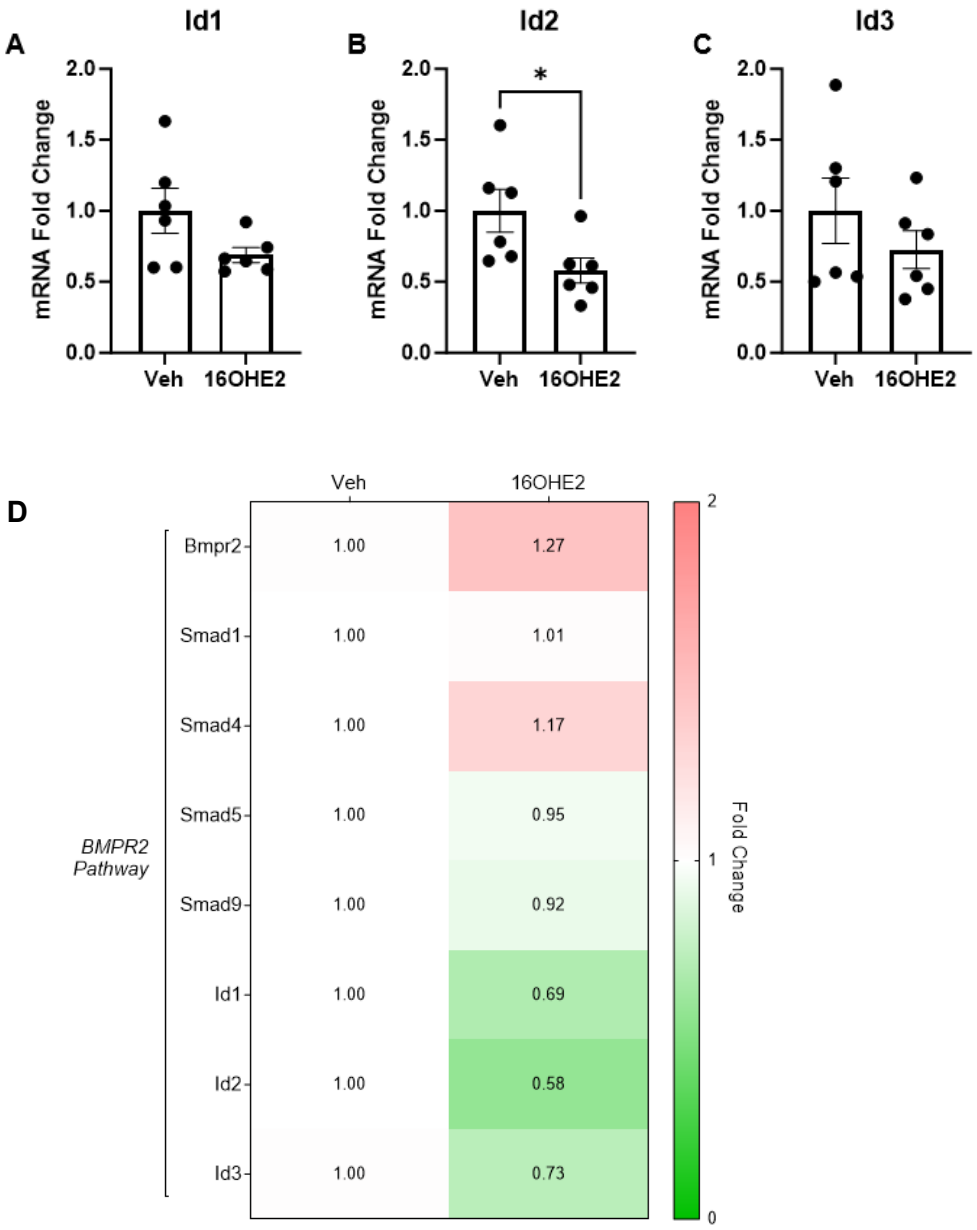

Figure 4.6: Effects of 2 hours stimulation with 16OHE2 on expression of genes within the BMPR2 signalling pathway in male rPASMCs.

Male rat pulmonary artery smooth muscle cells (rPASMCs) were seeded in 100 mm dishes at 2.2×10^6 cells/dish, cultured to ~70% confluency, quiesced (0.2% charcoal stripped fetal bovine serum (FBS) in phenol red-free Dulbecco's Modified Eagle Medium (DMEM)) for 24 hours, then stimulated with 10 nM 16α-hydroxyestradiol (16OHE2), or vehicle (Veh) control (10 nM ethanol) for 2 hours prior to RNA lysis. Stimulations were carried out in phenol red-free DMEM with 1% charcoal stripped FBS. Basal CT value = average CT value in the vehicle control group. FC= Fold change, calculated by ΔΔCT method and represented as relative to the vehicle (where the average vehicle fold change is 1). (A) *Id1* (B) *Id2* (C) *Id3* (D) Heatmap comparison of the fold change mRNA expression in response to 16OHE2 compared to the vehicle. Green = <1, white = 1, red = >1. Normality was assessed by Shapiro-Wilk test. Data are expressed as ±SEM and analysed by unpaired t-test. *p<0.05. n=6.

Table 4.10: Effects of 2 Hours Stimulation With 16OHE2 on Expression of Genes Within the BMPR2 Signalling Pathway in Male rPASMCs

PATHWAY	GENES	Basal CT value	16OHE2 vs. Veh	
			FC ± SEM	P-value
BMPR2 Pathway	***Bmpr2***	26.0	1.27 ± 0.16	0.1905
	Smad1	27.1	1.01 ± 0.14	0.9721
	Smad4	25.8	1.18 ± 0.12	0.2240
	Smad5	27.6	0.95 ± 0.09	0.7073
	Smad9	31.6	0.92 ± 0.10	0.5155
	Id1	29.0	0.69 ± 0.05	0.0933
	Id2	27.7	0.58 ± 0.09	0.0366*
	Id3	23.2	0.73 ± 0.13	0.3245

Table 4.10: Effects of 2 hours stimulation with 16OHE2 on expression of genes within the BMPR2 signalling pathway in male rPASMCs.

Male rat pulmonary artery smooth muscle cells (rPASMCs) were seeded in 100 mm dishes at 2.2×10^6 cells/dish, cultured to ~70% confluency, quiesced (0.2% charcoal stripped fetal bovine serum (FBS) in phenol red-free Dulbecco's Modified Eagle Medium (DMEM)) for 24 hours, then stimulated with 10 nM 16α-hydroxyestradiol (16OHE2), or vehicle (Veh) control (10 nM ethanol) for 2 hours prior to RNA lysis. Stimulations were carried out in phenol red-free DMEM with 1% charcoal stripped FBS. Basal CT value = average CT value in the vehicle control group. FC= Fold change, calculated by ΔΔCT method and represented as relative to the vehicle (where the average vehicle fold change is 1). Normality was assessed by Shapiro-Wilk test. Data are expressed as ±SEM and analysed by unpaired t-test. *$p<0.05$. n=6.

4.2.7 Basal Expression of the BMPR2 Signalling Pathway in Male and Female Rat Pulmonary Artery Smooth Muscle Cells

We hypothesised that decreased expression of *Bmpr2*, *Smad1*, *Smad4* and *Smad5* in response to 16OHE2 was only observed in male rPASMCs because basal BMPR2 levels were already suppressed in females. In the absence of PAH, basal BMPR2 signalling is lower in female control subject hPASMCs compared to males[104]. For example, Mair et al. observed decreased basal mRNA and protein expression of BMPR2, SMAD1, Id1 and Id3 in female control subject hPASMCs[104]. This appears to be dependent on E2, which significantly decreased the levels of Id1 and Id3 mRNA and protein in male control subject hPASMCs, resulting in expression levels akin to females[104]. Furthermore, only female Smad1$^{+/-}$ mice spontaneously develop PAH and this is reversed by ovariectomy[104]. Therefore, we wished to compare basal expression of the BMPR2 pathway in male and female rPASMCs.

The following genes within the BMPR2 signalling pathway were studied: *Bmpr2*, *Smad1*, *Smad2*, *Smad3*, *Smad4*, *Smad5*, *Smad6*, *Smad7*, *Smad9*, *Id1*, *Id2* and *Id3*. *Smad4* expression was significantly lower in female rPASMCs compared to males. On the other hand, basal expression of *Smad3* and *Id1* were significantly increased in female rPASMCs compared to males (Table 4.11, Figure 4.7). Basal BMPR2 protein levels were significantly lower in female rPASMCs compared to males (Figure 4.7).

Table 4.11: Basal Expression of Genes Within the BMPR2 Signalling Pathway in Female rPASMCs Compared to Male rPASMCs

PATHWAY	GENES	Basal CT value	Females vs. Males	
			FC ± SEM	P-value
BMPR2 Pathway	***Bmpr2***	26.2	0.72 ± 0.17	0.2192
	Smad1	26.9	1.05 ± 0.07	0.7196
	Smad2	27.7	0.84 ± 0.07	0.1372
	Smad3	27.9	1.38 ± 0.13	0.0487*
	Smad4	25.4	0.80 ± 0.06	0.0334*
	Smad5	27.5	0.86 ± 0.07	0.1307
	Smad6	26.3	0.86 ± 0.07	0.2256
	Smad7	28.1	0.92 ± 0.10	0.5439
	Smad9	30.5	0.98 ± 0.10	0.8537
	Id1	27.9	1.47 ± 0.15	0.0316*
	Id2	26.8	0.73 ± 0.12	0.1169
	Id3	23.2	1.04 ± 0.11	0.7859

Table 4.11: Basal expression of genes within the BMPR2 signalling pathway in female rPASMCs compared to male rPASMCs.

Rat pulmonary artery smooth muscle cells (rPASMCs) were seeded in 100 mm dishes at $2.2x10^6$ cells/dish and cultured for 3 days until 90-100% confluent before RNA lysis as previously described. Male and female rPASMCs were passage-matched at P3. Basal CT value = average CT value in male rPASMCs. FC= Fold change, calculated by ΔΔCT method and represented as relative to male rPASMCs (where the average male rPASMC fold change is 1). Normality was assessed by Shapiro-Wilk test. Data are expressed as ±SEM and analysed by unpaired t-test. *p<0.05. n=5-6.

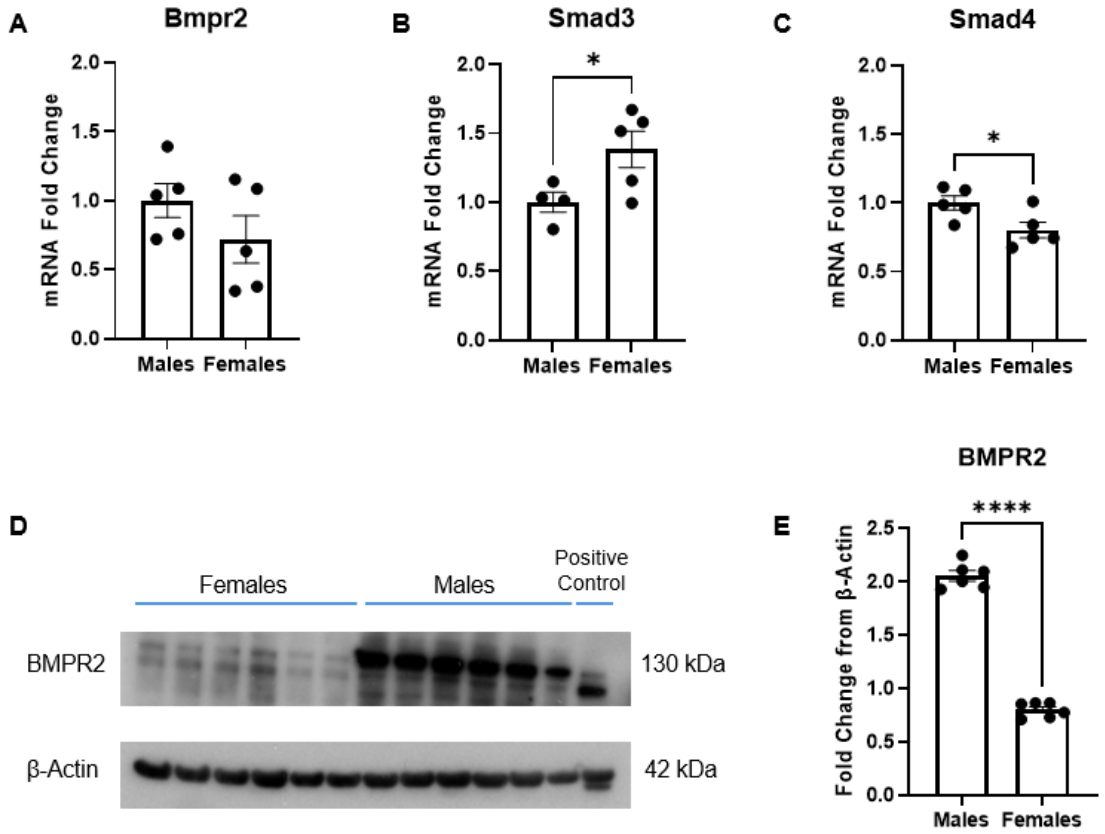

Figure 4.7: Basal expression of the BMPR2 signalling pathway in female rPASMCs compared to male rPASMCs.

Rat pulmonary artery smooth muscle cells (rPASMCs) were seeded in 100 mm dishes at 2.2×10^6 cells/dish and cultured for 3 days until 90-100% confluent before RNA and protein lysis as previously described. For qRT-PCR, male and female rPASMCs were passage-matched at P3. For western blots, male rPASMCs were passage 5-6 and female rPASMCs passage 3 due to the primary cell lines available at the time. Basal CT value = average CT value in the male rPASMCs. FC= Fold change, calculated by ΔΔCT method and represented as relative to male rPASMCs (where the average male rPASMC fold change is 1). (A) *Bmpr2*. (B) *Smad3*. (C) *Smad4*. (D) Immunoblot of BMPR2. Positive control = rat lung lysates. (E) Quantification of BMPR2 protein expression in male and female rPASMCs. Fold change is BMPR2 relative to β-actin expression. Normality was assessed by Shapiro-Wilk test. Data are expressed as ±SEM and analysed by unpaired t-test. *$p<0.05$, ****$p<0.0001$. n=5-6.

4.2.8 Effects of 16OHE2 on the Expression of Genes Within the BMPR2 Signalling Pathway in Human Male Control Subject Pulmonary Artery Smooth Muscle Cells

Following the observation that there was a decrease in *Bmpr2*, *Smad1*, *Smad4* and *Smad5* expression in response to 16OHE2 in male rPASMCs, we wished to investigate whether these effects would translate to hPASMCs. hPASMCs from male control subjects were used because basal BMPR2 signalling is suppressed in PAH patients, and, in the absence of PAH, BMPR2 expression is lower in female hPASMCs than male hPASMCs[102,141]. The hPASMCs were provided by Professor Nick Morrell (University of Cambridge, UK) with ethical permission and are isolated from small distal pulmonary arteries. Due to the shortage of human cells during the COVID-19 pandemic, experiments were repeated three times in three cell lines from individual donors (n=9). These are referred to by the anonymous internal identifiers 103MP, 79MP and 93MP. The characteristics of the human cell donors are shown in Table 4.12.

Table 4.12: Characteristics of the Human Male Control Subject Pulmonary Artery Smooth Muscle Cell Donors

ID	Sex	Age	Conditions	Medications
103MP	Male	52	Mild bronchiectasis, adenocarcinoma	Unknown
79MP	Male	60	Squamous cell carcinoma	Unknown
93MP	Male	75	Lobectomy (lung cancer)	Unknown

In male control subject hPASMCs, we studied the effects of 24 hours stimulation with 10 nM 16OHE2 on the following genes within the BMPR2 signalling pathway: *BMPR2*, *SMAD1*, *SMAD4*, *SMAD5*, *SMAD9*, *ID1*, *ID2,* and *ID3*. *BMPR2* and *SMAD4* expression significantly decreased in response to 16OHE2 (Figure 4.8, Table 4.13).

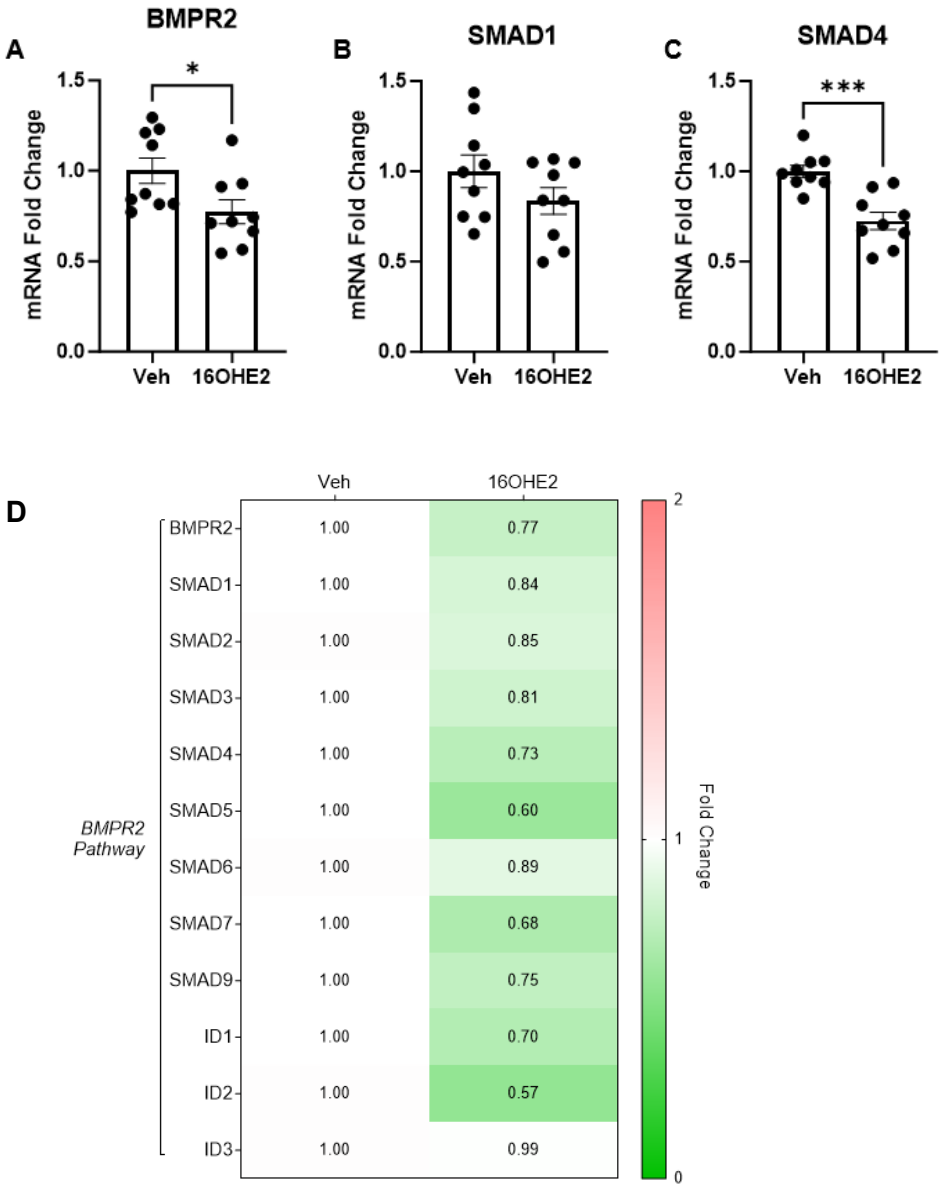

Figure 4.8: Effects 16OHE2 on expression of genes within the BMPR2 signalling pathway in male control subject hPASMCs.

Human male control subject pulmonary artery smooth muscle cells (hPASMCs) were seeded in 100 mm dishes at 2.2×10^6 cells/dish, cultured to ~70% confluency, quiesced (0.2% charcoal stripped fetal bovine serum (FBS) in phenol red-free Dulbecco's Modified Eagle Medium (DMEM)) for 24 hours, then stimulated with 10 nM 16α-hydroxyestradiol (16OHE2) or vehicle (Veh) control (10 nM ethanol) for 24 hours prior to RNA lysis. Stimulations were carried out in phenol red-free DMEM with 1% charcoal stripped FBS. Basal CT value = average CT value in the vehicle control group. FC= Fold change, calculated by ΔΔCT method and represented as relative to the vehicle (where the average vehicle fold change is 1). (A) *BMPR2*. (B) *SMAD1*. (C) *SMAD4*. (D) Heatmap comparison of the fold change mRNA expression in response to 16OHE2 compared to the vehicle. Green = <1, white = 1, red = >1. Normality was assessed using Shapiro-Wilk test. Data are expressed as ±SEM and analysed by unpaired t-test or Mann-Whitney test. *p<0.05, ***p<0.001. n=9.

Table 4.13: Effects of 16OHE2 on Expression of Genes Within the BMPR2 Signalling Pathway in Male Control Subject hPASMCs

PATHWAY	GENES	Basal CT value	16OHE2 vs. Veh	
			FC ± SEM	P-value
BMPR2 Pathway	***BMPR2***	31.2	0.77 ± 0.07	0.0315*
	SMAD1	32.6	0.84 ± 0.07	0.1792
	SMAD2	29.8	0.85 ± 0.15	0.4607
	SMAD3	27.1	0.81 ± 0.08	0.2470
	SMAD4	29.6	0.73 ± 0.05	0.0002*
	SMAD5	32.2	0.61 ± 0.09	0.0835
	SMAD6	30.1	0.89 ± 0.12	0.5110
	SMAD7	30.5	0.68 ± 0.26	0.2224
	SMAD9	34.3	0.75 ± 0.11	0.2153
	ID1	27.4	0.70 ± 0.35	0.2581
	ID2	30.4	0.57 ± 0.16	0.0625
	ID3	29.1	0.99 ± 0.52	0.6665

Table 4.13: Effects 16OHE2 on expression of genes within the BMPR2 signalling pathway in male control subject hPASMCs.

Human male control subject pulmonary artery smooth muscle cells (hPASMCs) were seeded in 100 mm dishes at 2.2×10^6 cells/dish, cultured to ~70% confluency, quiesced (0.2% charcoal stripped fetal bovine serum (FBS) in phenol red-free Dulbecco's Modified Eagle Medium (DMEM)) for 24 hours, then stimulated with 10 nM 16α-hydroxyestradiol (16OHE2) or vehicle (Veh) control (10 nM ethanol) for 24 hours prior to RNA lysis. Stimulations were carried out in phenol red-free DMEM with 1% charcoal stripped FBS. Basal CT value = average CT value in the vehicle control group. FC= Fold change, calculated by ΔΔCT method and represented as relative to the vehicle (where the average vehicle fold change is 1). Normality was assessed using Shapiro-Wilk test. Data are expressed as ±SEM and analysed by unpaired t-test or Mann-Whitney test. *$p<0.05$. n=9.

4.2.9 Effects of 16OHE2 on the Expression of Genes Within the BMPR2 Signalling Pathway in Rat Aorta Smooth Muscle Cells

The source of E2 synthesis may be important in PAH. Many studies have suggested that ovarian-synthesised E2 is protective against pulmonary vascular remodelling, haemodynamic alterations, and RV hypertrophy[36,37,38]. E2 is also a known vasodilator in the systemic circulation and is associated with cardioprotective effects in premenopausal women[113]. On the other hand, circulating E2 levels are higher in men and postmenopausal women with PAH compared to control subjects, and are associated with worse disease outcomes (e.g., decreased 6-minute walk distance)[30,31]. Furthermore, E2 has been demonstrated to increase proliferation of female control subject and PAH patient hPASMCs, and the aromatase inhibitor anastrozole has been investigated in clinical trials for PAH[35,102,279-281]. Aberrant proliferation of vascular smooth muscle cells is associated with several disease pathologies, e.g., atherosclerosis[355]. The bone morphogenetic protein 2/4/7 antagonist gremlin is constitutively expressed the normal vasculature[356]. Increased gremlin expression (and consequent reduction in BMPR2 signalling) are associated with vascular smooth muscle cell proliferation and migration and may be pathogenic in both systemic vascular injury and PAH[356,357]. Therefore, we wished to investigate the effects of 16OHE2 on the BMPR2 pathway in aorta smooth muscle cells (AoSMCs).

We investigated the effects of 24 hours stimulation with 10 nM 16OHE2 in male and female rat AoSMCs on the following genes within the BMPR2 signalling pathway: *Bmpr2*, *Smad1*, *Smad2*, *Smad3*, *Smad4*, *Smad5*, *Smad6*, *Smad7*, *Smad9*, *Id1*, *Id2* and *Id3*. In male rat AoSMCs, expression of *Smad3*, *Smad6*, *Id1*, *Id2* and *Id3* significantly decreased in response to 16OHE2 (Figure 4.9, Table 4.14). In female rat AoSMCs, *Smad2*, *Smad3*, *Smad4*, *Smad7*, *Id2* and *Id3* significantly decreased in response to 16OHE2 (Figure 4.10, Table 4.15).

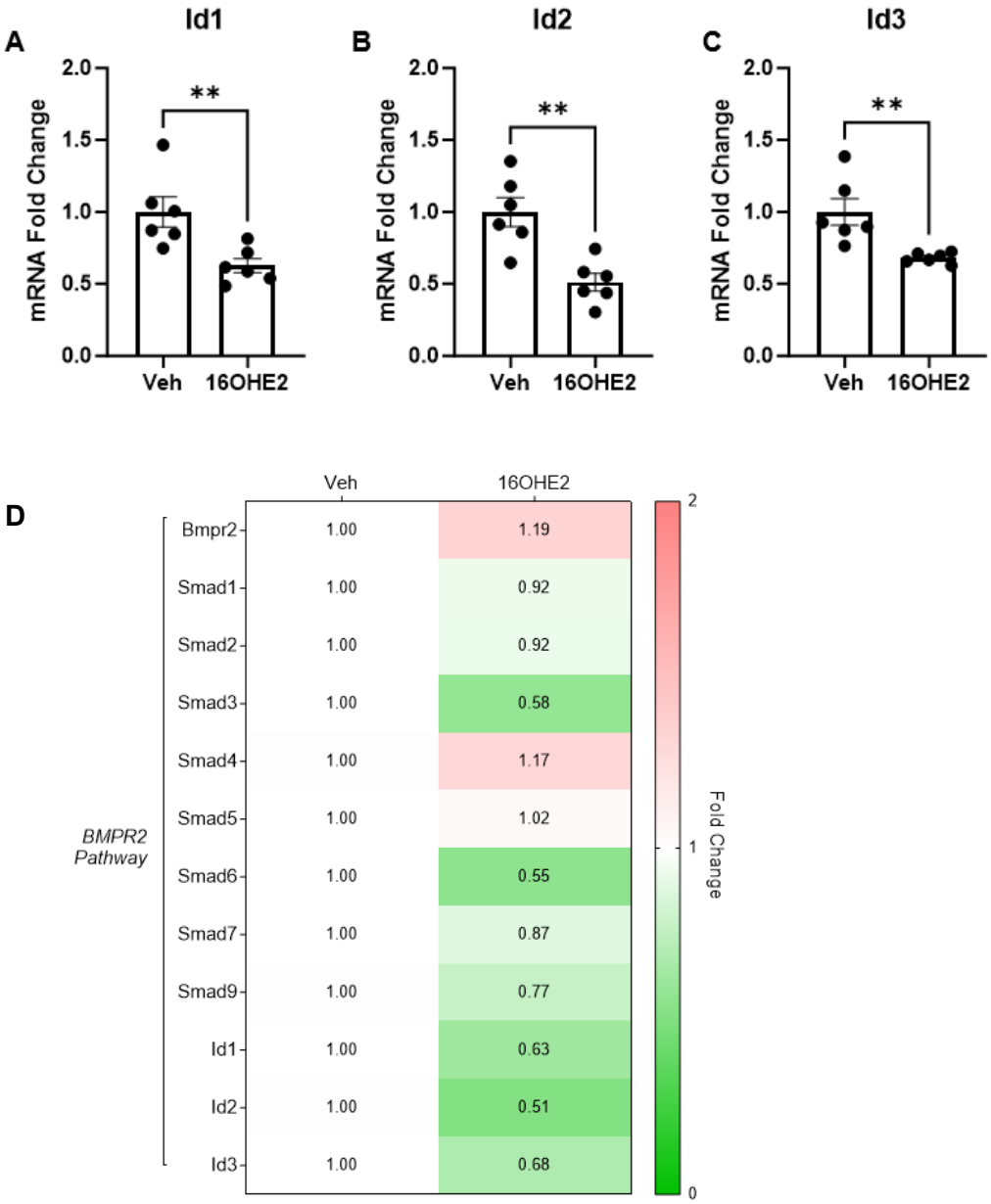

Figure 4.9: Effects 16OHE2 on expression of genes within the BMPR2 signalling pathway in male rat AoSMCs.

Male rat aorta smooth muscle cells (AoSMCs) were seeded in 6-well plates at $3x10^5$ cells/well, cultured to ~70% confluency, quiesced (0.2% charcoal stripped fetal bovine serum (FBS) in phenol red-free Dulbecco's Modified Eagle Medium (DMEM)) for 24 hours, then stimulated with 10 nM 16α-hydroxyestradiol (16OHE2), or vehicle (Veh) control (10 nM ethanol) for 24 hours prior to RNA lysis. Stimulations were carried out in phenol red-free DMEM with 1% charcoal stripped FBS. Basal CT value = average CT value in the vehicle control group. FC= Fold change, calculated by ΔΔCT method and represented as relative to the vehicle (where the average vehicle fold change is 1). (A) *Id1*. (B) *Id2*. (C) *Id3*. (D) Heatmap comparison of the fold change mRNA expression in response to 16OHE2 compared to the vehicle. Green = <1, white = 1, red = >1. Normality was assessed using Shapiro-Wilk test. Data are expressed as ±SEM and analysed by unpaired t-test. **p<0.01. n=6.

Table 4.14: Effects of 16OHE2 on Expression of Genes Within the BMPR2 Signalling Pathway in Male Rat AoSMCs

PATHWAY	GENES	Basal CT value	16OHE2 vs. Veh	
			FC ± SEM	P-value
BMPR2 Pathway	***Bmpr2***	26.5	1.19 ± 0.13	0.3399
	Smad1	27.8	0.92 ± 0.08	0.6491
	Smad2	27.8	0.92 ± 0.12	0.6753
	Smad3	28.3	0.58 ± 0.12	0.0074*
	Smad4	25.5	1.17 ± 0.18	0.5315
	Smad5	26.5	1.02 ± 0.10	0.9054
	Smad6	26.6	0.55 ± 0.06	0.0006*
	Smad7	28.1	0.87 ± 0.09	0.3257
	Smad9	31.1	0.77 ± 0.11	0.2483
	Id1	27.8	0.63 ± 0.05	0.0088*
	Id2	27.5	0.51 ± 0.06	0.0021*
	Id3	23.0	0.68 ± 0.02	0.0068*

Table 4.14: Effects 16OHE2 on expression of genes within the BMPR2 signalling pathway in male rat AoSMCs.

Male rat aorta smooth muscle cells (AoSMCs) were seeded in 6-well plates at $3x10^5$ cells/well, cultured to ~70% confluency, quiesced (0.2% charcoal stripped fetal bovine serum (FBS) in phenol red-free Dulbecco's Modified Eagle Medium (DMEM)) for 24 hours, then stimulated with 10 nM 16α-hydroxyestradiol (16OHE2), or vehicle (Veh) control (10 nM ethanol) for 24 hours prior to RNA lysis. Stimulations were carried out in phenol red-free DMEM with 1% charcoal stripped FBS. Basal CT value = average CT value in the vehicle control group. FC= Fold change, calculated by ΔΔCT method and represented as relative to the vehicle (where the average vehicle fold change is 1). Normality was assessed using Shapiro-Wilk test. Data are expressed as ±SEM and analysed by unpaired t-test. *$p<0.05$. n=6.

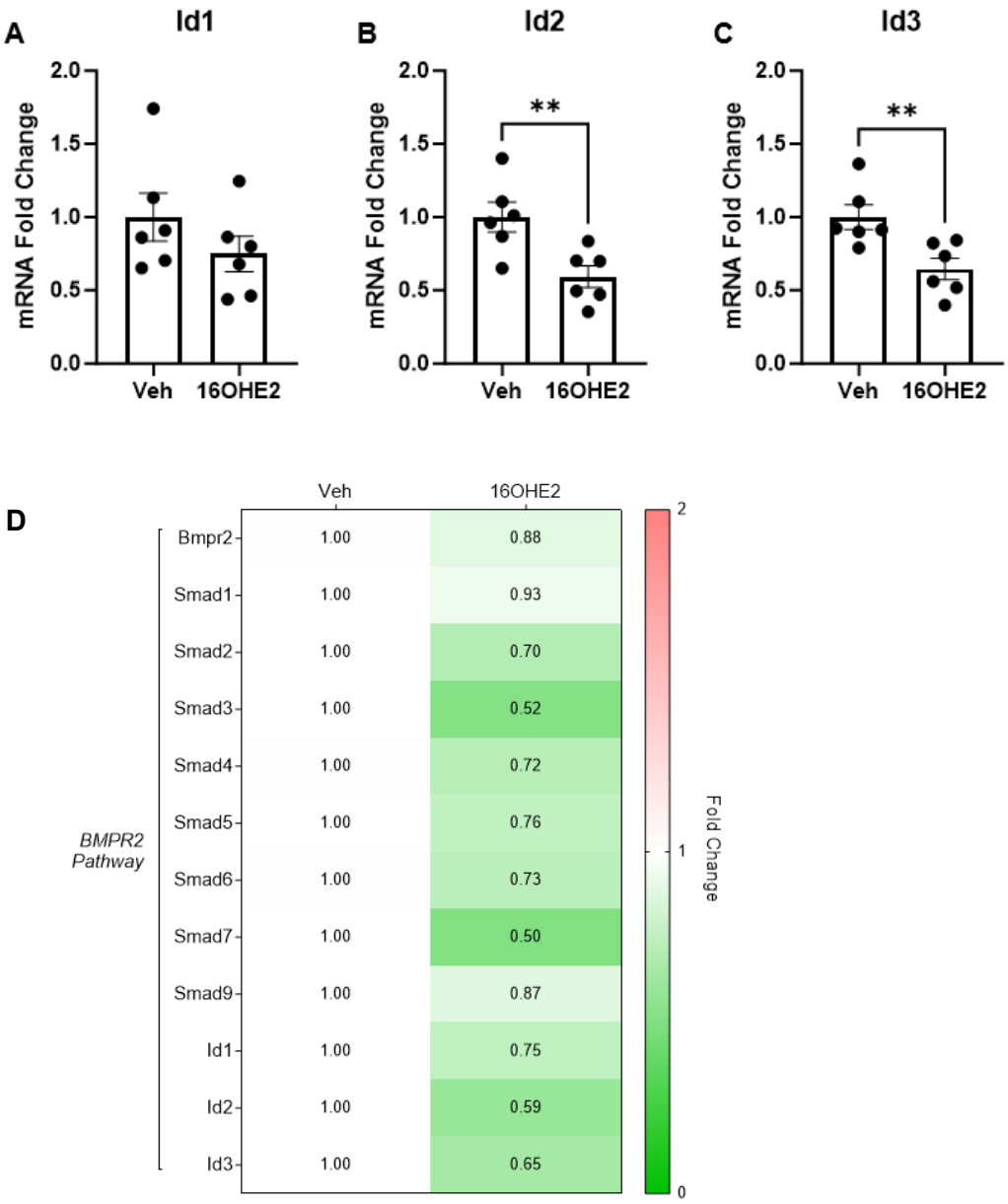

Figure 4.10: Effects 16OHE2 on expression of genes within the BMPR2 signalling pathway in female rat AoSMCs.

Female rat aorta smooth muscle cells (AoSMCs) were seeded in 6-well plates at $3x10^5$ cells/well, cultured to ~70% confluency, quiesced (0.2% charcoal stripped fetal bovine serum (FBS) in phenol red-free Dulbecco's Modified Eagle Medium (DMEM)) for 24 hours, then stimulated with 10 nM 16α-hydroxyestradiol (16OHE2) or vehicle (Veh) control (10 nM ethanol) for 24 hours prior to RNA lysis. Stimulations were carried out in phenol red-free DMEM with 1% charcoal stripped FBS. Basal CT value = average CT value in the vehicle control group. FC= Fold change, calculated by ΔΔCT method and represented as relative to the vehicle (where the average vehicle fold change is 1). (A) *Id1.* (B) *Id2* (C) *Id3.* (D) Heatmap comparison of the fold change mRNA expression in response to 16OHE2 compared to the vehicle. Green = <1, white = 1, red = >1. Normality was assessed using Shapiro-Wilk test. Data are expressed as ±SEM and analysed by unpaired t-test or Mann-Whitney test. **p<0.01. n=6.

Table 4.15: Effects of 16OHE2 on Expression of Genes Within the BMPR2 Signalling Pathway in Female Rat AoSMCs

PATHWAY	GENES	Basal CT value	16OHE2 vs. Veh	
			FC ± SEM	P-value
BMPR2 Pathway	***Bmpr2***	25.9	0.88 ± 0.17	0.6135
	Smad1	27.0	0.93 ± 0.09	0.6671
	Smad2	27.8	0.71 ± 0.04	0.0037*
	Smad3	27.5	0.52 ± 0.02	0.0009*
	Smad4	25.0	0.72 ± 0.06	0.0139*
	Smad5	27.4	0.76 ± 0.07	0.1319
	Smad6	27.6	0.73 ± 0.05	0.0931
	Smad7	29.4	0.50 ± 0.05	0.0022*
	Smad9	30.9	0.87 ± 0.16	0.5698
	Id1	28.0	0.75 ± 0.12	0.2458
	Id2	27.8	0.59 ± 0.07	0.0090*
	Id3	24.0	0.65 ± 0.07	0.0099*

Table 4.15: Effects 16OHE2 on expression of genes within the BMPR2 signalling pathway in female rat AoSMCs.

Female rat aorta smooth muscle cells (AoSMCs) were seeded in 6-well plates at $3x10^5$ cells/well, cultured to ~70% confluency, quiesced (0.2% charcoal stripped fetal bovine serum (FBS) in phenol red-free Dulbecco's Modified Eagle Medium (DMEM)) for 24 hours, then stimulated with 10 nM 16α-hydroxyestradiol (16OHE2) or vehicle (Veh) control (10 nM ethanol) for 24 hours prior to RNA lysis. Stimulations were carried out in phenol red-free DMEM with 1% charcoal stripped FBS. Basal CT value = average CT value in the vehicle control group. FC= Fold change, calculated by ΔΔCT method and represented as relative to the vehicle (where the average vehicle fold change is 1). Normality was assessed using Shapiro-Wilk test. Data are expressed as ±SEM and analysed by unpaired t-test or Mann-Whitney test. *$p<0.05$. n=6.

4.2.10 Effects of 16OHE2 on Fibrosis Markers in Rat Pulmonary Artery Smooth Muscle Cells in the Presence or Absence of Acute Hypoxia

In PAH, increased deposition and cross-linkage of collagen (converting soluble collagen to insoluble collagen) in the perivascular and intravascular compartments causes stiffening and reduced compliance of the pulmonary arteries[264]. Collagen deposition is highest in the intima, followed by the media and adventitia[265]. Fibril-forming collagens (e.g., COL1A1, COL3A1) assemble to build a microfibril and, when stabilised by cross-linking, provide structure and strength for the vessel wall[265]. Pulmonary collagen deposition is increased in BMPR2^{R899X} transgenic mice (with knock-in of a human R899X mutation)[105]. On the other hand, daily s/c injection with E2 decreased collagen deposition and fibrosis in the RV of male Sprague-Dawley rats with MCT-induced PAH[67]. Therefore, we wished to investigate the effects of 16OHE2 on *Col1a1* and *Col3a1* expression in rPASMCs.

We investigated the effects of 24 hours stimulation with 10 nM 16OHE2 on *Col1a1* and *Col3a1* mRNA expression in male and female rPASMCs under normoxic and acute hypoxic conditions (72 hours in 1% O_2, 5% CO_2, nitrogen). In male rPASMCs, *Col1a1* expression significantly decreased in response to 16OHE2 in normoxic conditions. However, there was no significant change in *Col1a1* under acute hypoxia, or in *Col3a1* expression (Figure 4.11). There were no changes in *Col1a1* or *Col3a1* expression in female rPASMCs under normoxic or acute hypoxic conditions (Figure 4.12).

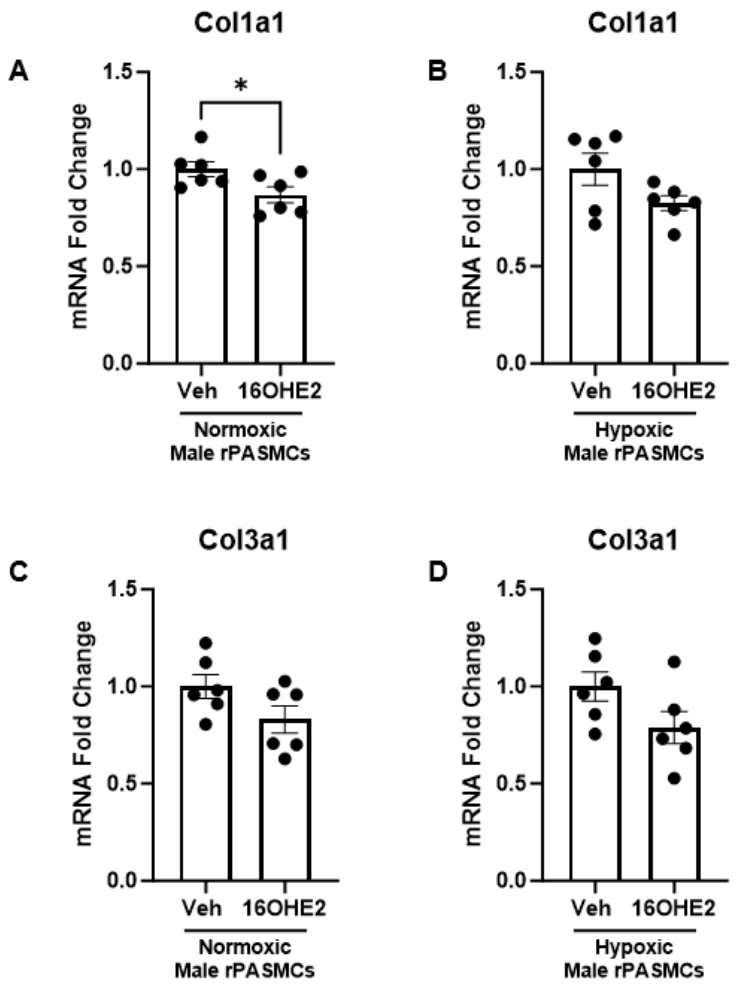

Figure 4.11: Effects 16OHE2 on fibrosis marker mRNA expression in the presence or absence of 72 hours acute hypoxia in male rPASMCs.

Male rat pulmonary artery smooth muscle cells (rPASMCs) were seeded in 100 mm dishes at 2.2×10^6 cells/dish. The following day, the culture media was refreshed, and the cells either maintained in normoxic conditions or placed into hypoxia (1% O_2/ 5% CO_2/ nitrogen) for 72 hours as previously described. On day 3, the cells (~70% confluency) were quiesced (0.2% charcoal stripped fetal bovine serum (FBS) in phenol red-free Dulbecco's Modified Eagle Medium (DMEM)) for 24 hours. Cells were stimulated with 10 nM 16α-hydroxyestradiol (16OHE2) or vehicle (Veh) control (10 nM ethanol) for 24 hours in phenol red-free DMEM with 1% charcoal stripped FBS. Basal CT value = average CT value in the vehicle control group. FC= Fold change, calculated by ΔΔCT method and represented as relative to the vehicle. (A) *Col1a1* in normoxic male rPASMCs. Basal CT=19.9. (B) *Col1a1* in hypoxic male rPASMCs. Basal CT = 20.9. (C) *Col3a1* in normoxic male rPASMCs. Basal CT = 18.8. (D) *Col3a1* in hypoxic male rPASMCs. Basal CT = 20.3. Normality was assessed by Shapiro-Wilk test. Data are expressed as ±SEM and analysed by unpaired t-test. *$p<0.05$. n=6.

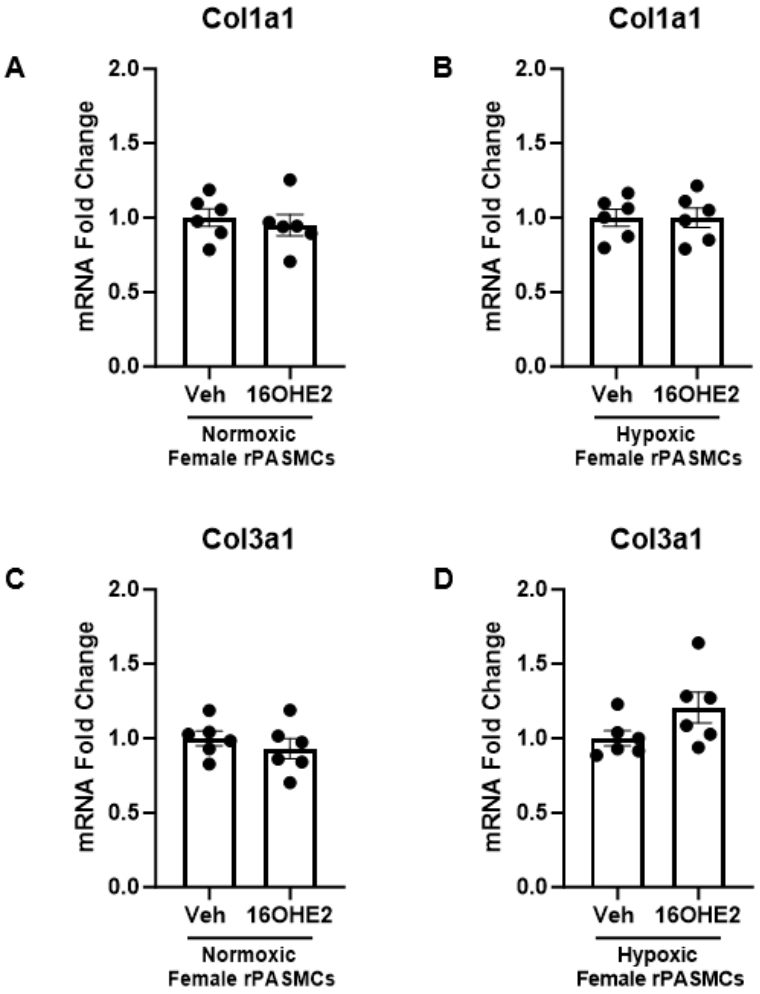

Figure 4.12: Effects 16OHE2 on fibrosis marker mRNA expression in the presence or absence of 72 hours acute hypoxia in female rPASMCs.

Female rat pulmonary artery smooth muscle cells (rPASMCs) were seeded in 100 mm dishes at $2.2x10^6$ cells/dish. The following day, the culture media was refreshed, and the cells either maintained in normoxic conditions or placed into hypoxia (1% O_2/ 5% CO_2/ nitrogen) for 72 hours as previously described. On day 3, the cells (~70% confluency) were quiesced (0.2% charcoal stripped fetal bovine serum (FBS) in phenol red-free Dulbecco's Modified Eagle Medium (DMEM)) for 24 hours. Cells were stimulated with 10 nM 16α-hydroxyestradiol (16OHE2) or vehicle (Veh) control (10 nM ethanol) for 24 hours in phenol red-free DMEM with 1% charcoal stripped FBS. Basal CT value = average CT value in the vehicle control group. FC= Fold change, calculated by ΔΔCT method and represented as relative to the vehicle. (A) *Col1a1* in normoxic female rPASMCs. Basal CT=19.0. (B) *Col1a1* in hypoxic female rPASMCs. Basal CT = 19.3. (C) *Col3a1* in normoxic female rPASMCs. Basal CT = 18.8. (D) *Col3a1* in hypoxic female rPASMCs. Basal CT = 18.9. Normality was assessed by Shapiro-Wilk test. Data are expressed as ±SEM and analysed by unpaired t-test. n=6.

4.3 Discussion

The female predominance of PAH has led to the hypothesis that estrogens and their metabolites may be involved in its pathogenesis[7]. Basal BMPR2 signalling is suppressed in the hPASMCs of PAH patients, and, in the absence of PAH, BMPR2 expression is lower in female hPASMCs than male hPASMCs[102,141]. Mair et al. observed that E2 suppressed Id1 and Id3 expression in male control subject hPASMCs to a similar level observed in female hPASMCs[104]. Similarly, Austin et al. also observed that E2 decreased *BMPR2* expression in human pulmonary microvascular endothelial cells[147]. Reduced BMPR2 signalling contributes to hyperactivation of the TGF-β pathway by shifting protective p-Smad1,5,8 signalling to the pathogenic p-Smad2,3 pathway, leading to cell proliferation, migration, and pulmonary vascular remodelling (Figure 1.5)[105]. Elevated plasma levels of 16OHE2 were recently observed in female idiopathic PAH patients, and in men and women with portopulmonary PAH[241,317]. However, its molecular effects are undetermined. We investigated the effects of 16OHE2 on the expression of genes within the estrogen pathway, BMPR2 signalling pathway, and fibrosis markers (*Col1a1*, *Col3a1*) in the presence or absence of acute hypoxia as a 'second hit'. 16OHE2 suppressed *Bmpr2*, *Smad1*, *Smad4* and *Smad5* expression in male rPASMCs, and decreased *Smad4* expression was reversed by MPP suggesting this occurs via ERα. Similarly, 16OHE2 suppressed *BMPR2* and *SMAD4* in male control subject hPASMCs. 16OHE2 decreased *Id1-3* mRNA expression in rat AoSMCs. In male rPASMCs, 16OHE2 decreased expression of the fibrosis marker *Col1a1* under normoxic conditions only.

As previously discussed in Chapter 3, β-actin (*Actb*) was used as the housekeeper for all experiments as it is stable under hypoxia (Figure 3.9). As many of the effects of estrogen metabolites in PAH result from direct interaction with estrogen receptors, we wished to investigate the effects of 16OHE2 on expression of genes within the estrogen pathway[33]. The following genes were studied in rPASMCs: *Esr1*, *Esr2*, *Gper1*, *Hsd17b1*, *Hsd17b2*, *Cyp19a1*, *Cyp1a1*, *Cyp1a2*, *Cyp1b1* and *Comt*. No significant changes were observed in expression of genes within the estrogen pathway in response to E2, 16OHE1 or 16OHE2 in male rPASMCs under normoxic or acute hypoxic conditions. However, *Gper1* expression significantly decreased in

female rPASMCs in response to 16OHE1 (under normoxic conditions only). This is intriguing given the known mitogenic effects of 16OHE1, and that the selective GPER agonist G1 attenuates MCT-induced PAH in male and ovariectomised female Wistar rats[35,125,126]. 16OHE1 forms strong covalent bonds with estrogen receptors and has a much higher estrogenic activity than 16OHE2[310]. However, plasma levels of 16OHE1 are only elevated in male PAH patients compared to control subjects[241]. Therefore, although decreased *Gper1* expression may be an additional pathogenic effect of 16OHE1, it would be interesting to investigate this in hPASMCs to determine whether this is a species-specific effect.

The effects of acute and prolonged estrogen exposure on PASMCs may also be different[345,346]. Circulating E2 levels are higher in men and postmenopausal women with PAH compared to control subjects, and are associated with worse disease outcomes[30,31]. PAH is presumed to develop in humans over several months or years[358]. However, this only takes days or weeks in experimental animal models of PAH[358]. Therefore *in vitro* and *in vivo* studies may not fully recapitulate the underlying mechanisms of human PAH[358]. Mair et al. observed that expression of the estrogen-synthesising enzyme aromatase was significantly increased in the medial (smooth muscle) layer of pulmonary arteries isolated from male and female chronic hypoxic C57BL/6 mice and SuHx Wistar Kyoto rats[33]. However, as the rPASMCs used in this study were isolated from control (non-PAH) rats, this may explain why few changes were observed in the expression of genes within the estrogen pathway in response to E2, 16OHE1 or 16OHE2. mRNA levels may also not directly correspond to protein levels. However, western blots to investigate this were unsuccessful due to the very low concentrations of the protein samples, which limited the amount of protein loaded to 10 µg per well. Attempts to concentrate the protein samples were unsuccessful.

The effects of acute hypoxia may also be different from chronic hypoxia[345,346]. Acute hypoxia leads to vasoconstriction in both humans and animal models (e.g., male Wistar rats), whereas pulmonary vascular remodelling and PAH only develop following chronic hypoxia[345,346]. CYP1B1 expression is upregulated in the pulmonary arteries of idiopathic and hereditary PAH patients[35]. It is also overexpressed in the pulmonary arteries of male and female C57BL/6 mice with chronic hypoxia- and SuHx-induced PAH[35]. CYP1A1 mRNA and protein expression is highly increased in the lungs of female SuHx Wistar rats, and this is reversed by

antagonism of the aryl hydrocarbon receptor[292]. There is a close link between hypoxia and estrogen metabolism as HIF1β (ARNT) is shared between HIF1α and the aryl hydrocarbon receptor (Figure 1.9)[292]. Cell proliferation and migration in PAH are analogous to the mechanisms observed in cancer, where a 'second hit' is required for carcinogenesis in addition to a tumour suppressor gene mutation[330,352,359]. Therefore, changes in estrogen pathway expression in rPASMCs may only occur with prolonged exposure to one or more 'second hits'.

Bmpr2, *Smad1* and *Smad4* mRNA expression significantly decreased in male rPASMCs following 24 hours stimulation with 10 nM 16OHE2 under normoxic and acute hypoxic conditions. *Smad5* also decreased under hypoxia only. This suggests that 16OHE2 may decrease protective BMP signalling through p-Smad1,5,9, resulting in decreased expression of Ids1-3 and leading to increased cell proliferation and decreased apoptosis[105,146]. However, as western blots for p-Smad1,5,9 were unsuccessful due to low protein sample concentrations, it cannot be confirmed that decreased mRNA expression translates to decreased protein expression. Similarly, Austin et al. observed that *BMPR2* expression decreased in response to 10 nM, 30 nM, and 100 nM 16OHE2 (estriol) in human pulmonary microvascular endothelial cells, with 10 nM being the optimal concentration[147]. On the other hand, in female rPASMCs no changes were observed in expression of genes within the BMPR2 signalling pathway under normoxic conditions, but *Bmpr2* expression significantly increased under acute hypoxia. Based on *in vivo* data presented in Chapter 5, increased *Bmpr2* expression may potentially be a compensatory response to decreased BMPR2 protein expression in the lung. However, this could not be determined in rPASMCs as western blots were unsuccessful.

A key question is whether 16OHE2 is modulating BMPR2 signalling pathway expression via the estrogen receptors. rPASMCs were stimulated with 16OHE2 in the presence or absence of the estrogen receptor antagonists MPP (ERα), PHTPP (ERβ), and G15 (GPER) for 24 hours. As per the previous experiment, *Bmpr2*, *Smad1*, *Smad4* and *Smad5* mRNA expression decreased in male rPASMCs in response to 16OHE2 alone. The decrease in *Smad4* was reversed by MPP, suggesting that this effect may occur via ERα. No changes were observed with the addition of PHTPP or G15. These findings are similar to a study by Wright et al., which demonstrated that continuous s/c dosing with MPP attenuated *Bmpr2*

suppression in the lung tissue of spontaneously pulmonary hypertensive female SERT^{+} mice[102]. MPP also inhibited E2-induced proliferation of female control subject hPASMCs, but PHTPP and G15 had no effect[102]. Furthermore, *BMPR2* is a known target gene of *ESR1* (ERα), and single nucleotide polymorphisms in *ESR1* are associated with portopulmonary hypertension[147,278]. Therefore, these findings are consistent with the hypothesis that 16OHE2 suppresses BMPR2 via ERα in a similar manner to E2. E2 is the parent compound of 16OHE2. Chemically, both E2 and 16OHE2 consist of one benzene ring, a phenolic hydroxyl group, and two (E2) or three (16OHE2) hydroxyl groups (Figure 4.13)[112,360]. Therefore, the structural similarity between E2 and 16OHE2 may potentially explain their similar pharmacological effects via ERα.

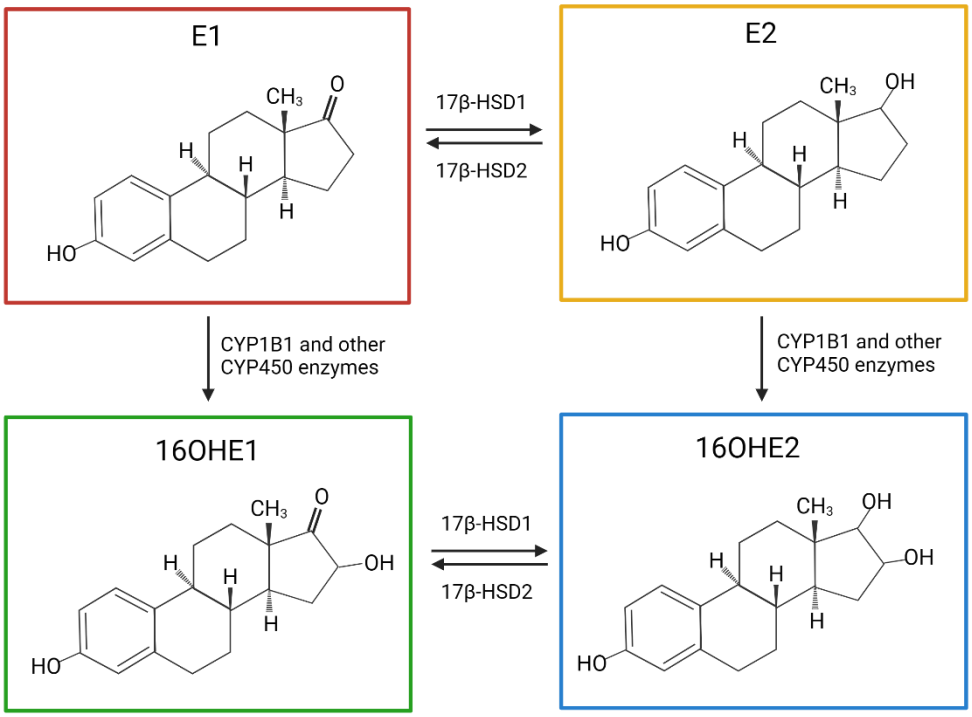

Figure 4.13: The chemical structures of estrone, estradiol, 16α-hydroxyestrone, and 16α-hydroxyestradiol.

Estrone (E1), estradiol (E2), 16α-hydroxyestrone (16OHE1) and 16α-hydroxyestradiol (16OHE2) contain 18 carbons and are collectively known as C18 steroids. In common, they all have one benzene ring and a phenolic hydroxyl group. However, estrone contains a ketone group whereas E2 has a hydroxyl group. 16OHE1 and 16OHE2 are formed via hydroxylation at C16. Created with BioRender.com.

On the other hand, increased *Bmpr2* mRNA expression in response to 16OHE2 in female rPASMCs under acute hypoxia was not mediated by the estrogen receptors (Supplementary Figure 9.3). This was surprising given that ERα is a known regulator of hypoxic genes (including HIF1α) and suggests this may be due to another mechanism (e.g. p38 mitogen-activated protein kinase signalling)[144,361]. Given the interaction between HIF1α and the aryl hydrocarbon receptor, and that 2ME2 downregulates HIF1α, it may be of interest to investigate the effects 16OHE2 on both HIF1α and the aryl hydrocarbon receptor[292,299]. As acute hypoxia leads to vasoconstriction but not pulmonary vascular remodelling in both humans and animal models (e.g., male Wistar rats), increased *Bmpr2* mRNA expression may potentially be a transient compensatory response prior to suppression under chronic hypoxic conditions resulting in increased cell proliferation[33]. This is consistent with the observation by Mair et al. that chronic hypoxia decreased BMPR2 expression in the lungs of male and female C57BL/6 mice[33].

The half-life of 16OHE2 is short. For example, the half-life of 16OHE2 after intramuscular injection was 3-4 hours in male and female Sprague-Dawley rats, and 1.5-5.3 hours in human female volunteers using the combined contraceptive pill[339,340]. *In vivo*, 16OHE2 undergoes extensive conjugation by enzymes such as β-glucuronidase and is excreted in the urine as 16OHE2-glucuronide[315,316]. However, these enzymes may not be present in the *in vitro* environment, which may explain why changes in the expression of genes within the BMPR2 signalling pathway were observed 24 hours after stimulation with 16OHE2. The effects of a shorter 2-hour stimulation with 10 nM 16OHE2 were investigated in male rPASMCs under normoxic conditions. The following genes within the BMPR2 signalling pathway were studied: *Bmpr2*, *Smad1*, *Smad4*, *Smad5*, *Smad9*, *Id1*, *Id2* and *Id3*. Expression of *Id2* significantly decreased in response to 16OHE2 but no other changes were observed. As this effect occurred rapidly, 16OHE2 may be acting through GPER and future work could involve challenging this with the antagonist G15[102]. Suppressed Id2 expression is associated with increased TGF-β mediated cell proliferation, increased cell differentiation, and decreased apoptosis[362,363]. Therefore, this further suggests that the effects of 16OHE2 in PAH may be pathogenic.

Another key question is why decreased *Bmpr2*, *Smad1*, *Smad4* and *Smad5* expression were only observed in male rPASMCs in response to 16OHE2 and not in females. Basal BMPR2 protein and *Smad4* mRNA expression were significantly lower in female rPASMCs than in males. This is in keeping with the hypothesis that expression of genes within the BMPR2 signalling pathway were only decreased in response to 16OHE2 in male rPASMCs because this was already suppressed in females. Similarly, Mair et al. observed decreased mRNA and protein levels of BMPR2, Smad1, Id1 and Id3 in female control subject hPASMCs compared to males[104]. Furthermore, in male control subject hPASMCs, Id1 and Id3 expression decreased in response to E2 to similar levels as observed in females[104]. Also, only female Smad1$^{+/-}$ mice spontaneously develop PAH, and this is attenuated by ovariectomy suggesting that it is E2-dependent[104]. Increased basal *Smad3* mRNA expression in female rPASMCs is consistent with a possible shift to increased pathogenic TGF-β signalling, and this may contribute to the female predominance of PAH[105]. On the other hand, Id1 is involved in many pathways (e.g, PI3K/Akt signalling, c-Myc signalling), therefore increased *Id1* mRNA expression in female rPASMCs could be independent of suppressed BMPR2 signalling[364]. This may also be a species difference.

ERα and ERβ protein levels are not significantly different between male and female control subject hPASMCs[102]. However, ERα levels are increased in female PAH patient hPASMCs, whereas ERβ is increased in male PAH patient hPASMCs[102]. In keeping with control subject hPASMCs, there was no significant difference in basal ERβ (ESR2) protein levels between male and female rPASMCs (Supplementary Figure 9.4). Western blots for ERα (ESR1) were unsuccessful.

BMPR2 and *SMAD4* mRNA expression were also decreased in response to 16OHE2 in male control subject hPASMCs, suggesting that the effects observed in rPASMCs may also translate to humans. The effects of 16OHE2 were not investigated in male PAH patient hPASMCs as basal BMPR2 signalling is already suppressed[102]. Contrary to the rPASMCs, there were no changes in *SMAD1* or *SMAD5*. However, the effects of 16OHE2 in hPASMCs may be influenced by many additional factors controlled for in the rats such as obesity, age, and medication[34,51].

In PAH patients, median survival ranges from 5 to 7 years after diagnosis, but no substantial improvements in survival have been realised during the past decade[365]. Although current treatments decrease pulmonary arterial pressure, they do not address the underlying pulmonary vascular remodelling[8]. Sotatercept is a novel fusion protein which acts as a ligand trap for selected TGF-β superfamily members to restore the balance between the pro-proliferative TGF-β pathway and the protective BMPR2 pathway[366]. Sotatercept is known to attenuate pulmonary vascular remodelling *in vivo* by reducing cell proliferation, reducing inflammation in the vessel wall, and promoting apoptosis[367,368,369]. Recent Phase 2 and 3 clinical trials have demonstrated that sotatercept improves exercise capacity (6-minute walk distance) and has a favourable clinical benefit-risk ratio in PAH patients[366,370-373]. Given the decreased *Bmpr2*, *Smad1*, *Smad4* and *Smad5* expression observed in male rPASMCs in response to 16OHE2, and the decreased *BMPR2* and *SMAD4* expression in male control subject hPASMCs, it would be intriguing to investigate whether this would be reversed by sotatercept, and whether sotatercept would attenuate increased plasma levels of 16OHE2 in female PAH patients[241].

The effects of estrogens in the systemic circulation may be different from the pulmonary vasculature[33,113]. Therefore, in addition to PASMCs, we also investigated the effects of 16OHE2 in rat aorta smooth muscle cells (AoSMCs). In male rPASMCs, *Bmpr2*, *Smad1*, *Smad4* and *Smad5* mRNA expression significantly decreased in response to 16OHE2, but this did not occur in females. There was no change in expression of *Smad2*, *Smad3*, *Smad4*, *Smad6*, *Smad7*, *Smad9*, *Id1*, *Id2* or *Id3*. On the other hand, in rat AoSMCs a response to 16OHE2 was observed in both sexes. In contrast to the male rPASMCs, there was no change in *Bmpr2*, *Smad1*, *Smad4* and *Smad5* in AoSMCs. However, *Smad3*, *Smad6*, *Id1*, *Id2* and *Id3* mRNA expression decreased in response to 16OHE2 in male rat AoSMCs, and *Smad2*, *Smad3*, *Smad4*, *Smad7*, *Id2* and *Id3* decreased in females. Suppressed *Id1-3* expression in rat AoSMCs may result from increased TGF-β signalling (Figure 1.5)[146]. This is consistent with decreased expression of the TGF-β inhibitor *Smad7* in female rat AoSMCs[145]. Hypothetically, decreased total *Smad2, Smad3* and *Smad4* expression could be due to increased phosphorylation to the p-Smad2,3,4 complex, leading to nuclear translocation and Id gene suppression[146]. Decreased inhibitory *Smad6* expression in male rat AoSMCs may be due to competition with *Smad4* for complex formation with p-Smad1[145].

Aberrant proliferation of vascular smooth muscle cells is associated with several disease pathologies, e.g., atherosclerosis[355]. E2 is a known vasodilator in the systemic circulation associated with cardioprotective effects in premenopausal women and demonstrates anti-mitogenic effects in vascular smooth muscle cells which may be associated with its sequential metabolism to 2ME2[109,113,374-376]. However, these effects are independent of ERα and ERβ[109,374,375]. On the other hand, Wright et al. demonstrated that selective activation of ERα in aorta endothelial cells increased extracellular signal-regulated kinase (ERK) expression and ERK1/2-mediated cell proliferation[102]. The bone morphogenetic protein 2/4/7 antagonist gremlin is constitutively expressed the normal vasculature[356]. Increased gremlin expression (and consequent reduction in BMPR2 signalling) is associated with vascular smooth muscle cell proliferation and migration and may be pathogenic in both systemic vascular injury and PAH[356,357]. Therefore, it would be intriguing to investigate whether 16OHE2 would increase proliferation and ERK1/2 expression in rat AoSMCs.

Increased collagen deposition in all layers of the pulmonary artery (including the fibril-forming collagens COL1A1 and COL3A1) plays a key role in stiffening and reduced compliance of the vessels in PAH[264,265]. In addition to quantifying mRNA or protein expression of collagens, another frequent method to assess fibrosis is immunohistochemical staining of tissue sections using picrosirius red or Masson's thricombe to selectively highlight collagen networks[105,265]. Using Masson's thricombe staining, Hoffmann et al. observed in idiopathic PAH patients that collagen deposition was highest in the intimal layer of the pulmonary artery, followed by the media, and then the perivascular tissue[265]. Intriguingly, Erewele et al. observed using picrosirius red staining that pulmonary arterial collagen deposition is increased in $BMPR2^{R899X}$ transgenic mice compared to their wild type controls[105]. On the other hand, while we observed that *Bmpr2* mRNA expression decreased in male rPASMCs in response to 16OHE2 under both normoxic and acute hypoxic conditions (72 hours in 1% O_2), *Col1a1* expression also significantly decreased under normoxia suggesting that 16OHE2 may be protective against fibrosis. Studies on the effects of E2 on collagen deposition have primarily focussed on the RV. For example, Liu et al observed that daily s/c injection with E2 decreased collagen deposition (Masson's thricombe staining) and fibrosis in the RV of male Sprague-Dawley rats with MCT-induced PAH[67]. This protective effect may be mediated via ERα as Cheng et al. observed that collagen deposition (picrosirius red staining) was

increased in the RV of female ERα-mutant Sprague-Dawley rats (with loss of function) compared to wild type controls, but no effect was observed in males[377]. However, the effects of collagen deposition in PAH may vary between the heart and the lungs. For example, Golob et al. observed that Col1a1$^{R/R}$ mice (with impairment of Type I collagen degradation and absence of deposition) developed SuHx-induced PAH with a comparable increase in RVSP to their wild type littermates[378]. However, RV hypertrophy was decreased in Col1a1$^{R/R}$ mice compared to wild type mice[378]. Future studies could investigate whether 16OHE2 is protective against fibrosis in an animal model of PAH (e.g., SuHx rats) by picrosirius red or Masson's thricombe staining of pulmonary artery and RV tissue sections in addition to quantification of *Col1a1* and *Col3a1* mRNA expression.

4.3.1 Limitations of this Study

Attempts to investigate BMPR2, p-Smad1,5,9 and Id1 protein expression by western blot were unsuccessful. Although mRNA expression of *Bmpr2*, *Smad1*, *Smad4,* and *Smad5* was decreased in male rPASMCs in response to 16OHE2, we cannot confirm this translates to decreased p-Smad1,5,9 signalling. Several attempts were made but only basal BMPR2 and ESR2 expression in untreated male and female rPASMCs were successfully quantified. This may be due to the very low concentration of the protein samples, which limited the amount of protein loaded per well to 20 µg in untreated rPASMCs and 10 µg in studies with 16OHE2. Attempts to concentrate the protein samples and different lysis methods were unsuccessful.

Due to the primary cell lines available at the time, male and female rPASMCs were not passage-matched when investigating basal BMPR2 protein expression (passage 3 females, passage 5-6 males). However, they were matched at passage 3 when investigating basal BMPR2 pathway mRNA expression later. The main caveat of higher passage primary cells is the risk of differentiation from the primary phenotype[331]. However, using the same isolation method, Peng et al. demonstrated that rPASMCs maintained their smooth muscle cell phenotype and were not contaminated with fibroblasts or endothelial cells between passage 5 and 7[331]. We also made the same observation up to passage 6. Therefore, it is unlikely that the

decreased BMPR2 protein levels in female rPASMCs are due to different passage numbers.

Expression of the sex markers associated with male or female cell phenotype may decrease with passage[379]. For example, there are two amelogenin genes present in humans – one on the X chromosome and the other on the Y chromosome containing an additional 6 base pair insertion[379]. SNU-449 (CRL-2234) hepatocellular carcinoma cells isolated from a male patient lose amelogenin-Y expression by passage 17, and amelogenin-Y is not expressed in PC-3 human prostate epithelial cells[379,380]. In qRT-PCR, the cycle threshold (CT) value is inversely proportional to gene expression. In this study, the basal CT value for *Esr1* was 36.1 in male rPASMCs and 34.5 in female rPASMCs. For *Esr2*, the basal CT value was 35.2 in male rPASMCs and 34.8 in female rPASMCs. Austin et al. previously observed that transfection of increasing quantities of ERα in COS-7 cells (which lack endogenous estrogen receptors) strongly correlates with decreasing *BMPR2* expression[147]. Therefore, the significantly lower basal BMPR2 protein expression in female rPASMCs compared to males may be associated with higher expression of *Esr1*. However, this is unclear as the male and female rPASMCs were run on different qPCR plates at different times so could not be directly compared. On the other hand, the basal CT value for *Gper1* was 33.0 in male rPASMCs and 33.6 in females. Androgen receptor expression was not investigated in rPASMCs. Estrogen receptor expression was not investigated in the hPASMCs as Wright et al. previously observed that there was no significant difference in the protein levels of ERα and ERβ between male and female control subject hPASMCs[102]. While this study did not investigate estrogen receptor expression in rat AoSMCs, Hutson et al. previously observed no significant difference in *Esr1*, *Esr2*, *Gper,* and *Cyp19a1* mRNA expression in the aorta (tissue) between male and female Sprague-Dawley rats[381]. However, *Gper* expression in A7r5 rat embroyonic AoSMCs (assumed to be mixed sex) was significantly higher than *Esr1*, *Esr2*, and *Cyp19a1,* which may mediate the protective effects of E2 on the aorta (e.g., vasodilation)[113,381]. Future studies could confirm whether the sex phenotype of rPASMCs is maintained with passage by PCR investigation of whether only amelogenin-X (females) or both amelogenin-X and amelogenin-Y (males) are present[379]. The basal expression of the estrogen receptor and androgen receptor genes could also be compared between male and female rPASMCs. This may be important when studying male

and female cells as sex differences in response to 16OHE2 could potentially be missed if the cells lose their phenotype.

The effects of normoxia and acute hypoxia were not directly compared as studies were carried out in primary cell lines from different rats at different times. While chronic hypoxia is an established *in vivo* model of PAH, the effects of acute hypoxia may be different[345,346]. However, the ability to maintain cells in a hypoxic environment for longer periods using a modular incubator chamber is limited. Attempts to investigate this using PASMCs from chronic and sugen-hypoxic rats were unsuccessful. Finally, PAH is assumed to develop in patients over several months or years[358]. This suggests that patients may be exposed to increased circulating E2 levels for prolonged periods of time[30,31]. However, *in vitro* studies only investigated a short 24-hour period of stimulation with 16OHE2.

4.3.2 Summary

In summary, 16OHE2 decreased *Bmpr2*, *Smad1*, *Smad4* and *Smad5* mRNA expression in male rPASMCs only, and the decrease in *Smad4* was reversed by MPP suggesting this occurs via ERα (Figure 4.14). This may be due to already suppressed basal BMPR2 protein levels in female rPASMCs compared to males. Basal *Smad4* mRNA expression was also lower in female rPASMCs, whereas *Smad3* and *Id1* were increased. On the other hand, 16OHE2 significantly increased *Bmpr2* expression in female rPASMCs under acute hypoxia. *BMPR2* and *SMAD4* expression were decreased by 16OHE2 in male control subject hPASMCs. *Smad3*, *Smad6*, *Id1*, *Id2* and *Id3* expression decreased in male rat AoSMCs in response to 16OHE2. *Smad2*, *Smad3*, *Smad4*, *Smad7*, *Id2* and *Id3* decreased in female rat AoSMCs. Suppressed *Id1-3* expression may result from increased TGF-β signalling[146]. *Col1a1* expression was decreased by 16OHE2 in male rPASMCs, but not in females. The *in vivo* effects of 16OHE2 in C57BL/6 mice are presented in Chapter 5.

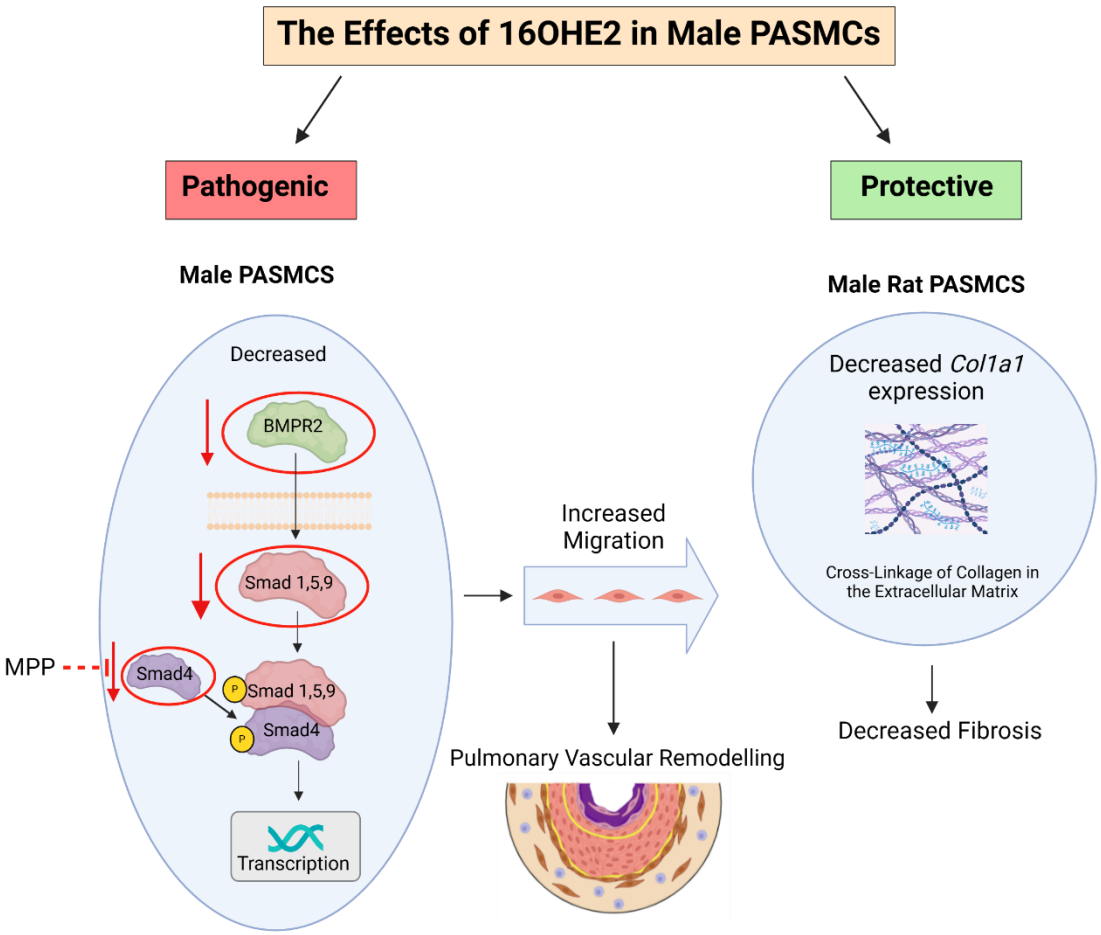

Figure 4.14: Summary of the molecular effects of 16OHE2 in male PASMCs. 16α-hydroxyestradiol (16OHE2) decreased *Bmpr2*, *Smad1*, *Smad4* and *Smad5* mRNA expression in male rat pulmonary artery smooth muscle cells (rPASMCs). The estrogen receptor-α antagonist MPP reversed the decrease in *Smad4* in response to 16OHE2, suggesting it may act via this receptor. *BMPR2* and *SMAD4* mRNA expression were also decreased by 16OHE2 in male control subject hPASMCs. Decreased expression of the bone morphogenetic protein receptor 2 (BMPR2) signalling pathway may lead to the increased rPASMC migration observed in Chapter 3 and contribute to pulmonary vascular remodelling in PAH. On the other hand, *Col1a1* expression decreased in response to 16OHE2 in male rPASMCs, suggesting that 16OHE2 may decrease fibrosis. These effects were not observed in female rPASMCs. Created with BioRender.com.

Chapter 5

The *In Vivo* Effects of 16α-Hydroxyestradiol in C57BL/6 Mice

5.1 Introduction

Pulmonary arterial hypertension (PAH) is characterised by progressive obstruction of the distal pulmonary arteries resulting in increased pulmonary arterial pressure leading to right ventricular (RV) hypertrophy and failure, and ultimately death[6]. The process of pulmonary vascular remodelling is complex, with multiple known mechanisms affecting all layers of the arterial wall[6]. These include proliferation, migration, genetic mutations, inflammation and oxidative stress[6]. Increased collagen deposition leads to stiffening and reduced compliance of the pulmonary arteries and maladaptive RV remodelling and fibrosis[264,266]. This includes the fibril-forming collagens COL1A1 and COL3A1, which provide structure and strength for the pulmonary artery and RV walls[264,266].

First noted by Dresdale et al. in 1951, numerous registries worldwide have observed that PAH is predominant in women[26-28,51,365]. This led to extensive research into the potential mechanisms by which estrogens may contribute to the development of PAH. On the other hand, once PAH has developed, women have better survival than men (known as the 'estrogen paradox')[28]. For example, according to the Swedish Pulmonary Arterial Hypertension Register, 5-year survival was 68% in women but 55% for men between 2008 and 2016[28]. RV hypertrophy and failure is the major cause of mortality in PAH[52]. A key prognostic marker of survival in PAH is the right ventricular ejection fraction (RVEF), which expresses the amount of deoxygenated blood pumped out of the RV (stroke volume) divided by the total amount of blood in the RV (end-diastolic volume) as a percentage[53,54]. According to Kawut et al., a 5% lower RVEF at diagnosis was associated with a 60% increased risk of death between January 1994 and June 2002[55]. In the absence of cardiovascular disease, both the Framingham Heart Study and Multi-Ethnic Study of Atherosclerosis observed that baseline RVEF is higher in women than men[56,57]. This may contribute to improved RV adaptability to high pulmonary arterial pressures and survival in female PAH patients[59]. There are many hypotheses for the estrogen paradox including poor translation of animal models to human PAH, altered estrogen metabolism, and extragonadal E2 synthesis in the peripheral tissues (e.g., lung, adipose)[29,33-35].

Suppression of Bone Morphogenetic Protein Receptor 2 (BMPR2) plays a key role in hereditary and idiopathic PAH[141]. Reduced BMP signalling through BMPR2 shifts protective p-Smad1,5,8 signalling to the pathogenic TGF-β pathway, leading to cell proliferation, migration, and pulmonary vascular remodelling (Figure 1.5)[105]. Basal *Bmpr2* expression is significantly lower in female SERT^{+} mouse lung tissue compared to their wild type littermates, but this was attenuated by continuous s/c dosing with the estrogen receptor-α (ERα) antagonist MPP[102]. White et al. observed that daily intraperitoneal injection of the estrogen metabolite 16α-hydroxyestrone (16OHE1) induced PAH in female C57BL/6 mice in the absence of any additional precipitating factors[35]. In male BMPR2^{R899X} transgenic mice (with a knock-in of the human R899X mutation), continuous s/c dosing with 16OHE1 increased pulmonary vascular resistance and decreased cardiac output[106]. Genetic variants associated with deficiency of SRY-related HMG-box 17 (*SOX17*) were recently observed in PAH patients[159]. Sangam et al. recently observed that 16OHE1 suppressed *SOX17* expression in human pulmonary artery endothelial cells (PAECs)[159]. Overexpression of *Sox17* in *Tie2-Sox17* transgenic mice attenuated 16OHE1-induced PAH and RV hypertrophy[159]. Therefore, SOX17 may be a key link between altered estrogen metabolism and PAH.

16α-hydroxyestradiol (16OHE2) is primarily produced during pregnancy (Figure 1.10)[314]. Increased plasma levels of 16OHE2 were recently observed in female idiopathic PAH patients, and in males and females with portopulmonary PAH[241,317]. While preliminary studies observed that 16OHE2 increases proliferation of female PAH patient hPASMCs and migration of blood outgrowth endothelial cells from male and female PAH patients, its effects *in vivo* are undetermined[241].

Aims of this chapter:

1. To investigate the physiological effects of 16OHE2 in C57BL/6 mice.

2. To investigate the effects of 16OHE2 on the BMPR2 signalling pathway, fibrosis marker expression, and *Sox17* expression in the lung and right ventricle.

All *in vivo* procedures were performed by Dr Smriti Sharma including intraperitoneal injections, pressure-volume (PV) loop measurement, and tissue harvest. For qRT-PCR experiments, RNA lysis and extractions from lung and RV tissue were carried out by Dr Sharma.

5.2 Results

5.2.1 Physiological Effects of 16OHE2 in C57BL/6 Mice

White et al. previously observed that daily intraperitoneal injection of 1.5 mg/kg 16OHE1 induced PAH in female C57BL/6 mice aged 10-12 weeks in the absence of any additional precipitating factors[35]. In this case, 16OHE1 significantly increased right ventricular systolic pressure (RVSP), pulmonary vascular remodelling and RV hypertrophy[35]. As the *in vivo* effects of 16OHE2 are undetermined, we repeated this study with 16OHE2 in male and female C57BL/6 mice aged 23-25 weeks.

PV loop analysis is the standard *in vivo* method of assessment for development of PAH[54]. Each PV loop represents a single cardiac cycle, with the width of the loop representing the stroke volume (amount of deoxygenated blood pumped out of the RV)[54]. The RVSP is the ratio of maximal pressure to volume for each loop and reflects the pulmonary arterial pressure[54]. Abnormal enlargement of the muscle mass in the RV (RV hypertrophy) often occurs in response to pressure overload and is the key driver of mortality in PAH[52]. On receipt of raw PV loop recordings from Dr Sharma, haemodynamic analysis was carried out to determine the RVSP. The Fulton Index (RV weight/ left ventricle plus septum (LV+S) weight) was also calculated as an indicator of RV hypertrophy[382]. Enlarged spleen size (splenomegaly) is associated with inflammation and is a common feature in patients with advanced idiopathic or hereditary PAH[383]. Therefore, we also investigated the effects of 16OHE2 on spleen weight.

In male mice, 16OHE2 did not affect either the RVSP or the Fulton index (Figure 5.1(A-B)). There was also no significant difference in body weight at the time of PV loop analysis (Figure 5.1(C)). However, spleen weight significantly increased in response to 16OHE2 (Figure 5.1(D)).

In female mice, 16OHE2 had no effect on the RVSP but significantly increased RV hypertrophy as measured by the Fulton Index (RV weight/ LV+S weight; Figure 5.2(A-B)). As previously observed in male mice, there was no significant difference

in body weight at the time of PV loop analysis, however spleen weight significantly increased in response to 16OHE2 (Figure 5.2(C-D)).

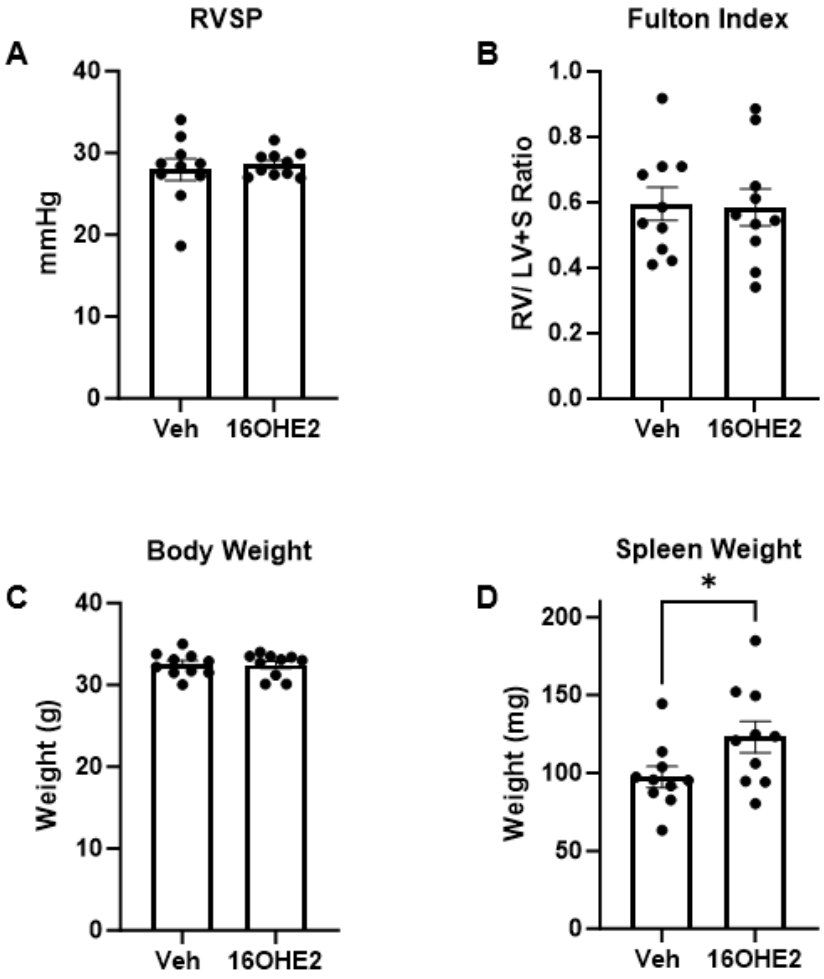

Figure 5.1: Physiological effects of 16OHE2 in male C57BL/6 mice.

Male C57BL/6 mice received 1.5 mg/kg/day 16α-hydroxyestradiol (16OHE2) by intraperitoneal injection for 14 days. No changes were observed in response to 16OHE2 in (A) RVSP, (B) Fulton Index (RV/ LV+S ratio), (C) Body weight at the time of PV loop analysis. (D) Spleen weight significantly increased following treatment with 16OHE2. RVSP = right ventricular systolic pressure, RV = right ventricle, LV+S = left ventricle plus septum. Normality was assessed by Shapiro-Wilk test. Data are expressed as ±SEM and analysed by unpaired t-test or Mann-Whitney test. *$p<0.05$. n=10.

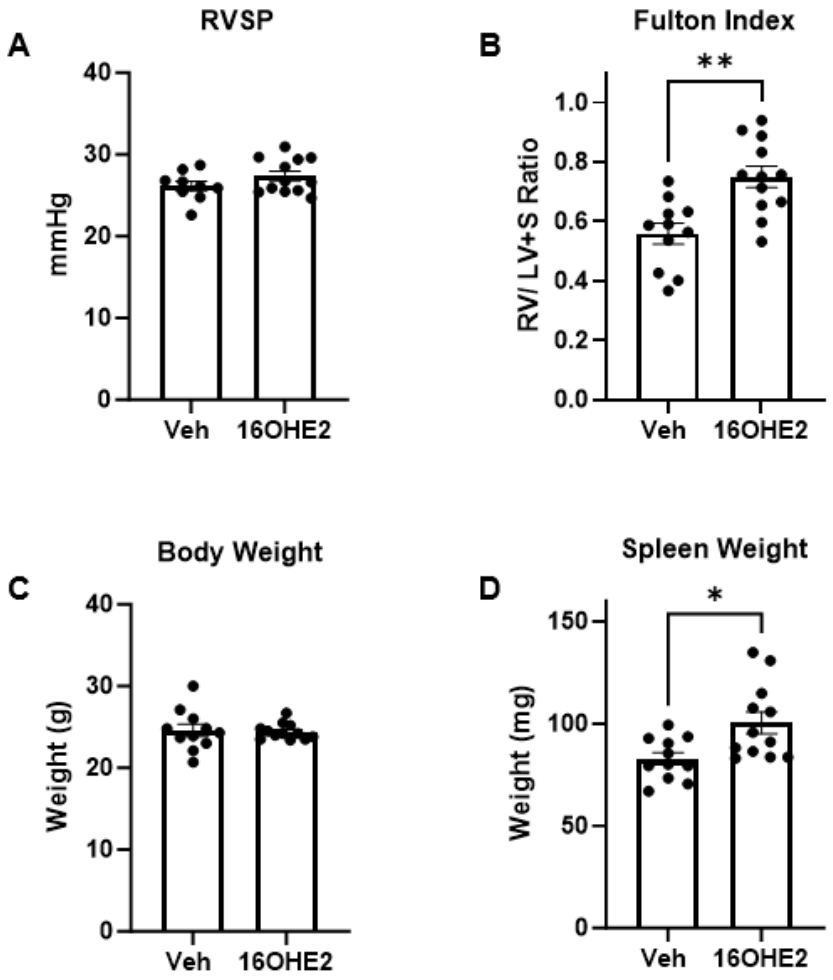

Figure 5.2: Physiological effects of 16OHE2 in female C57BL/6 mice.

Female C57BL/6 mice received 1.5 mg/kg/day 16α-hydroxyestradiol (16OHE2) by intraperitoneal injection for 14 days. (A) No change was observed in RVSP. (B) Fulton Index (RV/ LV+S ratio) significantly increased following treatment with 16OHE2. (C) There was no difference in body weight at the time of PV loop analysis. (D) Spleen weight significantly increased following treatment with 16OHE2. RVSP = right ventricular systolic pressure, RV = right ventricle, LV+S = left ventricle plus septum. Normality was assessed by Shapiro-Wilk test. Data are expressed as ±SEM and analysed by unpaired t-test or Mann-Whitney test. *$p<0.05$, **$p<0.01$. n=9-12.

5.2.2 Effects of 16OHE2 on the BMPR2 Signalling Pathway in Lung Tissue

According to Mair et al., basal *Bmpr2* mRNA expression in the lung is significantly lower in both female C57BL/6 mice and female Wistar Kyoto rats compared to males[33]. However, suppression of estrogen synthesis in female C57BL/6 mice by daily s/c anastrozole injection increased *Bmpr2* expression in the lung to a similar level as observed in males[33]. The effects of 16OHE2 on BMPR2 signalling in the lung are undetermined, therefore we wished to investigate this.

We investigated the effects of 16OHE2 in the lung tissue of C57BL/6 mice on the expression of the following genes within the BMPR2 signalling pathway: *Bmpr2*, *Smad1*, *Smad2*, *Smad3*, *Smad4*, *Smad5*, *Smad6*, *Smad7*, *Smad9*, *Id1*, *Id2*, and *Id3*. We also investigated the effects of 16OHE2 on the protein levels of BMPR2 and p-Smad1,5,9. In male mice, no significant changes were observed in gene expression but p-Smad1,5,9 levels significantly increased in response to 16OHE2 (Table 5.1, Figure 5.3). In female mice, no significant changes were observed in gene expression. However, BMPR2 protein levels significantly decreased in response to 16OHE2, whereas p-Smad1,5,9 significantly increased (Table 5.2, Figure 5.4).

Table 5.1: Effects of 16OHE2 on Expression of Genes Within the BMPR2 Signalling Pathway in the Lung Tissue of Male C57BL/6 Mice

PATHWAY	GENES	Basal CT value	16OHE2 vs. Veh	
			FC ± SEM	P-value
BMPR2 Pathway	***Bmpr2***	27.4	1.39 ± 0.21	0.1230
	Smad1	30.9	1.11 ± 0.09	0.2954
	Smad2	32.2	1.12 ± 0.06	0.1983
	Smad3	30.4	1.11 ± 0.08	0.3281
	Smad4	28.2	1.20 ± 0.09	0.0551
	Smad5	30.4	1.27 ± 0.11	0.0509
	Smad6	29.3	1.26 ± 0.16	0.2455
	Smad7	28.9	1.08 ± 0.06	0.4056
	Smad9	32.9	1.42 ± 0.17	0.0650
	Id1	27.1	1.09 ± 0.15	0.7326
	Id2	28.1	1.13 ± 0.14	0.5066
	Id3	26.2	0.96 ± 0.08	0.8155

Table 5.1: Effects of 16OHE2 on expression of genes within the BMPR2 signalling pathway in the lung tissue of male C57BL/6 mice.

Male C57BL/6 mice received 1.5 mg/kg/day 16α-hydroxyestradiol (16OHE2) by intraperitoneal injection for 14 days. Lung harvest, RNA lysis and qRT-PCR were carried out as previously described. FC= Fold change, calculated by ΔΔCT method and is represented as relative to the vehicle (where the average vehicle fold change is 1). Basal CT value = the average CT value of the vehicle control group. Normality was assessed by Shapiro-Wilk test. Data are expressed as ±SEM and analysed by unpaired t-test or Mann-Whitney test. n=10.

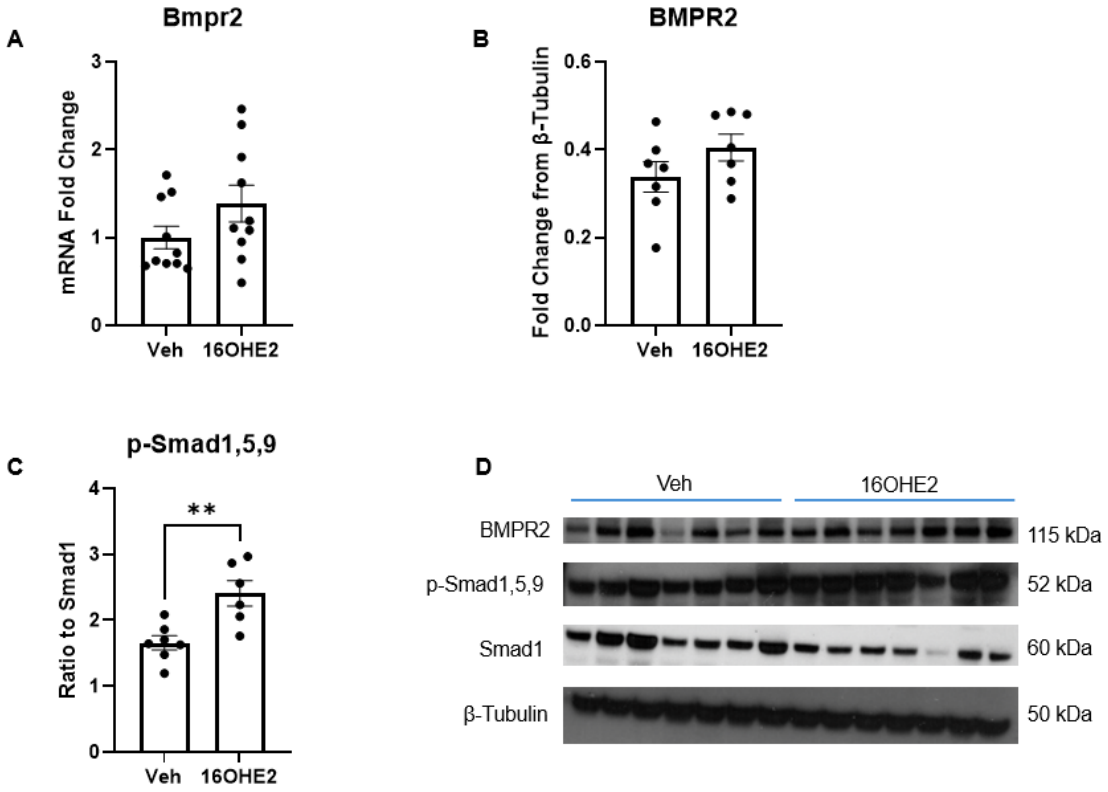

Figure 5.3: Effects of 16OHE2 on the BMPR2 signalling pathway in the lung tissue of male C57BL/6 mice.

Male C57BL/6 mice received 1.5 mg/kg/day 16α-hydroxyestradiol (16OHE2) by intraperitoneal injection for 14 days. Lung harvest, RNA and protein lysis, and qRT-PCR and western blot were carried out as previously described. (A) 16OHE2 did not affect *Bmpr2* mRNA expression. Fold change was calculated by the ΔΔCT method and is represented as relative to the vehicle (where the average vehicle fold change is 1). Basal CT (average vehicle) = 27.4. (B) Quantification of BMPR2 protein expression in lung tissue. Fold change is BMPR2 relative to β-tubulin expression. No significant change in BMPR2 was observed in response to 16OHE2. (C) Quantification of p-Smad1,5,9 expression in lung tissue. Ratio to Smad1 = (p-Smad1,5,9/ β-tubulin) divided by (Smad1/ β-tubulin). (D) Immunoblots of BMPR2, p-Smad1,5,9, Smad1, and β-tubulin). Normality was assessed by Shapiro-Wilk test. Data are expressed as ±SEM and analysed by unpaired t-test. n=7-10.

Table 5.2: Effects of 16OHE2 on Expression of Genes Within the BMPR2 Signalling Pathway in the Lung Tissue of Female C57BL/6 Mice

PATHWAY	GENES	Basal CT value	16OHE2 vs. Veh	
			FC ± SEM	P-value
BMPR2 Pathway	***Bmpr2***	27.1	0.98 ± 0.09	0.8743
	Smad1	30.8	0.97 ± 0.06	0.7512
	Smad2	32.4	0.91 ± 0.04	0.3252
	Smad3	30.3	0.93 ± 0.04	0.3685
	Smad4	28.7	1.03 ± 0.05	0.7672
	Smad5	30.6	0.90 ± 0.07	0.3881
	Smad6	28.9	0.99 ± 0.07	0.8350
	Smad7	28.7	1.04 ± 0.09	0.9759
	Smad9	32.6	0.71 ± 0.08	0.1185
	Id1	26.6	1.04 ± 0.12	0.8191
	Id2	28.1	1.05 ± 0.13	0.8303
	Id3	26.4	1.05 ± 0.12	0.8718

Table 5.2: Effects of 16OHE2 on expression of genes within the BMPR2 signalling pathway in the lung tissue of female C57BL/6 mice.
Female C57BL/6 mice received 1.5 mg/kg/day 16α-hydroxyestradiol (16OHE2) by intraperitoneal injection for 14 days. Lung harvest, RNA lysis and qRT-PCR were carried out as previously described. FC= Fold change, calculated by ΔΔCT method and represented as relative to the vehicle (where the average vehicle fold change is 1). Basal CT value = the average CT value of the vehicle control group. Normality was assessed by Shapiro-Wilk test. Data are expressed as ±SEM and analysed by unpaired t-test or Mann-Whitney test. n=11-12.

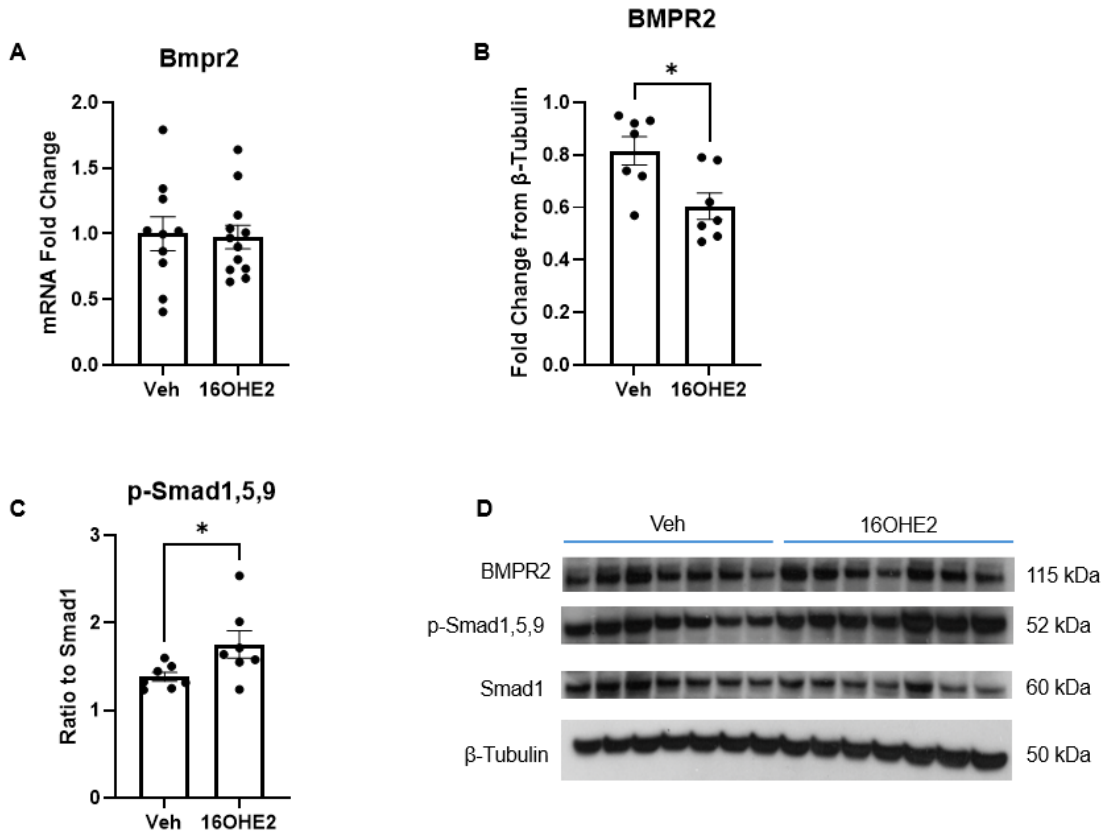

Figure 5.4: Effects of 16OHE2 on the BMPR2 signalling pathway in the lung tissue of female C57BL/6 mice.

Female C57BL/6 mice received 1.5 mg/kg/day 16α-hydroxyestradiol (16OHE2) by intraperitoneal injection for 14 days. Lung harvest, RNA and protein lysis, and qRT-PCR and western blot were carried out as previously described. (A) 16OHE2 did not affect *Bmpr2* mRNA expression. Fold change was calculated by the ΔΔCT method and is represented as relative to the vehicle (where the average vehicle fold change is 1). Basal CT (average vehicle) = 27.1. (B) Quantification of BMPR2 protein expression in lung tissue. Fold change is BMPR2 relative to β-tubulin expression. BMPR2 expression significantly decreased in response to 16OHE2. (C) Quantification of p-Smad1,5,9 expression in lung tissue. Ratio to Smad1 = (p-Smad1,5,9/ β-tubulin) divided by (Smad1/ β-tubulin). (D) Immunoblots of BMPR2, p-Smad1,5,9, Smad1 and β-tubulin). Normality was assessed by Shapiro-Wilk test. Data are expressed as ±SEM and analysed by unpaired t-test. n=7-12.

5.2.3 Effects of 16OHE2 on the Expression of Genes Within the BMPR2 Signalling Pathway in the Right Ventricle

Female PAH patients have improved survival rates compared to male patients, likely due to better RV adaptability to high pulmonary pressures[28,59]. Frump et al. observed that endogenous E2 depletion by ovariectomy worsened SuHx-induced RV hypertrophy in female Sprague-Dawley rats, and this was attenuated by continuous s/c administration of E2 in ovariectomised rats[108]. Similarly, they also observed that E2 attenuated SuHx-induced RV hypertrophy in male Sprague-Dawley rats[108]. Basal expression of BMPR2 in the lung is lower in female C57BL/6 mice and female Wistar Kyoto rats compared to males[33]. On the other hand, Frump et al. observed that basal expression of BMPR2 is higher in the RV of female Sprague-Dawley rats compared to males[384]. While BMPR2 expression in the RV was not affected by SuHx, it significantly increased in ovariectomised female SuHx Sprague-Dawley rats following continuous s/c administration of E2[384]. Therefore, we wished to investigate the effects of 16OHE2 on expression of genes within the BMPR2 signalling pathway in the RV.

We investigated the effects of 16OHE2 in the RV of C57BL/6 mice on the expression of the following genes within the BMPR2 signalling pathway: *Bmpr2*, *Smad1*, *Smad4*, *Smad5*, *Smad9*, *Id1*, *Id2*, and *Id3*. In male mice, no significant changes were observed (Figure 5.5, Table 5.3). However, in female mice, *Id1* and *Id3* expression significantly increased in response to 16OHE2 (Figure 5.6; Table 5.4).

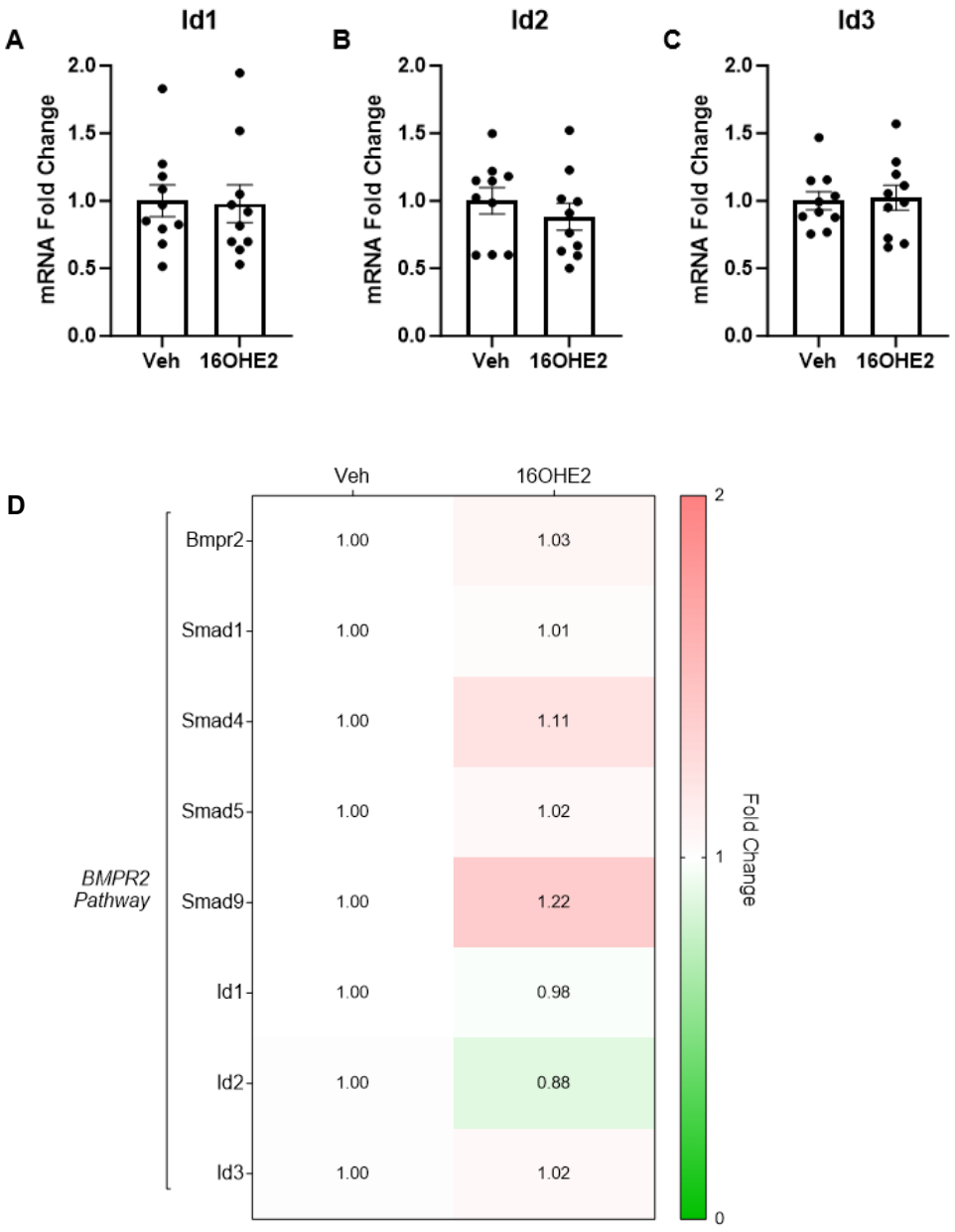

Figure 5.5: Effects of 16OHE2 on expression of genes within the BMPR2 signalling pathway in the right ventricle of male C57BL/6 mice.

Male C57BL/6 mice received 1.5 mg/kg/day 16α-hydroxyestradiol (16OHE2) by intraperitoneal injection for 14 days. Right ventricle (RV) harvest, RNA lysis, and qRT-PCR were carried out as previously described. 16OHE2 did not affect expression of (A) *Id1*, (B) *Id2*, (C) *Id3*. (D) Heatmap comparison of the fold change mRNA expression in response to 16OHE2 compared to the vehicle. Green = <1, white = 1, red = >1. Fold change was calculated by the ΔΔCT method and is represented as relative to the vehicle (where the average vehicle fold change is 1). Normality was assessed by Shapiro-Wilk test. Data are expressed as ±SEM and analysed by unpaired t-test. n=10.

Table 5.3: Effects of 16OHE2 on Expression of Genes Within the BMPR2 Signalling Pathway in the Right Ventricle of Male C57BL/6 Mice

PATHWAY	GENES	Basal CT value	16OHE2 vs. Veh	
			FC ± SEM	P-value
BMPR2 Pathway	***Bmpr2***	25.1	1.03 ± 0.07	0.8108
	Smad1	29.6	1.01 ± 0.06	0.8969
	Smad4	27.0	1.12 ± 0.09	0.2980
	Smad5	29.2	1.02 ± 0.08	0.8502
	Smad9	32.3	1.23 ± 0.11	0.1071
	Id1	25.7	0.98 ± 0.14	0.9048
	Id2	29.6	0.88 ± 0.10	0.4101
	Id3	26.0	1.02 ± 0.09	0.8490

Table 5.3: Effects of 16OHE2 on expression of genes within the BMPR2 signalling pathway in the right ventricle of male C57BL/6 mice.

Male C57BL/6 mice received 1.5 mg/kg/day 16α-hydroxyestradiol (16OHE2) by intraperitoneal injection for 14 days. Right ventricle (RV) harvest, RNA lysis, and qRT-PCR were carried out as previously described. FC= Fold change, calculated by ΔΔCT method and is represented as relative to the vehicle (where the average vehicle fold change is 1). Basal CT value = the average CT value of the vehicle control group. Normality was assessed by Shapiro-Wilk test. Data are expressed as ±SEM and analysed by unpaired t-test. n=10.

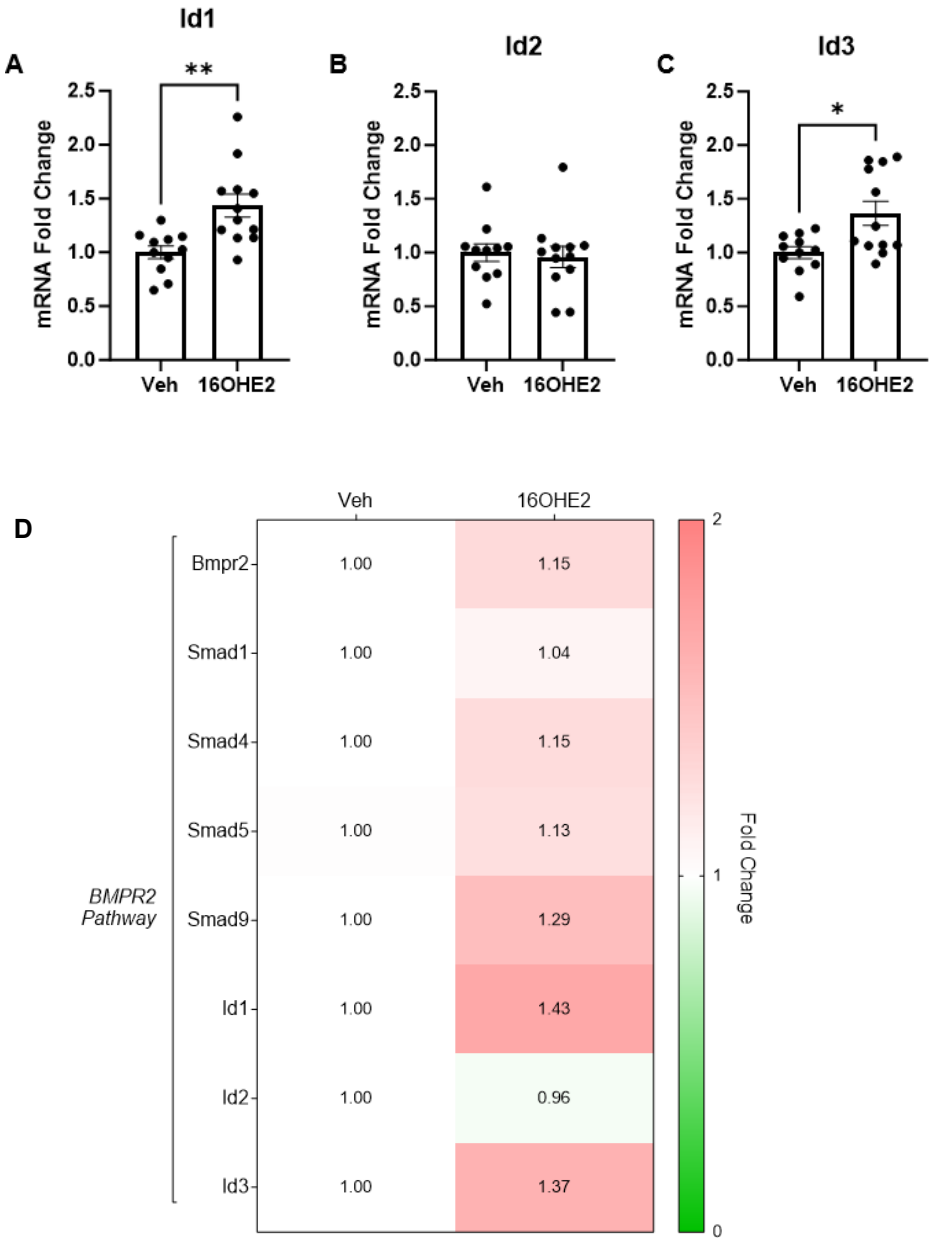

Figure 5.6: Effects of 16OHE2 on expression of genes within the BMPR2 signalling pathway in the right ventricle of female C57BL/6 mice.

Female C57BL/6 mice received 1.5 mg/kg/day 16α-hydroxyestradiol (16OHE2) by intraperitoneal injection for 14 days. Right ventricle (RV) harvest, RNA lysis, and qRT-PCR were carried out as previously described. (A) *Id1* significantly increased in response to 16OHE2. (B) No change was observed in *Id2*. (C) *Id3* significantly increased in response to 16OHE2. (D) Heatmap comparison of the fold change mRNA expression in response to 16OHE2 compared to the vehicle. Green = <1, white = 1, red = >1. Fold change was calculated by the ΔΔCT method and is represented as relative to the vehicle (where the average vehicle fold change is 1). Normality was assessed by Shapiro-Wilk test. Data are expressed as ±SEM and analysed by unpaired t-test or Mann-Whitney test. *p<0.05. **p<0.01. n=11-12.

Table 5.4: Effects of 16OHE2 on Expression of Genes Within the BMPR2 Signalling Pathway in the Right Ventricle of Female C57BL/6 Mice

PATHWAY	GENES	Basal CT value	16OHE2 vs. Veh	
			FC ± SEM	P-value
BMPR2 Pathway	***Bmpr2***	24.7	1.15 ± 0.06	0.1028
	Smad1	29.1	1.04 ± 0.06	0.9279
	Smad4	26.6	1.15 ± 0.04	0.0564
	Smad5	28.6	1.13 ± 0.08	0.2414
	Smad9	31.6	1.29 ± 0.10	0.0792
	Id1	25.1	1.44 ± 0.11	0.0024*
	Id2	28.8	0.96 ± 0.10	0.7626
	Id3	26.2	1.37 ± 0.11	0.0268*

Table 5.4: Effects of 16OHE2 on expression of genes within the BMPR2 signalling pathway in the right ventricle of female C57BL/6 mice.

Female C57BL/6 mice received 1.5 mg/kg/day 16α-hydroxyestradiol (16OHE2) by intraperitoneal injection for 14 days. Right ventricle (RV) harvest, RNA lysis, and qRT-PCR were carried out as previously described. FC= Fold change, calculated by ΔΔCT method and is represented as relative to the vehicle (where the average vehicle fold change is 1). Basal CT value = the average CT value of the vehicle control group. Normality was assessed by Shapiro-Wilk test. Data are expressed as ±SEM and analysed by unpaired t-test or Mann-Whitney test. *$p<0.05$. n=11-12.

5.2.4 Effects of 16OHE2 on Fibrosis Marker Expression in the Lung and Right Ventricle

In PAH, collagen deposition is increased in both the pulmonary arteries and RV[264,266]. This includes the fibril-forming collagens COL1A1 and COL3A1, which provide structure and strength for the pulmonary artery and RV walls[264,266]. Increased deposition of collagen causes stiffening and reduced compliance of the pulmonary arteries[264]. Erewele et al. observed that BMPR2 deficiency increased pulmonary collagen deposition in BMPR2^{R899X} transgenic mice (with knock-in of the human R899X mutation)[105]. Adaptation of the RV to high pulmonary pressures is the key determinant of survival in PAH[266]. Excess collagen formation is associated with maladaptive RV remodelling and fibrosis, which impair cardiac function and lead to RV failure[266]. E2 is known to be protective in the RV[67,108]. For example, daily s/c injection with E2 decreased MCT-induced collagen deposition and fibrosis in the RV of male Sprague-Dawley rats[67]. As the effects of 16OHE2 on collagen expression in the lung and RV are undetermined, we wished to investigate this.

We investigated the effects of 16OHE2 on gene expression of *Col1a1* and *Col3a1* in the lung and RV tissue of C57BL/6 mice. In male mice, no changes were observed in the lung tissue. However, in the RV, *Col3a1* expression significantly decreased in response to 16OHE2 (Figure 5.7). In female mice, *Col3a1* expression significantly decreased in the lung tissue in response to 16OHE2. *Col1a1* and *Col3a1* both significantly decreased in the RV (Figure 5.8).

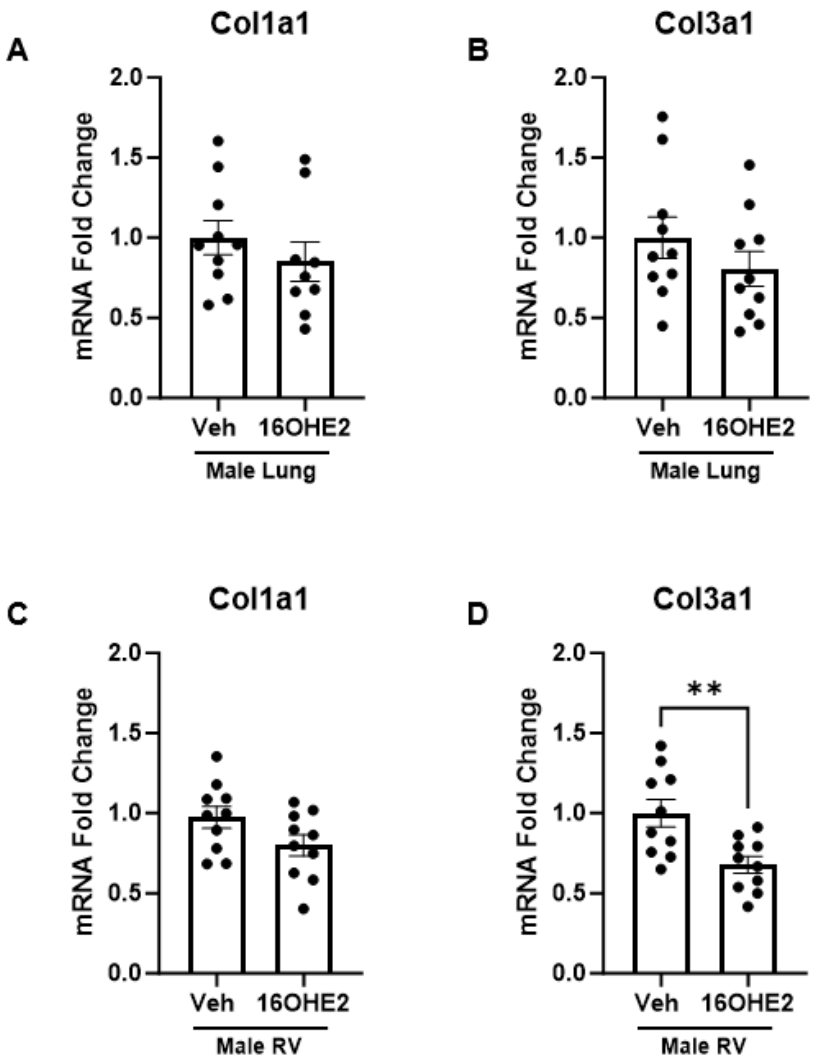

Figure 5.7: Effects of 16OHE2 on *Col1a1* and *Col3a1* mRNA expression in the lungs and right ventricle of male C57BL/6 mice.

Male C57BL/6 mice received 1.5 mg/kg/day 16α-hydroxyestradiol (16OHE2) by intraperitoneal injection for 14 days. Tissue harvest, RNA lysis, and qRT-PCR were carried out as previously described. No changes were observed in expression of (A) *Col1a1* in lung tissue (basal CT value = 25.1), (B) *Col3a1* in lung tissue (basal CT value = 25.5), (C) *Col1a1* in the RV (basal CT value = 24.9). (D) 16OHE2 significantly decreased *Col3a1* expression in the RV (basal CT value = 25.0). Fold change was calculated by the ΔΔCT method and is represented as relative to the vehicle (where the average vehicle fold change is 1). Basal CT value = the average CT value of the vehicle control group. Normality was assessed by Shapiro-Wilk test. Data are expressed as ±SEM and analysed by unpaired t-test. **$p<0.01$. n=10.

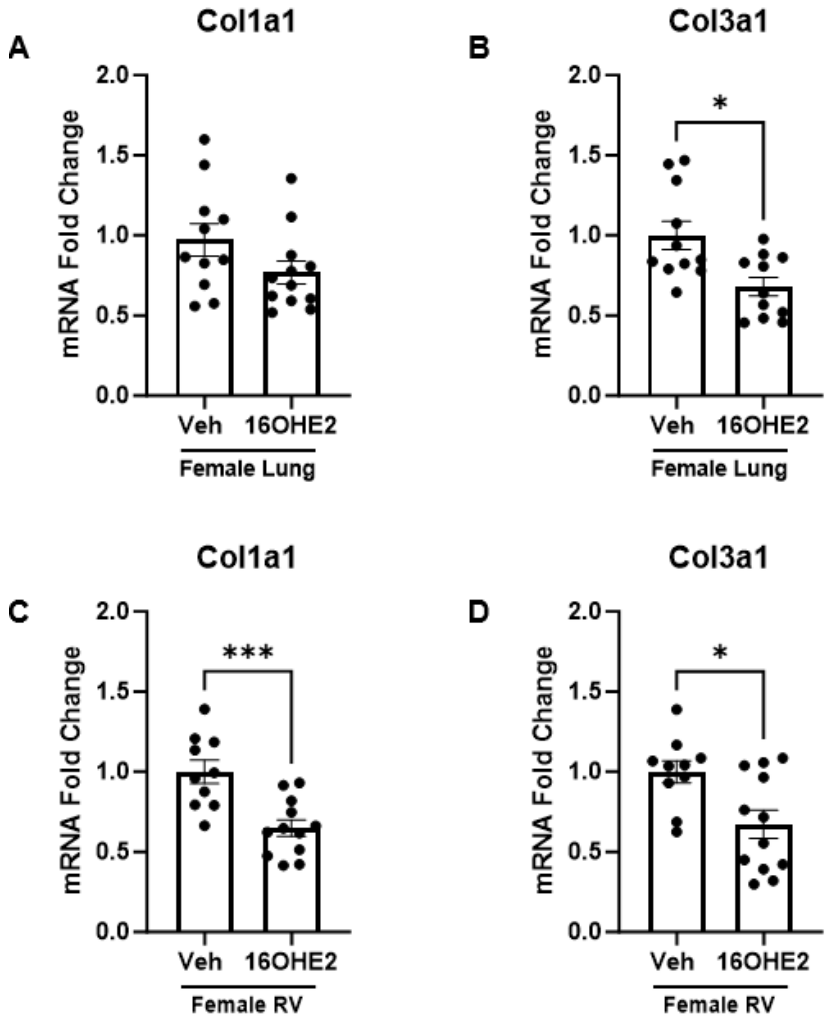

Figure 5.8: Effects of 16OHE2 on *Col1a1* and *Col3a1* mRNA expression in the lungs and right ventricle of female C57BL/6 mice.

Female C57BL/6 mice received 1.5 mg/kg/day 16α-hydroxyestradiol (16OHE2) by intraperitoneal injection for 14 days. Tissue harvest, RNA lysis, and qRT-PCR were carried out as previously described. (A) No change was observed in *Col1a1* in response to 16OHE2 in lung tissue (basal CT value = 25.0). (B) *Col3a1* significantly decreased in response to 16OHE2 in lung tissue (basal CT value = 24.9). (C) *Col1a1* significantly decreased in response to 16OHE2 in the RV (basal CT value = 24.3). (D) *Col3a1* significantly decreased in response to 16OHE2 in the RV (basal CT value = 24.2). Fold change was calculated by the ΔΔCT method and is represented as relative to the vehicle (where the average vehicle fold change is 1). Basal CT value = the average CT value of the vehicle control group. Normality was assessed by Shapiro-Wilk test. Data are expressed as ±SEM and analysed by unpaired t-test or Mann-Whitney test. *$p<0.05$, ***$p<0.001$. n=11-12.

5.2.5 Effects of 16OHE2 on *Sox17* Expression in the Lung and Right Ventricle

SOX17 was recently identified as a novel candidate gene associated with development of PAH[159]. SOX17 is specifically expressed in endothelial cells, and its expression is reduced in human pulmonary artery endothelial cells (PAECs) from PAH patients compared to control subjects[159]. SOX17 expression is also decreased in the endothelium of lung tissue sections from male and female Sprague-Dawley rats with SuHx-induced PAH[159]. Basal SOX17 levels in the lung tissue are significantly lower in female Sprague-Dawley rats compared to males, suggesting that E2 may be suppressive[159]. Sangam et al. recently observed that 16OHE1 suppressed SOX17 expression in human PAECs at concentrations ranging from 1-100 nM[159]. Its overexpression in Tie2-*Sox17* transgenic mice attenuated 16OHE1-induced PAH and RV hypertrophy[159]. Therefore, we wished to investigate the effect of 16OHE2 on *Sox17* expression.

We investigated the effects of 16OHE2 on *Sox17* mRNA expression in the lung and RV tissue of C57BL/6 mice. In male mice, no significant changes in *Sox17* expression were observed in response to 16OHE2 (Figure 5.9). In female mice, no change was observed in lung tissue, but *Sox17* expression significantly increased in the RV in response to 16OHE2 (Figure 5.10).

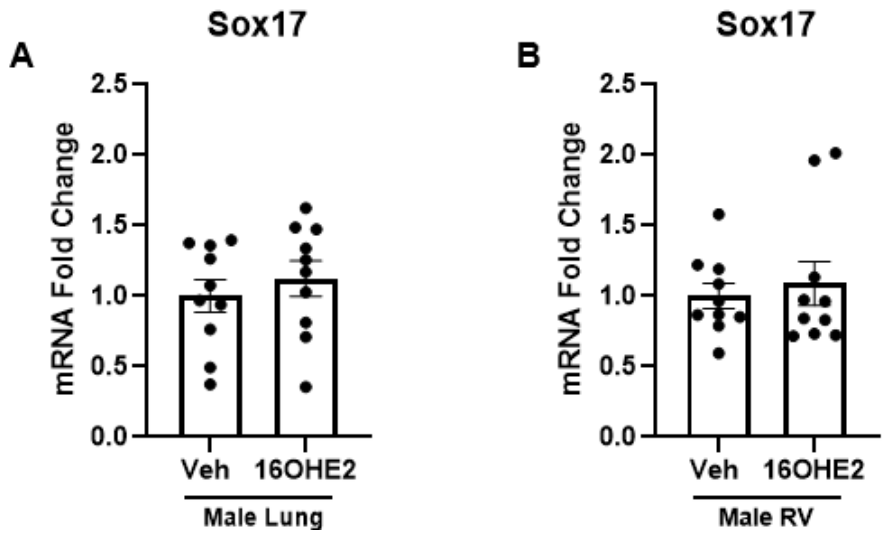

Figure 5.9: Effects of 16OHE2 on *Sox17* mRNA expression in the lung and right ventricle of male C57BL/6 mice.

Male C57BL/6 mice received 1.5 mg/kg/day 16α-hydroxyestradiol (16OHE2) by intraperitoneal injection for 14 days. Tissue harvest, RNA lysis, and qRT-PCR were carried out as previously described. (A) *Sox17* expression in lung tissue (basal CT value = 32.1). (B) *Sox17* expression in RV tissue (basal CT value = 30.2). Fold change was calculated by the ΔΔCT method and is represented as relative to the vehicle (where the average vehicle fold change is 1). Basal CT value = the average CT value of the vehicle control group. Normality was assessed by Shapiro-Wilk test. Data are expressed as ±SEM and analysed by unpaired t-test or Mann-Whitney test. n=10.

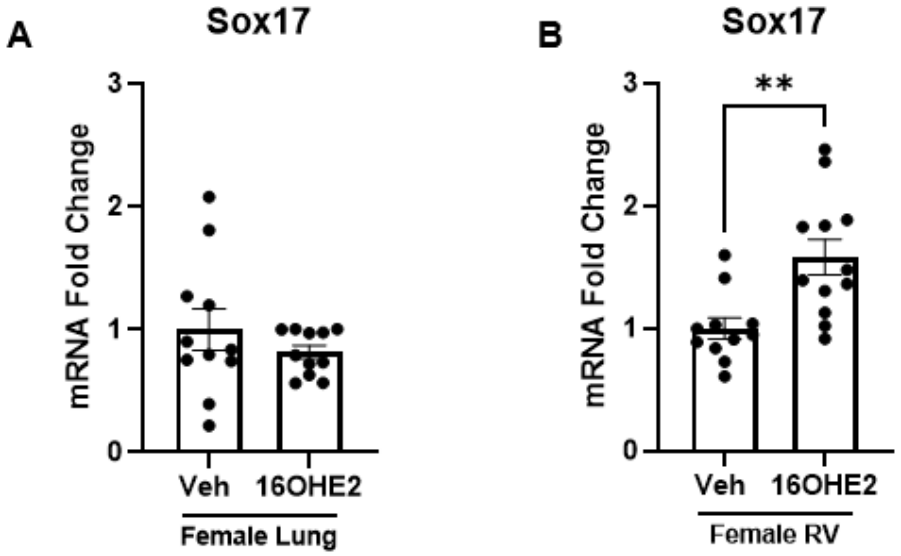

Figure 5.10: Effects of 16OHE2 on *Sox17* mRNA expression in the lung and right ventricle of female C57BL/6 mice.

Female C57BL/6 mice received 1.5 mg/kg/day 16α-hydroxyestradiol (16OHE2) by intraperitoneal injection for 14 days. Tissue harvest, RNA lysis, and qRT-PCR were carried out as previously described. (A) *Sox17* expression lung tissue (basal CT value = 31.2). (B) *Sox17* expression significantly increased in the RV in response to 16OHE2 (basal CT value = 29.6). Fold change was calculated by the ΔΔCT method and is represented as relative to the vehicle (where the average vehicle fold change is 1). Basal CT value = the average CT value of the vehicle control group. Normality was assessed by Shapiro-Wilk test. Data are expressed as ±SEM and analysed by unpaired t-test or Mann-Whitney test. **$p<0.01$. n=11-12.

5.3 Discussion

Female sex is a significant risk factor for PAH, with up to four-fold more women developing PAH than men[27]. On the other hand, once PAH has developed, women have better survival than men and this is likely due to improved RV adaptability to high pulmonary pressures[28,59]. Estrogens are also protective in certain animal models of PAH[29]. These issues are collectively known as the 'estrogen paradox'[29]. A key hypothesis for the estrogen paradox in PAH is a shift in estrogen metabolism from the protective 2-hydroxylation pathway towards pathogenic 16-hydroxylation (Figure 1.4)[274]. White et al. observed that daily intraperitoneal injection of 16OHE1 induced PAH in female C57BL/6 mice in the absence of any additional precipitating factors[35]. As the *in vivo* effects of 16OHE2 are undetermined, we repeated this study with 16OHE2 in male and female C57BL/6 mice. We demonstrated that 16OHE2 did not induce PAH, as assessed by no change in RVSP. However, 16OHE2 significantly increased RV hypertrophy only in female mice in the absence of raised RVSP. 16OHE2 also significantly increased spleen weight in both male and female mice. In lung tissue, no changes were observed in expression of genes within the BMPR2 signalling pathway in response to 16OHE2 in either sex. However, BMPR2 protein levels significantly decreased in the lung tissue of female mice, whereas p-Smad1,5,9 significantly increased in response to 16OHE2 in both sexes. In the RV, *Id1* and *Id3* mRNA expression significantly increased in response to 16OHE2 only in female mice. In the lung, *Col3a1* mRNA expression significantly decreased in response to 16OHE2 only in female mice. However, in the RV, *Col1a1* expression significantly decreased in female mice and *Col3a1* expression significantly decreased in both sexes. Finally, protective *Sox17* mRNA expression significantly increased in the RV of female mice in response to 16OHE2.

16OHE2 did not induce PAH in male or female C57BL/6 mice, as determined by no change in RVSP. However, in female mice 16OHE2 significantly increased RV hypertrophy in the absence of raised RVSP, suggesting that these effects occurred directly in the heart rather than in response to raised pulmonary arterial pressure. It is not unprecedented that estrogens may have direct effects in the heart independent of RVSP. For example, Frump et al. observed that continuous s/c E2 was protective against SuHx-induced RV hypertrophy despite the presence of raised

RVSP in male Sprague-Dawley rats[108]. Liu et al. also observed that continuous s/c E2 protected RV function in ovariectomised female SuHx C57BL/6 mice by stimulation of RV contractility[385]. We investigated the effects of 16OHE2 on RV contractility by analysing the maximum (dP/dt_{max}) and minimum (dP/dt_{min}) rate of pressure change in the ventricle. However, we did not observe any significant changes in RV contractility in response to 16OHE2 (Supplementary Figures 9.5 and 9.6).

White et al. administered intraperitoneal injections of 1.5 mg/kg 16OHE1 for 28 days[35]. However, due to time constraints our mice only received injections of 16OHE2 for 14 days prior to PV looping. Given the RV hypertrophy observed in female mice, it may be worth investigating whether continuing the dosing for the full 28 days would have an impact on RVSP. The half-life of 16OHE2 is short. For example, following intramuscular administration the half-life of 16OHE2 was 3-4 hours in male and female Sprague-Dawley rats and 1.5-5.3 hours in human female volunteers using the combined contraceptive pill[339,340]. 16OHE2 undergoes extensive conjugation by enzymes such as β-glucuronidase and is excreted in the urine as 16OHE2-glucuronide[315,316]. Therefore, continuous dosing with 16OHE2 using a subcutaneous pellet or osmotic minipump may be preferable to intermittent intraperitoneal injection. However, this is considerably more expensive. The effects of 16OHE2 in an animal model of PAH are undetermined. As rats exhibit a more severe disease phenotype than mice in response to both chronic hypoxia and SuHx, it may be interesting to investigate the effects of 16OHE2 in a rat model of PAH[80,99].

16OHE2 had no effect on body weight at the time of PV looping. However, spleen weight significantly increased in both sexes in response to 16OHE2. Increased spleen size (splenomegaly) is common in patients with advanced idiopathic or heritable PAH[383]. The spleen plays a key role in modulating immune response and splenomegaly is associated with inflammation[386]. Perivascular inflammation is a prominent pathological feature in PAH patients and in most animal models of PAH (particularly SuHx and MCT rats)[387]. This suggests that 16OHE2 may mediate inflammation. C-Reactive protein (CRP) is extensively used as a biomarker for inflammation[388]. Therefore, it would be interesting to investigate the effects of 16OHE2 on plasma levels of CRP.

In female mice, 16OHE2 significantly increased RV hypertrophy in the absence of raised RVSP, suggesting that the effects of 16OHE2 occur directly in the heart. Remodelling, hypertrophy, and dysfunction of the right, left, or both ventricles can occur in inflammatory cardiomyopathy where the immune system damages the muscle of the heart[389]. This occurs independently of pulmonary arterial pressures[389]. While predominantly triggered by viral infection, inflammatory cardiomyopathy can also be triggered by autoimmune diseases associated with PAH such as sarcoidosis[389]. In contrast to PAH, inflammatory cardiomyopathy is predominant in men, but this sex difference becomes less prominent with age[390,391,392]. E2 may mediate anti-inflammatory effects by inhibiting production and release of pro-inflammatory cytokines such as interleukin-1β (IL-1β) and tumour necrosis factor-α (TNF-α) in osteoblast-like cells, macrophages, and whole blood cultures[393-396]. During pregnancy, the severity of inflammation is reduced in autoimmune diseases such as multiple sclerosis, suggesting that production of 16OHE2 may mediate anti-inflammatory effects[397]. However, the immunological effects of 16OHE2 are not well characterised[397]. Vermillon et al. recently observed that 16OHE2 reduced inflammation in the lungs of female C57BL/6 mice with severe mouse adapted H1N1 influenza[398]. However, the effects of 16OHE2 on inflammation in the heart are undetermined. The significant increase in spleen weight suggests that increased RV hypertrophy in female mice in the absence of raised RVSP may be due to inflammation. Therefore, it would be intriguing to investigate the effects of 16OHE2 on expression of inflammatory markers such as IL-1β and TNF-α in the RV.

Following this, we investigated the effects of 16OHE2 on the BMPR2 signalling pathway in the lung and RV tissue of C57BL/6 mice. β-actin (*Actb*) was used as the housekeeper for all qRT-PCR experiments as we observed that it was stable in both lung and RV tissue across all experimental groups, as determined by no statistically significant difference in CT value (Figure 5.11). All samples were run on the same qRT-PCR plate to allow direct comparison.

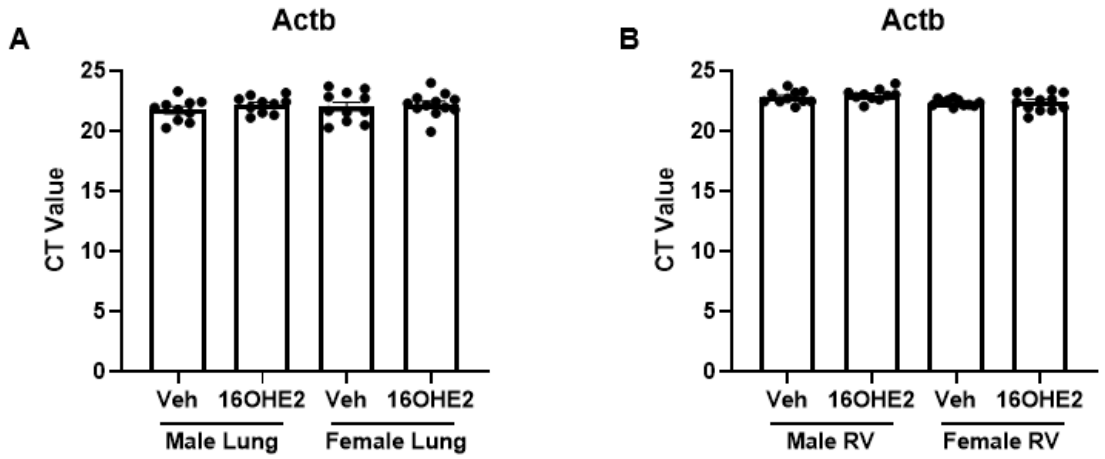

Figure 5.11: *Actb* expression is stable in the lung and right ventricle tissue of male and female C57BL/6 mice following treatment with 16OHE2.

Male and female C57BL/6 mice received 1.5 mg/kg/day 16α-hydroxyestradiol (16OHE2) or vehicle control by intraperitoneal injection for 14 days. Lung and right ventricle (RV) tissue harvest, RNA lysis, and qRT-PCR were carried out as previously described. There was no significant difference in the cycle threshold (CT) value for *Actb* expression in (A) Lung tissue, (B) RV tissue. Normality was assessed by Shapiro-Wilk test. Data are expressed as ±SEM and analysed by one-way ANOVA with post-hoc Tukey test. n=10-12.

β-tubulin was used as the housekeeper for western blots in lung tissue as Dr Sharma had previously observed this was stable and the antibody worked effectively in the lung tissue of the wild type littermates of BMPR2^{R899X} mice. No significant changes in gene expression were observed in lung tissue in response to 16OHE2 in either sex. However, BMPR2 protein levels significantly decreased in female mice in response to 16OHE2, whereas p-Smad1,5,9 expression significantly increased in both sexes. This suggests that 16OHE2 may have a protective effect against PAH in male C57BL/6 mice, as increased p-Smad1,5,9 signalling results in upregulation of Ids1-3, mediating cell cycle regulation[105,146]. However, the effect of 16OHE2 in females is unclear. It is not unprecedented that BMPR2 protein levels did not correspond to mRNA expression. For example, Wright et al. observed that continuous s/c dosing with the ERα antagonist MPP significantly increased BMPR2 protein levels in the lung tissue of female C57BL/6×CBA mice, but *Bmpr2* mRNA expression was significantly decreased[102]. BMPR2 also acts independently of p-Smad1,5,9 signalling via p38 mitogen-activated protein kinase (p38 MAPK; Figure 1.5)[399]. Harper et al. delivered the *BMPR2* gene to the pulmonary endothelium of

MCT-treated Sprague-Dawley rats using a targeted adenoviral vector (AdBMPR2Fab-9B9)[399]. Gene therapy with *BMPR2* significantly decreased phosphorylated-p38 MAPK expression in the lung tissue 2 days after treatment[399]. Therefore, in female C57BL/6 mice, the decrease in BMPR2 protein levels in response to 16OHE2 may potentially occur as a compensatory response to increased p38 MAPK signalling (independent of increased p-Smad1,5,9 signalling). Future studies could include western blots to confirm this.

In lung tissue, no changes in expression of genes within the BMPR2 signalling pathway were observed in either sex. On the other hand, 16OHE2 significantly increased the mRNA expression of *Id1* and *Id3* in the RV of female mice. It is not unprecedented that estrogens may have different effects on the BMPR2 pathway in the lung compared to the RV. For example, Mair et al. observed that basal BMPR2 expression in the lung is significantly lower in female C57BL/6 mice and female Wistar Kyoto rats compared to males[33]. However, suppression of estrogen synthesis in female C57BL/6 mice by daily s/c anastrozole injection increased *Bmpr2* expression in the lung to a similar level as observed in males[33]. On the other hand, Frump et al. reported that basal expression of BMPR2 is higher in the RV of female Sprague-Dawley rats compared to males[384]. Furthermore, BMPR2 expression in the RV significantly increased following continuous s/c E2 administration in ovariectomised female Sprague-Dawley rats[384].

The inhibitor of DNA-binding (Id) proteins regulate the cell cycle and cell differentiation[364]. Therefore, increased *Id1* and *Id3* expression in response to 16OHE2 in the RV of female mice may be protective against cell proliferation and RV remodelling. Some PAH patients develop adaptive RV hypertrophy where cardiac fibroblasts retain their function, however others develop maladaptive RV hypertrophy characterised by fibrosis, RV remodelling and loss of function[266]. Therefore, it is not unprecedented for female mice to develop RV hypertrophy in response to 16OHE2 despite increased expression of *Id1* and *Id3*. However, we did not investigate the effects of 16OHE2 on protein levels of Id1 and Id3 as western blots are technically challenging in the RV due the fibrous nature the tissue, and the small size of the Id proteins (~15 kDa) further adds to this challenge. We previously investigated the effects of 16OHE2 in pulmonary artery smooth muscle cells and aorta smooth muscle cells isolated from male and female Sprague-Dawley rats. Therefore, it may be interesting to isolate cardiac fibroblasts from the left and right

ventricles of these rats, and to investigate the effects of 16OHE2 on mRNA and protein expression of Id1 and Id3 in these cells. No significant changes were observed in any other genes within the BMPR2 signalling pathway. Id1 is known to be involved in many other pathways (e.g., PI3K/Akt signalling, c-Myc signalling), therefore increased *Id1* expression in the RV of female mice may be independent of BMPR2 signalling[364].

Increased collagen deposition in PAH causes stiffening and reduced compliance of the pulmonary arteries[264]. In lung tissue, *Col3a1* expression significantly decreased in response to 16OHE2 in female C57BL/6 mice but not in males. This suggests that 16OHE2 may increase compliance of the pulmonary arteries in female mice. Pulmonary vascular resistance (PVR) is a measure of compliance which describes the resistance blood must overcome to pass through the pulmonary vasculature[400]. PVR is increased in PAH patients and can be used to guide diagnosis and treatment[401]. A limitation of this study is that we did not investigate the effects of 16OHE2 on PVR. In mice, it is difficult to directly measure this during haemodynamic analysis due to their small size because a pulmonary artery segment long enough to facilitate cannulation is required[402]. However, PVR can be indirectly measured using wire myography or an organ bath[402]. English et al. observed that steroid hormones induced dose-dependent dilation during wire myography in pulmonary arteries isolated from male and female Wistar rats in the following order of activity – progesterone > testosterone > cortisol > E2[136]. On the other hand, White et al. did not observe any changes in pulmonary vascular contraction in arteries from female C57BL/6 mice treated with 16OHE1[35]. Therefore, it may be interesting to investigate whether 16OHE2 would affect pulmonary arterial collagen deposition in SuHx-induced PAH and whether this would have any impact on PVR.

In PAH, collagen deposition is also increased in the RV[266]. Adaptation of the RV to high pulmonary pressures is the key prognostic factor for survival in PAH[266]. Some patients develop adaptive RV hypertrophy where cardiac fibroblasts remain concentric with retained function[266]. However, others develop maladaptive RV hypertrophy characterised by transition of cardiac fibroblasts into myofibroblasts leading to excess collagen formation, disruption of cross-linking and collagen turnover, loss of extracellular matrix integrity, RV diastolic stiffness, and disruption of co-ordination and contraction[266]. RV adaptability is improved in female PAH patients

compared to males, suggesting that E2 may be protective[59]. Liu et al. observed that daily s/c injection with E2 decreased collagen deposition and fibrosis in the RV of male Sprague-Dawley rats with MCT-induced PAH[67]. On the other hand, Petrov et al. observed that E2 significantly increased *Col1a1* and *Col3a1* expression in cardiac fibroblasts isolated from male Wistar rats[270]. However, in cardiac fibroblasts isolated from female Wistar rats, E2 significantly decreased *Col1a1* and *Col3a1* expression[270]. We observed that *Col1a1* expression significantly decreased in response to 16OHE2 in the RV of female C57BL/6 mice, and *Col3a1* expression significantly decreased in the RV of both sexes. This suggests that 16OHE2 may be protective against fibrosis in the RV. It would be intriguing to investigate whether 16OHE2 may attenuate RV fibrosis in SuHx-induced PAH, for example by immunohistochemistry staining for collagen in sections of RV tissue.

SOX17 was recently identified as a novel candidate gene associated with development of PAH[159]. Variants associated with overexpression of *SOX17* were first described in patients with congenital abnormalities of the kidney and urinary tract (e.g., vesicoureteral reflux)[403]. However, PAH is associated with variants leading to *SOX17* deficiency[404]. Basal SOX17 levels in lung tissue are significantly lower in female Sprague-Dawley rats compared to males, suggesting that E2 may be suppressive[159]. Sangam et al. recently observed that 16OHE1 decreased *SOX17* expression in human PAECs[159]. However, we did not observe any significant effects of 16OHE2 on *Sox17* expression in the lung tissue of male or female C57BL/6 mice. On the other hand, *Sox17* expression significantly increased in the RV of female mice in response to 16OHE2. SOX17 is known to interact with Smad3, preventing formation of the p-Smad2,3 complex and the downstream effects of TGF-β signalling such as suppression of the Id genes[146,160]. Therefore, increased *Sox17* expression in the female RV is consistent with the increases observed in *Id1* and *Id3* expression and suggests that 16OHE2 may have a protective effect. SOX17 expression is decreased in the endothelium of human lung tissue sections from PAH patients compared to control subjects[159]. However, SOX17 expression was not stratified according to the subtype of PAH (e.g., idiopathic, heritable)[159]. A direct link between BMP2 and SOX17 has been identified during cardiogenesis, where BMP2 and SOX17 form a positive feedback loop and trigger induced pluripotent stem cells to become cardiac progenitor cells[161]. Therefore, it may be worth investigating whether there is a direct link between BMPR2 suppression and loss of SOX17 in heritable PAH.

5.3.1 Limitations of this Study

The Fulton Index (RV weight/ LV+S weight) measurement of RV hypertrophy was consistently higher than expected across all groups of C57BL/6 mice. For example, the average Fulton Index ratios in the male and female vehicle groups were 0.60 and 0.56 respectively. In comparison, Wang et al. reported a Fulton index of 0.26 ± 0.01 in normoxic male C57BL/6 mice[405]. The mouse RV is very small and fragile to handle. Therefore, this may have occurred due insufficient drying of the tissue prior to weighing.

We previously observed that 16OHE2 suppressed *Id1*, *Id2* and *Id3* expression in aorta smooth muscle cells isolated from male and female Sprague-Dawley rats (Chapter 4). However, we did not investigate the effects of 16OHE2 on systemic arterial pressure. Systemic arterial pressure can be measured by cannulation of the left common carotid artery[102]. However, prolonged anaesthesia in mice can change their haemodynamic state and additional systemic arterial pressure analysis may have affected the results[406].

The half-life of 16OHE2 is short. For example, following intramuscular administration, the half-life of 16OHE2 was 3-4 hours in male and female Sprague-Dawley rats and 1.5-5.3 hours in human female volunteers using the combined contraceptive pill[339,340]. Therefore, continuous s/c dosing with 16OHE2 using an implanted pellet or osmotic minipump may be preferable to intermittent intraperitoneal injection. However, this is considerably more expensive and may be more invasive for the animal.

Finally, most *in vitro* studies in this project were carried out in rats whereas the *in vivo* studies were performed in mice. Ideally, the *in vitro* and *in vivo* studies would be carried out in the same species, followed by investigation of whether these results translate to human cells. However, this was not possible due to the constraints of the COVID-19 pandemic.

5.3.2 Summary

In summary (Figure 5.12), 16OHE2 did not induce PAH in male or female C57BL/6 mice as determined by no change in RVSP. However, 16OHE2 significantly increased RV hypertrophy in female mice. Spleen weight was significantly increased in response to 16OHE2 in male and female mice. In lung tissue, no changes were observed in expression of genes within the BMPR2 signalling pathway in either sex. However, BMPR2 protein levels significantly decreased in the lung tissue of female mice, whereas p-Smad1,5,9 expression significantly increased in response to 16OHE2 in both sexes. 16OHE2 significantly increased *Id1* and *Id3* mRNA expression in the RV of female mice. On the other hand, 16OHE2 significantly decreased *Col3a1* expression in the lung tissue of female mice but not in males. *Col1a1* expression significantly decreased in response to 16OHE2 in the RV of female mice, and *Col3a1* expression significantly decreased in both sexes. Finally, *Sox17* expression significantly increased in the RV of female mice in response to 16OHE2. These results suggest that increased RV hypertrophy in female mice is due to direct effects of 16OHE2 on the heart. As spleen weight is significantly increased, this may occur due to increased inflammation independent of the RVSP and the protective molecular effects of 16OHE2 observed in the RV.

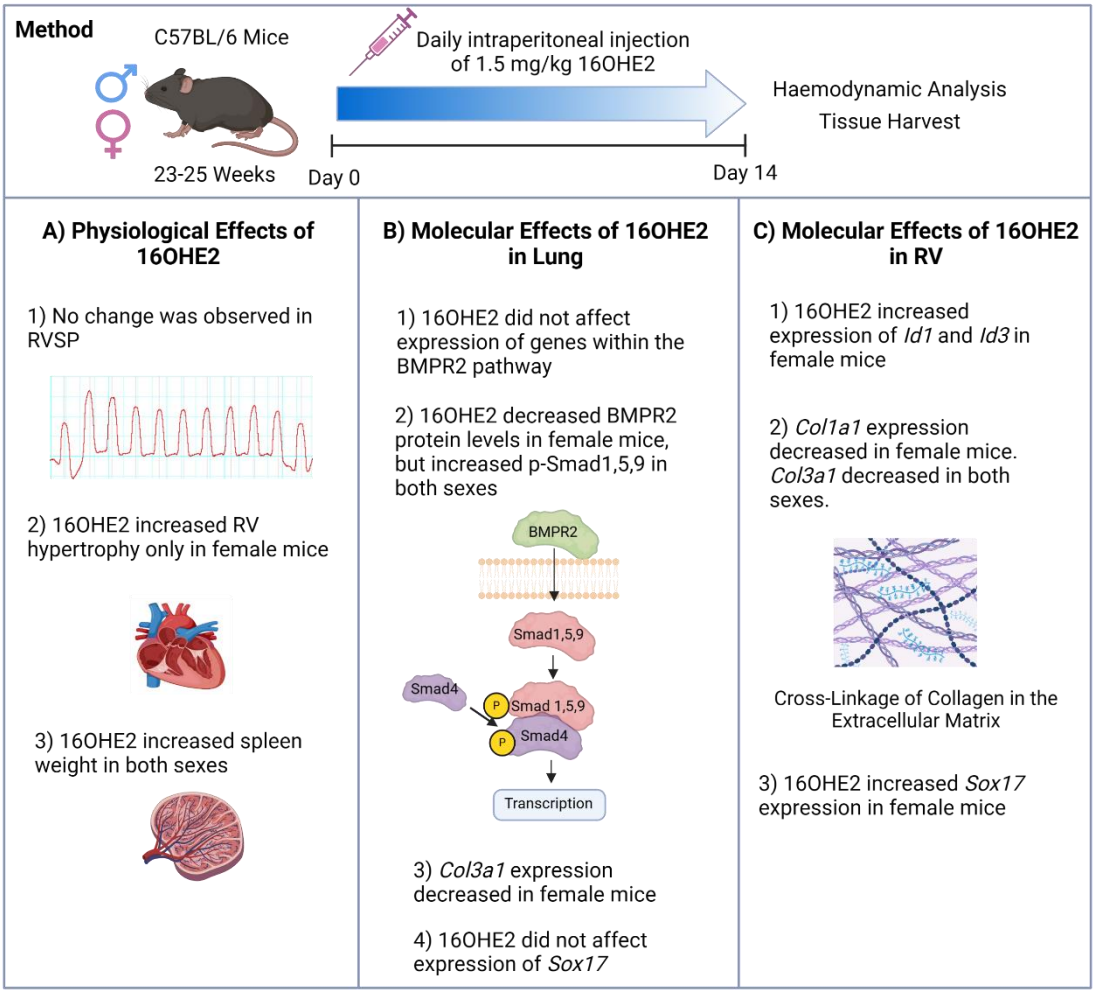

Figure 5.12: Summary of the *in vivo* effects of 16OHE2.
Male and female C57BL/6 mice aged 23-25 weeks received 1.5 mg/kg/day 16α-hydroxyestradiol (16OHE2) by intraperitoneal injection for 14 days before haemodynamic analysis and tissue harvest. (A) Physiological effects of 16OHE2. No change in right ventricular systolic pressure (RVSP) was observed in response to 16OHE2 in either sex. However, 16OHE2 significantly increased right ventricular (RV) hypertrophy in female mice. 16OHE2 significantly increased spleen weight in both sexes. (B) The molecular effects of 16OHE2 in lung tissue. 16OHE2 did not affect expression of genes within the bone morphogenetic protein receptor 2 (BMPR2) signalling pathway. However, BMPR2 protein levels significantly decreased in the lung tissue of female mice, whereas p-Smad1,5,9 significantly increased in response to 16OHE2 in both sexes. *Col3a1* expression significantly decreased in the lung tissue of female mice in response to 16OHE2. *Sox17* expression was not affected. (C) The molecular effects of 16OHE2 in the RV. 16OHE2 significantly increased expression of *Id1* and *Id3* in female mice. *Col1a1* expression significantly decreased in female mice, and *Col3a1* expression significantly decreased in both sexes in response to 16OHE2. *Sox17* expression significantly increased in response to 16OHE2 in female mice.

Chapter 6

General Discussion

6.1 General Discussion

Altered estrogen metabolism (Figure 1.4) is a key hypothesis for the estrogen paradox in PAH[274]. The estrogenic effects of 16α-hydroxyestrone (16OHE1) are more potent than those of other estrogen metabolites as it forms strong covalent bonds with estrogen receptors[274,310]. The effects of 16OHE1 in PAH appear to be predominantly pathogenic. For example, White et al. observed that daily intraperitoneal injection of 16OHE1 induced PAH in female C57BL/6 mice in the absence of any additional precipitating factors[35]. 16OHE1 also significantly increased proliferation of female control subject hPASMCs, and this further increased in female PAH patient hPASMCs[35,311]. On the other hand, 2-methoxyestradiol (2ME2) appears to be protective[299]. For example, continuous subcutaneous (s/c) 2ME2 attenuated chronic hypoxia-induced PAH in male and female Sprague-Dawley rats[299]. 2ME2 also significantly decreased proliferation of female control subject hPASMCs[299]. Elevated plasma ratios of 16OHE1/2ME2 and decreased urinary ratios of 2-hydroxyestrogen/16OHE1 have been observed in PAH patients[106,286]. Therefore, a shift in estrogen metabolism from the 2-hydroxylation pathway towards 16-hydroxylation may mediate development of PAH.

Increased plasma levels of 16OHE2 were recently observed in female idiopathic PAH patients, and in male and female patients with portopulmonary PAH[241,317]. Denver et al. observed that 16OHE2 significantly increased proliferation of female PAH patient hPASMCs and migration of blood outgrowth endothelial cells (BOECs) from male and female PAH patients[241]. During a study primarily focused on E2, Austin et al. (2012) incidentally observed that 24 hours stimulation with 16OHE2 (estriol) suppressed *BMPR2* expression in human pulmonary microvascular endothelial cells, with 10 nM being the optimal concentration[147]. However, this observation was made before increased plasma levels of 16OHE2 were detected in PAH patients (Denver et al. 2020)[241]. The molecular effects of 16OHE2 in PAH and its effects *in vivo* are undetermined. Therefore, we wished to investigate this.

In Chapter 3, we investigated the functional effects of 16OHE2 *in vitro.* We observed that 16OHE2 did not affect proliferation of Dede hamster lung fibroblasts or rat pulmonary artery smooth muscle cells (rPASMCs). Denver et al. previously observed that 16OHE2 significantly increased proliferation of female PAH patient

hPASMCs, but not of hPASMCs from male or female control subjects[241]. Therefore, we hypothesised that at least one 'second hit' was required. However, we did not observe any significant change in proliferation of male or female rPASMCs in response to 16OHE2 under acute hypoxia. Following this, we attempted to replicate the findings of Denver et al. in different female PAH patient hPASMCs, with the aim to carry out novel studies to investigate the underlying mechanism with estrogen receptor antagonists. However, we did not observe any significant change in proliferation. As previously discussed in Chapter 3, there are many potential confounding factors present in studies with hPASMCs including differences in passage number, age, weight, and genetic variance[34,51,141]. Therefore, different results may be due to use of different PAH patient cell lines.

A single 'second hit' with acute hypoxia was not sufficient to increase proliferation of rPASMCs in response to 16OHE2. It is not unprecedented that several 'hits' may be required to induce a proliferative response. There is substantial overlap between the mechanisms of pulmonary vascular remodelling in PAH and the 'hallmarks of cancer' as defined by Hanahan and Weinberg (Figure 6.1)[6,407-409]. Cancers are known to develop from a range of 2-7 somatic mutations (or 'hits') within cells which generate a growth advantage leading to uncontrolled proliferation or prohibition of cell death[410,411]. However, no single combination of hits has been identified for all instances of a specific type of cancer[410]. Somatic mutations may also be involved in development of PAH. For example, Aldred et al. identified a somatic mutation in *SMAD9* in the lung tissue of a hereditary PAH patient - an additional insult to *BMPR2* mutation[153]. Environmental factors are also involved in both cancer and PAH. For example, obesity is an established risk factor for estrogen receptor-positive (ER-positive) breast cancer and is also prevalent in PAH affecting 30-40% of patients[41,49]. Therefore, it is plausible that PAH may result from a different combination of genetic and environmental 'hits' in each patient. This may explain the difference between the increased proliferation in response to 16OHE2 observed in female PAH patient hPASMCs by Denver et al., and our own observation that 16OHE2 did not have any significant effect on proliferation in female PAH patient hPASMCs derived from different patients under different conditions[241].

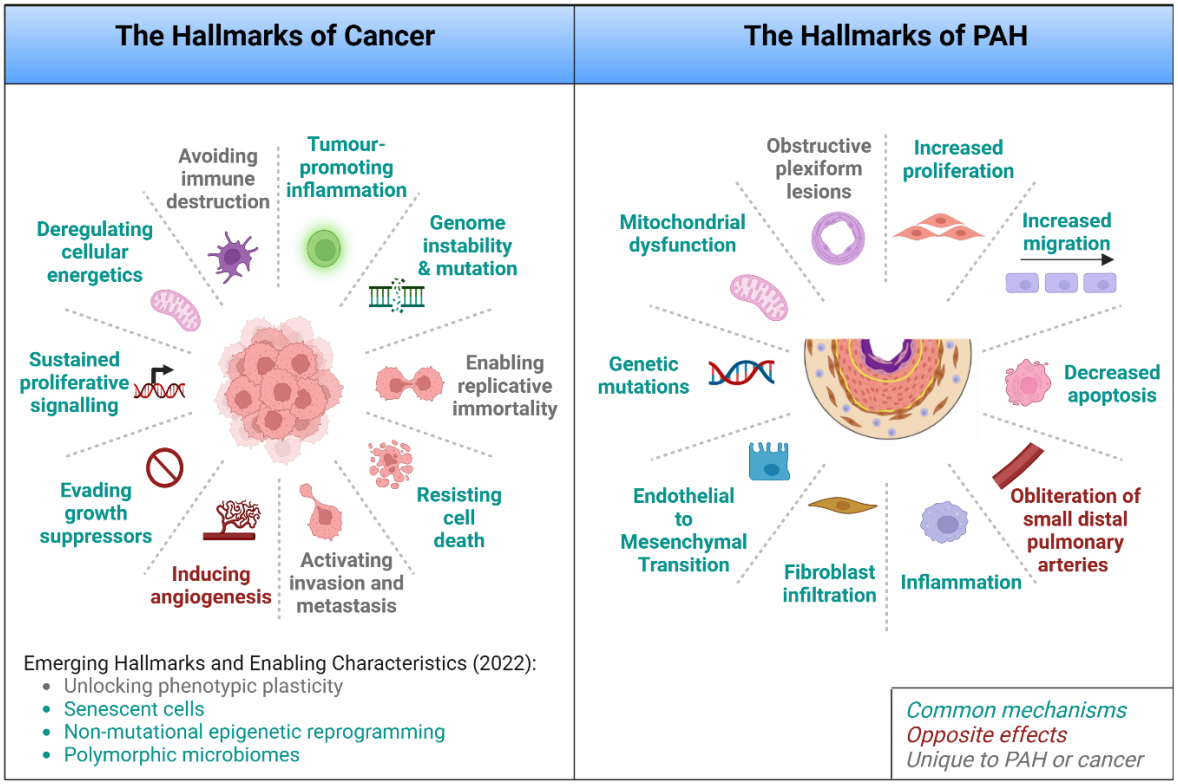

Figure 6.1: A direct comparison of the hallmarks of cancer and the hallmarks of PAH.

Hanan and Weinberg (2000) initially presented six 'hallmarks of cancer' – sustained proliferative signalling, evading growth suppressors, enabling replicative immortality, resisting cell death, inducing angiogenesis, and activating invasion and metastasis[407]. Two additional 'hallmarks' were introduced in 2011 (deregulating cellular energetics and avoiding immune destruction), along with the enabling characteristics inducing angiogenesis and tumour-promoting inflammation[408]. In 2022, Hanahan proposed four additional emerging hallmarks and enabling characteristics – unlocking phenotypic plasticity, senescent cells, non-mutational epigenetic reprogramming, and polymorphic microbiomes[409]. Here, we demonstrate that many of the hallmarks and enabling characteristics of cancer overlap with the underlying mechanisms of pulmonary arterial hypertension (PAH), and vice versa[6,407-409,412-416]. Adapted from "Hallmarks of Cancer (Circle Layout)", by BioRender.com (2024)[417].

In Chapter 3, we also demonstrated that 1 nM 16OHE2 increased migration of male and female rPASMCs following 8- and 24-hours stimulation. This occurred in the absence of a 'second hit' and suggests that 16OHE2 may independently mediate pulmonary vascular remodelling. Similarly, Denver et al. also observed that 1 nM 16OHE2 significantly increased migration of BOECs from male and female PAH patients following 24 hours stimulation[241]. We also observed that 1 nM E2 and 1 nM 16OHE1 significantly increased migration of male rPASMCs after 24 hours stimulation. While there is little published data on the effects of 16OHE1 and 16OHE2 on migration, the effects of E2 have been studied but are unclear. For example, E2 increased migration of MCF-7 breast cancer cells, and this was reversed by the ERα inhibitor fulvestrant which also decreased plasma levels of 16OHE2 in female PAH patients[117,352]. On the other hand, E2 inhibited migration of vascular smooth muscle cells isolated from the thoracic aorta of female Sprague-Dawley rats and this was reversed by fulvestrant[353]. Therefore, it would be intriguing to investigate whether ERα mediates increased rPASMC migration in response to 16OHE2.

Many of the hormonal therapies widely available for ER-positive breast cancer have been investigated in clinical trials for PAH, including fulvestrant and the selective ERα antagonist tamoxifen (Figure 6.2, Table 6.1)[117,121]. Kawut et al. observed that fulvestrant increased 6-minute walk distance, increased stroke volume, and decreased plasma 16OHE2 levels in postmenopausal women with PAH[117]. The results of the tamoxifen trial have not yet been posted[121]. The effects of 16OHE2 in cancer are not well defined. Intriguingly, Watson et al. observed that 16OHE2 increased proliferation of GH3/B6/F10 rat pituitary tumour cells, but this did not occur in a subline of these cells expressing low levels of ERα[318]. This adds further weight to the hypothesis that 16OHE2 may act through ERα. In practice, 16OHE2 (estriol) is used as a vaginal gel or cream as hormone replacement therapy (HRT)[91,418]. As 16OHE2 is readily absorbed into the systemic circulation, there has been some debate about its safety[418,419]. For example, adverse effects listed in the British National Formulary include increased risk of coronary artery disease, ischaemic stroke, and venous thromboembolism[91]. However, it is undetermined whether it has any association with PAH. On the other hand, Sánchez-Rovira et al. advised following a Phase 2 clinical trial that ultralow-dose 0.005% 16OHE2 vaginal gel is safe for menopausal symptoms associated with aromatase inhibitors in women with ER-positive breast cancer[419]. As 16OHE2 increased migration of

rPASMCs in both sexes, future studies could investigate whether this is attenuated by fulvestrant or tamoxifen because these widely available medicines could potentially benefit male and female PAH patients.

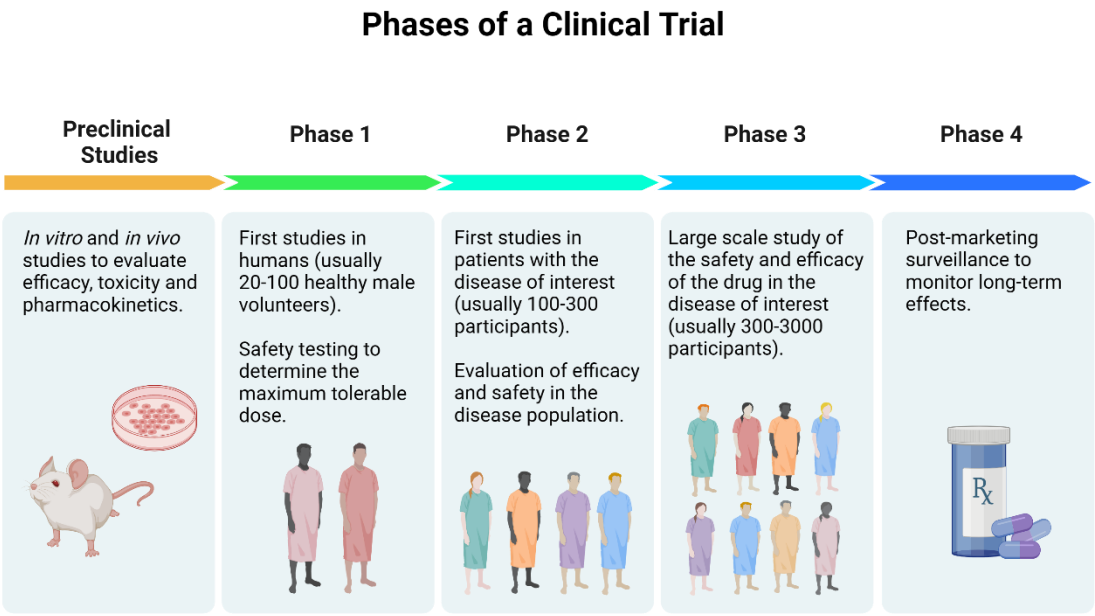

Figure 6.2: The phases of a clinical trial[420].

Created with BioRender.com

Table 6.1: Estrogen-dependent breast cancer drugs in clinical trials for PAH

Drug	Indications	Mechanism of Action	PAH Clinical Trial Phase	Year(s) of Completion	Ref.
Anastrozole	ER-positive breast cancer	Aromatase inhibitor	Phase 2	2015 2022	279 280 281
Fulvestrant	ER-positive breast cancer	ERα inhibitor	Phase 2	2018	117 118
Tamoxifen	ER-positive breast cancer	Selective ERα antagonist in breast tissue. Partial agonist in other tissues, e.g., endometrium).	Phase 2	2023	121

In Chapter 4, we investigated the molecular effects of 16OHE2 *in vitro*. We observed that the gene expression of *Bmpr2*, *Smad1*, *Smad4* and *Smad5* significantly decreased in male rPASMCs in response to 24 hours stimulation with 16OHE2 under both normoxia and acute hypoxia. Decreased *Smad4* expression was reversed by the ERα antagonist MPP, suggesting that 16OHE2 may act via this receptor. On the other hand, no changes were observed in expression of genes within the BMPR2 signalling pathway in female rPASMCs under normoxic conditions, however *Bmpr2* expression significantly increased in response to 16OHE2 under acute hypoxia. As previously discussed in Chapter 4, *Bmpr2* may only decrease in response to 16OHE2 in male rPASMCs because basal BMPR2 protein levels are already suppressed in females. *BMPR2* and *SMAD4* mRNA expression also significantly decreased in male control subject hPASMCs in response to 24 hours stimulation with 16OHE2. On the other hand, *Col1a1* significantly decreased in response to 16OHE2 in male rPASMCs, suggesting that it may be protective against fibrosis.

16OHE2 is known to have a short half-life. For example, following intramuscular administration the half-life of 16OHE2 was 3-4 hours in male and female Sprague-Dawley rats and 1.5-5.3 hours in human female volunteers using the combined contraceptive pill[339,340]. In male rPASMCs, we investigated the effects of 2 hours stimulation with 16OHE2 on expression of genes within the BMPR2 signalling pathway. However, the only change observed was a significant decrease in *Id2* expression. Furthermore, in Chapter 3 we only observed increased migration in response to 16OHE2 after 8- and 24-hours stimulation. However, as discussed in Chapter 4, the enzymes required to break down 16OHE2 may not be present in the cell culture environment. During pregnancy, 16OHE2 is synthesised from 16α-hydroxydehydroepiandrosterone (16-OH-DHEA) in the fetal liver then is released into the maternal circulation via the placenta as unconjugated 16OHE2[314]. It then undergoes extensive conjugation by enzymes such as β-glucuronidase and is excreted in the urine as 16OHE2-glucuronide (Figure 1.10)[315,316]. This leads to the questions of why plasma levels of 16OHE2 are elevated in PAH patients and where it is being synthesised[241,317]. Here, we present two hypotheses for elevated plasma levels of 16OHE2 in PAH.

Firstly, obesity may be more prevalent in PAH than the general population, affecting ~30-40% patients[43,45]. Adipose tissue was recently identified as an important endocrine organ[41]. Although it does not synthesise sex steroids *de novo*, adipose tissue highly expresses the estrogen-synthesising enzyme aromatase and interconverts stored or circulating sex steroids (Figure 1.8)[41,237]. Increased fat mass in obesity is positively correlated with increased estrogen synthesis via aromatase[49,50]. This effect is more pronounced in postmenopausal women as adipose tissue is the primary source of estrogen production after menopause[238]. According to the REVEAL registry, the average patient age at PAH diagnosis is 53 years old, suggesting that estrogen synthesis in adipose tissue may play an important role in the predisposition of postmenopausal women to PAH[51]. Adipose tissue is also known to metabolise estrogens[239]. CYP1B1 is one of several CYP450 enzymes which convert estrogens to 16α-hydroxyestrogens (Figure 1.4)[7]. CYP1B1 is highly expressed in visceral adipose tissue (VAT) and is also overexpressed in the pulmonary artery lesions of PAH patients[34,35,239,240]. Mair et al. recently observed that aromatase and CYP1B1 expression were significantly increased in the peri-renal VAT of male genetically obese *ob/ob* mice compared to their wildtype littermates[34]. However, this was not observed in female *ob/ob* mice[34]. In keeping with this, urinary levels of 16OHE1 were also elevated in male *ob/ob* mice[34]. On the other hand, Stirrat et al. observed that plasma 16OHE2 levels were significantly lower in severely obese pregnant women (BMI $\geq$40) compared to lean pregnant women at 28 and 36 weeks gestation[421]. Therefore, it would be intriguing to investigate whether there is any correlation between plasma 16OHE2 levels and BMI in PAH patients.

To further investigate the role of CYP1B1, Mair et al. incubated cell culture media with VAT harvested from male *ob/ob* mice for 24 hours[34]. VAT-conditioned media contained significantly lower levels of E2 compared to control media but significantly higher levels of 16OHE1, suggesting that E2 was metabolised by VAT[34]. Intriguingly, 24 hours stimulation with VAT-conditioned media significantly increased proliferation of PASMCs isolated from male *ob/ob* mice[34]. This was reversed by both anastrozole and the CYP1B1-inhibitor TMS[34]. Decreased BMPR2 signalling is associated with hyperactivation of the TGF-β pathway, leading to increased cell proliferation[105]. We observed that 16OHE2 significantly decreased gene expression of *BMPR2* in male rPASMCs and male control subject hPASMCs. Therefore, it is reasonable to hypothesise this may also occur in male mouse PASMCs. It would be intriguing to

repeat the experiment by Mair et al. in obese male *ob/ob* mice with two objectives: to investigate whether 16OHE2 is released by VAT and to investigate whether 24 hours incubation in VAT-conditioned media would decrease *Bmpr2* expression in male *ob/ob* mouse PASMCs.

Secondly, fluid retention is a key symptom of right heart failure in PAH, and this can lead to chronic kidney disease (CKD)[422,423]. CKD is prevalent in PAH (affecting up to 36% of patients) and is associated with worse outcomes including higher incidence of death or transplant[424,425]. 16OHE2 is predominantly excreted in the urine as 16OHE2-glucuronide[315,316]. Therefore, if 16OHE2 is synthesised in the peripheral tissues of PAH patients, then decreased elimination via the kidneys may result in accumulation of 16OHE2 in the circulation. Measurement of 16OHE2 at a single time point in pregnant women is imprecise because of pulsatile secretion, diurnal variation, and the short half-life of 16OHE2[314]. While a 24-hour urine collection may be the most accurate way to analyse 16OHE2, feasibility of this is a challenge as it is inconvenient for study subjects[426]. It would be interesting to measure urinary levels of 16OHE2 in PAH patients and investigate whether urinary or plasma levels of 16OHE2 correlate with kidney function.

In Chapter 4, we also demonstrated that 16OHE2 significantly decreased gene expression of *Smad3*, *Smad6*, *Id1*, *Id2* and *Id3* in male rat aorta smooth muscle cells (AoSMCs), and *Smad2*, *Smad3*, *Smad4*, *Smad7*, *Id2* and *Id3* in female rat AoSMCs. As previously discussed in Chapter 4, suppressed *Id1-3* expression may result from increased TGF-β signalling[146]. Aberrant proliferation of vascular smooth muscle cells is associated with several disease pathologies, e.g., atherosclerosis, restenosis[355]. Decreased *Id1-3* expression is associated with increased TGF-β mediated cell proliferation, increased cell differentiation, and decreased apoptosis[362,363,364]. Suppression of Ids1-3 also plays a key role in the uncontrolled proliferation of tumour cells in cancers[362,363,364]. Therefore, future studies could investigate the effects of 16OHE2 on proliferation of rat AoSMCs.

We observed that the ERα antagonist MPP attenuated decreased *Smad4* expression in response to 16OHE2 in male rPASMCs. However, the ERβ antagonist PHTPP and GPER antagonist G15 had no effect. Therefore, future studies could investigate whether decreased *Id1-3* expression in rat AoSMCs in response to 16OHE2 also occurs via ERα. Selective activation of ERα increased proliferation of mouse aorta endothelial cells via ERK1/2[102]. On the other hand, E2 is anti-mitogenic

in vascular smooth muscle cells and this may be associated with its sequential metabolism to 2ME2[109,374-376]. However, these effects occur independently of ERα and ERβ[109,374,375]. For example, E2 inhibits vascular injury response to the same extent in female wild-type, ERα knockout, ERβ knockout, and ERα/ERβ double knockout mice[109,374,375]. Kawut et al. recently observed that the ERα inhibitor fulvestrant decreased plasma 16OHE2 levels in postmenopausal women with PAH[117]. Therefore, future studies could investigate whether fulvestrant would attenuate *Id1-3* suppression in response to 16OHE2 in rat AoSMCs, because this widely available medicine could potentially be repurposed for several vascular diseases and benefit patients of either sex. However, fulvestrant is not recommended in premenopausal women as it is non-selective, resulting in the adverse effects of early menopause (e.g., increased risk of osteoporosis and cardiovascular disease)[119]. Tamoxifen is suitable for premenopausal women with ER-positive breast cancer as it is a selective ERα antagonist in breast tissue and a partial agonist in other tissues (e.g., endometrium)[120]. Therefore, it would also be interesting to investigate the effects of tamoxifen on *Id1-3* suppression in response to 16OHE2.

The *in vitro* studies in Chapters 3 and 4 predominantly focused on the effects of 16OHE2 in smooth muscle cells, which form the medial layer of the pulmonary artery (Figure 1.2)[6]. However, several other cell types also play a key role in the development of PAH, for example endothelial cells in the intimal layer and adventitial fibroblasts[6]. Therefore, it is important to consider the effects of 16OHE2 in different cell types and the whole blood vessel environment. In keeping with the migration we observed in male and female rPASMCs, Denver et al. also observed that 1 nM 16OHE2 increased migration of BOECs from male and female PAH patients[241]. However, while we observed that *Bmpr2* and *Smad1* mRNA expression significantly decreased in response to 16OHE2 in male rPASMCs, Dr Katie Yates Harvey observed no change in *BMPR2* mRNA expression but an increase in *SMAD1* in male hereditary PAH patient BOECs (unpublished data). Intriguingly, Frump et al. recently observed that ERα expression is decreased in PAECs from PAH patients, whereas Wright et al. observed that ERα expression is increased in female PAH patient hPASMCs[102,427]. In male rPASMCs, we observed that decreased *Smad4* mRNA expression in response to 16OHE2 was reversed by the ERα antagonist MPP. Therefore, differences in ERα expression between smooth muscle and endothelial cells may potentially explain the different molecular response to

16OHE2. Interaction between the endothelial and smooth muscle layers of the blood vessel also play a key role in PAH[428]. Vasoconstrictors secreted by the endothelium (e.g., endothelin-1, serotonin) act on smooth muscle cells in a paracrine fashion, and endothelial-to-mesenchymal cell transition contributes to increased muscularisation and neointima formation in the pulmonary artery[413.428]. Crosstalk between smooth muscle and endothelial cells also plays a key role, for example, miR-143-3p enriched exosomes from female hPASMCs increased migration of female human PAECs[429]. While increased migration of both rPASMCs and PAH patient BOECs suggest that 16OHE2 may contribute to remodelling in the whole blood vessel environment, a limitation of this project is that these effects are unclear[241]. Future studies could investigate this by studying the effects of 16OHE2 on release of vasoconstrictors (e.g., endothelin-1) from endothelial cells by enzyme-linked immunosorbent assay, endothelial-to-mesenchymal cell transition by loss of endothelial cell markers (e.g., CD31), and its effect on miR-143-3p expression in the exosomes of PASMCs.

Finally, in Chapter 5, we investigated the *in vivo* effects of 16OHE2 in C57BL/6 mice. *In vivo* work including dosing, haemodynamic measurements, and tissue harvest was carried out by Dr Smriti Sharma. 16OHE2 did not induce PAH in male or female C57BL/6 mice, as determined by no significant change in right ventricular systolic pressure (RVSP). However, 16OHE2 significantly increased RV hypertrophy in female mice in the absence of raised RVSP, suggesting that 16OHE2 acts directly on the heart. As previously discussed in Chapter 5, 16OHE2 also significantly increased spleen weight in male and female mice. Increased spleen size (splenomegaly) is common in patients with advanced idiopathic or heritable PAH[383]. The spleen plays a key role in modulating immune response and splenomegaly is associated with inflammation[386]. Therefore, RV hypertrophy in female mice may be due to inflammation, and future studies could investigate the effects of 16OHE2 on expression of inflammatory markers such as IL-1β and TNF-α.

Perivascular inflammation is a prominent pathological feature in PAH patients, and in most animal models of PAH (particularly sugen-hypoxic (SuHx) and monocrotaline (MCT) rats)[387]. Sotatercept is an activin receptor type IIA-Fc fusion protein which acts as a ligand trap for selected TGF-β superfamily members to restore the balance between the pro-proliferative TGF-β pathway and the protective BMPR2 signalling pathway[366,369]. Intriguingly, sotatercept was originally developed

for anaemia associated with end-stage CKD, and both anaemia and CKD are common comorbidities with PAH[430,431]. In addition to modulating immune response, the spleen plays a key role in filtering out senescent red blood cells from the circulation, and splenomegaly is associated with iron deficiency and other types of anaemia[432,433]. Therefore, splenomegaly may be a link between PAH and its comorbid anaemia and CKD. Given the increased spleen weight observed in male and female C57BL/6 mice, it may be interesting to investigate whether 16OHE2 also affects haemoglobin levels. Hepcidin is a small peptide hormone which regulates iron homeostasis[434]. Overexpression of hepcidin is associated with iron deficiency anaemia and anaemia of chronic or inflammatory disease[434]. Langdon et al. observed that the rodent sotatercept analogue RAP-011 increased production of red blood cells (erythropoiesis) in genetically iron deficient female Tg-*Hamp* mice overexpressing the hepcidin antimicrobial peptide (*Hamp1*)[434]. Joshi et al. recently observed that RAP-011 attenuated SuHx-induced elevated expression of several inflammatory markers (e.g., interleukin-6, chemokine ligand-2) in the lung tissue of male Sprague-Dawley rats[369]. However, the vasodilator sildenafil had no significant effect on inflammation despite being a first-line therapy for PAH[369]. In general, current therapies for PAH decrease pulmonary arterial pressure but do not address the underlying pulmonary vascular remodelling, and no substantial improvements have been made in patient survival in the last decade[435]. Sotatercept is a promising solution as it is known to attenuate pulmonary vascular remodelling *in vivo* by reducing cell proliferation, and clinical trials have demonstrated a favourable benefit-risk profile in PAH patients[366,370-373]. Having completed Phase 2 and 3 clinical trials, Sotatercept is in the post-marketing phase and is currently undergoing cost-benefit analysis for use within the NHS[436].

In Chapter 5, we also investigated the molecular effects of 16OHE2 in the lung and RV tissue of C57BL/6 mice. Tissue harvest and RNA extraction from the lung and RV was carried out by Dr Smriti Sharma. In lung tissue, no changes were observed in expression of genes within the BMPR2 signalling pathway in response to 16OHE2 in either sex. However, BMPR2 protein levels significantly decreased in the lung tissue of female mice, whereas p-Smad1,5,9 significantly increased in response to 16OHE2 in both sexes. *Id1* and *Id3* mRNA expression significantly increased in response to 16OHE2 in the RV of female mice (but not in males). As previously discussed in Chapter 5, decreased BMPR2 protein levels in the female mouse lung may occur independently of increased p-Smad1,5,9 signalling as a compensatory

response to increased p38 MAPK signalling (Figure 1.5)[399]. In female mice, increased *Id1* and *Id3* expression may be protective against RV remodelling. We also investigated the effects of 16OHE2 on the gene expression of *Col1a1* and *Col3a1*. In lung tissue, *Col3a1* significantly decreased in female mice but not in males. In the RV, *Col1a1* decreased in female mice in response to 16OHE2, and *Col3a1* decreased in male and female mice. This suggests that 16OHE2 may be protective against fibrosis. Finally, we observed that 16OHE2 increased gene expression of *Sox17* in the RV of female mice. This is consistent with increased *Id1* and *Id3* expression as SOX17 is known to interact with Smad3, preventing formation of the p-Smad2,3 complex and the downstream effects of TGF-β signalling such as suppression of the Id genes[146,160]. On the other hand, we observed in Chapters 3 and 4 that most of the *in vitro* effects of 16OHE2 were pathogenic including increased migration of male and female rPASMCs, decreased *BMPR2* expression in male rat and human male control subject PASMCs, and decreased *Id1-3* expression in male and female rat AoSMCs. The only exception was that 16OHE2 significantly decreased *Col1a1* expression in male rPASMCs. This leads to the question of why the effects of 16OHE2 are different *in vivo* than they are *in vitro*.

The chronic effects of 16OHE2 *in vivo* may be different to a single 24-hour stimulation *in vitro*. The effects of exogenous 16OHE2 in the circulation may also be different to its direct effects in the pulmonary artery. While the *in vivo* effects of 16OHE2 in PAH are undetermined, this has previously been observed with its parent estrogen E2. For example, Mair et al. observed that expression of the E2-synthesising enzyme aromatase was increased in the pulmonary arteries of chronic hypoxic C57BL/6 mice and SuHx Wistar Kyoto rats of both sexes compared to normoxic controls[33]. In females, daily s/c injection or oral dosing with anastrozole attenuated chronic hypoxia- and SuHx-induced PAH[33]. However, this was not observed in males[33]. Wright et al. also observed that E2 increased proliferation of female control subject hPASMCs via ERα[102]. On the other hand, Frump et al. observed that depletion of endogenous E2 by ovariectomy worsened RV hypertrophy in female SuHx Sprague-Dawley rats[108].

The effects of exogenous 16OHE2 may also be different in animals than in humans. This has previously been observed with E2. For example, circulating E2 levels are higher in male and postmenopausal female PAH patients compared to control subjects, and are associated with worse disease outcomes[30,31]. Exogenous E2 from

oral contraceptives and HRT may unmask or worsen pre-existing PAH, particularly in women with additional precipitating factors (e.g., genetic susceptibility, connective tissue disease)[32,39]. On the other hand, E2 is protective in certain animal models of PAH. For example, daily s/c injection with E2 attenuated MCT-induced PAH in male Sprague-Dawley rats[67]. Continuous s/c dosing with E2 also attenuated RV hypertrophy in male Sprague-Dawley rats with SuHx-induced PAH[108]. PAH is presumed to develop in humans over several months or years[358]. However, this only takes days or weeks in experimental animal models of PAH[358]. Therefore, the different effects of E2 (and potentially 16OHE2) observed in animal models of PAH compared to human PAH may occur because *in vivo* models do not fully recapitulate the underlying mechanisms of PAH[358].

6.2 Concluding Remarks

PAH is a life-limiting disease which is predominant in women[27]. However, once PAH has developed, women have better survival than men[28]. Many paradoxes have been observed in PAH, and here we provide evidence that the effects of 16OHE2 are also paradoxical (Figure 6.3). Most of the effects of 16OHE2 *in vitro* were pathogenic. 16OHE2 significantly increased migration of male and female rPASMCs. It also significantly decreased the expression of genes within the protective BMPR2 signalling pathway (*Bmpr2*, *Smad1*, *Smad4, Smad5*) in male rPASMCs under normoxic and acute hypoxic conditions. Decreased *Smad4* expression was attenuated by the ERα antagonist MPP, suggesting that 16OHE2 may act via this receptor. 16OHE2 also significantly decreased the gene expression of *BMPR2* and *SMAD4* in male control subject hPASMCs. On the other hand, 16OHE2 significantly increased *Col1a1* expression in male rPASMCs, suggesting it may be protective against fibrosis. 16OHE2 may also mediate pathogenic effects in the aorta. *Id1*, *Id2* and *Id3* expression significantly decreased in male rat AoSMCs in response to 16OHE2, and *Id2* and *Id3* expression significantly decreased in female rat AoSMCs.

On the other hand, 16OHE2 mediates both pathogenic and protective effects *in vivo*. 16OHE2 did not induce PAH in male or female C57BL/6 mice, as determined by no

significant change in RVSP. However, 16OHE2 significantly increased RV hypertrophy in female mice, suggesting that it acts directly on the heart. As spleen weight significantly increased in male and female mice, RV hypertrophy in females in response to 16OHE2 may result from inflammation. However, 16OHE2 significantly increased the gene expression of *Id1* and *Id3* in the RV of female mice, suggesting it may be protective against remodelling. In lung tissue, no changes were observed in expression of genes within the BMPR2 signalling pathway in response to 16OHE2 in either sex. However, BMPR2 protein levels significantly decreased in the lung tissue of female mice, whereas p-Smad1,5,9 increased in response to 16OHE2 in both sexes. 16OHE2 also decreased expression of *Col3a1* in female mouse lung tissue, *Col1a1* in female mouse RV, and *Col3a1* in male and female mouse RV. Finally, 16OHE2 also increased *Sox17* expression in the female mouse RV. Therefore, 16OHE2 appears to be protective against RV remodelling and fibrosis, particularly in female mice.

A key hypothesis for the estrogen paradox in PAH is that the effects of extragonadal E2 synthesis in peripheral tissues (e.g., lung, adipose) are different to circulating E2[33,34]. 16OHE2 is normally only present in the circulation during pregnancy as it is synthesised in the fetal liver[314]. Mair et al. observed that visceral adipose tissue (VAT) metabolised E2 to mitogenic 16OHE1 via CYP1B1 in male genetically obese *ob/ob* mice[34]. Intriguingly, proliferation of male *ob/ob* mouse PASMCs was significantly increased by 24 hours stimulation with VAT-conditioned media[34]. Therefore, adipose tissue may be the source of 16OHE2 synthesis in PAH patients. Future studies could investigate whether peripheral 16OHE2 synthesis is linked to localised pathogenic effects in pulmonary artery and aorta smooth muscle cells, whereas the protective effects of 16OHE2 may result from exogenous administration and/or be specific to rodents.

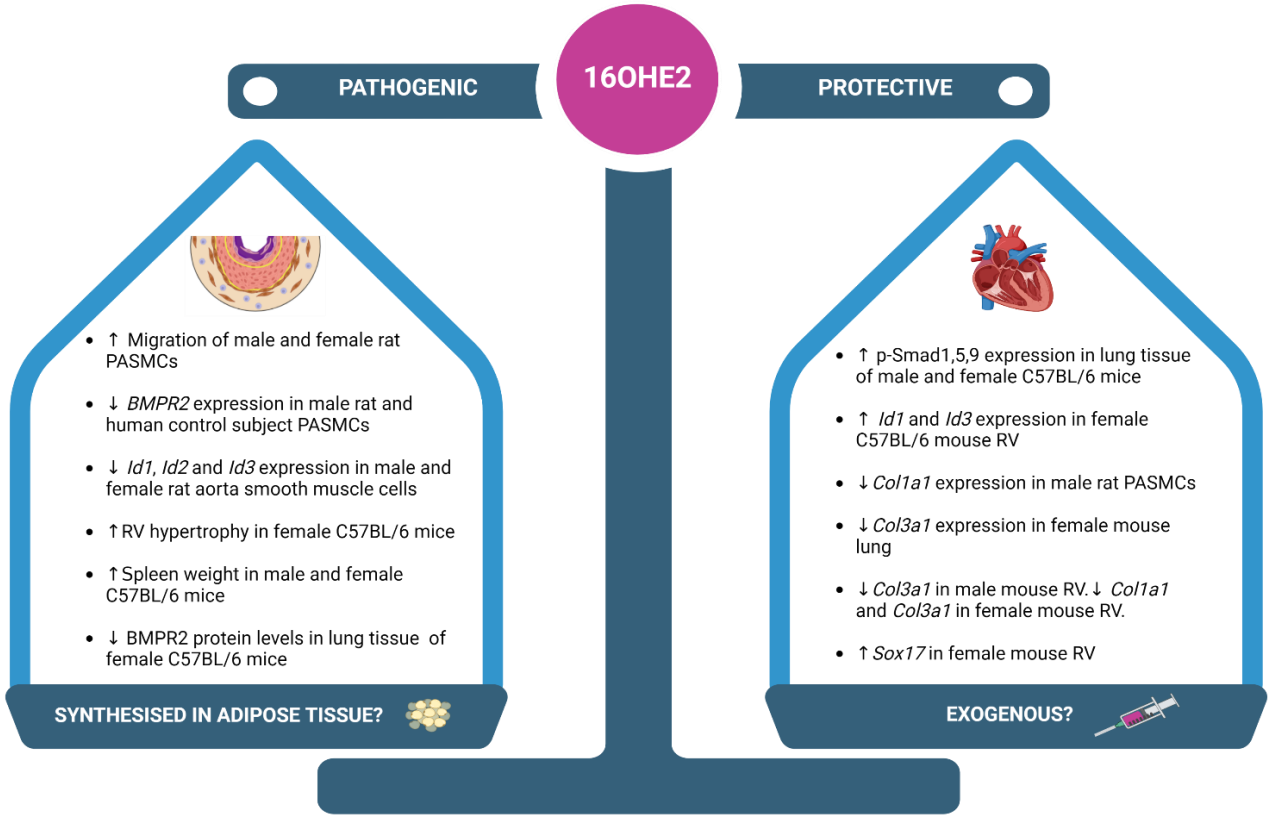

Figure 6.3: Summary of the effects of 16OHE2 in PAH.

The effects of 16α-hydroxyestradiol (16OHE2) in pulmonary arterial hypertension (PAH) appear to be paradoxical, as it mediates both pathogenic and protective effects. Most of the effects of 16OHE2 *in vitro* appear to be pathogenic, whereas 16OHE2 mediates both pathogenic and protective effects *in vivo*. Hypothetically, the pathogenic effects of 16OHE2 may result from synthesis in the peripheral tissues (e.g., lung, adipose), whereas its protective effects may result from exogenous administration or be specific to rodents. PASMCs = pulmonary artery smooth muscle cells, RV = right ventricle, BMPR2 = bone morphogenetic protein receptor 2, Id = inhibitor of DNA-binding, Col1a1 = collagen, type I, alpha 1, Col3a1 = collagen, type III, alpha 1, Sox17 = SRY-related HMG-box 17. Created with BioRender.com.

6.3 Future Perspective

Plasma levels of 16OHE2 are elevated in female idiopathic PAH patients, and in male and female patients with portopulmonary PAH[241,317]. Denver et al. previously observed that 16OHE2 significantly increased proliferation of female PAH patient hPASMCs[241]. However, we did not observe any change in proliferation in response to 16OHE2 in male or female rPASMCs. This suggests that at least one 'second hit' is required. We also did not observe any change in rPASMC proliferation in response to 16OHE2 under acute hypoxia. Attempts to isolate rPASMCs from chronic hypoxic and SuHx Sprague-Dawley rats were unsuccessful. Therefore, future studies could investigate the effects of combining 16OHE2 with exogenous hits (e.g., serotonin, endothelin) on proliferation.

We observed that 16OHE2 significantly increased migration of male and female rPASMCs. Similarly, Denver et al. demonstrated that 16OHE2 increased migration of BOECs from male and female PAH patients[241]. However, the underlying mechanism is undetermined. Therefore, this experiment could be repeated in future studies with the addition of estrogen receptor antagonists to determine whether any of these receptors mediate increased migration in response to 16OHE2.

16OHE2 is predominant during pregnancy, where it is synthesised in the fetal liver before entering the maternal circulation via the placenta[314]. However, the source of 16OHE2 synthesis in PAH patients is undetermined. Mair et al. recently demonstrated that CYP1B1 was elevated in visceral adipose tissue (VAT) from male and female genetically obese *ob/ob* mice compared with their wild type littermates[34]. In keeping with this, urinary 16OHE1 levels were also elevated in male *ob/ob* mice[34]. Cell culture media conditioned with VAT collected from male *ob/ob* mice also contained significantly higher levels of 16OHE1 compared to control media, suggesting that VAT releases 16OHE1 into the circulation[34]. Obesity may be more prevalent in PAH patients compared to the general population, and affects ~30-40% of patients[43,45]. Therefore, future studies could investigate whether adipose tissue is the source of 16OHE2 synthesis in PAH.

The *in vivo* effects of 16OHE2 have not yet been studied in an animal model of PAH. Rats exhibit a more severe disease phenotype than mice in both chronic hypoxia-

and SuHx-induced PAH[80,99]. Therefore, future studies could investigate the effects of 16OHE2 in a rat model of PAH. Due to the short half-life of 16OHE2, continuous dosing by subcutaneous pellet or osmotic minipump may be preferable to intermittent injection in future studies[339,340].

Finally, the estrogen pathway (Figure 1.4) provides many potential therapeutic targets for treating PAH[7]. Circulating E2 levels are higher in male and postmenopausal female PAH patients compared to control subjects, and are associated with worse disease outcomes[30,31]. Aromatase catalyses E2 synthesis from testosterone[6]. Kawut et al. observed that the aromatase inhibitor anastrozole significantly reduced plasma E2 levels, improved 6-minute walk distance, and was safe and well tolerated in men and postmenopausal women with PAH[279]. However, this only targets one part of the estrogen pathway. The CYP1B1 antagonist TMS attenuates PAH in chronic hypoxic C57BL/6 mice, SuHx C57BL/6 mice, obese male *ob/ob* mice, and female SERT^{+} mice (which overexpress gene for the human serotonin transporter)[34,35,240]. Therefore, future studies could investigate the effects of targeting both E2 synthesis and E2 metabolism with a combination of anastrozole and TMS. Finally, the novel fusion protein sotatercept acts as a ligand trap to restore the balance between the pro-proliferative TGF-β pathway and the protective BMPR2 signalling pathway[366]. Sotatercept attenuated pulmonary vascular remodelling *in vivo*, and improved exercise capacity (6-minute walk distance) in PAH patients in several clinical trials[366-373]. Although current therapies for PAH decrease pulmonary arterial pressure, they do not address the underlying pulmonary vascular remodelling[8]. Therefore, future studies could investigate whether combining sotatercept with anastrozole and/or TMS enhances its effects against pulmonary vascular remodelling.

7. References

1. Waxman AB. Exercise physiology and pulmonary arterial hypertension. Prog Cardiovasc Dis. 2012;55(2):172-9.

2. BioRender.com. Cross-section heart with human background (layout) [Internet]. Toronto: BioRender; [updated 2024; cited 2024 Apr 8]. Available from: https://app.biorender.com/biorender-templates.

3. Kovacs G, Dumitrescu D, Barner A, Greiner S, Grünig E, Hager A, et al. Definition, clinical classification and initial diagnosis of pulmonary hypertension: Updated recommendations from the Cologne Consensus Conference 2018. Int J Cardiol. 2018;272S:11-9.

4. Docherty CK, Harvey KY, Mair KM, Griffin S, Denver N, MacLean MR. The Role of Sex in the Pathophysiology of Pulmonary Hypertension. Adv Exp Med Biol. 2018;1065:511-28.

5. Benza RL, Miller DP, Barst RJ, Badesch DB, Frost AE, McGoon MD. An evaluation of long-term survival from time of diagnosis in pulmonary arterial hypertension from the REVEAL Registry. Chest. 2012;142(2):448-56.

6. Humbert M, Morrell NW, Archer SL, Stenmark KR, MacLean MR, Lang IM, et al. Cellular and molecular pathobiology of pulmonary arterial hypertension. J Am Coll Cardiol. 2004;43(12 Suppl S):13S-24S.

7. Morris H, Denver N, Gaw R, Labazi H, Mair K, MacLean MR. Sex Differences in Pulmonary Hypertension. Clin Chest Med. 2021;42(1):217-28.

8. Lan NSH, Massam BD, Kulkarni SS, Lang CC. Pulmonary Arterial Hypertension: Pathophysiology and Treatment. Diseases. 2018;6(2).

9. Lee H, Yeom A, Kim KC, Hong YM. Effect of Ambrisentan Therapy on the Expression of Endothelin Receptor, Endothelial Nitric Oxide Synthase and NADPH Oxidase 4 in Monocrotaline-induced Pulmonary Arterial Hypertension Rat Model. Korean Circ J. 2019;49(9):866-76.

10. Chester AH, Yacoub MH. The role of endothelin-1 in pulmonary arterial hypertension. Glob Cardiol Sci Pract. 2014;2014(2):62-78.

11. Dupuis J, Goresky CA, Fournier A. Pulmonary clearance of circulating endothelin-1 in dogs in vivo: exclusive role of ETB receptors. J Appl Physiol (1985). 1996;81(4):1510-5.

12. Dupuis J, Stewart DJ, Cernacek P, Gosselin G. Human pulmonary circulation is an important site for both clearance and production of endothelin-1. Circulation. 1996;94(7):1578-84.

13. Jankowich MD, Wu WC, Choudhary G. Association of Elevated Plasma Endothelin-1 Levels With Pulmonary Hypertension, Mortality, and Heart Failure in African American Individuals: The Jackson Heart Study. JAMA Cardiol. 2016;1(4):461-9.

14. Correale M, Ferraretti A, Monaco I, Grazioli D, Di Biase M, Brunetti ND. Endothelin-receptor antagonists in the management of pulmonary arterial hypertension: where do we stand? Vasc Health Risk Manag. 2018;14:253-64.

15. Montani D, Chaumais MC, Guignabert C, Günther S, Girerd B, Jaïs X, et al. Targeted therapies in pulmonary arterial hypertension. Pharmacol Ther. 2014;141(2):172-91.

16. Ahmad F, Murata T, Shimizu K, Degerman E, Maurice D, Manganiello V. Cyclic nucleotide phosphodiesterases: important signaling modulators and therapeutic targets. Oral Dis. 2015;21(1):e25-50.

17. Ting HJ, Murad JP, Espinosa EV, Khasawneh FT. Thromboxane A2 receptor: biology and function of a peculiar receptor that remains resistant for therapeutic targeting. J Cardiovasc Pharmacol Ther. 2012;17(3):248-59.

18. Chester AH, Yacoub MH, Moncada S. Nitric oxide and pulmonary arterial hypertension. Glob Cardiol Sci Pract. 2017;2017(2):14.

19. Jaitovich A, Jourd'heuil D. A Brief Overview of Nitric Oxide and Reactive Oxygen Species Signaling in Hypoxia-Induced Pulmonary Hypertension. Adv Exp Med Biol. 2017;967:71-81.

20. Xue C, Johns RA. Endothelial nitric oxide synthase in the lungs of patients with pulmonary hypertension. N Engl J Med. 1995;333(24):1642-4.

21. Mason NA, Springall DR, Burke M, Pollock J, Mikhail G, Yacoub MH, et al. High expression of endothelial nitric oxide synthase in plexiform lesions of pulmonary hypertension. J Pathol. 1998;185(3):313-8.

22. Milger K, Felix JF, Voswinckel R, Sommer N, Franco OH, Grimminger F, et al. Sildenafil versus nitric oxide for acute vasodilator testing in pulmonary arterial hypertension. Pulm Circ. 2015;5(2):305-12.

23. Thenappan T, Ormiston ML, Ryan JJ, Archer SL. Pulmonary arterial hypertension: pathogenesis and clinical management. BMJ. 2018;360:j5492.

24. Skoro-Sajer N, Lang I, Naeije R. Treprostinil for pulmonary hypertension. Vasc Health Risk Manag. 2008;4(3):507-13.

25. Mair KM, Johansen AK, Wright AF, Wallace E, MacLean MR. Pulmonary arterial hypertension: basis of sex differences in incidence and treatment response. Br J Pharmacol. 2014;171(3):567-79.

26. Dresdale DT, Schultz M, Michtom RJ. Primary pulmonary hypertension. I. Clinical and hemodynamic study. Am J Med. 1951;11(6):686-705.

27. Hoeper MM, Humbert M, Souza R, Idrees M, Kawut SM, Sliwa-Hahnle K, et al. A global view of pulmonary hypertension. Lancet Respir Med. 2016;4(4):306-22.

28. Kjellström B, Nisell M, Kylhammar D, Bartfay SE, Ivarsson B, Rådegran G, et al. Sex-specific differences and survival in patients with idiopathic pulmonary arterial hypertension 2008-2016. ERJ Open Res. 2019;5(3).

29. Lahm T, Tuder RM, Petrache I. Progress in solving the sex hormone paradox in pulmonary hypertension. Am J Physiol Lung Cell Mol Physiol. 2014;307(1):L7-26.

30. Ventetuolo CE, Baird GL, Barr RG, Bluemke DA, Fritz JS, Hill NS, et al. Higher Estradiol and Lower Dehydroepiandrosterone-Sulfate Levels Are Associated with Pulmonary Arterial Hypertension in Men. Am J Respir Crit Care Med. 2016;193(10):1168-75.

31. Baird GL, Archer-Chicko C, Barr RG, Bluemke DA, Foderaro AE, Fritz JS, et al. Lower DHEA-S levels predict disease and worse outcomes in post-menopausal women with idiopathic, connective tissue disease- and congenital heart disease-associated pulmonary arterial hypertension. Eur Respir J. 2018;51(6).

32. Baird GL, Walsh T, Aliotta J, Allahua M, Andrew R, Bourjeily G, et al. Insights from the Menstrual Cycle in Pulmonary Arterial Hypertension. Ann Am Thorac Soc. 2021;18(2):218-28.

33. Mair KM, Wright AF, Duggan N, Rowlands DJ, Hussey MJ, Roberts S, et al. Sex-dependent influence of endogenous estrogen in pulmonary hypertension. Am J Respir Crit Care Med. 2014;190(4):456-67.

34. Mair KM, Harvey KY, Henry AD, Hillyard DZ, Nilsen M, MacLean MR. Obesity alters oestrogen metabolism and contributes to pulmonary arterial hypertension. Eur Respir J. 2019;53(6).

35. White K, Johansen AK, Nilsen M, Ciuclan L, Wallace E, Paton L, et al. Activity of the estrogen-metabolizing enzyme cytochrome P450 1B1 influences the development of pulmonary arterial hypertension. Circulation. 2012;126(9):1087-98.

36. Earley S, Resta TC. Estradiol attenuates hypoxia-induced pulmonary endothelin-1 gene expression. Am J Physiol Lung Cell Mol Physiol. 2002;283(1):L86-93.

37. Lahm T, Albrecht M, Fisher AJ, Selej M, Patel NG, Brown JA, et al. 17β-Estradiol attenuates hypoxic pulmonary hypertension via estrogen receptor-mediated effects. Am J Respir Crit Care Med. 2012;185(9):965-80.

38. Lahm T, Patel KM, Crisostomo PR, Markel TA, Wang M, Herring C, et al. Endogenous estrogen attenuates pulmonary artery vasoreactivity and acute hypoxic pulmonary vasoconstriction: the effects of sex and menstrual cycle. Am J Physiol Endocrinol Metab. 2007;293(3):E865-71.

39. Morse JH, Horn EM, Barst RJ. Hormone replacement therapy: a possible risk factor in carriers of familial primary pulmonary hypertension. Chest. 1999;116(3):847.

40. Batton KA, Austin CO, Bruno KA, Burger CD, Shapiro BP, Fairweather D. Sex differences in pulmonary arterial hypertension: role of infection and autoimmunity in the pathogenesis of disease. Biol Sex Differ. 2018;9(1):15.

41. Mair KM, Gaw R, MacLean MR. Obesity, estrogens and adipose tissue dysfunction - implications for pulmonary arterial hypertension. Pulm Circ. 2020;10(3):2045894020952019.

42. Scottish Government. Diet & Healthy Weight Monitoring Report October 2020. [Internet]. Edinburgh: Scottish Government; [updated 2019 Oct 29; cited 2024 Jul 22]. Available from: https://www.gov.scot/binaries/content/documents/govscot/publications/statistics/2020/10/diet-healthy-weight-monitoring-report-2020/documents/diet-healthy-weight-monitoring-report/diet-healthy-weight-monitoring-report/govscot%3Adocument/diet-healthy-weight-monitoring-report.pdf.

43. McLean LL, Pellino K, Brewis M, Peacock A, Johnson M, Church AC. The obesity paradox in pulmonary arterial hypertension: the Scottish perspective. ERJ Open Res. 2019;5(4).

44. Fontbonne A, Currie A, Tounian P, Picot MC, Foulatier O, Nedelcu M, et al. Prevalence of Overweight and Obesity in France: The 2020 Obepi-Roche Study by the "Ligue Contre l'Obésité". J Clin Med. 2023;12(3).

45. Weatherald J, Huertas A, Boucly A, Guignabert C, Taniguchi Y, Adir Y, et al. Association Between BMI and Obesity With Survival in Pulmonary Arterial Hypertension. Chest. 2018;154(4):872-81.

46. Hales CM, Carroll MD, Fryar CD, Ogden CL. Prevalence of Obesity and Severe Obesity Among Adults: United States, 2017-2018. NCHS Data Brief. 2020(360):1-8.

47. Min J, Feng R, Badesch D, Berman-Rosenzweig E, Burger C, Chakinala M, et al. Obesity in Pulmonary Arterial Hypertension (PAH): The Pulmonary Hypertension Association Registry (PHAR). Ann Am Thorac Soc. 2020;18(2):229-37.

48. World Health Organization. Obesity and overweight. [Internet]. Geneva: World Health Organization; [updated 2024 Mar 1; cited 2024 Jul 22]. Available from: https://www.who.int/news-room/fact-sheets/detail/obesity-and-overweight.

49. Bhardwaj P, Au CC, Benito-Martin A, Ladumor H, Oshchepkova S, Moges R, et al. Estrogens and breast cancer: Mechanisms involved in obesity-related development, growth and progression. J Steroid Biochem Mol Biol. 2019;189:161-70.

50. Baglietto L, English DR, Hopper JL, MacInnis RJ, Morris HA, Tilley WD, et al. Circulating steroid hormone concentrations in postmenopausal women in relation to body size and composition. Breast Cancer Res Treat. 2009;115(1):171-9.

51. Farber HW, Miller DP, Poms AD, Badesch DB, Frost AE, Muros-Le Rouzic E, et al. Five-Year outcomes of patients enrolled in the REVEAL Registry. Chest. 2015;148(4):1043-54.

52. Hester J, Ventetuolo C, Lahm T. Sex, Gender, and Sex Hormones in Pulmonary Hypertension and Right Ventricular Failure. Compr Physiol. 2019;10(1):125-70.

53. Bruss ZS, Raja A. Physiology, Stroke Volume. [Updated 2022 Sep 12]. In: StatPearls [Internet]. Treasure Island (FL): StatPearls Publishing; 2024 Jan-. Available from: https://www.ncbi.nlm.nih.gov/books/NBK547686/.

54. Houston BA, Brittain EL, Tedford RJ. Right Ventricular Failure. N Engl J Med. 2023;388(12):1111-25.

55. Kawut SM, Horn EM, Berekashvili KK, Garofano RP, Goldsmith RL, Widlitz AC, et al. New predictors of outcome in idiopathic pulmonary arterial hypertension. Am J Cardiol. 2005;95(2):199-203.

56. Foppa M, Arora G, Gona P, Ashrafi A, Salton CJ, Yeon SB, et al. Right Ventricular Volumes and Systolic Function by Cardiac Magnetic Resonance and the Impact of Sex, Age, and Obesity in a Longitudinally Followed Cohort Free of Pulmonary and Cardiovascular Disease: The Framingham Heart Study. Circ Cardiovasc Imaging. 2016;9(3):e003810.

57. Kawut SM, Lima JA, Barr RG, Chahal H, Jain A, Tandri H, et al. Sex and race differences in right ventricular structure and function: the multi-ethnic study of atherosclerosis-right ventricle study. Circulation. 2011;123(22):2542-51

58. Ventetuolo CE, Ouyang P, Bluemke DA, Tandri H, Barr RG, Bagiella E, et al. Sex hormones are associated with right ventricular structure and function: The MESA-right ventricle study. Am J Respir Crit Care Med. 2011;183(5):659-67.

59. Kawut SM, Al-Naamani N, Agerstrand C, Berman Rosenzweig E, Rowan C, Barst RJ, et al. Determinants of right ventricular ejection fraction in pulmonary arterial hypertension. Chest. 2009;135(3):752-9.

60. Jacobs W, van de Veerdonk MC, Trip P, de Man F, Heymans MW, Marcus JT, et al. The right ventricle explains sex differences in survival in idiopathic pulmonary arterial hypertension. Chest. 2014;145(6):1230-6.

61. Marra AM, Benjamin N, Eichstaedt C, Salzano A, Arcopinto M, Gargani L, et al. Gender-related differences in pulmonary arterial hypertension targeted drugs administration. Pharmacol Res. 2016;114:103-9.

62. Gabler NB, French B, Strom BL, Liu Z, Palevsky HI, Taichman DB, et al. Race and sex differences in response to endothelin receptor antagonists for pulmonary arterial hypertension. Chest. 2012;141(1):20-6.

63. Mathai SC, Hassoun PM, Puhan MA, Zhou Y, Wise RA. Sex differences in response to tadalafil in pulmonary arterial hypertension. Chest. 2015;147(1):188-97.

64. Memon HA, Park MH. Pulmonary Arterial Hypertension in Women. Methodist Debakey Cardiovasc J. 2017;13(4):224-37.

65. Hemnes AR, Kiely DG, Cockrill BA, Safdar Z, Wilson VJ, Al Hazmi M, et al. Statement on pregnancy in pulmonary hypertension from the Pulmonary Vascular Research Institute. Pulm Circ. 2015;5(3):435-65.

66. Resta TC, Kanagy NL, Walker BR. Estradiol-induced attenuation of pulmonary hypertension is not associated with altered eNOS expression. Am J Physiol Lung Cell Mol Physiol. 2001;280(1):L88-97.

67. Liu Z, Duan YL, Ge SL, Zhang CX, Gong WH, Xu JJ. Effect of estrogen on right ventricular remodeling of monocrotaline-induced pulmonary arterial hypertension in rats and its mechanism. Eur Rev Med Pharmacol Sci. 2019;23(4):1742-50.

68. Gomez-Arroyo JG, Farkas L, Alhussaini AA, Farkas D, Kraskauskas D, Voelkel NF, et al. The monocrotaline model of pulmonary hypertension in perspective. Am J Physiol Lung Cell Mol Physiol. 2012;302(4):L363-9.

69. Taraseviciene-Stewart L, Kasahara Y, Alger L, Hirth P, Mc Mahon G, Waltenberger J, et al. Inhibition of the VEGF receptor 2 combined with chronic hypoxia causes cell death-dependent pulmonary endothelial cell proliferation and severe pulmonary hypertension. FASEB J. 2001;15(2):427-38.

70. Hoshikawa Y, Nana-Sinkam P, Moore MD, Sotto-Santiago S, Phang T, Keith RL, et al. Hypoxia induces different genes in the lungs of rats compared with mice. Physiol Genomics. 2003;12(3):209-19.

71. Fagan KA, Fouty BW, Tyler RC, Morris KG, Hepler LK, Sato K, et al. The pulmonary circulation of homozygous or heterozygous eNOS-null mice is hyperresponsive to mild hypoxia. J Clin Invest. 1999;103(2):291-9.

72. Fagan KA, Tyler RC, Sato K, Fouty BW, Morris KG, Huang PL, et al. Relative contributions of endothelial, inducible, and neuronal NOS to tone in the murine pulmonary circulation. Am J Physiol. 1999;277(3):L472-8.

73 Hales CA, Kradin RL, Brandstetter RD, Zhu YJ. Impairment of hypoxic pulmonary artery remodeling by heparin in mice. Am Rev Respir Dis. 1983;128(4):747-51.

74. Kay JM, Harris P, Heath D. Pulmonary hypertension produced in rats by ingestion of Crotalaria spectabilis seeds. Thorax. 1967;22(2):176-9.

75. Lee J, Reich R, Xu F, Sehgal PB. Golgi, trafficking, and mitosis dysfunctions in pulmonary arterial endothelial cells exposed to monocrotaline pyrrole and NO scavenging. Am J Physiol Lung Cell Mol Physiol. 2009;297(4):L715-28.

76. Ramos M, Lamé MW, Segall HJ, Wilson DW. Monocrotaline pyrrole induces Smad nuclear accumulation and altered signaling expression in human pulmonary arterial endothelial cells. Vascul Pharmacol. 2007;46(6):439-48.

77. Stenmark KR, Morganroth ML, Remigio LK, Voelkel NF, Murphy RC, Henson PM, et al. Alveolar inflammation and arachidonate metabolism in monocrotaline-induced pulmonary hypertension. Am J Physiol. 1985;248(6 Pt 2):H859-66.

78. Stenmark KR, Davie N, Frid M, Gerasimovskaya E, Das M. Role of the adventitia in pulmonary vascular remodeling. Physiology (Bethesda). 2006;21:134-45.

79. Stenmark KR, Nozik-Grayck E, Gerasimovskaya E, Anwar A, Li M, Riddle S, et al. The adventitia: Essential role in pulmonary vascular remodeling. Compr Physiol. 2011;1(1):141-61.

80. Gomez-Arroyo J, Saleem SJ, Mizuno S, Syed AA, Bogaard HJ, Abbate A, et al. A brief overview of mouse models of pulmonary arterial hypertension: problems and prospects. Am J Physiol Lung Cell Mol Physiol. 2012;302(10):L977-91.

81. Roth RA, Dotzlaf LA, Baranyi B, Kuo CH, Hook JB. Effect of monocrotaline ingestion on liver, kidney, and lung of rats. Toxicol Appl Pharmacol. 1981;60(2):193-203.

82. Pullamsetti S, Krick S, Yilmaz H, Ghofrani HA, Schudt C, Weissmann N, et al. Inhaled tolafentrine reverses pulmonary vascular remodeling via inhibition of smooth muscle cell migration. Respir Res. 2005;6(1):128.

83. Yuyama H, Fujimori A, Sanagi M, Koakutsu A, Sudoh K, Sasamata M, et al. The orally active nonpeptide selective endothelin ETA receptor antagonist YM598 prevents and reverses the development of pulmonary hypertension in monocrotaline-treated rats. Eur J Pharmacol. 2004;496(1-3):129-39.

84. Mitani Y, Mutlu A, Russell JC, Brindley DN, DeAlmeida J, Rabinovitch M. Dexfenfluramine protects against pulmonary hypertension in rats. J Appl Physiol (1985). 2002;93(5):1770-8.

85. Tanaka Y, Schuster DP, Davis EC, Patterson GA, Botney MD. The role of vascular injury and hemodynamics in rat pulmonary artery remodeling. J Clin Invest. 1996;98(2):434-42.

86. Okada K, Tanaka Y, Bernstein M, Zhang W, Patterson GA, Botney MD. Pulmonary hemodynamics modify the rat pulmonary artery response to injury. A neointimal model of pulmonary hypertension. Am J Pathol. 1997;151(4):1019-25.

87. Rudolph AM, Neuhauser EB, Golinko RJ, Auld PA. Effects of pneumonectomy on pulmonary circulation in adult and young animals. Circ Res. 1961;9:856-61.

88. Deslauriers J, Ugalde P, Miro S, Deslauriers DR, Ferland S, Bergeron S, et al. Long-term physiological consequences of pneumonectomy. Semin Thorac Cardiovasc Surg. 2011;23(3):196-202.

89. Kramer MS, Lane DA. Aminorex, dexfenfluramine, and primary pulmonary hypertension. J Clin Epidemiol. 1998;51(4):361-4.

90. Li MF, Cheung BM. Rise and fall of anti-obesity drugs. World J Diabetes. 2011;2(2):19-23.

91. Joint Formulary Committee. British National Formulary [Internet]. London: British Medical Association and Royal Pharmaceutical Society of Great Britain; [updated 2024 Feb 20; cited 2024 Mar 14]. Available from https://bnf.nice.org.uk/.

92. Dempsie Y, MacRitchie NA, White K, Morecroft I, Wright AF, Nilsen M, et al. Dexfenfluramine and the oestrogen-metabolizing enzyme CYP1B1 in the development of pulmonary arterial hypertension. Cardiovasc Res. 2013;99(1):24-34.

93. Simonneau G, Humbert M. Amphetamine Derivatives and the Risk of Pulmonary Arterial Hypertension. A New Chapter of the Story. Am J Respir Crit Care Med. 2018;197(6):704-6.

94. Chin KM, Channick RN, Rubin LJ. Is methamphetamine use associated with idiopathic pulmonary arterial hypertension? Chest. 2006;130(6):1657-63.

95. Labazi H, Nilsen M, MacLean MR. Sex-dependent right ventricular hypertrophic gene changes after methamphetamine treatment in mice. Eur J Pharmacol. 2021;900:174066.

96. Lahm T, Douglas IS, Archer SL, Bogaard HJ, Chesler NC, Haddad F, et al. Assessment of Right Ventricular Function in the Research Setting: Knowledge Gaps

and Pathways Forward. An Official American Thoracic Society Research Statement. Am J Respir Crit Care Med. 2018;198(4):e15-e43.

97. Labazi H, Axelsen JB, Hillyard D, Nilsen M, Andersen A, MacLean MR. Sex-Dependent Changes in Right Ventricular Gene Expression in Response to Pressure Overload in a Rat Model of Pulmonary Trunk Banding. Biomedicines. 2020;8(10).

98. Abe K, Toba M, Alzoubi A, Ito M, Fagan KA, Cool CD, et al. Formation of plexiform lesions in experimental severe pulmonary arterial hypertension. Circulation. 2010;121(25):2747-54.

99. Vitali SH, Hansmann G, Rose C, Fernandez-Gonzalez A, Scheid A, Mitsialis SA, et al. The Sugen 5416/hypoxia mouse model of pulmonary hypertension revisited: long-term follow-up. Pulm Circ. 2014;4(4):619-29.

100. Wu XH, Ma JL, Ding D, Ma YJ, Wei YP, Jing ZC. Experimental animal models of pulmonary hypertension: Development and challenges. Animal Model Exp Med. 2022;5(3):207-16.

101. White K, Dempsie Y, Nilsen M, Wright AF, Loughlin L, MacLean MR. The serotonin transporter, gender, and 17β oestradiol in the development of pulmonary arterial hypertension. Cardiovasc Res. 2011;90(2):373-82.

102. Wright AF, Ewart MA, Mair K, Nilsen M, Dempsie Y, Loughlin L, et al. Oestrogen receptor alpha in pulmonary hypertension. Cardiovasc Res. 2015;106(2):206-16.

103. Dempsie Y, Nilsen M, White K, Mair KM, Loughlin L, Ambartsumian N, et al. Development of pulmonary arterial hypertension in mice over-expressing S100A4/Mts1 is specific to females. Respir Res. 2011;12:159.

104. Mair KM, Yang XD, Long L, White K, Wallace E, Ewart MA, et al. Sex affects bone morphogenetic protein type II receptor signaling in pulmonary artery smooth muscle cells. Am J Respir Crit Care Med. 2015;191(6):693-703.

105. Erewele EO, Castellon M, Loya O, Marshboom G, Schwartz A, Yerlioglu K, et al. Hypoxia-induced pulmonary hypertension upregulates eNOS and TGF-β contributing to sex-linked differences in. Pulm Circ. 2022;12(4):e12163.

106. Fessel JP, Chen X, Frump A, Gladson S, Blackwell T, Kang C, et al. Interaction between bone morphogenetic protein receptor type 2 and estrogenic compounds in pulmonary arterial hypertension. Pulm Circ. 2013;3(3):564-77.

107. Frump AL, Selej M, Wood JA, Albrecht M, Yakubov B, Petrache I, et al. Hypoxia Upregulates Estrogen Receptor β in Pulmonary Artery Endothelial Cells in a HIF-1α-Dependent Manner. Am J Respir Cell Mol Biol. 2018;59(1):114-26.

108. Frump AL, Goss KN, Vayl A, Albrecht M, Fisher A, Tursunova R, et al. Estradiol improves right ventricular function in rats with severe angioproliferative pulmonary hypertension: effects of endogenous and exogenous sex hormones. Am J Physiol Lung Cell Mol Physiol. 2015;308(9):L873-90.

109. Karas RH, Schulten H, Pare G, Aronovitz MJ, Ohlsson C, Gustafsson JA, et al. Effects of estrogen on the vascular injury response in estrogen receptor alpha, beta (double) knockout mice. Circ Res. 2001;89(6):534-9.

110. Badawi AF, Cavalieri EL, Rogan EG. Role of human cytochrome P450 1A1, 1A2, 1B1, and 3A4 in the 2-, 4-, and 16alpha-hydroxylation of 17beta-estradiol. Metabolism. 2001;50(9):1001-3.

111. Deroo BJ, Korach KS. Estrogen receptors and human disease. J Clin Invest. 2006;116(3):561-70.

112. Fuentes N, Silveyra P. Estrogen receptor signaling mechanisms. Adv Protein Chem Struct Biol. 2019;116:135-70.

113. Aryan L, Younessi D, Zargari M, Banerjee S, Agopian J, Rahman S, et al. The Role of Estrogen Receptors in Cardiovascular Disease. Int J Mol Sci. 2020;21(12).

114. Hamidi SA, Dickman KG, Berisha H, Said SI. 17β-estradiol protects the lung against acute injury: possible mediation by vasoactive intestinal polypeptide. Endocrinology. 2011;152(12):4729-37.

115. Vegeto E, Cuzzocrea S, Crisafulli C, Mazzon E, Sala A, Krust A, et al. Estrogen receptor-alpha as a drug target candidate for preventing lung inflammation. Endocrinology. 2010;151(1):174-84.

116. Rajkumar R, Konishi K, Richards TJ, Ishizawar DC, Wiechert AC, Kaminski N, et al. Genomewide RNA expression profiling in lung identifies distinct signatures in idiopathic pulmonary arterial hypertension and secondary pulmonary hypertension. Am J Physiol Heart Circ Physiol. 2010;298(4):H1235-48.

117. Kawut SM, Pinder D, Al-Naamani N, McCormick A, Palevsky HI, Fritz J, et al. Fulvestrant for the Treatment of Pulmonary Arterial Hypertension. Ann Am Thorac Soc. 2019;16(11):1456-9.

118. ClinicalTrials.gov [Internet]. Bethesda (MD): National Library of Medicine (US). Identifier NCT02911844, Estrogen receptor antagonist in patients with pulmonary arterial hypertension (ERA-PAH); [updated 2019 Dec 9; cited 2024 Mar 14]. Available from: https://www.clinicaltrials.gov/study/NCT02911844?cond=Pulmonary%20Arterial%20Hypertension&term=Fulvestrant&rank=1.

119. Rocca A, Maltoni R, Bravaccini S, Donati C, Andreis D. Clinical utility of fulvestrant in the treatment of breast cancer: a report on the emerging clinical evidence. Cancer Manag Res. 2018;10:3083-99.

120. Chen X, Austin ED, Talati M, Fessel JP, Farber-Eger EH, Brittain EL, et al. Oestrogen inhibition reverses pulmonary arterial hypertension and associated metabolic defects. Eur Respir J. 2017;50(2).

121. ClinicalTrials.gov [Internet]. Bethesda (MD): National Library of Medicine (US). Identifier NCT03528902, Tamoxifen therapy to treat pulmonary arterial hypertension (T3PAH); [updated 2023 Aug 1; cited 2024 Mar 14]. Available from: https://www.clinicaltrials.gov/study/NCT03528902?cond=Pulmonary%20Arterial%20Hypertension&term=Tamoxifen&rank=1.

122. Lindsey SH, Cohen JA, Brosnihan KB, Gallagher PE, Chappell MC. Chronic treatment with the G protein-coupled receptor 30 agonist G-1 decreases blood pressure in ovariectomized mRen2.Lewis rats. Endocrinology. 2009;150(8):3753-8.

123. Lindsey SH, da Silva AS, Silva MS, Chappell MC. Reduced vasorelaxation to estradiol and G-1 in aged female and adult male rats is associated with GPR30 downregulation. Am J Physiol Endocrinol Metab. 2013;305(1):E113-8.

124. Lindsey SH, Yamaleyeva LM, Brosnihan KB, Gallagher PE, Chappell MC. Estrogen receptor GPR30 reduces oxidative stress and proteinuria in the salt-sensitive female mRen2.Lewis rat. Hypertension. 2011;58(4):665-71.

125. Alencar AK, Montes GC, Montagnoli T, Silva AM, Martinez ST, Fraga AG, et al. Activation of GPER ameliorates experimental pulmonary hypertension in male rats. Eur J Pharm Sci. 2017;97:208-17.

126. Alencar AKN, Montes GC, Costa DG, Mendes LVP, Silva AMS, Martinez ST, et al. Cardioprotection Induced by Activation of GPER in Ovariectomized Rats With Pulmonary Hypertension. J Gerontol A Biol Sci Med Sci. 2018;73(9):1158-66.

127. Rabinovitch M. Molecular pathogenesis of pulmonary arterial hypertension. J Clin Invest. 2012;122(12):4306-13.

128. Mueller JW, Gilligan LC, Idkowiak J, Arlt W, Foster PA. The Regulation of Steroid Action by Sulfation and Desulfation. Endocr Rev. 2015;36(5):526-63.

129. Turcu A, Smith JM, Auchus R, Rainey WE. Adrenal androgens and androgen precursors-definition, synthesis, regulation and physiologic actions. Compr Physiol. 2014;4(4):1369-81.

130. Dessouroux A, Akwa Y, Baulieu EE. DHEA decreases HIF-1alpha accumulation under hypoxia in human pulmonary artery cells: potential role in the treatment of pulmonary arterial hypertension. J Steroid Biochem Mol Biol. 2008;109(1-2):81-9.

131. Liu D, Dillon JS. Dehydroepiandrosterone stimulates nitric oxide release in vascular endothelial cells: evidence for a cell surface receptor. Steroids. 2004;69(4):279-89.

132. Alzoubi A, Toba M, Abe K, O'Neill KD, Rocic P, Fagan KA, et al. Dehydroepiandrosterone restores right ventricular structure and function in rats with severe pulmonary arterial hypertension. Am J Physiol Heart Circ Physiol. 2013;304(12):H1708-18.

133. Homma N, Nagaoka T, Karoor V, Imamura M, Taraseviciene-Stewart L, Walker LA, et al. Involvement of RhoA/Rho kinase signaling in protection against

monocrotaline-induced pulmonary hypertension in pneumonectomized rats by dehydroepiandrosterone. Am J Physiol Lung Cell Mol Physiol. 2008;295(1):L71-8.

134. Chen YM, Lee HC, Chen MT, Huang CC, Chen WC. Dehydroepiandrosterone supplementation combined with Weight-Loading Whole-Body Vibration Training (WWBV) affects exercise performance and muscle glycogen storage in middle-aged C57BL/6 mice. Int J Med Sci. 2018;15(6):564-73.

135. Dumas de La Roque E, Savineau JP, Metivier AC, Billes MA, Kraemer JP, Doutreleau S, et al. Dehydroepiandrosterone (DHEA) improves pulmonary hypertension in chronic obstructive pulmonary disease (COPD): a pilot study. Ann Endocrinol (Paris). 2012;73(1):20-5.

136. English KM, Jones RD, Jones TH, Morice AH, Channer KS. Gender differences in the vasomotor effects of different steroid hormones in rat pulmonary and coronary arteries. Horm Metab Res. 2001;33(11):645-52.

137. Rowell KO, Hall J, Pugh PJ, Jones TH, Channer KS, Jones RD. Testosterone acts as an efficacious vasodilator in isolated human pulmonary arteries and veins: evidence for a biphasic effect at physiological and supra-physiological concentrations. J Endocrinol Invest. 2009;32(9):718-23.

138. Wen J, Wang J, Tang X, Deng S, Dai J, Li X, et al. DHT deteriorates the progression of monocrotaline-induced pulmonary arterial hypertension: effects of endogenous and exogenous androgen. Am J Transl Res. 2019;11(9):5752-63.

139. Ventetuolo CE, Mitra N, Wan F, Manichaikul A, Barr RG, Johnson C, et al. Oestradiol metabolism and androgen receptor genotypes are associated with right ventricular function. Eur Respir J. 2016;47(2):553-63.

140. Austin ED, Loyd JE. The genetics of pulmonary arterial hypertension. Circ Res. 2014;115(1):189-202.

141. Morrell NW, Aldred MA, Chung WK, Elliott CG, Nichols WC, Soubrier F, et al. Genetics and genomics of pulmonary arterial hypertension. Eur Respir J. 2019;53(1).

142. Humbert M, Deng Z, Simonneau G, Barst RJ, Sitbon O, Wolf M, et al. BMPR2 germline mutations in pulmonary hypertension associated with fenfluramine derivatives. Eur Respir J. 2002;20(3):518-23.

143. Sztrymf B, Coulet F, Girerd B, Yaici A, Jais X, Sitbon O, et al. Clinical outcomes of pulmonary arterial hypertension in carriers of BMPR2 mutation. Am J Respir Crit Care Med. 2008;177(12):1377-83.

144. Awad KS, West JD, de Jesus Perez V, MacLean M. Novel signaling pathways in pulmonary arterial hypertension (2015 Grover Conference Series). Pulm Circ. 2016;6(3):285-94.

145. ten Dijke P, Korchynskyi O, Valdimarsdottir G, Goumans MJ. Controlling cell fate by bone morphogenetic protein receptors. Mol Cell Endocrinol. 2003;211(1-2):105-13.

146. Zhang Y, Alexander PB, Wang XF. TGF-β Family Signaling in the Control of Cell Proliferation and Survival. Cold Spring Harb Perspect Biol. 2017;9(4).

147. Austin ED, Hamid R, Hemnes AR, Loyd JE, Blackwell T, Yu C, et al. BMPR2 expression is suppressed by signaling through the estrogen receptor. Biol Sex Differ. 2012;3(1):6.

148. Ichimori H, Kogaki S, Takahashi K, Ishida H, Narita J, Nawa N, et al. Drastic shift from positive to negative estrogen effect on bone morphogenetic protein signaling in pulmonary arterial endothelial cells under hypoxia. Circ J. 2013;77(8):2118-26.

149. Johnson DW, Berg JN, Baldwin MA, Gallione CJ, Marondel I, Yoon SJ, et al. Mutations in the activin receptor-like kinase 1 gene in hereditary haemorrhagic telangiectasia type 2. Nat Genet. 1996;13(2):189-95.

150. McAllister KA, Grogg KM, Johnson DW, Gallione CJ, Baldwin MA, Jackson CE, et al. Endoglin, a TGF-beta binding protein of endothelial cells, is the gene for hereditary haemorrhagic telangiectasia type 1. Nat Genet. 1994;8(4):345-51.

151. Gregson CL, Bergen DJM, Leo P, Sessions RB, Wheeler L, Hartley A, et al. A Rare Mutation in SMAD9 Associated With High Bone Mass Identifies the SMAD-

Dependent BMP Signaling Pathway as a Potential Anabolic Target for Osteoporosis. J Bone Miner Res. 2020;35(1):92-105.

152. Austin ED, Hamid R, Ahmad F. Somatic mutations in pulmonary arterial hypertension: primary or secondary events? Am J Respir Crit Care Med. 2010;182(9):1094-6.

153. Aldred MA, Comhair SA, Varella-Garcia M, Asosingh K, Xu W, Noon GP, et al. Somatic chromosome abnormalities in the lungs of patients with pulmonary arterial hypertension. Am J Respir Crit Care Med. 2010;182(9):1153-60.

154. Drake KM, Zygmunt D, Mavrakis L, Harbor P, Wang L, Comhair SA, et al. Altered MicroRNA processing in heritable pulmonary arterial hypertension: an important role for Smad-8. Am J Respir Crit Care Med. 2011;184(12):1400-8.

155. Davis BN, Hilyard AC, Lagna G, Hata A. SMAD proteins control DROSHA-mediated microRNA maturation. Nature. 2008;454(7200):56-61.

156. Chen X, Talati M, Fessel JP, Hemnes AR, Gladson S, French J, et al. Estrogen Metabolite 16α-Hydroxyestrone Exacerbates Bone Morphogenetic Protein Receptor Type II-Associated Pulmonary Arterial Hypertension Through MicroRNA-29-Mediated Modulation of Cellular Metabolism. Circulation. 2016;133(1):82-97.

157. Chun HJ, Bonnet S, Chan SY. Translational Advances in the Field of Pulmonary Hypertension. Translating MicroRNA Biology in Pulmonary Hypertension. It Will Take More Than "miR" Words. Am J Respir Crit Care Med. 2017;195(2):167-78.

158. Yamada Y, Takanashi M, Sudo K, Ueda S, Ohno SI, Kuroda M. Novel form of miR-29b suppresses bleomycin-induced pulmonary fibrosis. PLoS One. 2017;12(2):e0171957.

159. Sangam S, Sun X, Schwantes-An TH, Yegambaram M, Lu Q, Shi Y, et al. SOX17 Deficiency Mediates Pulmonary Hypertension: At the Crossroads of Sex, Metabolism, and Genetics. Am J Respir Crit Care Med. 2023;207(8):1055-69.

160. Feng XH, Lin X, Derynck R. Smad2, Smad3 and Smad4 cooperate with Sp1 to induce p15(Ink4B) transcription in response to TGF-beta. EMBO J. 2000;19(19):5178-93.

161. Stefanovic S, Abboud N, Désilets S, Nury D, Cowan C, Pucéat M. Interplay of Oct4 with Sox2 and Sox17: a molecular switch from stem cell pluripotency to specifying a cardiac fate. J Cell Biol. 2009;186(5):665-73.

162. Ma L, Roman-Campos D, Austin ED, Eyries M, Sampson KS, Soubrier F, et al. A novel channelopathy in pulmonary arterial hypertension. N Engl J Med. 2013;369(4):351-61.

163. Weise-Cross L, Resta TC, Jernigan NL. Redox Regulation of Ion Channels and Receptors in Pulmonary Hypertension. Antioxid Redox Signal. 2019;31(12):898-915.

164. Bedoya M, Rinné S, Kiper AK, Decher N, González W, Ramírez D. TASK Channels Pharmacology: New Challenges in Drug Design. J Med Chem. 2019;62(22):10044-58.

165. Austin ED, Ma L, LeDuc C, Berman Rosenzweig E, Borczuk A, Phillips JA, et al. Whole exome sequencing to identify a novel gene (caveolin-1) associated with human pulmonary arterial hypertension. Circ Cardiovasc Genet. 2012;5(3):336-43.

166. Wertz JW, Bauer PM. Caveolin-1 regulates BMPRII localization and signaling in vascular smooth muscle cells. Biochem Biophys Res Commun. 2008;375(4):557-61.

167. Nickel NP, Spiekerkoetter E, Gu M, Li CG, Li H, Kaschwich M, et al. Elafin Reverses Pulmonary Hypertension via Caveolin-1-Dependent Bone Morphogenetic Protein Signaling. Am J Respir Crit Care Med. 2015;191(11):1273-86.

168. ClinicalTrials.gov [Internet]. Bethesda (MD): National Library of Medicine (US). Identifier NCT03522935, Subcutaneous elafin in healthy subjects; [updated 2021 Apr 28; cited 2024 Mar 19]. Available from: https://www.clinicaltrials.gov/study/NCT03522935?term=NCT03522935%23&rank=1

169. Berger M, Gray JA, Roth BL. The expanded biology of serotonin. Annu Rev Med. 2009;60:355-66.

170. Bakshi A, Tadi P. Biochemistry, Serotonin. [Updated 2022 Oct 5]. In: StatPearls [Internet]. Treasure Island (FL): StatPearls Publishing; 2024 Jan. Available from https://www.ncbi.nlm.nih.gov/books/NBK560856/.

171. Aiello RJ, Bourassa PA, Zhang Q, Dubins J, Goldberg DR, De Lombaert S, et al. Tryptophan hydroxylase 1 Inhibition Impacts Pulmonary Vascular Remodeling in Two Rat Models of Pulmonary Hypertension. J Pharmacol Exp Ther. 2017;360(2):267-79.

172. Walther DJ, Peter JU, Bashammakh S, Hörtnagl H, Voits M, Fink H, et al. Synthesis of serotonin by a second tryptophan hydroxylase isoform. Science. 2003;299(5603):76.

173. Adnot S, Houssaini A, Abid S, Marcos E, Amsellem V. Serotonin transporter and serotonin receptors. Handb Exp Pharmacol. 2013;218:365-80.

174. Hervé P, Launay JM, Scrobohaci ML, Brenot F, Simonneau G, Petitpretz P, et al. Increased plasma serotonin in primary pulmonary hypertension. Am J Med. 1995;99(3):249-54.

175. Eddahibi S, Guignabert C, Barlier-Mur AM, Dewachter L, Fadel E, Dartevelle P, et al. Cross talk between endothelial and smooth muscle cells in pulmonary hypertension: critical role for serotonin-induced smooth muscle hyperplasia. Circulation. 2006;113(15):1857-64.

176. Dempsie Y, Martin P, Upton PD. Connexin-mediated regulation of the pulmonary vasculature. Biochem Soc Trans. 2015;43(3):524-9.

177. MacLean MMR. The serotonin hypothesis in pulmonary hypertension revisited: targets for novel therapies (2017 Grover Conference Series). Pulm Circ. 2018;8(2):2045894018759125.

178. Long L, MacLean MR, Jeffery TK, Morecroft I, Yang X, Rudarakanchana N, et al. Serotonin increases susceptibility to pulmonary hypertension in BMPR2-deficient mice. Circ Res. 2006;98(6):818-27.

179. Eddahibi S, Adnot S. [Serotonin and pulmonary arterial hypertension]. Rev Mal Respir. 2006;23 Suppl 2:4S45-4S51.

180. Morecroft I, Dempsie Y, Bader M, Walther DJ, Kotnik K, Loughlin L, et al. Effect of tryptophan hydroxylase 1 deficiency on the development of hypoxia-induced pulmonary hypertension. Hypertension. 2007;49(1):232-6.

181. Dempsie Y, Morecroft I, Welsh DJ, MacRitchie NA, Herold N, Loughlin L, et al. Converging evidence in support of the serotonin hypothesis of dexfenfluramine-induced pulmonary hypertension with novel transgenic mice. Circulation. 2008;117(22):2928-37.

182. Ciuclan L, Hussey MJ, Burton V, Good R, Duggan N, Beach S, et al. Imatinib attenuates hypoxia-induced pulmonary arterial hypertension pathology via reduction in 5-hydroxytryptamine through inhibition of tryptophan hydroxylase 1 expression. Am J Respir Crit Care Med. 2013;187(1):78-89.

183. Hoeper MM, Barst RJ, Bourge RC, Feldman J, Frost AE, Galié N, et al. Imatinib mesylate as add-on therapy for pulmonary arterial hypertension: results of the randomized IMPRES study. Circulation. 2013;127(10):1128-38.

184. Sitbon O, Gomberg-Maitland M, Granton J, Lewis MI, Mathai SC, Rainisio M, et al. Clinical trial design and new therapies for pulmonary arterial hypertension. Eur Respir J. 2019;53(1).

185. Goldberg DR, De Lombaert S, Aiello R, Bourassa P, Barucci N, Zhang Q, et al. Optimization of spirocyclic proline tryptophan hydroxylase-1 inhibitors. Bioorg Med Chem Lett. 2017;27(3):413-9.

186. Petrassi M, Barber R, Be C, Beach S, Cox B, D'Souza AM, et al. Identification of a Novel Allosteric Inhibitory Site on Tryptophan Hydroxylase 1 Enabling Unprecedented Selectivity Over all Related Hydroxylases. Front Pharmacol. 2017;8:240.

187. ClinicalTrials.gov [Internet]. Bethesda (MD): National Library of Medicine (US). Identifier NCT04712669, A study of rodatristat ethyl in patients with pulmonary arterial hypertension (ELEVATE 2); [updated 2023 Oct 5; cited 2024 Mar 19]. Available from: https://www.clinicaltrials.gov/study/NCT04712669?cond=Pulmonary%20Arterial%20Hypertension&term=rodatristat&rank=1.

188. Crane JD, Palanivel R, Mottillo EP, Bujak AL, Wang H, Ford RJ, et al. Inhibiting peripheral serotonin synthesis reduces obesity and metabolic dysfunction by promoting brown adipose tissue thermogenesis. Nat Med. 2015;21(2):166-72.

189. MacIntyre PD, Bhargava B, Hogg KJ, Gemmill JD, Hillis WS. Effect of subcutaneous sumatriptan, a selective 5HT1 agonist, on the systemic, pulmonary, and coronary circulation. Circulation. 1993;87(2):401-5.

190. Dickenson JM, Hill SJ. Human 5-HT1B receptor stimulated inositol phospholipid hydrolysis in CHO cells: synergy with Gq-coupled receptors. Eur J Pharmacol. 1998;348(2-3):279-85.

191. Sweeney G, Templeton A, Clayton RA, Baird M, Sheridan S, Johnston ED, et al. Contractile responses to sumatriptan in isolated bovine pulmonary artery rings: relationship to tone and cyclic nucleotide levels. J Cardiovasc Pharmacol. 1995;26(5):751-60.

192. MacLean MR, Sweeney G, Baird M, McCulloch KM, Houslay M, Morecroft I. 5-Hydroxytryptamine receptors mediating vasoconstriction in pulmonary arteries from control and pulmonary hypertensive rats. Br J Pharmacol. 1996;119(5):917-30.

193. Hood KY, Mair KM, Harvey AP, Montezano AC, Touyz RM, MacLean MR. Serotonin Signaling Through the 5-HT. Arterioscler Thromb Vasc Biol. 2017;37(7):1361-70.

194. MacLean MR, Clayton RA, Templeton AG, Morecroft I. Evidence for 5-HT1-like receptor-mediated vasoconstriction in human pulmonary artery. Br J Pharmacol. 1996;119(2):277-82.

195. Delaney C, Sherlock L, Fisher S, Maltzahn J, Wright C, Nozik-Grayck E. Serotonin 2A receptor inhibition protects against the development of pulmonary hypertension and pulmonary vascular remodeling in neonatal mice. Am J Physiol Lung Cell Mol Physiol. 2018;314(5):L871-L81.

196. Launay JM, Hervé P, Peoc'h K, Tournois C, Callebert J, Nebigil CG, et al. Function of the serotonin 5-hydroxytryptamine 2B receptor in pulmonary hypertension. Nat Med. 2002;8(10):1129-35.

197. Blanpain C, Le Poul E, Parma J, Knoop C, Detheux M, Parmentier M, et al. Serotonin 5-HT(2B) receptor loss of function mutation in a patient with fenfluramine-associated primary pulmonary hypertension. Cardiovasc Res. 2003;60(3):518-28.

198. Glusa E, Pertz HH. Further evidence that 5-HT-induced relaxation of pig pulmonary artery is mediated by endothelial 5-HT(2B) receptors. Br J Pharmacol. 2000;130(3):692-8.

199. West JD, Carrier EJ, Bloodworth NC, Schroer AK, Chen P, Ryzhova LM, et al. Serotonin 2B Receptor Antagonism Prevents Heritable Pulmonary Arterial Hypertension. PLoS One. 2016;11(2):e0148657.

200. Lawrie A, Spiekerkoetter E, Martinez EC, Ambartsumian N, Sheward WJ, MacLean MR, et al. Interdependent serotonin transporter and receptor pathways regulate S100A4/Mts1, a gene associated with pulmonary vascular disease. Circ Res. 2005;97(3):227-35.

201. MacLean MR, Deuchar GA, Hicks MN, Morecroft I, Shen S, Sheward J, et al. Overexpression of the 5-hydroxytryptamine transporter gene: effect on pulmonary hemodynamics and hypoxia-induced pulmonary hypertension. Circulation. 2004;109(17):2150-5.

202. Morecroft I, Loughlin L, Nilsen M, Colston J, Dempsie Y, Sheward J, et al. Functional interactions between 5-hydroxytryptamine receptors and the serotonin transporter in pulmonary arteries. J Pharmacol Exp Ther. 2005;313(2):539-48.

203. Mair KM, MacLean MR, Morecroft I, Dempsie Y, Palmer TM. Novel interactions between the 5-HT transporter, 5-HT1B receptors and Rho kinase in vivo and in pulmonary fibroblasts. Br J Pharmacol. 2008;155(4):606-16.

204. Liu Y, Suzuki YJ, Day RM, Fanburg BL. Rho kinase-induced nuclear translocation of ERK1/ERK2 in smooth muscle cell mitogenesis caused by serotonin. Circ Res. 2004;95(6):579-86.

205. ClinicalTrials.gov [Internet]. Bethesda (MD): National Library of Medicine (US). Identifier NCT03638908, Fluoxetine in pulmonary arterial hypertension (PAH) Trial (PAH); [updated 2020 Jun 26; cited 2024 Mar 20]. Available from:

https://www.clinicaltrials.gov/study/NCT03638908?cond=Pulmonary%20Arterial%20Hypertension&term=serotonin&rank=2.

206. ClinicalTrials.gov [Internet]. Bethesda (MD): National Library of Medicine (US). Identifier NCT00942708, Safety and efficacy of fluoxetine in pulmonary arterial hypertension; [updated 2020 Jun 2; cited 2024 Mar 20]. Available from: https://www.clinicaltrials.gov/study/NCT00942708?cond=Pulmonary%20Arterial%20Hypertension&term=serotonin&rank=4.

207. ClinicalTrials.gov [Internet]. Bethesda (MD): National Library of Medicine (US). Identifier NCT00190333, Serotonin transporter escitalopram in pulmonary hypertension; [updated 2011 Feb 18; cited 2024 Mar 20]. Available from: https://www.clinicaltrials.gov/study/NCT00190333?cond=Pulmonary%20Arterial%20Hypertension&term=serotonin&rank=5.

208. Sadoughi A, Roberts KE, Preston IR, Lai GP, McCollister DH, Farber HW, et al. Use of selective serotonin reuptake inhibitors and outcomes in pulmonary arterial hypertension. Chest. 2013;144(2):531-41.

209. Fox BD, Azoulay L, Dell'Aniello S, Langleben D, Lapi F, Benisty J, et al. The use of antidepressants and the risk of idiopathic pulmonary arterial hypertension. Can J Cardiol. 2014;30(12):1633-9.

210. Bhat-Nakshatri P, Wang G, Collins NR, Thomson MJ, Geistlinger TR, Carroll JS, et al. Estradiol-regulated microRNAs control estradiol response in breast cancer cells. Nucleic Acids Res. 2009;37(14):4850-61.

211. Wallace E, Morrell NW, Yang XD, Long L, Stevens H, Nilsen M, et al. A Sex-Specific MicroRNA-96/5-Hydroxytryptamine 1B Axis Influences Development of Pulmonary Hypertension. Am J Respir Crit Care Med. 2015;191(12):1432-42.

212. Docherty CK, Denver N, Fisher S, Nilsen M, Hillyard D, Openshaw RL, et al. Direct Delivery of MicroRNA96 to the Lungs Reduces Progression of Sugen/Hypoxia-Induced Pulmonary Hypertension in the Rat. Mol Ther Nucleic Acids. 2020;22:396-405.

213. McQuillan BM, Picard MH, Leavitt M, Weyman AE. Clinical correlates and reference intervals for pulmonary artery systolic pressure among echocardiographically normal subjects. Circulation. 2001;104(23):2797-802.

214. Weyman AE, Davidoff R, Gardin J, Ryan T, St John Sutton M, Weissman NJ. Echocardiographic evaluation of pulmonary artery pressure with clinical correlates in predominantly obese adults. J Am Soc Echocardiogr. 2002;15(5):454-62.

215. Carbone S, Canada JM, Billingsley HE, Siddiqui MS, Elagizi A, Lavie CJ. Obesity paradox in cardiovascular disease: where do we stand? Vasc Health Risk Manag. 2019;15:89-100.

216. Poms AD, Turner M, Farber HW, Meltzer LA, McGoon MD. Comorbid conditions and outcomes in patients with pulmonary arterial hypertension: a REVEAL registry analysis. Chest. 2013;144(1):169-76.

217. Hu EC, He JG, Liu ZH, Ni XH, Zheng YG, Gu Q, et al. Survival advantages of excess body mass index in patients with idiopathic pulmonary arterial hypertension. Acta Cardiol. 2014;69(6):673-8.

218. Agarwal M, Agrawal S, Garg L, Lavie CJ. Relation Between Obesity and Survival in Patients Hospitalized for Pulmonary Arterial Hypertension (from a Nationwide Inpatient Sample Database 2003 to 2011). Am J Cardiol. 2017;120(3):489-93.

219. Vishvanath L, Gupta RK. Contribution of adipogenesis to healthy adipose tissue expansion in obesity. J Clin Invest. 2019;129(10):4022-31.

220. Fantuzzi G. Adipose tissue, adipokines, and inflammation. J Allergy Clin Immunol. 2005;115(5):911-9; quiz 20.

221. Chait A, den Hartigh LJ. Adipose Tissue Distribution, Inflammation and Its Metabolic Consequences, Including Diabetes and Cardiovascular Disease. Front Cardiovasc Med. 2020;7:22.

222. Houstis N, Rosen ED, Lander ES. Reactive oxygen species have a causal role in multiple forms of insulin resistance. Nature. 2006;440(7086):944-8.

223. Furukawa S, Fujita T, Shimabukuro M, Iwaki M, Yamada Y, Nakajima Y, et al. Increased oxidative stress in obesity and its impact on metabolic syndrome. J Clin Invest. 2004;114(12):1752-61.

224. Yamauchi T, Kamon J, Waki H, Terauchi Y, Kubota N, Hara K, et al. The fat-derived hormone adiponectin reverses insulin resistance associated with both lipoatrophy and obesity. Nat Med. 2001;7(8):941-6.

225. Stern JH, Rutkowski JM, Scherer PE. Adiponectin, Leptin, and Fatty Acids in the Maintenance of Metabolic Homeostasis through Adipose Tissue Crosstalk. Cell Metab. 2016;23(5):770-84.

226. Morioka T, Emoto M, Yamazaki Y, Kawano N, Imamura S, Numaguchi R, et al. Leptin is associated with vascular endothelial function in overweight patients with type 2 diabetes. Cardiovasc Diabetol. 2014;13:10.

227. Ponrartana S, Hu HH, Gilsanz V. On the relevance of brown adipose tissue in children. Ann N Y Acad Sci. 2013;1302:24-9.

228. Chondronikola M, Volpi E, Børsheim E, Porter C, Saraf MK, Annamalai P, et al. Brown Adipose Tissue Activation Is Linked to Distinct Systemic Effects on Lipid Metabolism in Humans. Cell Metab. 2016;23(6):1200-6.

229. BioRender.com. Adipose tissue depots [Internet]. Toronto: Biorender; [updated 2024; cited 2024 Apr 9]. Available from: https://app.biorender.com/biorender-templates.

230. Siegel-Axel DI, Häring HU. Perivascular adipose tissue: An unique fat compartment relevant for the cardiometabolic syndrome. Rev Endocr Metab Disord. 2016;17(1):51-60.

231. Virdis A, Duranti E, Rossi C, Dell'Agnello U, Santini E, Anselmino M, et al. Tumour necrosis factor-alpha participates on the endothelin-1/nitric oxide imbalance in small arteries from obese patients: role of perivascular adipose tissue. Eur Heart J. 2015;36(13):784-94.

232. Shields KJ, Verdelis K, Passineau MJ, Faight EM, Zourelias L, Wu C, et al. Three-dimensional micro computed tomography analysis of the lung vasculature

and differential adipose proteomics in the Sugen/hypoxia rat model of pulmonary arterial hypertension. Pulm Circ. 2016;6(4):586-96.

233. Ibrahim MM. Subcutaneous and visceral adipose tissue: structural and functional differences. Obes Rev. 2010;11(1):11-8.

234. Sacks HS, Fain JN, Holman B, Cheema P, Chary A, Parks F, et al. Uncoupling protein-1 and related messenger ribonucleic acids in human epicardial and other adipose tissues: epicardial fat functioning as brown fat. J Clin Endocrinol Metab. 2009;94(9):3611-5.

235. Gaborit B, Sengenes C, Ancel P, Jacquier A, Dutour A. Role of Epicardial Adipose Tissue in Health and Disease: A Matter of Fat? Compr Physiol. 2017;7(3):1051-82.

236. Iacobellis G. Local and systemic effects of the multifaceted epicardial adipose tissue depot. Nat Rev Endocrinol. 2015;11(6):363-71.

237. Simpson ER, Brown KA. Obesity and breast cancer: role of inflammation and aromatase. J Mol Endocrinol. 2013;51(3):T51-9.

238. Key TJ, Appleby PN, Reeves GK, Roddam A, Dorgan JF, Longcope C, et al. Body mass index, serum sex hormones, and breast cancer risk in postmenopausal women. J Natl Cancer Inst. 2003;95(16):1218-26.

239. Ellero S, Chakhtoura G, Barreau C, Langouët S, Benelli C, Penicaud L, et al. Xenobiotic-metabolizing cytochromes p450 in human white adipose tissue: expression and induction. Drug Metab Dispos. 2010;38(4):679-86.

240. Johansen AK, Dean A, Morecroft I, Hood K, Nilsen M, Loughlin L, et al. The serotonin transporter promotes a pathological estrogen metabolic pathway in pulmonary hypertension via cytochrome P450 1B1. Pulm Circ. 2016;6(1):82-92.

241. Denver N, Homer NZM, Andrew R, Harvey KY, Morrell N, Austin ED, et al. Estrogen metabolites in a small cohort of patients with idiopathic pulmonary arterial hypertension. Pulm Circ. 2020;10(1):2045894020908783.

242. Ye J. Mechanisms of insulin resistance in obesity. Front Med. 2013;7(1):14-24.

243. Niswender KD. Basal insulin: physiology, pharmacology, and clinical implications. Postgrad Med. 2011;123(4):17-26.

244. Narayan KM, Boyle JP, Thompson TJ, Gregg EW, Williamson DF. Effect of BMI on lifetime risk for diabetes in the U.S. Diabetes Care. 2007;30(6):1562-6.

245. Zamanian RT, Hansmann G, Snook S, Lilienfeld D, Rappaport KM, Reaven GM, et al. Insulin resistance in pulmonary arterial hypertension. Eur Respir J. 2009;33(2):318-24.

246. Pugh ME, Robbins IM, Rice TW, West J, Newman JH, Hemnes AR. Unrecognized glucose intolerance is common in pulmonary arterial hypertension. J Heart Lung Transplant. 2011;30(8):904-11.

247. Xu W, Koeck T, Lara AR, Neumann D, DiFilippo FP, Koo M, et al. Alterations of cellular bioenergetics in pulmonary artery endothelial cells. Proc Natl Acad Sci U S A. 2007;104(4):1342-7.

248. Janani C, Ranjitha Kumari BD. PPAR gamma gene--a review. Diabetes Metab Syndr. 2015;9(1):46-50.

249. West J, Niswender KD, Johnson JA, Pugh ME, Gleaves L, Fessel JP, et al. A potential role for insulin resistance in experimental pulmonary hypertension. Eur Respir J. 2013;41(4):861-71.

250. Sutliff RL, Kang BY, Hart CM. PPARgamma as a potential therapeutic target in pulmonary hypertension. Ther Adv Respir Dis. 2010;4(3):143-60.

251. Idris-Khodja N, Ouerd S, Trindade M, Gornitsky J, Rehman A, Barhoumi T, et al. Vascular smooth muscle cell peroxisome proliferator-activated receptor γ protects against endothelin-1-induced oxidative stress and inflammation. J Hypertens. 2017;35(7):1390-401.

252. Ali DE, Shah M, Ali A, Malik MO, Rehman F, Badshah H, et al. Treatment with Metformin and Combination of Metformin Plus Pioglitazone on Serum Levels of IL-6 and IL-8 in Polycystic Ovary Syndrome: A Randomized Clinical Trial. Horm Metab Res. 2019;51(11):714-22.

253. Ameshima S, Golpon H, Cool CD, Chan D, Vandivier RW, Gardai SJ, et al. Peroxisome proliferator-activated receptor gamma (PPARgamma) expression is decreased in pulmonary hypertension and affects endothelial cell growth. Circ Res. 2003;92(10):1162-9.

254. Hansmann G, de Jesus Perez VA, Alastalo TP, Alvira CM, Guignabert C, Bekker JM, et al. An antiproliferative BMP-2/PPARgamma/apoE axis in human and murine SMCs and its role in pulmonary hypertension. J Clin Invest. 2008;118(5):1846-57.

255. Achari AE, Jain SK. Adiponectin, a Therapeutic Target for Obesity, Diabetes, and Endothelial Dysfunction. Int J Mol Sci. 2017;18(6).

256. Summer R, Fiack CA, Ikeda Y, Sato K, Dwyer D, Ouchi N, et al. Adiponectin deficiency: a model of pulmonary hypertension associated with pulmonary vascular disease. Am J Physiol Lung Cell Mol Physiol. 2009;297(3):L432-8.

257. Choi HM, Doss HM, Kim KS. Multifaceted Physiological Roles of Adiponectin in Inflammation and Diseases. Int J Mol Sci. 2020;21(4).

258. Woodcock CC, Chan SY. The Search for Disease-Modifying Therapies in Pulmonary Hypertension. J Cardiovasc Pharmacol Ther. 2019;24(4):334-54.

259. Furukawa S, Fujita T, Shimabukuro M, Iwaki M, Yamada Y, Nakajima Y, et al. Increased oxidative stress in obesity and its impact on metabolic syndrome. J Clin Invest. 2004;114(12):1752-61.

260. Legchenko E, Chouvarine P, Borchert P, Fernandez-Gonzalez A, Snay E, Meier M, et al. PPARγ agonist pioglitazone reverses pulmonary hypertension and prevents right heart failure via fatty acid oxidation. Sci Transl Med. 2018;10(438).

261. ClinicalTrials.gov [Internet]. Bethesda (MD): National Library of Medicine (US). Identifier NCT00825266, Insulin resistance in pulmonary arterial hypertension; [updated 2017 Mar 31; cited 2024 Mar 20]. Available from: https://www.clinicaltrials.gov/study/NCT00825266?cond=Pulmonary%20Arterial%20Hypertension&term=Pioglitazone&rank=1.

262. Nissen SE, Wolski K. Rosiglitazone revisited: an updated meta-analysis of risk for myocardial infarction and cardiovascular mortality. Arch Intern Med. 2010;170(14):1191-201.

263. Hansmann G, Calvier L, Risbano MG, Chan SY. Activation of the Metabolic Master Regulator PPARγ: A Potential PIOneering Therapy for Pulmonary Arterial Hypertension. Am J Respir Cell Mol Biol. 2020;62(2):143-56.

264. Thenappan T, Chan SY, Weir EK. Role of extracellular matrix in the pathogenesis of pulmonary arterial hypertension. Am J Physiol Heart Circ Physiol. 2018;315(5):H1322-H31.

265. Hoffmann J, Marsh LM, Pieper M, Stacher E, Ghanim B, Kovacs G, et al. Compartment-specific expression of collagens and their processing enzymes in intrapulmonary arteries of IPAH patients. Am J Physiol Lung Cell Mol Physiol. 2015;308(10):L1002-13.

266. Andersen S, Nielsen-Kudsk JE, Vonk Noordegraaf A, de Man FS. Right Ventricular Fibrosis. Circulation. 2019;139(2):269-85.

267. Merklinger SL, Wagner RA, Spiekerkoetter E, Hinek A, Knutsen RH, Kabir MG, et al. Increased fibulin-5 and elastin in S100A4/Mts1 mice with pulmonary hypertension. Circ Res. 2005;97(6):596-604.

268. Jones PL, Rabinovitch M. Tenascin-C is induced with progressive pulmonary vascular disease in rats and is functionally related to increased smooth muscle cell proliferation. Circ Res. 1996;79(6):1131-42.

269. Ruffenach G, Chabot S, Tanguay VF, Courboulin A, Boucherat O, Potus F, et al. Role for Runt-related Transcription Factor 2 in Proliferative and Calcified Vascular Lesions in Pulmonary Arterial Hypertension. Am J Respir Crit Care Med. 2016;194(10):1273-85.

270. Petrov G, Regitz-Zagrosek V, Lehmkuhl E, Krabatsch T, Dunkel A, Dandel M, et al. Regression of myocardial hypertrophy after aortic valve replacement: faster in women? Circulation. 2010;122(11 Suppl):S23-8.

271. Chan SY, Rubin LJ. Metabolic dysfunction in pulmonary hypertension: from basic science to clinical practice. Eur Respir Rev. 2017;26(146).

272. Diebold I, Hennigs JK, Miyagawa K, Li CG, Nickel NP, Kaschwich M, et al. BMPR2 preserves mitochondrial function and DNA during reoxygenation to promote endothelial cell survival and reverse pulmonary hypertension. Cell Metab. 2015;21(4):596-608.

273. Fitzgerald G, Soro-Arnaiz I, De Bock K. The Warburg Effect in Endothelial Cells and its Potential as an Anti-angiogenic Target in Cancer. Front Cell Dev Biol. 2018;6:100.

274. Tofovic SP, Jackson EK. Estradiol Metabolism: Crossroads in Pulmonary Arterial Hypertension. Int J Mol Sci. 2019;21(1).

275. Samavat H, Kurzer MS. Estrogen metabolism and breast cancer. Cancer Lett. 2015;356(2 Pt A):231-43.

276. Machado-Linde F, Pelegrin P, Sanchez-Ferrer ML, Leon J, Cascales P, Parrilla JJ. 2-methoxyestradiol in the pathophysiology of endometriosis: focus on angiogenesis and therapeutic potential. Reprod Sci. 2012;19(10):1018-29.

277. Khan WA. 16 α-Hydroxyestrone induced adduct generate high affinity autoantibodies in SLE. Adv Med Sci. 2019;64(1):72-8.

278. Roberts KE, Fallon MB, Krowka MJ, Brown RS, Trotter JF, Peter I, et al. Genetic risk factors for portopulmonary hypertension in patients with advanced liver disease. Am J Respir Crit Care Med. 2009;179(9):835-42.

279. Kawut SM, Archer-Chicko CL, DeMichele A, Fritz JS, Klinger JR, Ky B, et al. Anastrozole in Pulmonary Arterial Hypertension. A Randomized, Double-Blind, Placebo-controlled Trial. Am J Respir Crit Care Med. 2017;195(3):360-8.

280. ClinicalTrials.gov [Internet]. Bethesda (MD): National Library of Medicine (US). Identifier NCT01545336, Anastrozole in patients with pulmonary arterial hypertension (AIPH); [updated 2016 Oct 27; cited 2024 Mar 14]. Available from: https://www.clinicaltrials.gov/study/NCT01545336?cond=Pulmonary%20Arterial%20Hypertension&term=anastrozole&rank=2.

281. ClinicalTrials.gov [Internet]. Bethesda (MD): National Library of Medicine (US). Identifier NCT03229499, Pulmonary hypertension and anastrozole trial (PHANTOM); [updated 2023 Aug 31; cited 2024 Mar 14]. Available from: https://www.clinicaltrials.gov/study/NCT03229499?cond=Pulmonary%20Arterial%20Hypertension&term=anastrozole&rank=1.

282. Rojas LB, Gomes MB. Metformin: an old but still the best treatment for type 2 diabetes. Diabetol Metab Syndr. 2013;5(1):6.

283. Dean A, Nilsen M, Loughlin L, Salt IP, MacLean MR. Metformin Reverses Development of Pulmonary Hypertension via Aromatase Inhibition. Hypertension. 2016;68(2):446-54.

284. ClinicalTrials.gov [Internet]. Bethesda (MD): National Library of Medicine (US). Identifier NCT03617458, Interventions against insulin resistance in pulmonary arterial hypertension; [updated 2023 Oct 10; cited 2024 Mar 21]. Available from: https://www.clinicaltrials.gov/study/NCT03617458?cond=Pulmonary%20Arterial%20Hypertension&term=Metformin&rank=3.

285. Kwant CT, van der Horst FAL, Bogaard HJ, de Man FS, Vonk Noordegraaf A. Nutritional status in pulmonary arterial hypertension. Pulm Circ. 2022;12(4):e12173.

286. Austin ED, Cogan JD, West JD, Hedges LK, Hamid R, Dawson EP, et al. Alterations in oestrogen metabolism: implications for higher penetrance of familial pulmonary arterial hypertension in females. Eur Respir J. 2009;34(5):1093-9.

287. West J, Cogan J, Geraci M, Robinson L, Newman J, Phillips JA, et al. Gene expression in BMPR2 mutation carriers with and without evidence of pulmonary arterial hypertension suggests pathways relevant to disease penetrance. BMC Med Genomics. 2008;1:45.

288. Larigot L, Juricek L, Dairou J, Coumoul X. AhR signaling pathways and regulatory functions. Biochim Open. 2018;7:1-9.

289. Murray IA, Patterson AD, Perdew GH. Aryl hydrocarbon receptor ligands in cancer: friend and foe. Nat Rev Cancer. 2014;14(12):801-14.

290. Xu CX, Wang C, Zhang ZM, Jaeger CD, Krager SL, Bottum KM, et al. Aryl hydrocarbon receptor deficiency protects mice from diet-induced adiposity and metabolic disorders through increased energy expenditure. Int J Obes (Lond). 2015;39(8):1300-9.

291. Sato S, Shirakawa H, Tomita S, Ohsaki Y, Haketa K, Tooi O, et al. Low-dose dioxins alter gene expression related to cholesterol biosynthesis, lipogenesis, and glucose metabolism through the aryl hydrocarbon receptor-mediated pathway in mouse liver. Toxicol Appl Pharmacol. 2008;229(1):10-9.

292. Dean A, Gregorc T, Docherty CK, Harvey KY, Nilsen M, Morrell NW, et al. Role of the Aryl Hydrocarbon Receptor in Sugen 5416-induced Experimental Pulmonary Hypertension. Am J Respir Cell Mol Biol. 2018;58(3):320-30.

293. Lee HJ, Han HJ. Role of Microtubule-Associated Factors in HIF1α Nuclear Translocation. Adv Exp Med Biol. 2020;1232:271-6.

294. Lu YR, Song J, Zhabihula BX, Zhang JR. 2-Methoxyestradiol promotes radiosensitivity of esophageal squamous cell carcinoma by suppressing hypoxia-inducible factor-1α expression. Eur Rev Med Pharmacol Sci. 2019;23(24):10785-95.

295. Tofovic SP, Salah EM, Mady HH, Jackson EK, Melhem MF. Estradiol metabolites attenuate monocrotaline-induced pulmonary hypertension in rats. J Cardiovasc Pharmacol. 2005;46(4):430-7.

296. Veith C, Schermuly RT, Brandes RP, Weissmann N. Molecular mechanisms of hypoxia-inducible factor-induced pulmonary arterial smooth muscle cell alterations in pulmonary hypertension. J Physiol. 2016;594(5):1167-77.

297. Schultz K, Fanburg BL, Beasley D. Hypoxia and hypoxia-inducible factor-1alpha promote growth factor-induced proliferation of human vascular smooth muscle cells. Am J Physiol Heart Circ Physiol. 2006;290(6):H2528-34.

298. Ball MK, Waypa GB, Mungai PT, Nielsen JM, Czech L, Dudley VJ, et al. Regulation of hypoxia-induced pulmonary hypertension by vascular smooth muscle hypoxia-inducible factor-1α. Am J Respir Crit Care Med. 2014;189(3):314-24.

299. Docherty CK, Nilsen M, MacLean MR. Influence of 2-Methoxyestradiol and Sex on Hypoxia-Induced Pulmonary Hypertension and Hypoxia-Inducible Factor-1-α. J Am Heart Assoc. 2019;8(5):e011628.

300. Manavathi B, Acconcia F, Rayala SK, Kumar R. An inherent role of microtubule network in the action of nuclear receptor. Proc Natl Acad Sci U S A. 2006;103(43):15981-6.

301. Esteve JM, Launay JM, Kellermann O, Maroteaux L. Functions of serotonin in hypoxic pulmonary vascular remodeling. Cell Biochem Biophys. 2007;47(1):33-44.

302. Salama SA, Kamel MW, Botting S, Salih SM, Borahay MA, Hamed AA, et al. Catechol-o-methyltransferase expression and 2-methoxyestradiol affect microtubule dynamics and modify steroid receptor signaling in leiomyoma cells. PLoS One. 2009;4(10):e7356.

303. Jiang H, Xie T, Ramsden DB, Ho SL. Human catechol-O-methyltransferase down-regulation by estradiol. Neuropharmacology. 2003;45(7):1011-8.

304. Boudíková B, Szumlanski C, Maidak B, Weinshilboum R. Human liver catechol-O-methyltransferase pharmacogenetics. Clin Pharmacol Ther. 1990;48(4):381-9.

305. Tofovic SP, Jones TJ, Bilan VP, Jackson EK, Petrusevska G. Synergistic therapeutic effects of 2-methoxyestradiol with either sildenafil or bosentan on amelioration of monocrotaline-induced pulmonary hypertension and vascular remodeling. J Cardiovasc Pharmacol. 2010;56(5):475-83.

306. Kulke MH, Chan JA, Meyerhardt JA, Zhu AX, Abrams TA, Blaszkowsky LS, et al. A prospective phase II study of 2-methoxyestradiol administered in combination with bevacizumab in patients with metastatic carcinoid tumors. Cancer Chemother Pharmacol. 2011;68(2):293-300.

307. ClinicalTrials.gov [Internet]. Bethesda (MD): National Library of Medicine (US). Identifier NCT00030095, 2-Methoxyestradiol in treating patients with advanced solid tumours; [updated 2015 Apr 30; cited 2024 Mar 22]. Available from: https://www.clinicaltrials.gov/study/NCT00030095?term=2%20methoxyestradiol&rank=1.

308. Tofovic SP, Zhang X, Zhu H, Jackson EK, Rafikova O, Petrusevska G. 2-Ethoxyestradiol is antimitogenic and attenuates monocrotaline-induced pulmonary hypertension and vascular remodeling. Vascul Pharmacol. 2008;48(4-6):174-83.

309. Park SA, Lee MH, Na HK, Surh YJ. 4-Hydroxyestradiol induces mammary epithelial cell transformation through Nrf2-mediated heme oxygenase-1 overexpression. Oncotarget. 2017;8(1):164-78.

310. Swaneck GE, Fishman J. Covalent binding of the endogenous estrogen 16 alpha-hydroxyestrone to estradiol receptor in human breast cancer cells: characterization and intranuclear localization. Proc Natl Acad Sci U S A. 1988;85(21):7831-5.

311. Hood KY, Montezano AC, Harvey AP, Nilsen M, MacLean MR, Touyz RM. Nicotinamide Adenine Dinucleotide Phosphate Oxidase-Mediated Redox Signaling and Vascular Remodeling by 16α-Hydroxyestrone in Human Pulmonary Artery Cells: Implications in Pulmonary Arterial Hypertension. Hypertension. 2016;68(3):796-808.

312. ClinicalTrials.gov [Internet]. Bethesda (MD): National Library of Medicine (US). Identifier NCT03068130, Extended access program to assess long-term safety of bardoxolone methyl in patients with pulmonary hypertension RANGER (RANGER); [updated 2024 Feb 6; cited 2024 Mar 19]. Available from: https://www.clinicaltrials.gov/study/NCT03068130?cond=Pulmonary%20Arterial%20Hypertension&term=bardoxolone&rank=1.

313. Johnson JA, Hemnes AR, Perrien DS, Schuster M, Robinson LJ, Gladson S, et al. Cytoskeletal defects in Bmpr2-associated pulmonary arterial hypertension. Am J Physiol Lung Cell Mol Physiol. 2012;302(5):L474-84.

314. Falah N, Torday J, Quinney SK, Haas DM. Estriol review: Clinical applications and potential biomedical importance. Clinical Research and Trials. 2015;1.

315. Kuhl H. Pharmacology of estrogens and progestogens: influence of different routes of administration. Climacteric. 2005;8 Suppl 1:3-63.

316. Mattison DR, Karyakina N, Goodman M, LaKind JS. Pharmaco- and toxicokinetics of selected exogenous and endogenous estrogens: a review of the data and identification of knowledge gaps. Crit Rev Toxicol. 2014;44(8):696-724.

317. Al-Naamani N, Krowka MJ, Forde KA, Krok KL, Feng R, Heresi GA, et al. Estrogen Signaling and Portopulmonary Hypertension: The Pulmonary Vascular Complications of Liver Disease Study (PVCLD2). Hepatology. 2021;73(2):726-37.

318. Watson CS, Jeng YJ, Kochukov MY. Nongenomic actions of estradiol compared with estrone and estriol in pituitary tumor cell signaling and proliferation. FASEB J. 2008;22(9):3328-36.

319. Ciscato F, Ferrone L, Masgras I, Laquatra C, Rasola A. Hexokinase 2 in Cancer: A Prima Donna Playing Multiple Characters. Int J Mol Sci. 2021;22(9).

320. Julian GS, Oliveira RW, Tufik S, Chagas JR. Analysis of the stability of housekeeping gene expression in the left cardiac ventricle of rats submitted to chronic intermittent hypoxia. J Bras Pneumol. 2016;42(3):211-4.

321. Masoud GN, Li W. HIF-1α pathway: role, regulation and intervention for cancer therapy. Acta Pharm Sin B. 2015;5(5):378-89.

322. Muñoz-Sánchez J, Chánez-Cárdenas ME. The use of cobalt chloride as a chemical hypoxia model. J Appl Toxicol. 2019;39(4):556-70.

323. Merck. Protocol for charcoal-stripping FBS to deplete hormones. [Internet]. Darmstadt: Merck; 2020 [updated 2023; cited 2023 Aug 17]. Available from: https://www.sigmaaldrich.com/technical-documents/articles/biology/cell-culture/charcoal-stripped-heat-inactivated-fbs-protocols.html.

324. Thermo Fisher Scientific Inc. Phenol red, 0.5% solution, MP biomedicals. [Internet]. UK: Thermo Fisher Scientific; 1995 [updated 2023; cited 2023 Aug 17]. Available from https://www.fishersci.com/shop/products/phenol-red-0-5-solution-mp-biomedicals/MP091690049.

325. Hagan C. When are mice considered old? [Internet]. Maine: The Jackson Laboratory; [updated 2017 Nov 7; cited 2024 Jul 4]. Available from:

https://www.jax.org/news-and-insights/jax-blog/2017/november/when-are-mice-considered-old.

326. Long L, Ormiston ML, Yang X, Southwood M, Gräf S, Machado RD, et al. Selective enhancement of endothelial BMPR-II with BMP9 reverses pulmonary arterial hypertension. Nat Med. 2015;21(7):777-85.

327. Department of Biostatistics. Power and Sample Size [Internet]. Nashville: Vanderbilt University [updated 2021 Feb 15; cited 2024 Mar 25]. Available from: https://vbiostatps.app.vumc.org/ps/t-test/ind.

328. Paredes F, Williams HC, San Martin A. Metabolic adaptation in hypoxia and cancer. Cancer Lett. 2021;502:133-42.

329. Tan SC, Carr CA, Yeoh KK, Schofield CJ, Davies KE, Clarke K. Identification of valid housekeeping genes for quantitative RT-PCR analysis of cardiosphere-derived cells preconditioned under hypoxia or with prolyl-4-hydroxylase inhibitors. Mol Biol Rep. 2012;39(4):4857-67.

330. Diller M, Schüler S, Buchholz S, Lattrich C, Treeck O, Ortmann O. Effects of estriol on growth, gene expression and estrogen response element activation in human breast cancer cell lines. Maturitas. 2014;77(4):336-43.

331. Peng G, Xu J, Liu R, Fu Z, Li S, Hong W, et al. Isolation, culture and identification of pulmonary arterial smooth muscle cells from rat distal pulmonary arteries. Cytotechnology. 2017;69(5):831-40.

332. Tarbit E, Singh I, Peart JN, Rose'Meyer RB. Biomarkers for the identification of cardiac fibroblast and myofibroblast cells. Heart Fail Rev. 2019;24(1):1-15.

333. Muñoz-Sánchez J, Chánez-Cárdenas ME. The use of cobalt chloride as a chemical hypoxia model. J Appl Toxicol. 2019;39(4):556-70.

334. Martier AT, Maurice YV, Conrad KM, Mauvais-Jarvis F, Mondrinos MJ. Sex-specific actions of estradiol and testosterone on human fibroblast and endothelial cell proliferation, bioenergetics, and vasculogenesis. bioRxiv. 2023.

335. Luo H, Yang G, Yu T, Luo S, Wu C, Sun Y, et al. GPER-mediated proliferation and estradiol production in breast cancer-associated fibroblasts. Endocr Relat Cancer. 2014;21(2):355-69.

336. Luo N, Guan Q, Zheng L, Qu X, Dai H, Cheng Z. Estrogen-mediated activation of fibroblasts and its effects on the fibroid cell proliferation. Transl Res. 2014;163(3):232-41.

337. Santana LCL, Spolidorio LC, Pitombo JCP, Basso FG, Guarenghi GG, Prates RC, et al. Testosterone Increases Fibroblast Proliferation in vitro Through Androgen and Estrogen Receptor Activation. J Int Acad Periodontol. 2020;22(3):146-55.

338. Yang X, Wang Y, Yan S, Sun L, Yang G, Li Y, et al. Effect of testosterone on the proliferation and collagen synthesis of cardiac fibroblasts induced by angiotensin II in neonatal rat. Bioengineered. 2017;8(1):14-20.

339. Heithecker R, Aedo AR, Landgren BM, Cekan SZ. Plasma estriol levels after intramuscular injection of estriol and two of its esters. Horm Res. 1991;35(6):234-8.

340. Zhang H, Meng Z, Ye T, Liu T, Li J, Ma F, Gu R et al. An UPLC-MS/MS method to monitor estriol injection and comparison of pharmacokinetic characteristics after irradiation. Radiat Med Prot. 2021;2(2):72-78.

341. Wu D, Yotnda P. Induction and testing of hypoxia in cell culture. J Vis Exp. 2011(54).

342. Braunschweig L, Meyer AK, Wagenführ L, Storch A. Oxygen regulates proliferation of neural stem cells through Wnt/β-catenin signalling. Mol Cell Neurosci. 2015;67:84-92.

343. Cheng J, Yang HL, Gu CJ, Liu YK, Shao J, Zhu R, et al. Melatonin restricts the viability and angiogenesis of vascular endothelial cells by suppressing HIF-1α/ROS/VEGF. Int J Mol Med. 2019;43(2):945-55.

344. Strese S, Fryknäs M, Larsson R, Gullbo J. Effects of hypoxia on human cancer cell line chemosensitivity. BMC Cancer. 2013;13:331.

345. Shimoda LA, Laurie SS. HIF and pulmonary vascular responses to hypoxia. J Appl Physiol (1985). 2014;116(7):867-74.

346. Mogami H, Kojima I. Stimulation of calcium entry is prerequisite for DNA synthesis induced by platelet-derived growth factor in vascular smooth muscle cells. Biochem Biophys Res Commun. 1993;196(2):650-8.

347. Sweeney M, Yu Y, Platoshyn O, Zhang S, McDaniel SS, Yuan JX. Inhibition of endogenous TRP1 decreases capacitative Ca2+ entry and attenuates pulmonary artery smooth muscle cell proliferation. Am J Physiol Lung Cell Mol Physiol. 2002;283(1):L144-55.

348. Xie X, Li S, Zhu Y, Liu L, Pan Y, Wang J, et al. MicroRNA-27a/b mediates endothelin-1-induced PPARγ reduction and proliferation of pulmonary artery smooth muscle cells. Cell Tissue Res. 2017;369(3):527-3.

349. Maruyama H, Sakai S, Ieda M. Endothelin-1 alters BMP signaling to promote proliferation of pulmonary artery smooth muscle cells. Can J Physiol Pharmacol. 2022;100(10):1018-27.

350. Liao H, He H, Chen Y, Zeng F, Huang J, Wu L. Effects of long-term serial cell passaging on cell spreading, migration, and cell-surface ultrastructures of cultured vascular endothelial cells. Cytotechnology. 2014;66(2):229-38.

351. Cao J, Wu X, Qin X, Li Z. Uncovering the Effect of Passage Number on HT29 Cell Line Based on the Cell Metabolomic Approach. J Proteome Res. 2021;20(3):1582-90.

352. Vazquez Rodriguez G, Abrahamsson A, Jensen LD, Dabrosin C. Estradiol Promotes Breast Cancer Cell Migration via Recruitment and Activation of Neutrophils. Cancer Immunol Res. 2017;5(3):234-47.

353. Zheng S, Chen X, Hong S, Long L, Xu Y, Simoncini T, et al. 17β-Estradiol inhibits vascular smooth muscle cell migration via up-regulation of striatin protein. Gynecol Endocrinol. 2015;31(8):618-24.

354. Maruyama H, Dewachter C, Sakai S, Belhaj A, Rondelet B, Remmelink M, et al. Bosentan reverses the hypoxia-induced downregulation of the bone

morphogenetic protein signaling in pulmonary artery smooth muscle cells. Life Sci. 2016;159:111-5.

355. Ranganna K, Yousefipour Z, Yatsu FM, Milton SG, Hayes BE. Gene expression profile of butyrate-inhibited vascular smooth muscle cell proliferation. Mol Cell Biochem. 2003;254(1-2):21-36.

356. Maciel TT, Melo RS, Schor N, Campos AH. Gremlin promotes vascular smooth muscle cell proliferation and migration. J Mol Cell Cardiol. 2008;44(2):370-9.

357. Cahill E, Costello CM, Rowan SC, Harkin S, Howell K, Leonard MO, et al. Gremlin plays a key role in the pathogenesis of pulmonary hypertension. Circulation. 2012;125(7):920-30.

358. Happé C, Kurakula K, Sun XQ, da Silva Goncalves Bos D, Rol N, Guignabert C, et al. The BMP Receptor 2 in Pulmonary Arterial Hypertension: When and Where the Animal Model Matches the Patient. Cells. 2020;9(6).

359. Wang LH, Wu CF, Rajasekaran N, Shin YK. Loss of Tumor Suppressor Gene Function in Human Cancer: An Overview. Cell Physiol Biochem. 2018;51(6):2647-93.

360. Denver N, Khan S, Homer NZM, MacLean MR, Andrew R. Current strategies for quantification of estrogens in clinical research. J Steroid Biochem Mol Biol. 2019;192:105373.

361. Chaltel-Lima L, Domínguez F, Domínguez-Ramírez L, Cortes-Hernandez P. The Role of the Estrogen-Related Receptor Alpha (ERRa) in Hypoxia and Its Implications for Cancer Metabolism. Int J Mol Sci. 2023;24(9).

362. Florio M, Hernandez MC, Yang H, Shu HK, Cleveland JL, Israel MA. Id2 promotes apoptosis by a novel mechanism independent of dimerization to basic helix-loop-helix factors. Mol Cell Biol. 1998;18(9):5435-44.

363. Kowanetz M, Valcourt U, Bergström R, Heldin CH, Moustakas A. Id2 and Id3 define the potency of cell proliferation and differentiation responses to transforming growth factor beta and bone morphogenetic protein. Mol Cell Biol. 2004;24(10):4241-54.

364. Zhao Z, Bo Z, Gong W, Guo Y. Inhibitor of Differentiation 1 (Id1) in Cancer and Cancer Therapy. Int J Med Sci. 2020;17(8):995-1005.

365. lahm MM, Pausch C, Grünig E, Staehler G, Huscher D, Pittrow D, et al. Temporal trends in pulmonary arterial hypertension: results from the COMPERA registry. Eur Respir J. 2022;59(6).

366. Hoeper MM, Badesch DB, Ghofrani HA, Gibbs JSR, Gomberg-Maitland M, McLaughlin VV, et al. Phase 3 Trial of Sotatercept for Treatment of Pulmonary Arterial Hypertension. N Engl J Med. 2023;388(16):1478-90.

367. Andre P, Joshi SR, Briscoe SD, Alexander MJ, Li G, Kumar R. Therapeutic Approaches for Treating Pulmonary Arterial Hypertension by Correcting Imbalanced TGF-β Superfamily Signaling. Front Med (Lausanne). 2021;8:814222.

368. Yung LM, Yang P, Joshi S, Augur ZM, Kim SSJ, Bocobo GA, et al. ACTRIIA-Fc rebalances activin/GDF versus BMP signaling in pulmonary hypertension. Sci Transl Med. 2020;12(543).

369. Joshi SR, Liu J, Bloom T, Karaca Atabay E, Kuo TH, Lee M, et al. Sotatercept analog suppresses inflammation to reverse experimental pulmonary arterial hypertension. Sci Rep. 2022;12(1):7803.

370. Humbert M, McLaughlin V, Gibbs JSR, Gomberg-Maitland M, Hoeper MM, Preston IR, et al. Sotatercept for the Treatment of Pulmonary Arterial Hypertension. N Engl J Med. 2021;384(13):1204-15.

371. Gomberg-Maitland M, McLaughlin VV, Badesch DB, Ghofrani HA, Hoeper MM, Humbert M, et al. Long-Term Effects of Sotatercept on Right Ventricular Function: Results From the PULSAR Study. JACC Heart Fail. 2023;11(10):1457-9.

372. Humbert M, McLaughlin V, Gibbs JSR, Gomberg-Maitland M, Hoeper MM, Preston IR, et al. Sotatercept for the treatment of pulmonary arterial hypertension: PULSAR open-label extension. Eur Respir J. 2023;61(1).

373. Souza R, Badesch DB, Ghofrani HA, Gibbs JSR, Gomberg-Maitland M, McLaughlin VV, et al. Effects of sotatercept on haemodynamics and right heart function: analysis of the STELLAR trial. Eur Respir J. 2023;62(3).

374. Iafrati MD, Karas RH, Aronovitz M, Kim S, Sullivan TR, Lubahn DB, et al. Estrogen inhibits the vascular injury response in estrogen receptor alpha-deficient mice. Nat Med. 1997;3(5):545-8.

375. Karas RH, Hodgin JB, Kwoun M, Krege JH, Aronovitz M, Mackey W, et al. Estrogen inhibits the vascular injury response in estrogen receptor beta-deficient female mice. Proc Natl Acad Sci U S A. 1999;96(26):15133-6.

376. Zacharia LC, Gogos JA, Karayiorgou M, Jackson EK, Gillespie DG, Barchiesi F, et al. Methoxyestradiols mediate the antimitogenic effects of 17beta-estradiol: direct evidence from catechol-O-methyltransferase-knockout mice. Circulation. 2003;108(24):2974-8.

377. Cheng TC, Philip JL, Tabima DM, Kumari S, Yakubov B, Frump AL, et al. Estrogen receptor-α prevents right ventricular diastolic dysfunction and fibrosis in female rats. Am J Physiol Heart Circ Physiol. 2020;319(6):H1459-H73.

378. Golob MJ, Wang Z, Prostrollo AJ, Hacker TA, Chesler NC. Limiting collagen turnover via collagenase-resistance attenuates right ventricular dysfunction and fibrosis in pulmonary arterial hypertension. Physiol Rep. 2016;4(11).

379. Shah K, McCormack CE, Bradbury NA. Do you know the sex of your cells? Am J Physiol Cell Physiol. 2014;306(1):C3-18.

380. Park SJ, Jeong SY, Kim HJ. Y chromosome loss and other genomic alterations in hepatocellular carcinoma cell lines analyzed by CGH and CGH array. Cancer Genet Cytogenet. 2006;166(1):56-64.

381. Hutson DD, Gurrala R, Ogola BO, Zimmerman MA, Mostany R, Satou R, et al. Estrogen receptor profiles across tissues from male and female Rattus norvegicus. Biol Sex Differ. 2019;10(1):4.

382. Spyropoulos F, Vitali SH, Touma M, Rose CD, Petty CR, Levy P, et al. Echocardiographic markers of pulmonary hemodynamics and right ventricular hypertrophy in rat models of pulmonary hypertension. Pulm Circ. 2020;10(2):2045894020910976.

383. Tonelli AR, Yadav R, Gupta A, Arrossi AV, Heresi GA, Dweik RA. Spleen size in idiopathic and heritable pulmonary arterial hypertension. Respiration. 2013;85(5):391-9.

384. Frump AL, Albrecht M, Yakubov B, Breuils-Bonnet S, Nadeau V, Tremblay E, et al. 17β-Estradiol and estrogen receptor α protect right ventricular function in pulmonary hypertension via BMPR2 and apelin. J Clin Invest. 2021;131(6).

385. Liu A, Schreier D, Tian L, Eickhoff JC, Wang Z, Hacker TA, et al. Direct and indirect protection of right ventricular function by estrogen in an experimental model of pulmonary arterial hypertension. Am J Physiol Heart Circ Physiol. 2014;307(3):H273-83.

386. Lori A, Perrotta M, Lembo G, Carnevale D. The Spleen: A Hub Connecting Nervous and Immune Systems in Cardiovascular and Metabolic Diseases. Int J Mol Sci. 2017;18(6).

387. Hu Y, Chi L, Kuebler WM, Goldenberg NM. Perivascular Inflammation in Pulmonary Arterial Hypertension. Cells. 2020;9(11).

388. Sproston NR, Ashworth JJ. Role of C-Reactive Protein at Sites of Inflammation and Infection. Front Immunol. 2018;9:754.

389. Tschöpe C, Ammirati E, Bozkurt B, Caforio ALP, Cooper LT, Felix SB, et al. Myocarditis and inflammatory cardiomyopathy: current evidence and future directions. Nat Rev Cardiol. 2021;18(3):169-93.

390. Barcena ML, Tonini G, Haritonow N, Breiter P, Milting H, Baczko I, et al. Sex and age differences in AMPK phosphorylation, mitochondrial homeostasis, and inflammation in hearts from inflammatory cardiomyopathy patients. Aging Cell. 2023;22(8):e13894.

391. Li S, Gupte AA. The Role of Estrogen in Cardiac Metabolism and Diastolic Function. Methodist Debakey Cardiovasc J. 2017;13(1):4-8.

392. Baritussio A, Schiavo A, Basso C, Giordani AS, Cheng CY, Pontara E, et al. Predictors of relapse, death or heart transplantation in myocarditis before the introduction of immunosuppression: negative prognostic impact of female gender,

fulminant onset, lower ejection fraction and serum autoantibodies. Eur J Heart Fail. 2022;24(6):1033-44.

393. Pfeilschifter J, Köditz R, Pfohl M, Schatz H. Changes in proinflammatory cytokine activity after menopause. Endocr Rev. 2002;23(1):90-119.

394. Rickard D, Russell G, Gowen M. Oestradiol inhibits the release of tumour necrosis factor but not interleukin 6 from adult human osteoblasts in vitro. Osteoporos Int. 1992;2(2):94-102.

395. Kimble RB, Srivastava S, Ross FP, Matayoshi A, Pacifici R. Estrogen deficiency increases the ability of stromal cells to support murine osteoclastogenesis via an interleukin-1and tumor necrosis factor-mediated stimulation of macrophage colony-stimulating factor production. J Biol Chem. 1996;271(46):28890-7.

396. Rogers A, Eastell R. The effect of 17beta-estradiol on production of cytokines in cultures of peripheral blood. Bone. 2001;29(1):30-4.

397. Robinson DP, Klein SL. Pregnancy and pregnancy-associated hormones alter immune responses and disease pathogenesis. Horm Behav. 2012;62(3):263-71.

398. Vermillion MS, Ursin RL, Attreed SE, Klein SL. Estriol Reduces Pulmonary Immune Cell Recruitment and Inflammation to Protect Female Mice From Severe Influenza. Endocrinology. 2018;159(9):3306-20.

399. Harper RL, Reynolds AM, Bonder CS, Reynolds PN. BMPR2 gene therapy for PAH acts via Smad and non-Smad signalling. Respirology. 2016;21(4):727-33.

400. Kwan WC, Shavelle DM, Laughrun DR. Pulmonary vascular resistance index: Getting the units right and why it matters. Clin Cardiol. 2019;42(3):334-8.

401. Deng J. Clinical application of pulmonary vascular resistance in patients with pulmonary arterial hypertension. J Cardiothorac Surg. 2021;16(1):311.

402. Ko EA, Song MY, Donthamsetty R, Makino A, Yuan JX. Tension Measurement in Isolated Rat and Mouse Pulmonary Artery. Drug Discov Today Dis Models. 2010;7(3-4):123-30.

403. Gimelli S, Caridi G, Beri S, McCracken K, Bocciardi R, Zordan P, et al. Mutations in SOX17 are associated with congenital anomalies of the kidney and the urinary tract. Hum Mutat. 2010;31(12):1352-9.

404. Wu Y, Wharton J, Walters R, Vasilaki E, Aman J, Zhao L, et al. The pathophysiological role of novel pulmonary arterial hypertension gene. Eur Respir J. 2021;58(3).

405. Wang Z, Schreier DA, Hacker TA, Chesler NC. Progressive right ventricular functional and structural changes in a mouse model of pulmonary arterial hypertension. Physiol Rep. 2013;1(7):e00184.

406. Janssen BJ, De Celle T, Debets JJ, Brouns AE, Callahan MF, Smith TL. Effects of anesthetics on systemic hemodynamics in mice. Am J Physiol Heart Circ Physiol. 2004;287(4):H1618-24.

407. Hanahan D, Weinberg RA. The hallmarks of cancer. Cell. 2000;100(1):57-70.

408. Hanahan D, Weinberg RA. Hallmarks of cancer: the next generation. Cell. 2011;144(5):646-74.

409. Hanahan D. Hallmarks of Cancer: New Dimensions. Cancer Discov. 2022;12(1):31-46.

410. Anandakrishnan R, Varghese RT, Kinney NA, Garner HR. Estimating the number of genetic mutations (hits) required for carcinogenesis based on the distribution of somatic mutations. PLoS Comput Biol. 2019;15(3):e1006881.

411. Futreal PA, Coin L, Marshall M, Down T, Hubbard T, Wooster R, et al. A census of human cancer genes. Nat Rev Cancer. 2004;4(3):177-83.

412. Pokharel MD, Marciano DP, Fu P, Franco MC, Unwalla H, Tieu K, et al. Metabolic reprogramming, oxidative stress, and pulmonary hypertension. Redox Biol. 2023;64:102797.

413. Gorelova A, Berman M, Al Ghouleh I. Endothelial-to-Mesenchymal Transition in Pulmonary Arterial Hypertension. Antioxid Redox Signal. 2021;34(12):891-914.

414. Liu L, Wei Y, Giunta S, He Q, Xia S. Potential role of cellular senescence in pulmonary arterial hypertension. Clin Exp Pharmacol Physiol. 2022;49(10):1042-9.

415. Hudson J, Farkas L. Epigenetic Regulation of Endothelial Dysfunction and Inflammation in Pulmonary Arterial Hypertension. Int J Mol Sci. 2021;22(22).

416. Moutsoglou DM, Tatah J, Prisco SZ, Prins KW, Staley C, Lopez S, et al. Pulmonary Arterial Hypertension Patients Have a Proinflammatory Gut Microbiome and Altered Circulating Microbial Metabolites. Am J Respir Crit Care Med. 2023;207(6):740-56.

417. BioRender.com. Hallmarks of cancer (circle layout) [Internet]. Toronto: BioRender; [updated 2024; cited 2024 Apr 13]. Available from: https://app.biorender.com/biorender-templates.

418. Aspen. Estriol 1mg/g cream. Summary of product characteristics [Internet]. Surrey: Electronic Medicines Compendium; [updated 2023 Nov 9; cited 2024 Mar 14]. Available from: https://www.medicines.org.uk/emc/product/5384/smpc.

419. Sánchez-Rovira P, Hirschberg AL, Gil-Gil M, Bermejo-De Las Heras B, Nieto-Magro C. A Phase II Prospective, Randomized, Double-Blind, Placebo-Controlled and Multicenter Clinical Trial to Assess the Safety of 0.005% Estriol Vaginal Gel in Hormone Receptor-Positive Postmenopausal Women with Early Stage Breast Cancer in Treatment with Aromatase Inhibitor in the Adjuvant Setting. Oncologist. 2020;25(12):e1846-54.

420. Umscheid CA, Margolis DJ, Grossman CE. Key concepts of clinical trials: a narrative review. Postgrad Med. 2011;123(5):194-204.

421. Stirrat LI, O'Reilly JR, Barr SM, Andrew R, Riley SC, Howie AF, et al. Decreased maternal hypothalamic-pituitary-adrenal axis activity in very severely obese pregnancy: Associations with birthweight and gestation at delivery. Psychoneuroendocrinology. 2016;63:135-43.

422. Vonk-Noordegraaf A, Haddad F, Chin KM, Forfia PR, Kawut SM, Lumens J, et al. Right heart adaptation to pulmonary arterial hypertension: physiology and pathobiology. J Am Coll Cardiol. 2013;62(25 Suppl):D22-33.

423. Forfia PR, Mathai SC, Fisher MR, Housten-Harris T, Hemnes AR, Champion HC, et al. Hyponatremia predicts right heart failure and poor survival in pulmonary arterial hypertension. Am J Respir Crit Care Med. 2008;177(12):1364-9.

424. Shah SJ, Thenappan T, Rich S, Tian L, Archer SL, Gomberg-Maitland M. Association of serum creatinine with abnormal hemodynamics and mortality in pulmonary arterial hypertension. Circulation. 2008;117(19):2475-83.

425. Nickel NP, O'Leary JM, Brittain EL, Fessel JP, Zamanian RT, West JD, et al. Kidney dysfunction in patients with pulmonary arterial hypertension. Pulm Circ. 2017;7(1):38-54.

426. Longcope C. Estriol production and metabolism in normal women. J Steroid Biochem. 1984;20(4B):959-62.

427. Frump AL, Yakubov B, Walts A, Fisher A, Cook T, Chesler NC, et al. Estrogen Receptor-α Exerts Endothelium-Protective Effects and Attenuates Pulmonary Hypertension. Am J Respir Cell Mol Biol. 2023;68(3):341-4.

428. Gao Y, Chen T, Raj JU. Endothelial and Smooth Muscle Cell Interactions in the Pathobiology of Pulmonary Hypertension. Am J Respir Cell Mol Biol. 2016;54(4):451-60.

429. Deng L, Blanco FJ, Stevens H, Lu R, Caudrillier A, McBride M, et al. MicroRNA-143 Activation Regulates Smooth Muscle and Endothelial Cell Crosstalk in Pulmonary Arterial Hypertension. Circ Res. 2015;117(10):870-83.

430. Coyne DW, Singh HN, Smith WT, Giuseppi AC, Connarn JN, Sherman ML, et al. Sotatercept Safety and Effects on Hemoglobin, Bone, and Vascular Calcification. Kidney Int Rep. 2019;4(11):1585-97.

431. Ramakrishnan L, Pedersen SL, Toe QK, Quinlan GJ, Wort SJ. Pulmonary Arterial Hypertension: Iron Matters. Front Physiol. 2018;9:641.

432. Vogt AS, Arsiwala T, Mohsen M, Vogel M, Manolova V, Bachmann MF. On Iron Metabolism and Its Regulation. Int J Mol Sci. 2021;22(9).

433. Wei YH, He YZ, Guo XY, Lin XY, Zhu HB, Guo XJ. Investigation and Analysis of Iron-Deficiency Anemia Complicated by Splenomegaly. Int J Gen Med. 2021;14:4155-9.

434. Langdon JM, Barkataki S, Berger AE, Cheadle C, Xue QL, Sung V, et al. RAP-011, an activin receptor ligand trap, increases hemoglobin concentration in hepcidin transgenic mice. Am J Hematol. 2015;90(1):8-14.

435. Hoeper MM, Pausch C, Grünig E, Staehler G, Huscher D, Pittrow D, et al. Temporal trends in pulmonary arterial hypertension: results from the COMPERA registry. Eur Respir J. 2022;59(6).

436. National Institute for Health and Care Excellence. Sotatercept for treating pulmonary arterial hypertension [ID6163] [Internet]. London: NICE; [updated 2024 Mar 12; cited 2024 Mar 14]. Available from: https://www.nice.org.uk/guidance/indevelopment/gid-ta11103.

404.

8. Supplemental Methods

8.1 Protocol for *Mycoplasma* Testing Using a PCR Kit

During earlier experiments, *Mycoplasma* testing was carried out by Gregor Aitchison and Ayman Gebril using a PCR Mycoplasma Test Kit (PromoCell, UK). 1 mL culture media (taken at 90-100% cell confluency) was stored in an Eppendorf tube. The sample was heated at 95°C for 10 minutes, then centrifuged at 500g for 5 minutes to pellet cellular debris. The supernatant was transferred to a fresh tube and centrifuged at 14,000g for 15 minutes. The supernatant was removed, and the pellet re-suspended in 100 µL RNase-free water.

The test reaction tubes were rehydrated by adding 23 µL Rehydration Buffer. 2 µL media was added to each tube and 2µL DNA Elution Buffer was added to one as a negative control. A positive control reaction tube was rehydrated by adding 23 µL Rehydration Buffer and 2 µL DNA-free water was added. The contents were mixed thoroughly by flicking the tube and the lyophilised components allowed to dissolve by incubating for 5 minutes at room temperature. The PCR tubes were placed in a PTC-100™ Programmable Thermal Controller (MJ Research Inc., Quebec, Canada) and the following program run:

1 cycle	95°C for 2 minutes
40 cycles	94°C for 30 seconds
	55°C for 30 seconds
	72°C for 40 seconds
	Cool down to 4-8°C

Agarose gel electrophoresis was carried out using a 1.5% standard agarose gel with 5 mm comb. The reaction tube was vortexed gently then 8µL of DNA ladder, positive control, negative control, and each sample were loaded. Gel electrophoresis was carried out at 100V for 30 minutes, and the bands visualised under UV light on an Azure imaging system.

8.2 *Mycoplasma* Testing Using a MycoStrip™ Detection Kit

During later experiments, *Mycoplasma* testing was carried out by Gregor Aitchison and Ayman Gebril using a MycoStrip™ Mycoplasma Detection Kit (Invivogen, San Diego, US) as this was less time consuming. 1 mL culture media (taken at 90-100% cell confluency) was transferred to an RNase-free Eppendorf tube and centrifuged at 16,000g for 5 minutes to pellet any *Mycoplasma*. The supernatant was discarded, ensuring that no more than 50 µL media remained. 500 µL sterile PBS was added and the sample was mixed by pipetting. The kit provided a positive control containing *Mycoplasma* DNA. Sterile PBS was used as a negative control. 5 µL reaction buffer was added to 5 µL of prepared sample or control and heated at 65°C for 40 minutes. 200 µL migration buffer was added to the tube and mixed well. 100 µL processed sample was added to the test strip. One band (‘C’ band only) indicates that *Mycoplasma* was not detected in the processed sample. Two bands (‘C’ and ‘T') indicate that the processed sample is contaminated by *Mycoplasma*. If no ‘T’ band appears after 5 minutes, the test is considered negative.

8.3 Protein Transfer Using the Trans-Blot Turbo Transfer System

Sodium dodecyl sulfate polyacrylamide gel electrophoresis was carried out as per 2.9.3. The Trans-Blot Turbo Transfer Pack was opened, and the bottom part placed in the tray of the Trans-Blot Turbo Transfer system (Bio-Rad Laboratories Ltd, UK). The gel was removed from the cassette and placed on top of the PVDF membrane. A small amount of TBS was poured over and any bubbles removed. The top half of the gel pack was placed over the gel and any bubbles removed. The transfer was run for 7 minutes. The blot was rinsed in distilled water and Ponceau S stain used to assess transfer. Immunoblotting was carried out as per 2.9.5.

8.4 Visualisation of Protein Bands Using the LI-COR Imaging System

Sodium dodecyl sulfate polyacrylamide gel electrophoresis, protein transfer and immunoblotting with primary antibodies were carried out as per 2.9.3, 2.9.4, and 2.9.5. The following fluorophore-labelled secondary antibodies were used: IRDye® 680RD Donkey anti-Rabbit IgG (LI-COR Inc., Lincoln, US), IRDye® 800CW Donkey anti-Mouse IgG (LI-COR Inc., Lincoln, US) at 1:20,000 dilution in TBST. The blots were incubated in secondary antibody for 1 hour at room temperature and rinsed 1x10 minutes in TBST then 2x10 minutes in TBS. The blots were imaged using an Odyssey® M Imaging System (LI-COR Inc., Lincoln, US). Densitometry was quantified using ImageJ, and analysis carried out as per 2.9.5.

9. Supplemental Data

9.1 The Effect of 24 Hours Incubation in 1% O_2 on Female Rat Pulmonary Artery Smooth Muscle Cells

Following 24 hours incubation in 1% O_2, 5% CO_2, nitrogen mix, HIF1α remained present in both the nucleus and cytoplasm of female rPASMCs (Figure 9.1). There was also no change in *Hk2* expression. This suggests that a longer incubation period is required to induce a hypoxic response, and 72 hours was found to be sufficient (Figure 3.4).

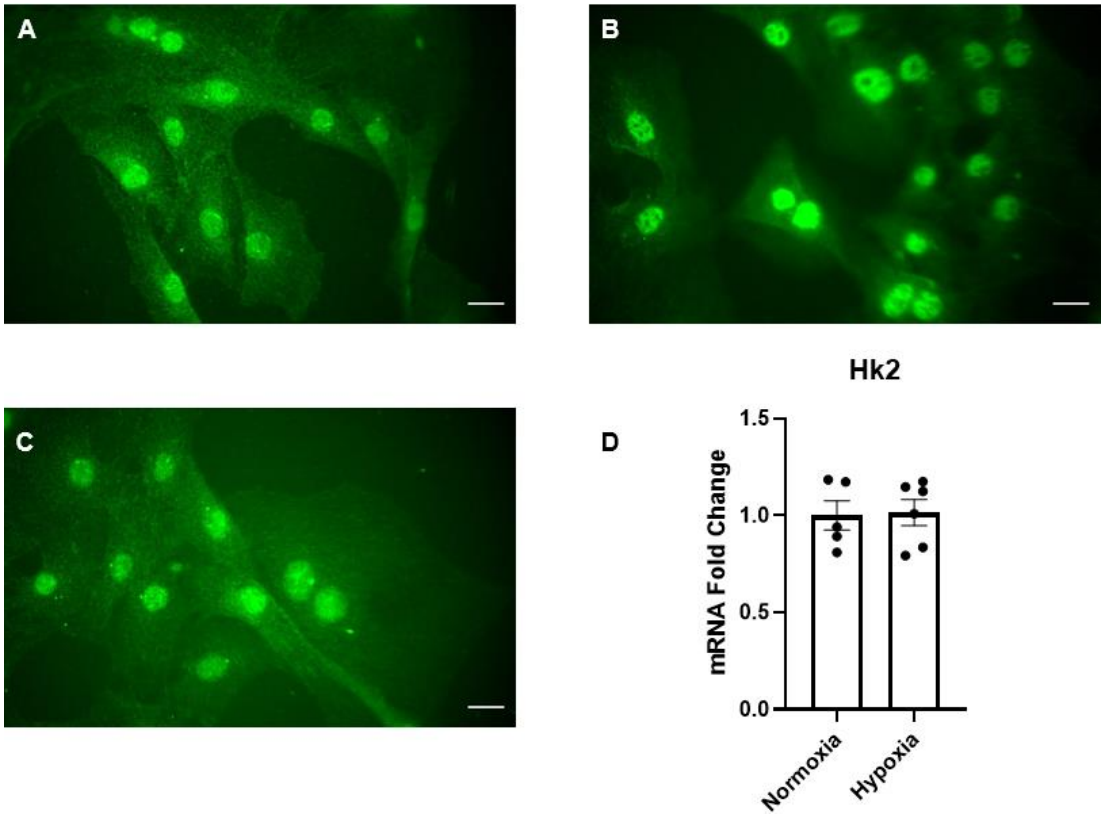

Figure 9.1: 24 hours incubation in 1% O_2 is insufficient to induce a hypoxic response in rPASMCs.

(A-C) Female rat pulmonary artery smooth muscle cells (rPASMCs) at passage 3 were seeded on to collagen coated coverslips in a 12-well plate at $1x10^5$ cells/well, cultured until 50-60% confluent, and immunocytochemistry carried out as previously described. HIF1α is shown in green. HIF1α was strongly present in both the cytoplasm and nucleus under (A) normoxic conditions, (B) 24 hours treatment with 200 μM cobalt chloride, (C) 24 hours incubation in 1% O_2/ 5% CO_2 in N_2, indicating that a longer incubation period was required to induce a hypoxic response. Images are representative of HIF1α immunofluorescence. Scale bars = 20 μm. (D) Female rPASMCs were seeded into 6-well plates at $3x10^5$ cells/well, cultured until ~70% confluent, and incubated in normoxia or 1% O_2/ 5% CO_2 in N_2 for 24 hours prior to RNA collection. qRT-PCR was carried out as previously described. Basal *Hk2* CT (normoxia) = 33.0. Data are expressed as ±SEM and analysed by unpaired t-test. n=6 technical replicates performed in one female rPASMC cell line.

9.2 Physiological Data from Sprague-Dawley Rats

Table 9.1: Physiological Data from Male Sprague-Dawley Rats

Parameter	Untreated	Sugen-Hypoxic
Age (Weeks)	11-12	15
Body Weight (g)	320-344	269-300
RV Weight (mg) (Mean ± SEM)	184.70 ± 5.12	520.40 ± 17.49
LV+S Weight (mg) (Mean ± SEM)	751.60 ± 11.39	825.90 ± 44.61
Fulton Index (Mean ± SEM)	0.25 ± 0.01	0.63 ± 0.03
Spleen Weight (mg) (Mean ± SEM)	549.00 ± 51.80	850.60 ± 70.22

Table 9.1: Physiological data from male Sprague-Dawley rats.
Rat pulmonary artery smooth muscle cells (rPASMCs) were isolated from untreated healthy male Sprague-Dawley rats aged 11-12 weeks as previously described. rPASMCs were also isolated from Sprague-Dawley rats treated with a single 20 mg/kg dose of Sugen 5416 followed by 3 weeks hypoxia (reduced atmospheric pressure of 550 mBar) then 3 weeks re-exposure to normal atmospheric pressure (~1050 mBar), however these cell cultures failed due to poor growth. Physiological data are shown in Table 9.1 and expressed as the range or mean ± SEM. RV = right ventricle, LV+S = left ventricle plus septum. n=4-9.

Table 9.2: Physiological Data from Female Sprague-Dawley Rats

Parameter	Untreated	Chronic Hypoxic	Sugen-Hypoxic
Age (Weeks)	11-13	18	15
Body Weight (g)	210-265	241-260	205-241
RV Weight (mg) (Mean ± SEM)	159.70 ± 4.91	217.90 ± 6.76	406.00 ± 116.10
LV+S Weight (mg) (Mean ± SEM)	603.70 ± 24.33	533.60 ± 17.95	713.90 ± 125.10
Fulton Index (Mean ± SEM)	0.26 ± <0.01	0.41 ± 0.03	0.56 ± 0.13
Spleen Weight (mg) (Mean ± SEM)	578.00 ± 60.11	426.80 ± 35.74	706.5 ± 92.22

Table 9.2: Physiological data from female Sprague-Dawley rats.
Rat pulmonary artery smooth muscle cells (rPASMCs) were isolated from untreated healthy female Sprague-Dawley rats aged 11-13 weeks as previously described. rPASMCs were also isolated from female Sprague-Dawley rats treated with a single 20 mg/kg dose of Sugen 5416 followed by 3 weeks hypoxia (reduced atmospheric pressure of 550 mBar) then 3 weeks re-exposure to normal atmospheric pressure (~1050 mBar), however these cell cultures failed due to poor growth. rPASMCs were successfully isolated from female Sprague-Dawley rats treated with 2 weeks hypoxia (550 mBar) alone. Physiological data are shown in Table 9.2 and expressed as the range or mean ± SEM. RV = right ventricle, LV+S = left ventricle plus septum. n=4-9.

9.3 Wound Migration Assay

In male rPASMCs, the percentage wound area closed was significantly lower in response to 10 nM 16OHE2 compared to 1 nM (Figure 3.7), and there was no significant difference in migration between DMEM containing 1% FBS and the vehicle control (10 nM ethanol, Figure 9.2). This suggests that the 10 nM ethanol concentration was not responsible for this effect, and that migration in response to 16OHE2 is concentration dependent.

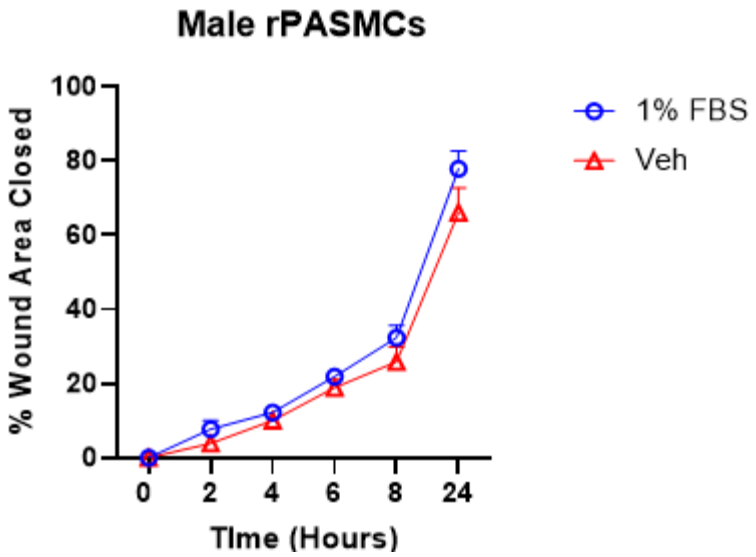

Figure 9.2: Comparison of migration in response to 1% FBS and vehicle in male rPASMCs. Rat pulmonary artery smooth muscle cells (rPASMCs) were seeded in a 6-well plate at $3x10^5$ cells/well, cultured to 90-100% confluency, and quiesced (0.2% charcoal stripped FBS in phenol red-free DMEM) for 24 hours. Two wounds were created per well using a 200 µL pipette tip, the cells were washed three times with PBS, then stimulated with 16α-hydroxyestradiol (16OHE2) as previously described or controls. Stimulations were carried out in phenol red-free DMEM with 1% charcoal stripped FBS. Images were taken at 0, 2, 4, 6, 8, and 24 hours, and the % wound area closed calculated as a measure of cell migration. No significant difference was observed between stimulation with the vehicle (10 nM ethanol) and 1% FBS. Data are expressed as ±SEM and analysed by two-way ANOVA with post-hoc Tukey test. n=6.

9.4 Effects of 16OHE2 on *Bmpr2* Expression in the Presence of Estrogen Receptor Antagonists in Female Rat Pulmonary Artery Smooth Muscle Cells Under Acute Hypoxia

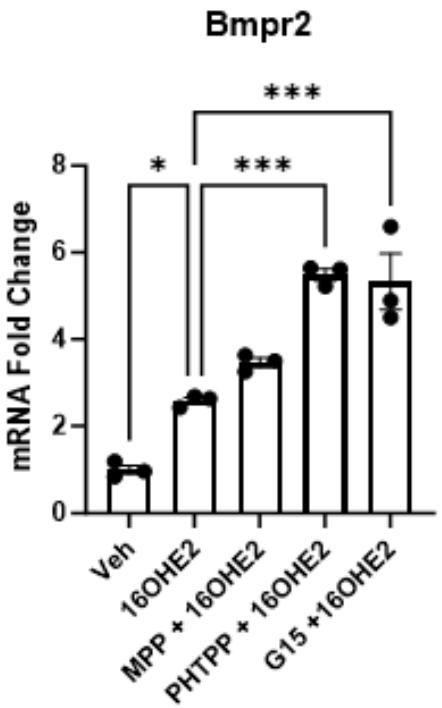

Figure 9.3: Effects of 16OHE2 in the presence of estrogen receptor antagonists on *Bmpr2* mRNA expression in female rPASMCs under acute hypoxia.
Female rat pulmonary artery smooth muscle cells (rPASMCs) were seeded in 100 mm dishes at $2.2x10^6$ cells/dish. The following day, the culture media was refreshed, and the cells were placed into hypoxia (1% O_2/ 5% CO_2/ nitrogen) for 72 hours as previously described. On day 3, the cells (~70% confluency) were quiesced (0.2% charcoal stripped FBS in phenol red-free DMEM) for 24 hours. On day 4, cells were stimulated with 10 nM 16α-hydroxyestradiol (16OHE2) in the presence or absence of the estrogen receptor antagonists 1 μM MPP (ERα), 1μM PHTPP (ERβ) or 1μM G15 (GPER), or with the vehicle control (10 nM ethanol) for 24 hours prior to RNA lysis. Stimulations were carried out in phenol red-free DMEM with 1% charcoal stripped FBS. Basal CT value = 29.1 (average CT value in the vehicle control group). FC= Fold change, calculated by ΔΔCT method and represented as relative to the vehicle (where the average vehicle fold change is 1). Data are expressed as ±SEM and analysed by one-way ANOVA with post-hoc Tukey test. *$p<0.05$, ***$p<0.001$. n=3.

9.5 Basal ESR2 Expression in Female Rat Pulmonary Artery Smooth Muscle Cells Compared to Males

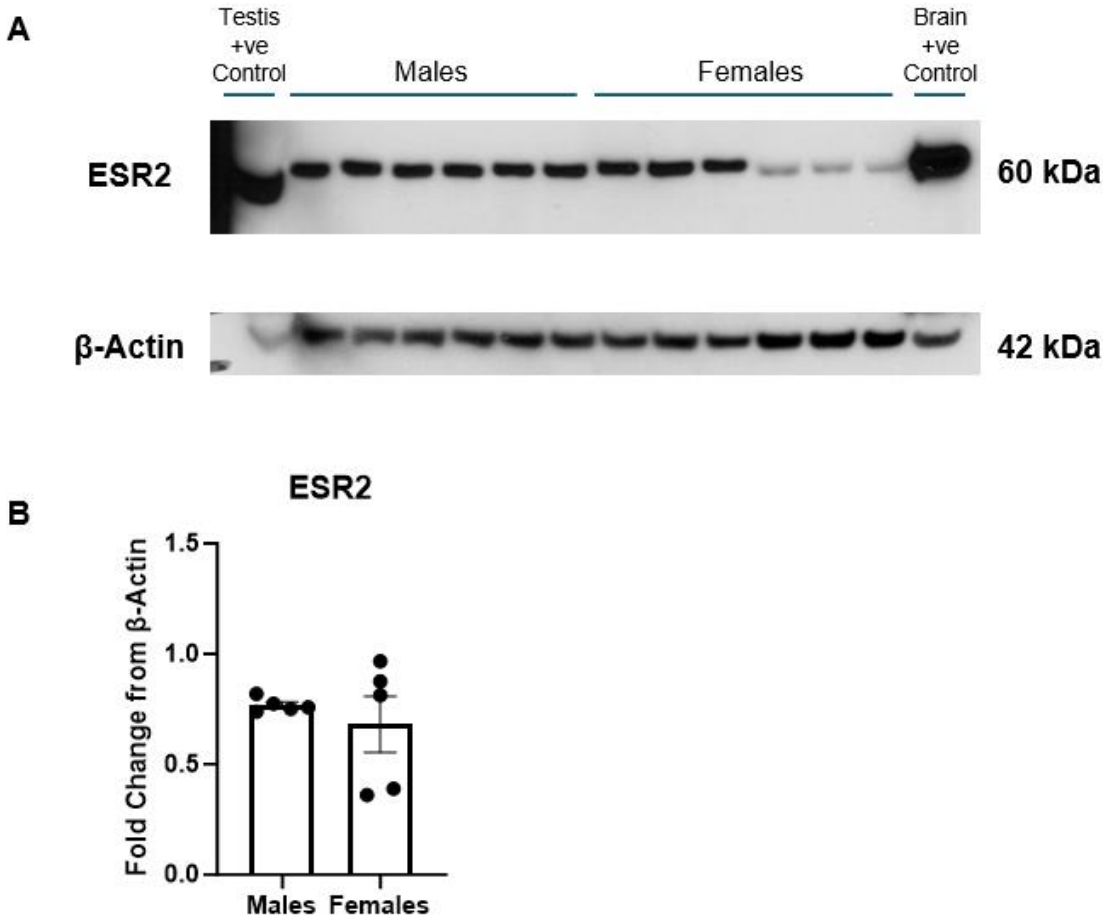

Figure 9.4: Basal expression of ESR2 in female rPASMCs compared to male rPASMCs. Rat pulmonary artery smooth muscle cells (rPASMCs) were seeded in 100 mm dishes at 2.2×10^6 cells/dish and cultured for 3 days until 90-100% confluent before protein lysis as previously described. Male rPASMCs were passage 5-6 and females passage 3 due to the primary cell lines available at the time. (A) Immunoblots of ESR2 and β-actin. Positive controls = rat testis and rat brain lysates. (B) Quantification of basal ESR2 expression in male and female rPASMCs. Fold change is ESR2 relative to β-actin expression. Data are expressed as ±SEM and analysed by unpaired t-test. n=6.

9.6 Physiological Effects of 16OHE2 in C57BL/6 Mice

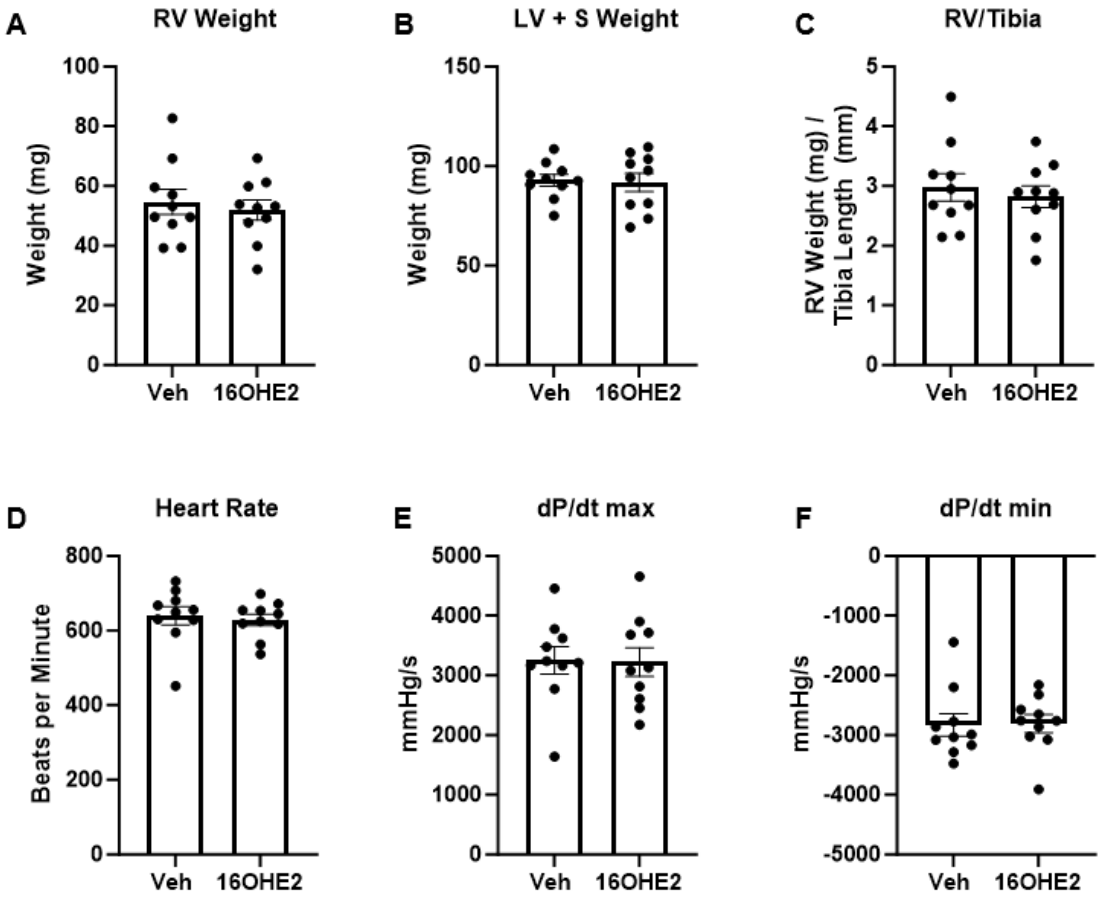

Figure 9.5: Physiological effects of 16OHE2 in male C57BL/6 mice.

Male C57BL/6 mice received 1.5 mg/kg/day 16α-hydroxyestradiol (16OHE2) by intraperitoneal injection for 14 days. No significant changes were observed in response to 16OHE2 in (A) Right ventricular (RV) weight, (B) Weight of the left ventricle plus septum (LV+S), (C) Ratio of RV weight/ tibia length, (D) Heart rate, (E) Maximum rate of pressure change in the RV (dP/dt_{max}), or (F) Minimum rate of pressure change in the RV (dP/dt_{min}). Normality was assessed by Shapiro-Wilk test. Data are expressed as ±SEM and analysed by unpaired t-test. n=10.

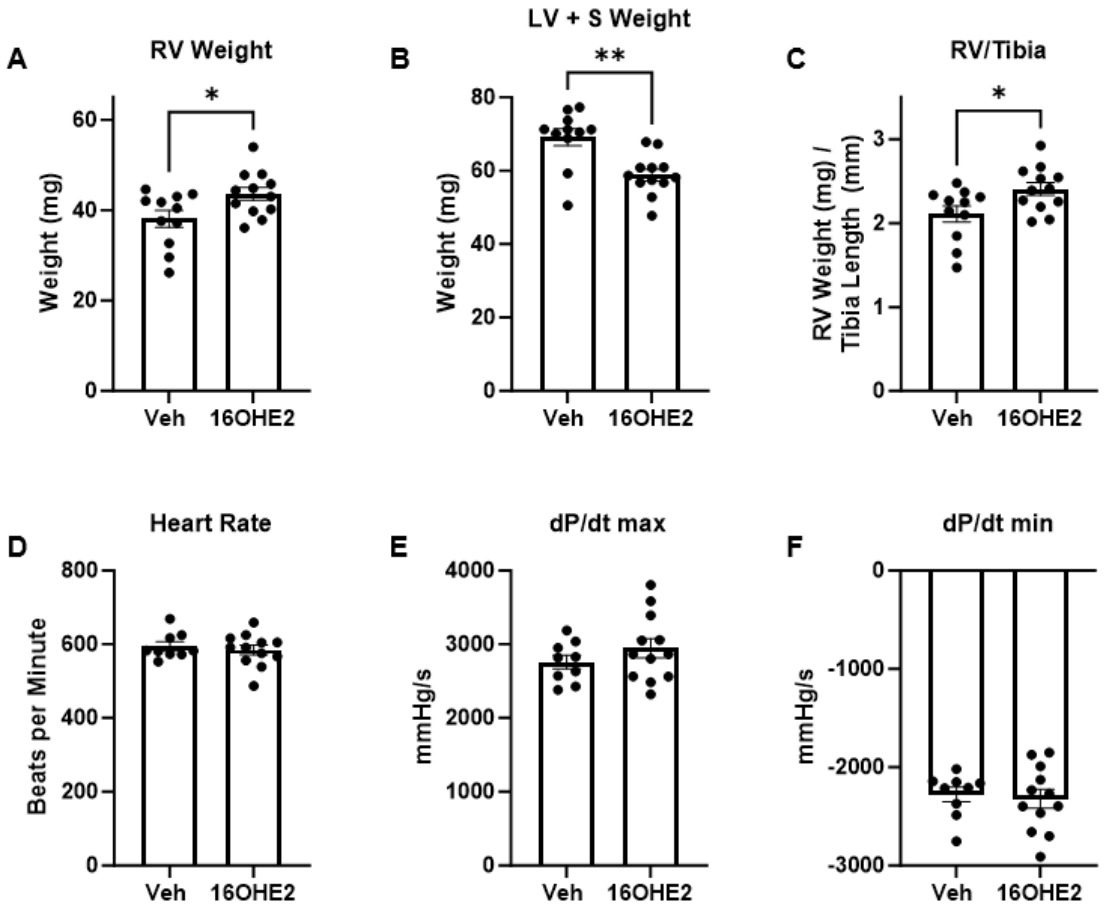

Figure 9.6: Physiological effects of 16OHE2 in female C57BL/6 mice.

Female C57BL/6 mice received 1.5 mg/kg/day 16α-hydroxyestradiol (16OHE2) by intraperitoneal injection for 14 days. (A) Right ventricle (RV) weight significantly increased in response to 16OHE2. (B) Weight of the left ventricle plus septum (LV+S) significantly decreased in response to 16OHE2. (C) Ratio of RV weight/ tibia length significantly increased in response to 16OHE2. (D) There was no change in heart rate. (E) There was no change in the maximum rate of pressure change in the RV (dP/dt_{max}). (F) There was no change in the minimum rate of pressure change in the RV (dP/dt_{min}). Normality was assessed by Shapiro-Wilk test. Data are expressed as ±SEM and analysed by unpaired t-test or Mann-Whitney test. n=9-12.